Biotechnology and Biological Sciences Research Council

University of East Anglia

norwich research park
Doctoral Training Partnership

Investigating the role of microRNAs in the development of Xenopus neural crest

Thesis for a PhD degree
Submitted to University of East Anglia
By

Alice May Godden

This copy of the thesis has been supplied on condition that anyone who consults it is understood to recognise that its copyright rests with the author and that use of any information derived there from must be in accordance with the current UK copyright Law. In addition, any quotation or extract must include full attribution.

Word count: 59,034

Principal Investigator: Prof. Grant N. Wheeler
Submission date: 26/07/2021

Acknowledgements

I want to pay special thanks to Dr. Aida Rajic for inspiring me into the field of developmental biology and the role that microRNAs may play in embryonic development.

I would like to thank my PI Prof. Grant Wheeler for the opportunity to carry out the project and acknowledge my second and third supervisors Prof. Simon Moxon and Prof. Andrea Munsterberg for their advice during the project.

I want to thank lab alumni Dr Nicole Ward, Dr Ines Desanlis, Dr Katy Saide and Dr Marta Marín-Barba for teaching me how to work with (catch) the *Xenopus*. I also want to thank Michael van der Lee for helping with the frozen sperm project, so many thousands of embryos!

I'd also like to show my appreciation to all the technicians in BIO: Elaine, Jordan and Andy for keeping the place going and all the nitrogen flowing for the injectors. I'd like to thank Simon Deakin and the Animal technicians: John, Emma, Rich, Anya, and Imogen for keeping the frogs happy, healthy and very well-looked after.

For advanced training, I would like to thank a few people: Prof. Matthew Guille and all the team at the European Xenopus resource centre for their continued advice, technical support and generation of data and frog lines. Prof. Anne-Hélène Monsoro-Burq for continued interest and ideas for the project. Dr. Timothy Grocott and Dr. Johannes Wittig for molecular support and wider training and advice not only in my PhD but when I joined the lab as a research technician. Dr. Paige Paddy and Dr. Tracey Swingler for microRNA, q-RT-PCR and other microRNA related queries.

I would like to say a big thank you to the UKRI and NRP DTP programme team for funding and continued support and advice. I would also like to thank Prof. Alastair Grant for guidance and mentorship.

Last, but not least I want to thank some very important people who kept me going throughout this project. I want to thank my Mum and Dad, as well as my sister Emily for all the support they have provided me throughout my studies. Most importantly I want to acknowledge the support of my fiancé Dr. Benjamin Rix. For all the late-night pick-ups, missed events, freshly cooked lasagne, technical advice, and generally keeping me going. Without you I would not have made it this far.

Abstract

The neural crest is a multipotent stem-cell population that is specified during early neurulation and that undergoes epithelial-mesenchymal-transition and proceeds to migrate to various points in the developing embryo where they give rise to several tissues including parts of the peripheral nervous system and craniofacial skeleton. The molecular background and detailed fine-tuning of neural crest specification is increasingly being elucidated but many questions remain. Dysregulation of neural crest results in several different diseases grouped under the term neurocristopathies. These include in-born defects like Waardenburg syndrome, presenting with *Pax3* mutations, pigment defects and mild craniofacial dysmorphogenesis through to cancers such as neuroblastoma.

MicroRNAs are short non-coding RNAs approximately 20 nucleotides long which affect gene expression through post-transcriptional repression and have known roles in development and disease. As part of an ongoing project microRNAs miR-196a and miR-219 were identified to be expressed in *Xenopus* neural crest.

I have investigated the molecular pathways affected by these microRNAs by using morpholinos and developed a novel CRISPR-Cas9 knockout approach. Development of neural crest and other tissues has been evaluated using whole mount *in situ* hybridization of key neural crest, neural plate border and hatching gland markers including Sox10, Snail2, Pax3 and Xhe2; Alcian blue testing, q-RT-PCR, phenotype, and genotype analysis. Craniofacial and pigment phenotypes were observed following miRNA-knockouts, and miRNA-knockdowns showed neural crest, neural plate, neural and placodal phenotypes.

Access Condition and Agreement

Each deposit in UEA Digital Repository is protected by copyright and other intellectual property rights, and duplication or sale of all or part of any of the Data Collections is not permitted, except that material may be duplicated by you for your research use or for educational purposes in electronic or print form. You must obtain permission from the copyright holder, usually the author, for any other use. Exceptions only apply where a deposit may be explicitly provided under a stated licence, such as a Creative Commons licence or Open Government licence.

Electronic or print copies may not be offered, whether for sale or otherwise to anyone, unless explicitly stated under a Creative Commons or Open Government license. Unauthorised reproduction, editing or reformatting for resale purposes is explicitly prohibited (except where approved by the copyright holder themselves) and UEA reserves the right to take immediate ‘take down’ action on behalf of the copyright and/or rights holder if this Access condition of the UEA Digital Repository is breached. Any material in this database has been supplied on the understanding that it is copyright material and that no quotation from the material may be published without proper acknowledgement.

Table of Contents

Abbreviations

AGO- Argonaute
AGO-CLASH- AGO cross-linking, ligation, and sequencing of hybrids
BMP- Bone morphogenetic protein
CHARGE (syndrome)- Coloboma in the eye, Heart defects, Atresia of choanae, Retardation of growth/development, Genital abnormalities, and Ear abnormalities
cRNA- Capped RNA
crRNA- CRISPR RNA
CRISPs- Cysteine- rich secretory proteins
CRISPR- Clustered regularly interspaced short palindromic repeats
EMT- Epithelial-to-mesenchymal transition
FGF- Fibroblast growth factor
gDNA- Genomic DNA
GRN- Gene regulatory network
HDR- Homology directed repair
HG- Hatching gland
HITS-CLIP- High-throughput sequencing of RNA isolated by crosslinking immunoprecipitation
INDEL-Insertion deletion mutation
KD- Knockdown
KO- Knockout
LNA- Locked nucleic acid
miRNA(s)- microRNA(s)
MM- Mismatch
MO- Morpholino
mRNA- Messenger RNA
NC- Neural crest
NHEJ- Non-homologous end-joining
NPB- Neural plate border
PAM- Protospacer adjacent motif
PPE- Preplacodal ectoderm
PSED- Pax-Six-Eya-Dach
RA- Retinoic acid
RISC- RNA-induced silencing complex
sgRNA- single guide RNA
tracrRNA- Trans-activating CRISPR RNA
UTR- Untranslated region
Wnt- Wingless related

List of Figures

List of Tables

CHAPTER I

INTRODUCTION

1.0.0 Introduction

1.1.0 *Xenopus* as a model system

The *Xenopus* species are commonly used as a model organism for developmental biology research. *Xenopus laevis* and *tropicalis* are easily induced to lay large clutches of eggs on demand in the laboratory for research. These develop outside of the mother and can develop readily in salt solutions (Karpinka et al., 2015). *Xenopus* embryos are a great model system to experiment with, particularly for molecular manipulation, owing to the larger embryo size compared to Zebrafish embryos. *Xenopus* crucially is evolutionarily close to mammals (Liu, 2016; Sater and Moody, 2017).

Within the genus of *Xenopus* there are benefits to using different species, for different studies. For genetics-based studies it is optimal to use *Xenopus tropicalis*, due to its diploid genome. This contrasts with *Xenopus laevis* which has a tetraploid genome. Other advantages with using the *tropicalis,* is that it has a far shorter generation time. The *X. tropicalis* therefore makes a preferred model when making lines of experimental animals due to its diploid genome and short generation time(Grainger, 2012). In contrast *X. laevis* are good for dissection experiments like animal caps, due to their larger size (Ward et al., 2018). These reasons make *Xenopus* a good model to study neural crest (NC) and will be used in this project (Liu, 2016; Sater and Moody, 2017).

1.2.0 *Xenopus* development

Xenopus embryo staging of development has been documented by Nieuwkoop and Faber, hence the Xenopus development was named “NF” stages (Nieuwkoop, 1967). *Xenopus* eggs are easily fertilized in the lab by *in vitro* fertilization. *Xenopus* embryos can develop quickly with the rate of development dependent upon environmental temperature, a summary of the key stages of development can be seen in Fig.1.1. The embryo initially undergoes rapid cleavages without growing, before going through gastrulation and neurulation where the embryos will change shape and begin to grow and develop a nervous system before organogenesis and metamorphosis into a frog. *X. tropicalis*, can develop much more quickly than *X. laevis,* going through

to the metamorphosis stages within a month (Showell and Conlon, 2009; Wlizla et al., 2018).

Once a *Xenopus* embryo is fertilized, the embryo undergoes a series of dynamic morphological and physical changes (Fig.1.1). Initially, the *Xenopus* egg is a single cell that is split into a vegetal and animal pole. The vegetal pole contains all the necessary maternal proteins for sustenance of the embryo and the animal pole contains the maternal messenger RNAs (mRNA)s, (White and Heasman, 2008). Once the egg is fertilized, the embryo undergoes a process called cortical rotation. The entry point of the sperm will specify the pole of the embryo, with the opposing side of sperm entry becoming the dorsal side (Heasman, 2006). The cortical rotation shifts dorsalizing factors in the vegetal pole of the embryo 30^{o} (Vonica and Gumbiner, 2007). This leads to the activation of signalling pathways including canonical Wingless related (Wnt) signalling on the dorsal side of the embryo due to accumulation of beta-catenin. At this stage the embryo is undergoing rapid cleavages. Later after blastula development, the *Xenopus* organizer, the Spemann organizer forms at the dorsal lip (blastopore) at NF stage 8 (Ding et al., 2017; Nieuwkoop, 1969). The Spemann organizer is in the marginal zone and secretes growth factor antagonists: Dickkopf, Frzb1, Cerberus, Follistatin, Noggin and Chordin which lead to the induction of embryonic cell differentiation and the formation of a dorsal-ventral gradient for bone morphogenetic protein (BMP) signalling and activity (Moriyama and De Robertis, 2018). The embryo is now at a gastrula stage of development. By the gastrula stages of development, patterning of germ layers has begun (Ding et al., 2017; Nieuwkoop, 1969). During gastrulation the antero-posterior axis forms. The Spemann organizer has a significant role in the development of the head organizer, with Dickkopf-1 signalling enough to cause head induction alone, as shown in overexpression experiments (Glinka et al., 1998). During gastrulation the involuting endoderm and mesoderm move inwards and upwards towards the animal pole, giving rise to the antero-posterior axis. This lays the foundation for the formation of internal structures and organs laying down the body plan (Glinka et al., 1997; Heasman, 2006), (Fig. 1.1).

The embryo is now at neurula stage of development and will undergo neurulation. This phase, starting from NF stage 13, includes the development of the nervous system. This comes from the developing neural plate tissue, which is induced by BMP signalling gradients, generated by expression of BMP antagonists in the Spemann organizer (Glinka et al., 1998; Heasman, 2006; Moriyama and De Robertis, 2018). During neurula development the neural tube will be laid down in the embryo. The embryo will then begin to elongate and develop into a tadpole with organs growing and developing during metamorphosis before becoming an adult frog (Honore et al., 2003; Yaoita, 2019). These key stages of development are summarized in Fig 1.1, taken from (Wolpert and Tickle, 2011).

1.3.0 Neural plate border, placode, and neural crest development

1.3.1 Neural plate & neural border specification

The neural plate border (NPB), is situated between the non-neural ectoderm, and neural ectodermal region, which contains precursory neural crest (NC), neural tube and the pre-placodal ectoderm (PPE), (Betancur et al., 2010). The location of this tissue is shown in Fig. 1.2. Pax3 and Zic1 are transcription factors that are expressed within the NPB region in the developing *Xenopus* embryo and are thought to be involved in the specification of NC (Hong and Saint-Jeannet, 2017a). Pax3 is a key neural border specifier and is activated by fibroblast growth factor (FGF) and BMP signalling, which triggers *Hairy2* and *Msx1* to induce *Pax3* expression. Wnt, BMP and FGF gradients and signalling leads to induction of NC (Milet and Monsoro-Burq, 2012).

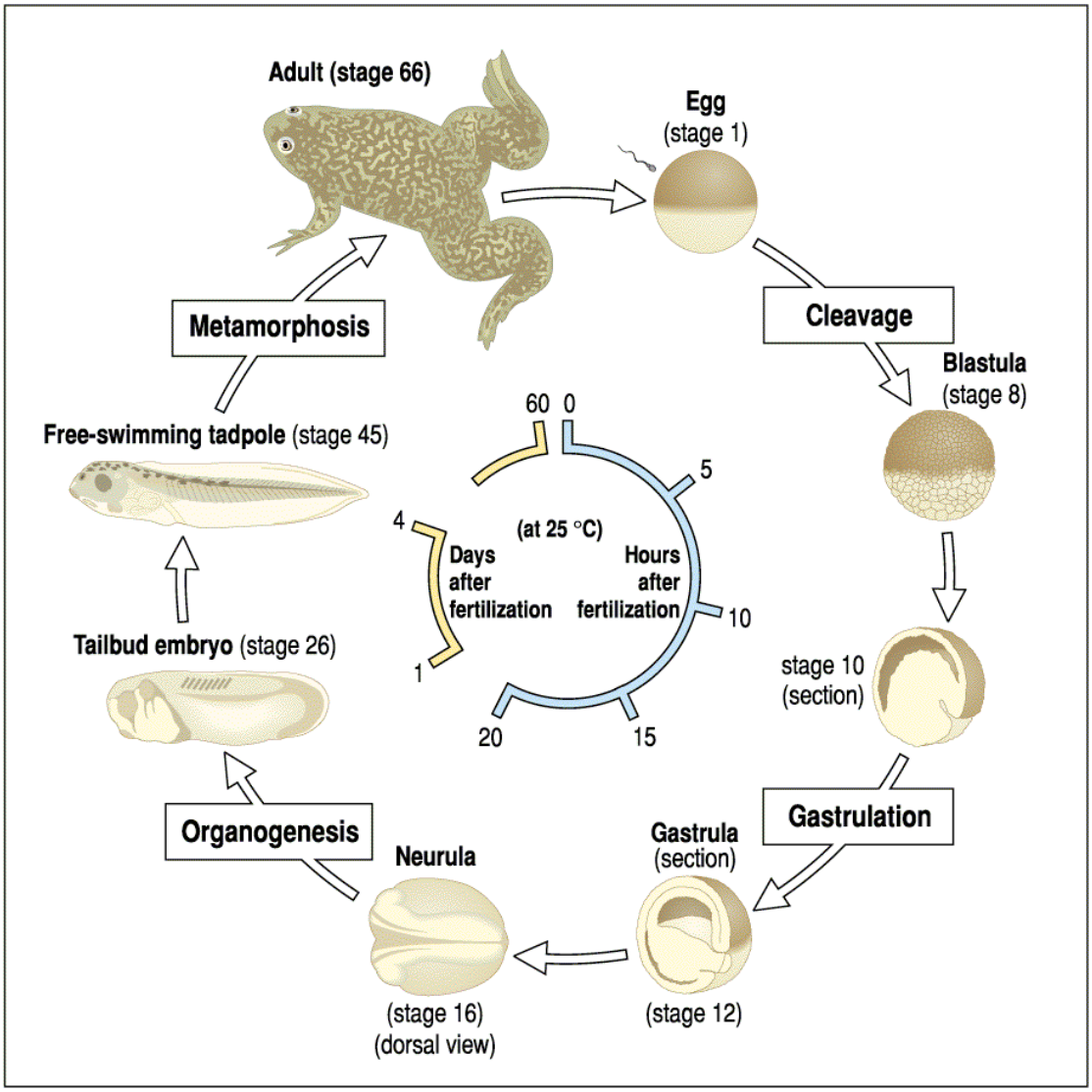

Figure 1.1- *Xenopus* life cycle and embryonic development from an unfertilized egg through to metamorphosis and a swimming frog. Taken from: (Wolpert and Tickle, 2011).

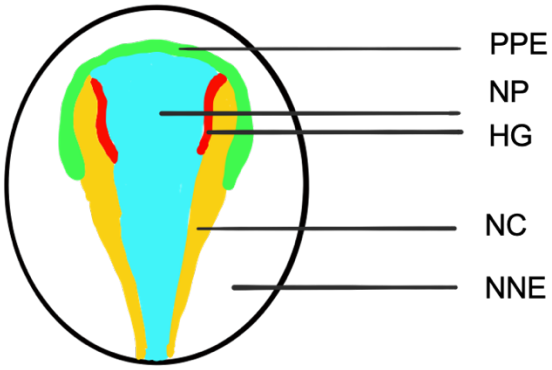

Figure 1.2- Location of embryonic tissues in Xenopus neurula development. Pre-placodal ectoderm (PPE) is located most anteriorly in a horse-shoe shape around the neural plate (NP). Lateral to the neural plate is the hatching gland (HG) in red, and neural crest (NC) in yellow. Most laterally is the non-neural ectoderm (NNE) in white. Figure based on information from (Hong and Saint-Jeannet, 2007) . Drawn by Alice Godden.

In the developing *Xenopus* embryo at gastrulation stage, the neural border region is surrounded by non-neural ectoderm neural plate and mesoderm (Hong et al., 2008). The neural border itself is induced by several signalling pathways. These include Wnt, FGF and BMP signalling, all co-operating in early ectodermal patterning (Borday et al., 2018; Hong and Saint-Jeannet, 2017b; Monsoro-Burq et al., 2005). BMP signals are released from neighbouring non-neural ectoderm and are antagonized by signals from the Spemann organizer. This forms a BMP gradient of activity in the ectoderm. In regions where BMP signalling is higher epidermal fates are promoted, however where BMP signalling is lower neural tissues are specified. Balanced and maintained BMP signalling is important for the specification of the neural border (Hong et al., 2008; Tribulo et al., 2003)

The neural plate, and neural border areas express transcription factors including Zic1. In areas with lower BMP signalling, neural plate and neural plate border markers Pax3 and Msx1 are attenuated; whereas in areas of higher BMP signalling Zic1, is upregulated. Expression of BMP antagonists and FGF signalling is also required in NB specification (Hong and Saint-Jeannet, 2007). Pax3 and Zic1 are critical in specification of the neural border. The development of the neural border involves a complex and much debated gene regulatory network (GRN), (Hong and Saint-Jeannet, 2017a), (Fig. 1.4).

FGF signalling can activate NB markers like *Pax3, Hes4, Ap2* and *Msx1*. FGF signalling between the paraxial mesoderm and ectoderm lead to development of NPB (Monsoro-Burq et al., 2005). Wnt signalling is expressed in the neural border, but it limited to more posterior regions. Early in *Xenopus* development Wnt signalling is also found in parts of the neural plate (Borday et al., 2018).

The neural plate gives rises to the neural tube. This happens through the formation of neural folds that rise either side of the midline and eventually meet and close to form a tube-shaped hollow structure (Fig. 1.5). The formation of the neural tube is significant in development as there are many life-threatening diseases associated with failure of closure of the neural tube, including spina bifida (Suzuki et al., 2010). The morphogenetic drivers behind formation and closure of the neural tube involved convergent extension and apical constriction to bend and constrict the neural plate into the correct position and shape. The bending is thought to be affected by the stiffness of the neural plate and myosin and cytoskeletal cellular organization (Rolo et al., 2009).

1.3.2 Placode development

In *Xenopus,* placodes are derived from ectoderm and are thicker specialized epidermis around the anterior neural plate (Fig. 1.2). Placodes give rise to sensory organs, there are many types of placode for all sensory organs, but not limited to: olfactory placode, profundal placode, and lens placode (Fig. 1.3). Interestingly, *Eya1* is expressed in all placodes, except lens placode. Another highly expressed gene in placodal regions is *Pax3*, which is also expressed in neural plate, ectoderm, and future NC (Hong and Saint-Jeannet, 2007; Plouhinec et al., 2017; Schlosser and Ahrens, 2004). Placodal development begins with the formation of PPE (Schlosser, 2014a). Ectoderm tissue can give rise to: placodes, epidermis, neural plate, and NC (Plouhinec et al., 2017).

PPE is a specialized ectodermal tissue that initially is induced in the neural plate border region in *Xenopus* neurulation. The PPE is a horseshoe shaped thick tissue located anteriorly and laterally to the neural plate (Watanabe et al.,

2018), (Fig. 1.2). Neural plate, NC and epidermis are specified alongside PPE (Schlosser, 2014b). PPE is where all cranial placodes arise from in the developing neural plate stage embryo (Fig. 1.3). For development of PPE from the neural border, BMP signalling needs to be inhibited (Watanabe et al., 2018). Key regulatory genes within this are thought to be the *Six* and *Eya* gene families (Schlosser and Ahrens, 2004).

Cranial placodes are ectodermal thickenings in the head of a vertebrate embryo at the NPB (Fig. 1.3). The *Pax-Six-Eya-Dach* network of genes has a role in placodal induction, with overlapping expression throughout embryonic development (Baker and Bronner-Fraser, 2001). High levels of the transcription factor Zic1 in *Xenopus* embryos can promote pre-placodal progenitors. This is significant in the context of NC development, as Zic1 can induce expression of Sox9 and Snail2 which are significant in the development and specification of NC (Betancur et al., 2010; Hong and Saint-Jeannet, 2017a).

1.3.3 Neural Crest

The NC is a vertebrate multipotent stem-cell population. The NC is located laterally to the neural plate (Fig 1.2). This population gives rise to many cell and tissue types such as derivatives of the peripheral nervous system, craniofacial skeleton, sensory ganglia, smooth muscle of major blood vessels (Betancur et al., 2010; Hatch et al., 2016). The NC has a complex GRN that has been much debated. Areas of the network require further research and clarification (Betancur et al., 2010), (Fig. 1.4).

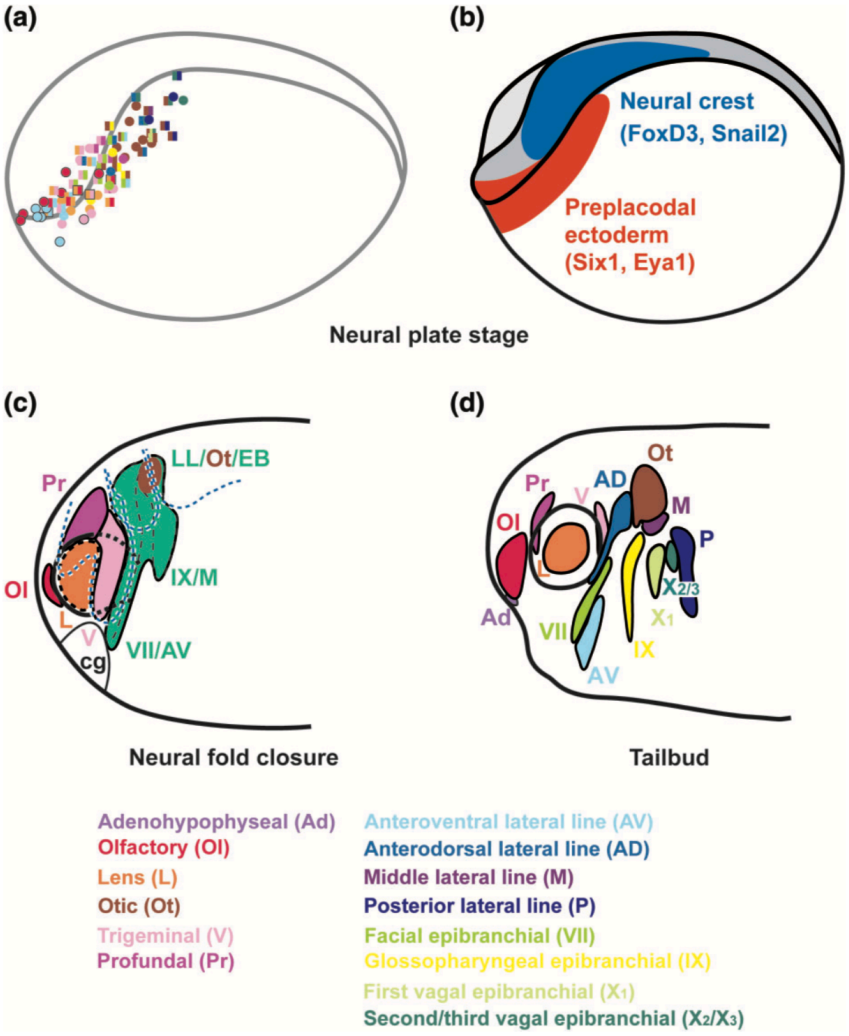

Figure 1.3- Cranial placode development and origins in Xenopus. A) Fate map of st.14 neural-plate stage embryo. B) Pre-placodal ectoderm and neural crest C) St.21 embryo, showing neural fold closure and all Lateral line (LL), otic (Ot), and epibranchial (EB) placodes will arise from a common posterior placodal area (LL/Ot/EB). Neural crest streams are shown as blue broken lines. (d) At tailbud stages (stage 27), placodes have become segregated. Colour code matches fate map in (a). Taken from (Schlosser, 2014b).

1.3.4 Neural Crest gene regulatory network

Many signalling molecules and transcription factors are implicated in the NC GRN and contribute to the fine control of NC development. The GRN can orchestrate and modulate the regulatory elements required for the NC to develop its diverse properties, including but not limited to cell migration and multipotency. The GRN starts with several signalling pathways: Wnts, BMPs, Notch and FGF signalling (Litsiou et al., 2005; Sauka-Spengler et al., 2007). These signalling pathways will induce the NC, (Fig. 1.4).

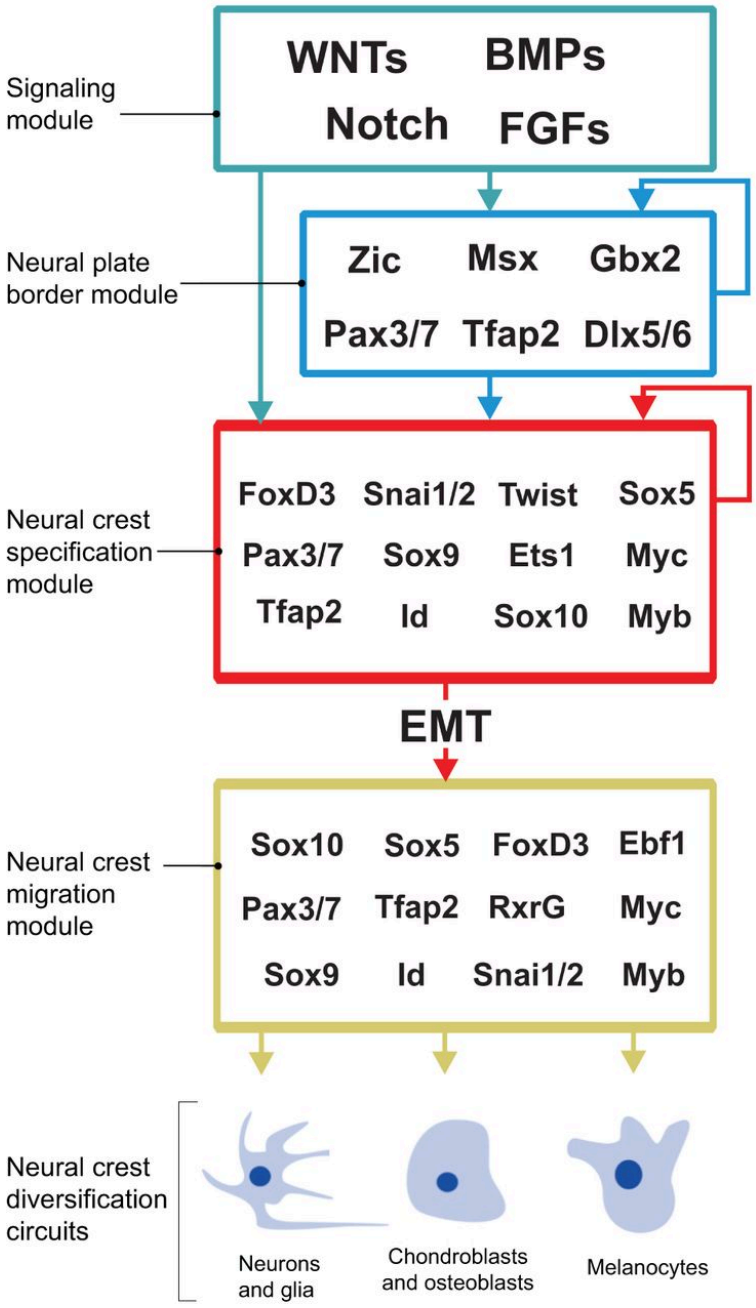

Figure 1.4- Neural crest gene regulatory network. Figure taken from: (Simoes-Costa and Bronner, 2015).

After the closure of the neural tube, the NC cells will then differentiate after migrating to their destination. Generation of a BMP dorsal-ventral gradient along the developing embryo allow for specification of the NC by lower levels of BMP than neural plate (Steventon et al., 2005; Steventon and Mayor, 2012).

BMP signalling is regulated by BMP antagonists Chordin and Noggin in the generation of NC. Through use of mutants, it has previously been found that Noggin has a more major role than Chordin, with Chordin having a degree of

redundancy in NC formation. This was because, in dorsal tissue where Noggin is lower in expression, BMP signaling was upregulated, and further upregulated when Chordin was also reduced in expression. A low level of BMP signalling is required in the development of NC, to allow for delamination of NC cells (Anderson et al., 2006).

Animal cap experiments revealed the role of signalling molecules in the development of NC with the generation of explants. Animal cap explants are generated through careful excision of a small square of animal pole tissue at the gastrula stage and are then cultured and left to develop to a neurula stage of development. To do this, embryos are injected with different mRNAs to generate different fated tissue. If embryos are injected with Pax3 and Zic1 mRNA, NC explants can be generated (Bang et al., 1999; Mayor et al., 1995; Milet and Monsoro-Burq, 2014).

A Wnt, FGF and BMP signalling gradient is established through the expression of BMP antagonists from the Spemann organizer in the medial plane, and in the anterior end of the embryo Wnt antagonists are enriched. These gradients lead to the patterning of neural plate and induction of NC (Marchant et al., 1998; Steventon et al., 2009). To induce NC, Wnt, FGF and retinoic acid (RA) signalling is essential and feeds into the NPB specifiers and transcriptional network including: *Msx, Ap2* (*tfap2a*), *Dlx, Zic, c-Myc* and *Hairy2* (Steventon et al., 2005; Steventon and Mayor, 2012). NC specification occurs during neurulation stages of development. Wnt signalling combined with the combination of expression of Pax3 and Zic1 leads to upregulation of NC specifiers like *Snail* and *FoxD3* (Aybar et al., 2003).

Signals that induce migratory NC emanate from the neural border region. For example, *Hairy2* has been shown to specify NC through promoting cell survival, migration and maintenance and activation of *Id3*; in turn promoting NC differentiation (Milet and Monsoro-Burq, 2012; Vega-Lopez et al., 2015). The NC becomes specified once the NPB is specified. The NC specifiers include the following transcription factors: Snail1, Snail2/Slug, Sox10, Sox9, Sox8, FoxD3 and C-myc (Hatch et al., 2016; Milet and Monsoro-Burq, 2012).

Before migration, the NC cells begin to proliferate and produce a pool of multipotent cells. Expression of *Myc* allows for proliferation and *Id3* for multipotency (Light et al., 2005). Proto-oncogene *c-myc* is expressed at the NPB region and is an early NC marker. In a morpholino (MO) knockdown (KD) experiment, loss of c-myc expression is correlated to loss of NC precursors, and increased expression of central nervous system progenitors (Bellmeyer et al., 2003; Light et al., 2005). *Id3* is a target of c-myc and is vital in maintaining a pool of NC cells. MO KD of *Id3* leads to a reduction in the formation of NC. This highlights how NC cells can maintain anti-apoptotic properties in their development (Light et al., 2005).

Overexpression of *Sox9* and *Snail* antiapoptotic markers, allow NC cells to avoid cell death and thus maintains a pool of pre-migratory multipotent NC cells (Cheung et al., 2005). *Sox9* has been shown to be upstream of *Snail2* and can induce *Snail2* expression (Sakai et al., 2006). If *Sox9* expression is absent, NC cells will undergo apoptosis in their migratory pathways. The co-expression of *Snail* and *Sox9* will then induce the NC cells to go through epithelial-to-mesenchymal transition (EMT), (Cheung et al., 2005). This can be seen in Fig. 1.5.

1.3.5 Neural Crest migration

Once the neural tube forms the NC cells will then delaminate, undergoing EMT, and will then proceed to migrate away from the neural tube to various destinations. NC cells can then migrate collectively, responding to external cues to gain directional and positional information. This information can be gained through cell-cell contact and interactions (Theveneau and Mayor, 2012). NC cells can be facilitated to undergo migration by expression of transcription factors such as *Snail* and *Twist*. Tissue stiffness also has been shown to have a role in collective NC cell migration. The mesodermal tissue that can becomes more rigid during convergent extension processes from gastrulation is thought to promote NC migration (Barriga et al., 2018).

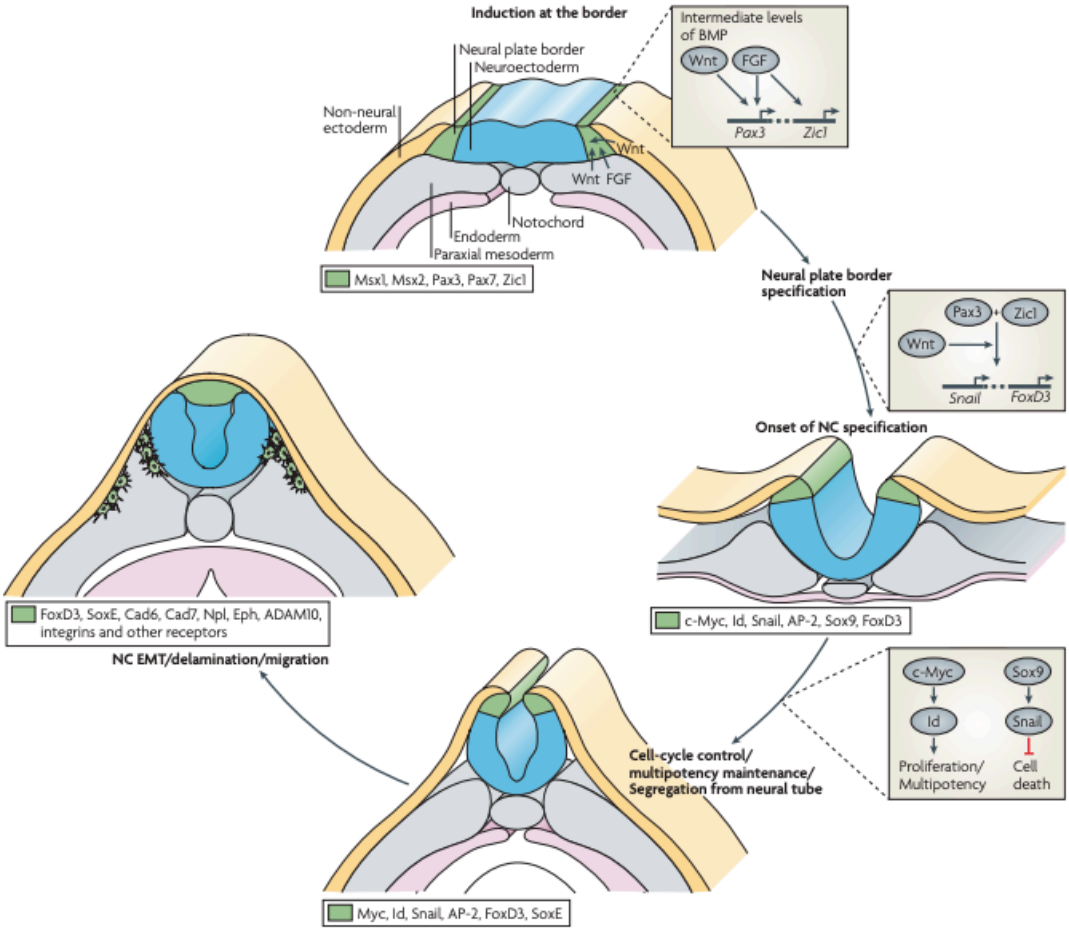

Figure 1.5- Induction and Specification of Xenopus neural crest. Taken from: (Sauka-Spengler and Bronner-Fraser, 2008).

NC cells migrate from the trunk NC in separate migratory streams (Hwang et al., 2009). NC delamination is the process where these streams form, when they migrate, they differentiate into different NC cell populations. Meanwhile the neural tube is beginning to close as shown in Fig. 1.5 (Aybar et al., 2003). Migration of NC is a good model for investigating collective cell migration and better understanding cancer cell invasion (Barriga et al., 2018). NC migration has similarities to cancer metastasis (Gonzalez Malagon et al., 2018; Gouignard et al., 2016).

1.3.6 Neural crest cell differentiation

The NC has the potential to differentiate into many different cell types and differentiated tissues. The NC can migrate substantial distances and become parts of the peripheral nervous system, neurons, pigment and much more

(Aoto et al., 2015; Cheung and Briscoe, 2003; Sauka-Spengler and Bronner-Fraser, 2008).

Sox genes have an impact on the specification of NC (Stanchina et al., 2006). Sox10 is a key NC marker and when combined with other signals can lead to different differentiation paths. This can be seen in Fig. 1.6, as Sox10 and MITF expression can lead to generation of melanocytes, whereas Sox10 and NGN1 can lead to generation of sensory neurons (Sauka-Spengler and Bronner-Fraser, 2008). *Sox10* can transcriptionally regulate key genes in melanogenesis such as *Dct (Dopachrome tautomerase)* and *Tyr* (tyrosinase). Sox10 expression leads to upregulation of master pigmentation gene *Mitf* and subsequently *Dct* and *Tyr* (Harris et al., 2010).

1.3.7 Cranial neural crest development

As mentioned, the NC population is multipotent. The cranial NC is a divergent population that gives rise to the key cranial structures such as: the cranial nerves, head mesenchyme and muscles, the jaw and skull (Cordero et al., 2011; Simoes-Costa and Bronner, 2015).

Cranial NC originates and migrates from the anterior neural tube (Gilmour et al., 2002). The transcription factor Sox9 is essential in cranial NC development in *Xenopus*. *Sox9* is implicated in chondrogenesis, so it is unsurprising it is involved in craniofacial development. In heterozygous *Sox9* mutants, severe craniofacial impairments were observed. Sox9 MO KD *Xenopus* tadpoles were shown by Alcian blue staining to have abnormal pharyngeal arches and deformed cranial skeletal elements (Spokony et al., 2002). The location of the branchial, mandibular and hyoid arches and overview of cranial neural crest populations are summarised in Fig. 1.7 (Baltzinger et al., 2005).

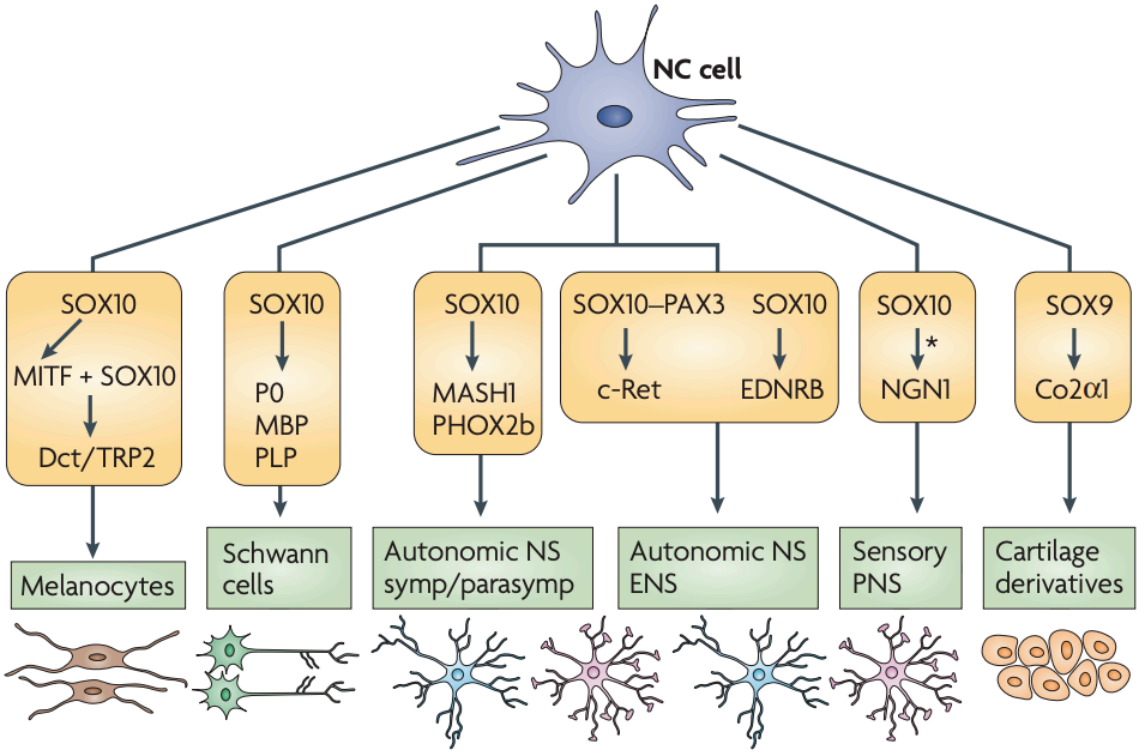

Figure 1.6- Sox expression and neural crest cell differentiation pathways. Figure taken from: (Sauka-Spengler and Bronner-Fraser, 2008).

FoxD3 is expressed in migratory cranial NC cells (Lukoseviciute et al., 2018). As NC cells become more specified, the level of FoxD3 expression reduces. In mouse FoxD3 mutants newborn mice exhibited cleft palates and faces. Without maintenance of FoxD3 cranial NC development is impaired (Teng et al., 2008).

Recent work has shown the potential importance of the *Ventx* network in NC migration. Ventx2 KD studies showed a reduction in cranial NC migration in the pharyngeal arches in tailbud *Xenopus* embryos. The report offers conclusions that Ventx/NANOG network could be implicated in development of cranial tissues (Scerbo and Monsoro-Burq, 2020).

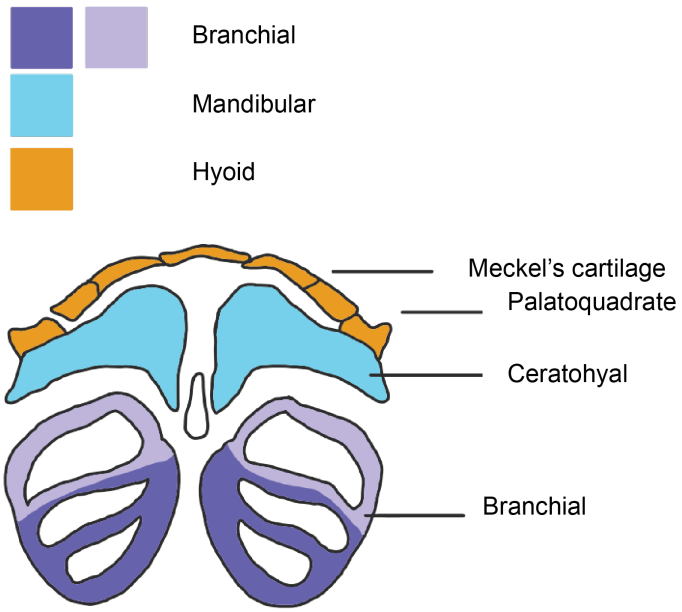

Figure 1.7- Xenopus cranial neural crest in craniofacial development. Based on information from (Baltzinger et al., 2005) Drawn by Alice Godden.

Cranial NC cells initially migrate in sheets of cells. Cranial NC cells can be explanted in embryo experiments due to their cohesive nature. This is evidenced by a leading edge and a trailing edge in migration (Alfandari et al., 2010). A summary of cranial NC migratory streams in chick and *Xenopus* can be seen in Fig. 1.8.

1.3.8 Cardiac, trunk, vagal and sacral neural crest populations

Posterior to the cranial NC, other NC derivatives include the trunk, sacral, vagal, and cardiac NC. The cardiac NC contributes to the development of the outflow tract of the heart in amniotes. In *Xenopus* the cardiac NC reside in the aortic sac and arch arteries. Genes important for cardiac NC development include Ets-1; which is embryonic lethal in knockout (KO) mice (Gao et al., 2010).

The trunk NC gives rises to pigment forming cells and parts of the peripheral nervous system (Collazo et al., 1993). These NC cells migrate along the dorsal side of the embryo through the somites and give rise to pigment producing cells. Trunk NC cells also give rise to adrenal chromaffin cells, and parts of the

peripheral nervous system (Klymkowsky et al., 2010). Vagal crest and sacral NC combine and together can give rise to parts of the enteric nervous system. They also contribute to parts of the heart and gut tracts (Burns and Douarin, 1998).

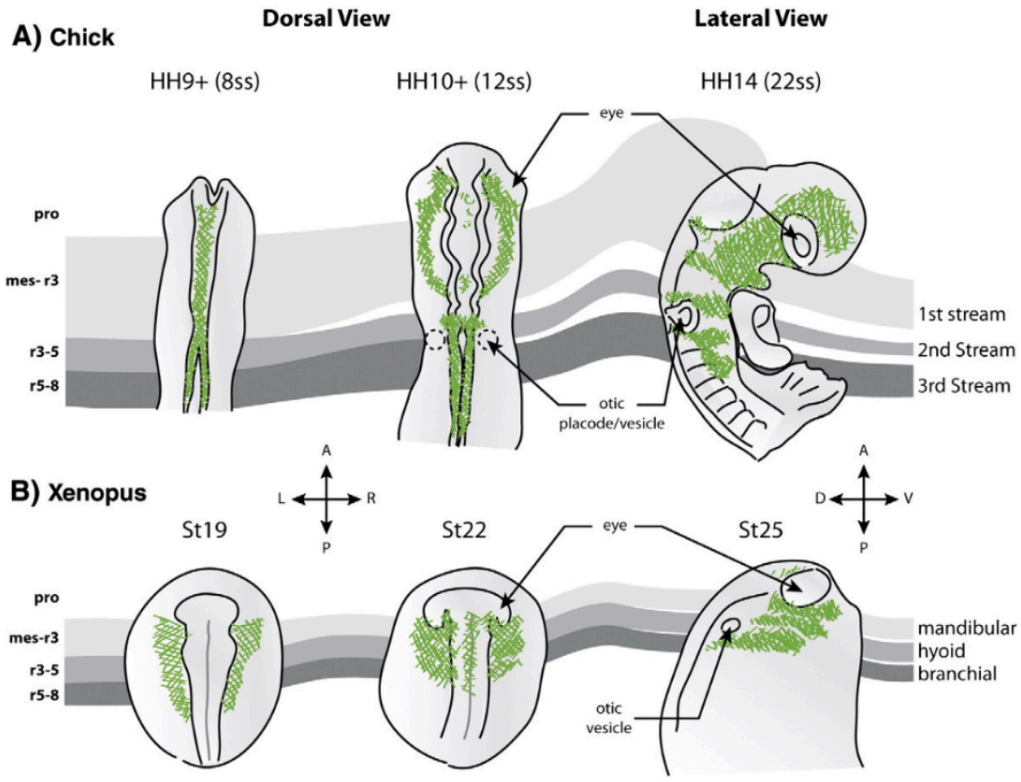

Figure 1.8- Early migration of cephalic neural crest cells. A) Migration of chick cephalic NC cells. B) Migration of Xenopus cephalic NC cells. Abbreviations mes, mesencephalon; pro, proencephalon; r, rhombomere; ss, somites. Nieuwkoop and Faber stages of Xenopus embryos. Figure taken from: (Theveneau and Mayor, 2012).

1.3.9 Hatching gland

There are three distinct cell populations that arise at the NPB in *Xenopus*: the NC, the PPE, and the hatching gland (HG). The HG is situated in the superficial ectoderm of the anterior neural folds and expresses the hatching enzyme, *Xhe.* The gene *Pax3* is also expressed in HG and its progenitors (Hong and Saint-Jeannet, 2007). The HG in *Xenopus* produces proteolytic enzymes to digest the surrounding vitelline membrane around the developing embryo. The HG cells are ectodermal-derived. Likewise with NC, HG needs Wnt and BMP signalling for induction. It is likely that HG development is induced by upstream events and specifiers in NPB development (Kurauchi et al., 2010).

One of the first reports on *Xenopus* HG, showed that *Xhe* is exclusively expressed in the HG and by HG cells. The enzyme is 425 amino acids long. The proteolytic part is only 200 amino acids long and is derived from the astacin family (Katagiri et al., 1997). Cysteine-rich secretory proteins (CRISPs) are a homologue of the mammalian family of CRISPs, in *Xenopus* they are expressed exclusively in the HG. These proteins are highly conserved in vertebrates and were first identified in mice. Overexpression of XCRISP leads to early hatching events, signifying a potential key role of CRISPs in HG development (Schambony et al., 2003).

1.3.10 Neurocristopathies

Neurocristopathies are developmental congenital disorders where there is aberrant NC migration, specification, or differentiation (Gouignard et al., 2016; Ward et al., 2018). Neurocristopathies also include some cancers such as neuroblastoma and melanoma, DiGeorge syndrome and cranio-fronto-nasal dysplasia (Gouignard et al., 2016; Ward et al., 2018).

Recklinghausen disease affects Schwann cells and melanocytes to produce tumours, neurofibromas. It is one of the most common neurocristopathies, affecting up to 1: 2,000 live births (Etchevers et al., 2006). Hirschsprung's disease is a neurocristopathy and is one of the most common intestinal inborn defects in new-borns, with 1 in 5,000 new-borns affected in the UK and Ireland alone; affecting males at a 3:1 ratio versus females (Bradnock et al., 2017; Heanue and Pachnis, 2007). Many patients present with melanocyte deficiencies. In a mouse model of Hirschsprung's disease, mice with *Sox10* mutations have an absence of NC due to NC cell death (Southard-Smith et al., 1998). More critical to the survival of new born babies, in Hisrchsprung's the enteric nervous system is not innervated which can be fatal if not identified quickly (Heanue and Pachnis, 2007).

Defects in the development of the cardiac NC population results in congenital heart diseases. This is through the lack of development of the cardiac outflow tract (Gao et al., 2010). Examples of cardiac NC diseases includes CHARGE

(Coloboma in the eye, Heart defects, Atresia of choanae, Retardation of growth/development, Genital abnormalities, and Ear abnormalities) syndrome which can affect both cranial and cardiac NC derivatives. The extent to which an individual patient suffers and presents with these abnormalities varies significantly. The molecular mechanisms driving progression of CHARGE syndrome involve homozygous mutations in the gene *CHD7.* Chromatin remodelling is thought to be the driver of CHARGE syndrome, as CHD7 regulated nucleosome positioning within enhancer rich regions (Berube-Simard and Pilon, 2019). Further molecular analysis of *CHD7* mutations and the impact on the carboxyterminal of CHD7 may uncover treatment for this neurocristopathy (Vuorela et al., 2007).

Treacher Collin's is a rare syndrome that affects 1: 50,000 live births (Avery and Dalton, 2016). Treacher Collin's is an inborn neurocristopathy affecting craniofacial development. It is caused by mutations in *TCOF1* gene which produces the protein Treacle. If one copy of the *TCOF1* gene is mutated there is insufficient ribosome production. Symptoms of Treacher Collin's include: hearing loss, cleft palate, and abnormal ear development. The molecular mechanism behind Treacher Collin's is thought to be neuroepithelial apoptosis and reduced expression of NC cells. Possible treatments to alleviate Treacher Collins involve targeting p53 function to modulate NC apoptosis levels (Jones et al., 2008). The molecular mechanisms of many neurocristopathies are not fully understood, therefore it is critical to establish the development of these diseases, and what role microRNAs (miRNAs) may play, as this could lead to therapeutic interventions.

1.4.0 miRNAs

MiRNAs are short non-coding, single stranded RNAs, approximately 20-22 nucleotides in length (Alberti and Cochella, 2017; Lee et al., 1993; Shah et al., 2017). It took many years for these short RNA oligos to be recognised, beginning with transcripts from the gene *lin-4* (Ruvkun et al., 2004). This was the discovery of small RNAs that had antisense complementarity to *lin-14*. These small RNAs were shown to bind to 3' untranslated region (UTR) in *lin-*

14 mRNA in *C. elegans,* regulating larval development (Lee et al., 1993). After being first discovered in *C. elegans*, miRNAs have since been identified in plants and animals (Alberti and Cochella, 2017; Lee et al., 1993; Mok et al., 2017). MiRNAs have also been implicated in development and disease, most predominantly cancer. MiRNAs are also reportedly involved in tissue pluripotency, regulating multipotent states and differentiation (Ambros, 2011). Notably, complete absence of miRNAs results in embryonic lethality, thus demonstrating the crucial importance of miRNAs in embryonic development (Alberti and Cochella, 2017).

1.4.1 MiRNA biogenesis and mechanism of action

MiRNAs are highly conserved and abundant between species with many orthologues discovered (Bartel, 2004). MiRNAs can be produced from independent genes and can also be encoded in intronic regions of the genome (Olena and Patton, 2010). Currently on miRbase, a miRNA database and repository; there are 2,656 mature miRNA sequences. It is thought that there are 2,300 or more different miRNAs in humans alone (Alles et al., 2019). Recent reports suggest that 60% of all protein coding genes in mammals are regulated by one, or more, miRNAs (Li et al., 2018). Within the human genome it is estimated that up to 2% of genes encode for miRNAs (Miska, 2005).

MiRNAs in plants and animals are both transcribed from the genome to produce precursor molecules that undergo cleavage. The key difference in biogenesis of plant and animal miRNAs, is that animal miRNAs are cleaved by Drosha and Dicer, but in plants it is *DCL1* and helicase in the cell nucleus that are involved in mature miRNA biogenesis. Another key difference is how they exert their effect. Plant miRNAs regulate gene expression through targeting cleavage of mRNAs in single sites (Millar and Waterhouse, 2005).

In animals, miRNAs impact gene expression through post-transcriptional silencing of genes. MiRNAs are recruited to the RNA-induced silencing complex (RISC) bound to an argonaute (AGO) protein (Agarwal et al., 2015; Shah et al., 2017). The region of the miRNA that is complementary to the 3’

UTR is known as the seed region (Agarwal et al., 2015). A summary of the mechanism of action and biogenesis of miRNAs in animals shown in Fig. 1.9, (Inui et al., 2010), and consists of these main stages of processing:

1. Transcription of the pri-miRNA by RNA Pol II
2. DROSHA processing of the pri-miRNA to form a hairpin precursor structure
3. Export of the hairpin by exportin-5 complex into the cell cytoplasm from the nucleus
4. Dicer cleaves the now pre-miRNA structure, producing a mature miRNA
5. AGO complex formation and binding of the miRNA through 5' seed sequence complementarity to a complementary 3' UTR
6. Alterations in gene expression through mRNA cleavage, translational repression, or mRNA de-adenylation

(Agarwal et al., 2015; Alberti and Cochella, 2017; Bartel, 2004; Inui et al., 2010).

1.4.2 MiRNA-mRNA binding, 3'UTRs and seed region binding

MiRNAs post transcriptionally regulate gene expression through complementary miRNA-mRNA seed region binding of the miRNA to the mRNA's 3' UTR (Witkos et al., 2011). If the miRNA and target bind in perfect hybridization this leads to cleavage of the target mRNA. If the hybridization is imperfect, it is more likely that the target will be blocked from being translated rather than degraded (Kruger and Rehmsmeier, 2006). See Fig. 1.10 for overview of miRNA-mRNA binding and interactions.

Prediction of miRNA-mRNA binding is challenging. There are many online tools, algorithms and bioinformatical resources to help predict miRNA-mRNA interactions and predict miRNA targets. These include databases: Tarbase, MiRecords, Targetscan, PicTar and DIANA (Witkos et al., 2011). These tools provide a shortlist of candidate miRNAs and mRNAs for the researcher to analyse further. This can save much time, however they still all need to be

experimentally validated and tested in systems to be of any use. Experimental validation techniques of miRNA-mRNA interactions include the luciferase assay (Witkos et al., 2011; Wong and Wang, 2015). Other techniques for identification miRNA-mRNA interaction and locations include AGO High-throughput sequencing of RNA isolated by crosslinking immunoprecipitation (HITS-CLIP). This method enables the user to analyse miRNA-mRNA interactions in the cell cytoplasm and nucleus (Zhang et al., 2019). Similar methods include AGO cross-linking, ligation, and sequencing of hybrids (AGO-CLASH). This looks at RNA-RNA interactions by sequencing of crosslinked and ligated hybrids. CLASH is advantageous as it can map miRNA binding sites and detect chimeras (Helwak et al., 2013).

1.4.3 MiRNAs in development

MiRNAs have been found to be implicated in development of vertebrate tissues, including: chick, mouse, frog and fish (Mok et al., 2017; Ward et al., 2018); as well as invertebrates like the worm and fruit fly (Chandra et al., 2017).

A group of miRNAs termed myomiRs are implicated in muscle development, having important roles in cell fate specification. The same myomiRs, miR-133, -1 and -206 have been linked to somite differentiation in chicken embryos (Goljanek-Whysall et al., 2014). These miRNAs have also been found in mouse and human. MiR-1 and miR-206 in chick and miR-27b in mouse have a role in a negatively regulating *Pax3* expression in muscle progenitors (Goljanek-Whysall et al., 2014; Mok et al., 2017).

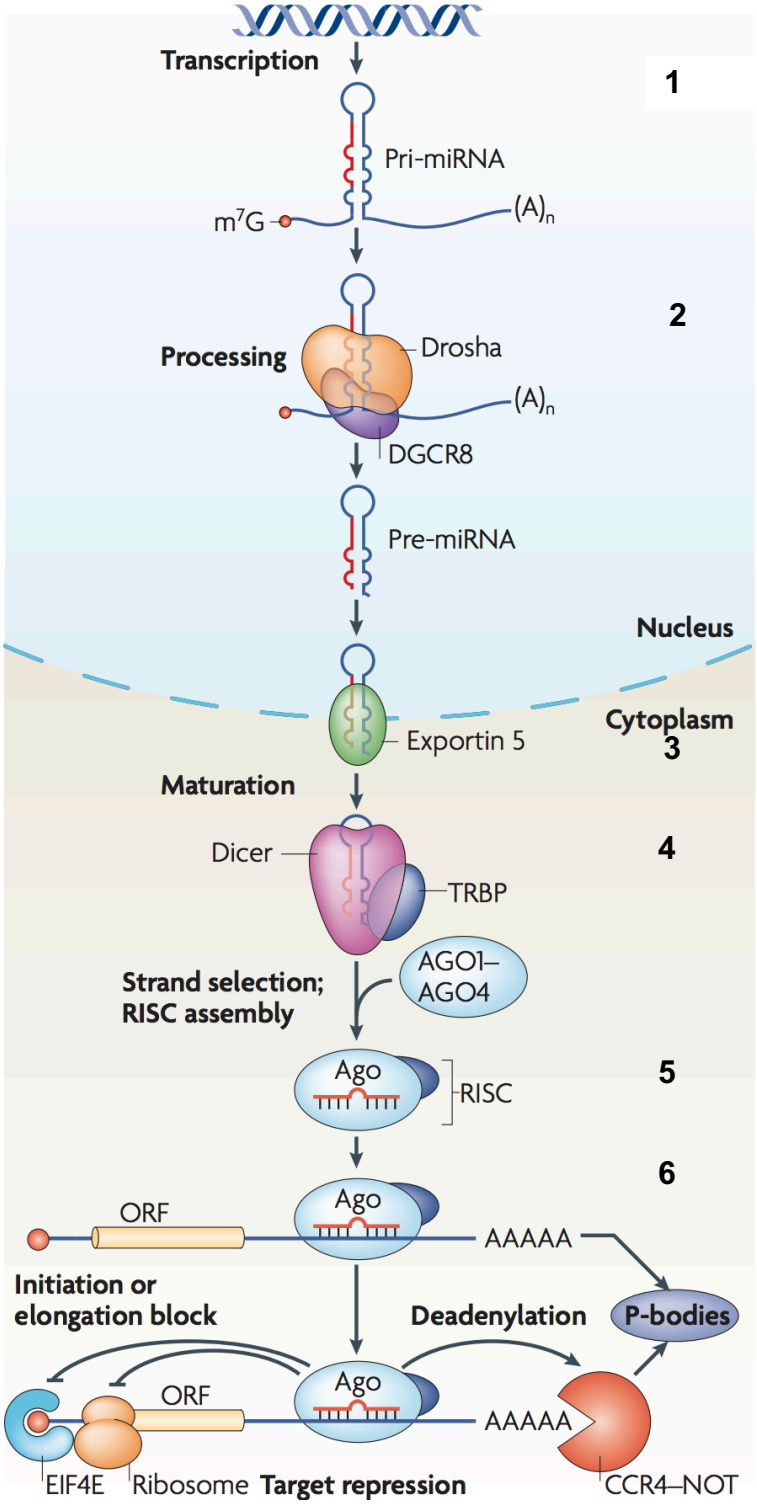

Figure 1.9- miRNA biogenesis and action pathway showing transcription, processing, maturation, and gene silencing and repression mechanisms. Taken from (Inui et al., 2010).

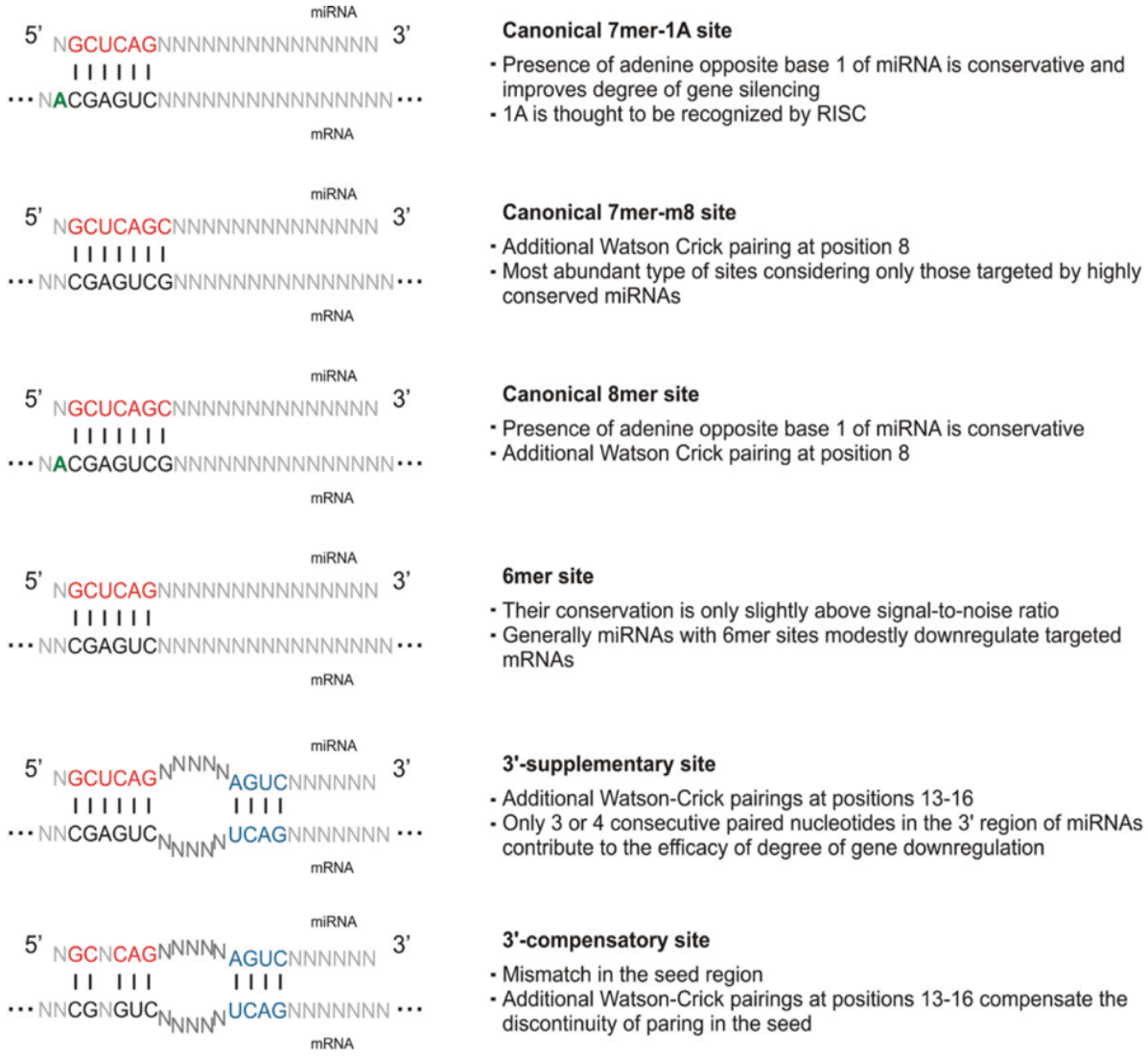

Figure 1.10- miRNA-mRNA interactions and binding. Figure taken from (Witkos et al., 2011).

MiRNAs have also been found to have a role in the developing chick heart. qPCR data shows distinct expression of miRNAs in the ventricular and atrial regions of the developing chicken heart. Notably during chamber formation at Hamilton and Hamburger (HH) stage 14 chicken embryo the septum develops toward the endocardial cushions in the atrioventricular canal. It has been reported that miR-15a, -23b and -199a are upregulated during the atrioventricular canal formation (Wittig and Munsterberg, 2016). In support of this, miR-130 has also been found to have a role in cardiac specification by regulating an FGF8 BMP-2 negative feedback loop in chick gastrulation (Lopez-Sanchez et al., 2015). Blood specific miRNA, miR-451 is a highly conserved vertebrate miRNA. It is involved in the maturation of erythrocytes. miR-451 in Zebrafish and links up with miR-144 in a negative feedback loop

during erythropoiesis. This works by miR-144 repressing Dicer processing of pre-miRNAs and allows for AGO-2 dependent processing for miR-451 (Kretov et al., 2020).

MiRNAs are expressed in a vast range of developing tissues. Interestingly, there is a sex-determined bias in the development of *Drosophila*, in the expression of miRNAs. The intronic miR-995 is involved in cellular proliferation and is conserved among other insects and has a 3.4-fold change in expression in female *Drosophila* over males. This highlights an interesting role of miRNAs in in gametes (Marco, 2014). There are thought to be 129 genes with the GO term “developmental process” in *Drosophila*. The most prominent family of miRNAs implicated in this was miR-2, and its products are thought to target neural genes and neural development (Marco et al., 2012).

Following on the theme of neural development, a miRNA array revealed a number of miRNAs in mouse brain development where miR-9 and miR-131 were found to be important (Krichevsky et al., 2003). In support of this, a more recent review found that miR-9 has three identical mature miRNA transcripts, and when knocked out completely, a reduction in neurogenesis was observed (Petri et al., 2014). Brain-specific miR-134 was found to regulate dendritic spine development in rat hippocampus neurons and inhibits the translation of the mRNA for *Limk1*. Experiments to reduce the inhibition of Limk1 by miR-134 through extracellular stimulus highlight how miR-134 may be linked to synaptic development (Schratt et al., 2006).

MiR-199 is implicated in chick embryonic craniofacial development. MiR-199 is one of a family of miRNAs involved in Sonic Hedgehog signalling. MiR-199 is involved in the formation of the jaw in chick embryos, relying on Sonic Hedgehog signalling from the brain. KD of miR-199 in chick embryos led to wider faces, and upregulation led to the development of narrower faces (Richbourg et al., 2020)

Overall, the evidence highlights how miRNAs are imperative in many organisms in the fine-tuning and cell-specification in many developmental

processes and suggests unknown and potential roles in many molecular processes.

1.4.4 MiRNAs in Xenopus development

In comprehensive publications, the Harland and Wheeler labs showed the expression of miRNAs in *Xenopus* embryonic development (Ahmed et al., 2015; Walker and Harland, 2008).

Harland and Walker's expression paper showed development of *in situ* hybridisation probes designed to target the primary miRNA transcript. The group produced 60 antisense probes against miRNAs, of these 42 failed to give a result, but as the authors mention this could be due to the processing and turnover of the miRNAs (Walker and Harland, 2008).

Of the miRNAs tested miR-1a-1, miR-7-2, miR-9a-1, miR-9a-2, miR-9-3, mi-10c, miR-18a, miR23b, miR-24a, miR-96, miR-98, miR-124, miR-130a, miR-133b, miR-181a-2, miR-219 and miR-429 had an expression pattern at the neurula and tadpole stages. Of these, notably miR-9 was found in neuronal progenitors, and supports other mouse work as mentioned above, highlighted a conserved role of miR-9 (Krichevsky et al., 2003; Petri et al., 2014; Walker and Harland, 2008).

In *Xenopus* muscle development the vertebrate specific miRNA, miR-206 was shown to be regulating somite morphogenesis by maintaining changes in cell adhesion properties. The impact was shown through KD experiments through morpholino injected *Xenopus* embryos. It was found that KD of miR-206 disrupted the formation of actin filaments, and thus affected muscle morphogenesis (Sweetman et al., 2006; Vergara et al., 2018). The first reported images of a miRNA in a developing *Xenopus* embryo were first seen in embryos generated by the lab (Sweetman et al., 2006).

MiRNA expression in the developing *Xenopus laevis* has been documented within the Wheeler lab, providing a database of expression patterns of 179

miRNAs tested, using LNA oligonucleotide probes, see Table 1.1 below (Ahmed et al., 2015). An online catalogue of the expression profiles can be accessed on Xenbase by the following link http://www.xenbase.org/geneExpression/static/miRNA/body/mirTable.jsp.

Table 1.1- Expression pattern of miRNA in Xenopus. Shows expression in a range of developing organs, based on data from (Ahmed et al., 2015).

miRNA	Expression
34b	Pancreas
128	Brain
107	Gut
122	Liver
126	Blood vessels
200a	Olfactory placodes
455	Liver
30d	Brain
100	Brain
96	Brain & Olfactory placodes

The work of Ahmed and colleagues also looked to profile miRNA expression at different stages of *Xenopus* embryo development by using sequencing miRNAs. A time course of stages was analysed, from blastula, gastrula, neurula, tailbud, tadpole and late tadpole were analysed. From this, five novel miRNAs were discovered, miR-GNW8, miR-GNW9, miR-GNW11, miR-GNW12, miR-GNW13. These were highly expressed from gastrula stage of development onwards in dorsal, mesodermal and neuroectoderm structures. Expression at the later stages of development can be seen in the anterior structures such as the branchial arches and parts of the trunk of the tadpoles. Overall, the expression profile of 179 miRNAs in *X. laevis* were characterised and discussed with individual expression profiles and patterns (Ahmed et al., 2015).

In addition to this work, a further 125 unidentified miRNAs were found in a next-generation sequencing experiment in *Xenopus* (Shah et al., 2017). This demonstrates a role for miRNAs in development of tissues and organs. In

recently published small RNA sequencing data NC and ectodermal explants were analysed for miRNA expression profiles. This was done using high-definition adapters and next generation sequencing of libraries. By using explants, it was possible to analyse miRNA expression in blastula, neural, ectoderm and NC tissue. This made it possible to identify NC uniquely expressed miRNAs (Ward et al., 2018).

MiRNAs miR-338 and miR-301a were found to be expressed in all explants. They were most enriched in blastula and NC tissue. It was suggested that these miRNAs may be involved in maintenance of stemness in NC cell populations (Ward et al., 2018). 11 miRNAs were found significantly highly expressed in the NC compared to all other tissues analysed. This included: miR-196a, miR-130b/c, miR-17, miR-20b, miR-196a, miR-10b and miR-219 (Ward et al., 2018).

During this project, other researchers have helped show that clustered regularly interspaced short palindromic repeats- Cas9 (CRISPR-Cas9), is a valid approach to study and KO miRNAs (Kretov et al., 2020). There has also been the production of CRISPR resources for Drosophila, so this helps the development of miRNA CRISPR in flies (Bassett and Liu, 2014). More recently single guide RNAs (sgRNA)s were individually used to repress miRNA activity and expression by up to 96% (Chang et al., 2016). At the time of writing, CRISPR-Cas9 had not yet been used to KO a miRNA in *Xenopus* species. This gap in methodology will be filled during the thesis. This gap hopes to be filled through production of a miRNA KO line of *Xenopus*. This would circumvent complex technological development of AGO-CLASH (cross-linking, ligation, and sequencing of hybrids) and serve as a tool for more complex molecular analysis.

1.4.5 MiRNAs and miR-196a and miR-219 in disease

MiRNAs have widely been implicated in many diseases, particularly cancers. MiRNAs have been implicated in development and pathogenesis of Alzheimer's disease (Wang et al., 2019).

miR-196a in disease

Unsurprisingly, miRNAs, particularly miR-196a has been implicated in numerous cancers. A recent report showed that miR-196a-5p targets IκBα by luciferase assays. Upregulation of miR-196a-5p by overexpression in colorectal cancer cell lines promoted migration of colorectal cancer cells by EMT and pathogenesis of colorectal cancer (Xin et al., 2019). In addition to cancers, miR-196a holds potential as a biomarker in prediction of progression of chronic kidney disease in patients. In a recent study it was found that those with kidney disease had marked increases in levels of miR-196a in their urine (Zhang et al., 2018).

miR-219 in disease

The candidate miRNAs for this project have been implicated in many diseases. miR-219 has been found to be down-regulated in the brain tissue of autopsied Alzheimer's disease patients. It was thought that this reduction in miR-219 could explain the increased toxicity of Tau proteins in the progression of the disease (Santa-Maria et al., 2015). In cancer miR-219 has been likened to a tumour suppressor. With a recent study in metastatic ovarian cancer cells overexpression of miR-219-5p led to a reduction in cell proliferation, invasion, and migration (Xing et al., 2018).

There is limited research in miRNAs in *Xenopus* NC development. Only limited papers have been listed on Pubmed that cover this research topic. An older report looked at our candidate miRNA, miR-196a in *X. laevis* eye development. The study used an LNA *in situ* hybridisation probe to visualise and track miR-196a expression in developing *Xenopus* embryos. The study also utilised an antisense oligonucleotide designed against the mature miRNA sequence of miR-196a to analyse and predict expression of miR-196a on eye development. Using bioinformatic miRNA target prediction tools like RNAhybrid it was found that miR-196a in *X. laevis* targets eye development genes like Pax6 (Qiu et al., 2009). Despite this work there lies a huge gap in understanding miRNAs in *Xenopus* NC development. Therefore, there lies many unanswered questions in this area. Previous research in the Wheeler

lab has identified candidate miRNAs for follow up in NC development (Ward et al., 2018). This forms the basis of studying miR-196a and miR-219 in more detail in this research project and report.

1.5.0 Rationale, Aim & Objectives

The rationale of this project was based on a set of pilot data from a previous student who investigated miRNAs in NC development more broadly (Ward, 2017). This generated a lot of data, and in particular RNA-seq data. The main objective of the project was to focus in on the role of miR-196a and miR-219 in the molecular development of NC. By discovering and contributing to the molecular understanding of the development of NC, it could be hoped that more will be understood in the development of neurocristopathies, developmental disorders and cancer. From this the following rationale, hypotheses and aims were set out.

Hypotheses

It was hypothesised that miR-196a and miR-219 are important in initial cell fate choices setting up induction and specification of NC. Furthermore, miR-196a and miR-219 are predicted to target and have impact genes and gene expression involved in NC and placodal specification.

Rationale and Aims

We have previously shown that miR-196a and miR-219 are almost exclusively expressed in *Xenopus* developing NC through small RNA-sequencing. It would be predicted that these miRNAs are expressed in NC tissue, through whole mount *in situ* hybridisation to reveal spatial and temporal miRNA expression in the developing *Xenopus* embryo.

When this project was started, and still at time of writing, there was no published method to KO a miRNA with CRISPR-Cas9 in *Xenopus*. Therefore, methodology needed to be developed to KO miRNAs and begin to generate viable miRNA KO lines of *X. tropicalis.* Alongside this, miRNAs were knocked down with morpholino experiments, and impact on NC, NPB, placodal and HG development was be assayed

CHAPTER II

MATERIALS & METHODS

2.0.0 Methods

2.1.0 *Xenopus* husbandry

Personal licensing from the Home Office was attained to conduct this PhD research. Ethical guidelines of the University of East Anglia and Home Office rules were strictly adhered to. Female *X. laevis* were primed approximately 5 days before embryos were requires. Priming is a 100 unit (U) injection of Pregnant mare serum gonadotropin (PMSG, Intervet, 1,000 U/ mL) into one dorsal lymph sac. A further two injections, into both dorsal lymph sacs of human chorionic gonadotrophin (hCG, Chorulon, Intervet, 1,000 U/ mL) was conducted the afternoon before oocytes were required, this is inducing. For *X. tropicalis,* frogs were primed with 10 U/Chorulon 24-72 hours before inducing. Females were induced with 200-250 U/Chorulon.

To fertilize the *Xenopus* oocytes, a male is anaesthetised in 1g MS-222 in 300 mL of water. The male is then dissected, and schedule 1 euthanasia is completed by dislocation of the neck and destruction and or removal of the heart. The testes were then removed and stored in testes buffer (80% fetal calf serum, 20% 1X MMR, gentamycin (Sigma 1:1000U).

To obtain oocytes, the female is “milked/squeezed”, by gentle squeezing the abdomen, applying pressure to release oocytes into a petri dish. A piece of testes is homogenized in 1 mL of 1 x MMR (100 mM NaCl, 2mM KCl, 1mM $MgCl_2$, 2 mM $CaCl_2$, 5mM HEPES p.H 7.5), and pipetted over the clutch of eggs, left for 5 mins. All washes are carried out at 18°C. 0.1 X MMR (10 mM NaCl, 2mM KCl, 1mM $MgCl_2$, 2 mM $CaCl_2$, 5mM HEPES p.H 7.5), is then applied to the embryos and left for 20 mins, before de-jellying the embryos with 2% L-cysteine in 1 X MMR p.H 7.8-8.0. Embryos are carefully mixed in the solution to help remove jelly. A further two washes of 1 X MMR and two washes of 0.1 X MMR are carried out before plating embryos on bovine serum albumin (BSA) coated plates. Embryos are then left in the appropriate temperature incubator to reach the desired embryonic stage in accordance with Niewkoop and Faber, 1967 *X. laevis* normal table of development (Nieuwkoop, 1967).

2.2.0 Injecting embryos with Morpholinos

MO stocks are kept at room temperature, if aliquots are frozen, they must be warmed up to 65 °C for 10 minutes and then kept on ice before use. Sequences of MOs are listed in Table 2.1. Embryos were injected at the desired stage with 60 ng/ 10nL of MO with 5 ng of GFP capped RNA (See Table 2 for MO sequence data). Embryos were lined up in 3% ficoll (6 g Ficoll GE Healthcare PM400, 60 mL 1 X MMR, 140 mL dH_2O) before injecting, and then left to develop in 3% ficoll at 23 °C. After 2 hrs Ficoll was replaced with 0.1 X MMR and embryos left to developed to desired stages.

Needles were calibrated before injection using microscope graticule eyepiece to inject 10 nL at 2 cell stage embryos and 5 nL at 4 cell stage embryos on a Harvard apparatus injector (Medical Systems Research), the injector was set to the parameters: $P_{out=}$ = 90, $P_{balance}$ = 0.6 and P_{inject} = 16. *X. tropicalis* maximum injection volume was 4.2 nL, and for *X. laevis* was 10 nL.

Table 2.1 - Injected morpholino and miRNA mimic sequence data.

Morpholino	Sequence
miR-196a MO	5'- CAATCCCAACAACATGAAACTACCT-3'
miR-196a Mismatch	5'-CATTGCCAAGAACATCAAAGTACCT-3'
miR-219 MO	5'-AGAATTGCGTTTGGACAATCAAGGG-3'
miR-219 Mismatch	5' ACAATTGCCTTTCGAGAATCAACGG-3'
Xl-Pax3 MO (Monsoro-Burq et al., 2005)	5'- TCTCAGTTCCCTTGCCAAGTATTAA- 3'

2.2.1 Capped RNA synthesis

Capped RNA (cRNA) for GFP and LacZ was produced by digesting 1 µg of plasmid DNA. This was done using 5 µL of buffer with 2 µL of restriction enzyme (Not1), in a total volume of 50 µL of nuclease free water. This was then incubated overnight at 37°C before purification with Qiagen PCR purification kit according to manufacturer protocol. Linearized DNA concentration was quantified using a Nanodrop before transcription. Transcription of linearized plasmid used reagents from mMessage mMachine SP6 Transcription, Ambion, AM1340. See Table 2.2 below for plasmid

information. 1 µL of DNase was added to the transcription reaction, left 15 mins at 37°C before lithium chloride purification, quantification and aliquoting into 2 µL 5 ng and 50 ng aliquots and stored at -80°C.

Table *2.2*- Plasmid information for cRNA synthesis*.*

Plasmid	***Plasmid Source***	***Restriction Enzyme***	***Transcription***
pCS GFP2	Dr. Maggie Walmesly	Not1	SP6
pCS+nuc beta-gal (LacZ)	Dr. Maggie Walmesly	Not1	SP6

2.2.2 Fixing embryos

Once embryos had reached the desired stage, they were fixed in MEMFA (3.7% formaldehyde, 1 X MEM salts, DEPC H_2O at a ratio of 1:1:8, MEM Salts. Embryos were fixed 2 hrs at RT or overnight at 4°C with rocking. The MEMFA was then removed and replaced with 2 washes of phosphate buffered saline 0.1% Tween (PBST), and washed twice in 100% ethanol, before storage at -20°C.

2.3.0 Whole-mount *in situ* hybridisation

2.3.1 Preparation of competent cells & bacterial transformation

5 mL of *E. coli* strain DH5alpha was grown overnight in Luria broth at 37°C with shaking at 200 rpm. 1 mL of the culture was then added to 200 mL of LB media and incubated with shaking at 37°C testing optical density (OD600) until it reaches 0.3-0.4. Cultures were then cooled on ice for 15 mins and centrifuged for 10 mins, at 4°C and 2000 rpm. The supernatant was discarded, and bacterial pellet was resuspended in 16 mL of filter sterilized TB I buffer. Cells were put on ice for a further 15 mins and centrifuged at 4°C and 20,000 rpm for 10 mins. The supernatant was discarded, and the pellet was resuspended in 4ml of sterilized TB II, aliquots were then stored at -80°C.

Materials:

- TB I pH 5.8: $RbCl_2$ 0.1M, $MnCl_2H_2O$ 0.068M, $CaCl_2$, 0.01M, KAc 1 M pH 7.5, 37.5 mL Glycerol adjust to 250 mL and pH using 0.2 M HAc
- TB II: MOPS 0.5M pH 6.8, $RbCL_2$ 0.01M, $CaCl_2$ H_2O 1.04 M, 37.5 mL Glycerol adjust to 250 mL aliquoted and stored at -80°C

Transformation

1-4 µL of plasmid DNA was transformed into 100 µL of bacterial competent cell strain DH5alpha and left for 30 mins on ice. Heat shock was carried out for 90 secs at 42°C before being placed back on ice for 2 mins. 1 mL of Luria broth media (LB) was added and left to grow at 37°C 180 rpm shaking for 1 hr before pelleting and plating out onto antibiotic resistant plates. Plates were incubated overnight at 37°C.

2.3.2 Midi prep

A single colony was picked from the bacterial plate, and a 5 mL starter culture including 5 µL of respective antibiotic was added to 5 mL LB media. This was grown overnight at 37°C with 180 rpm shaking. A 50 mL culture was inoculated using 100 µL of previous culture and 50 µL of antibiotic (10 mg/ mL). Nucleobond Xtra Midi plasmid purification kit (Machery-Nagal, Germany) was used according to manufacturer protocol. DNA concentration was quantified using Nanodrop machine.

2.3.3 Riboprobe synthesis

Plasmid DNA for desired probes was digested using an appropriate restriction enzyme to give an antisense fragment and confirmed by running on a 1% agarose gel for 40 mins at 100 V, imaged using a UV analyser Biorad Chemidoc XRS (Biorad, California, USA). This linearized DNA was then purified using a QioQuick PCR Purification kit, Qiagen, according to manufacturer protocol and then transcribed to produce RNA riboprobe with the reagents in Table 2.3. Plasmids used in this study are shown in Table 2.4.

Table 2.3- Riboprobe synthesis transcription reaction reagents. All reagents supplied by Promega, except DIG/FITC labelled-UTPS, Roche, 11093274910).

Reagent	Per reaction
Linearized DNA	1 µg
5 X Transcription buffer	4 µL
DDT 100 mM	2 µL
DIG/FITC-labelled UTPs	2 µL
RNAsin	1 µL
RNA polymerase	2 µL
Final volume	20 µL

The transcription reaction was carried out overnight at 37°C and a further 2% agarose gel was run for 30 mins at 90 V. Using Illustra ProbeQuant G-50 Micro Columns, 27-5330-01 (GE Healthcare, UK). RNA riboprobes were radiolabelled and purified on a G50 column and diluted in hybridisation buffer to give a concentration of 1 µg/ mL.

2.3.4 Whole mount in situ hybridisation & LacZ tracer development

Before *in situ* hybridisation can be conducted, if embryos were injected with a lacZ tracer, this was developed first and as follows: embryos were fixed for 30 mins in MEMFA at room temperature and examined for beta-galactosidase staining, see Table 2.5 below for solution. Embryos were incubated with solution at 37°C no shaking until red staining was observed as in (Monsoro-Burq, 2007). Embryos then underwent a further 1 hr 30 mins of fixation in MEMFA before further processing.

Table 2.4- Riboprobe synthesis plasmids information. Some information such as insert size was not provided, but plasmids were sequenced to verify correct insert mRNA.

Clone name	Antibiotic resistance	Backbone	Sense RE	Sense polymerase	Antisense RE	Antisense Polymerase	Insert Size	Source
Pax3	Ampicillin				BglII	SP6		AH.Monsoro-Burq
Sox10	Ampicillin	pBSK			EcoRI	T3	1.3kb	JP. Saint-Jeannet
Snail2	Ampicillin	pCS107			EcoRI/BamHI	T7		EXRC
Xhe2	Ampicillin	pBSK			XbaI	T7		AH.Monsoro-Burq
EYA1	Ampicillin	pT-Adv			HindIII	T7		Schlosser
PAX6	Ampicillin	pBSK	XhoI	T3	XbaI	T7		Bill Harris
En2					XbaI	T3		Nancy PapalopμLus
Zic1	Ampicillin				EcoRI	T3		Dr Jung Aruga
Sox2	Ampicillin	pCS2+	NotI	SP6	EcoRI	T7		Prof. Yoshiki Sasai
c-myc	Ampicillin				ApaI	SP6		

Table 2.5- Beta-galactosidase staining solution.

Reagent	Amount to add	Final concentration
1 M K3Fe(Cn)6	250 μL	5 mM
1 M K4Fe(Cn)6	250 μL	5 mM
1 M MgCl2	10 μL	2 mM
20 mg/mL Red-Gal	250 μL	1 mg/ mL
DEPC-PBS	4.24 mL	

All steps, except for the proteinase K incubation are carried out with gentle rocking. Embryos were rehydrated in graded methanol washes from 100%, 75%, 50% and 25% methanol DEPC-PBST for 5 mins each. Embryos were then washed twice for 5 mins in DEPC-PBST before proteinase K treatment at 20mg/ mL, diluted in DEPC-PBST, followed by re-fixation in 3.7% formaldehyde for 20 mins at RT. Embryos were rinsed in hybridisation buffer then replaced with fresh hybridisation buffer and incubated for 1 hr at 60°C,

after this embryos underwent hybridisation with riboprobe overnight at 60°C. Probe was removed and saved for re-use, and embryos underwent a series of 2 x SSC at 60°C. Embryos were then RNase treated (RNase A/T1- Thermo Scientific, EN0551, 2 mg/mL, use 1 µL/mL of 2X SSC) for 30 mins at 37°C. Embryos were then washed in a series of 0.2X SSC washes and then MAB (p.H 9.5) before blocking (MAB with 2% BMB) at room temperature with rocking for 1 hr and then incubation overnight with anti-DIG antibody (1:4000) in blocking buffer, at 4°C. At least 6, 1X MAB washes preceded alkaline phosphatase treatment and colour development with NBT/BCIP at 37°C.

Colour reaction was stopped with PBST, and embryos were fixed before bleaching (bleaching 44.75 mL depc water, 20 x SSC p.H 7 1.25 mL, 1.5 mL 30% hydrogen peroxide- Sigma, 2.5 mL formamide) before imaging.

Solutions for WISH and Double WISH:

- PBS – 10X: 2.5 g $NaH_2PO_4H_2O$, 11.94 g $NaHPO_4.H_2O$, 102.2 g NaCl
- PBST – PBS with 0.1% Tween-20
- 2% Blocking reagent: MABT/ 2% Roche blocking reagent: 50 mL MABT + 1 g blocking reagent (possibly use half). Dissolve at 65 ^oC
- Blocking Solution (MABT/2% blocking reagent/20% goat serum): 40 mL MABT + 1 g blocking reagent + 10 mL goat serum
- 2% Blocking reagent (MAB/2% blocking reagent/10% goat serum) for a minimum of 60 mins.
- Blocking solution containing 1:2000 dilution of Anti-Dig-AP Fab fragments (Roche 11093274910)
- NTMT- To make 200mL: 5M NaCL- 4 mL, 1 M Tris-Cl (pH 9.5) 20 mL, 1 M $MgCl_2$ 10 mL, Tween20 2mL, + 164mL H_2O. Colour reaction- 25 mL NTMT + 22.5 µL NBT and 87.5 µL BCIP
- BCIP: 50 mg/mL in 100% DMF
- NBT (Nitro Blue tetrazolium): 75 mg/ mL in 70% dimethylformamide (DMF)

- Proteinase K treatment 1 µL / mL of 20 mg/ mL stock in DEPC-PBST. ST.10.5 – 1MIN, ST 12-16 – 2 MIN, ST. 16-20 – 3 MIN, ST. 20-25 – 4 MIN, ST. 25-30 – 5 MIN, ST. 30-33 – 6 MIN, ST. 33-36 – 8 MIN, ST. 36-40 – 18 MIN, ST. 40- 45 – 20 MIN

- Hybridisation buffer: 50% formamide, 5X SSC, 1 mg/ml Torula RNA, 100 µg/ml Heparin, 1X Denhardt's solution, 0.1% Tween 20, 0.1% CHAPS, 10 mM EDTA.

- MEMFA: 10% MEM salts, 10% formaldehyde in DEPC-water

- MEM salts: 0.1 M MOPS, 2 mM EGTA, 1 mM $MgSO_4$, pH 7.4

- 20 X SSC: Dissolve 175.3 g NaCl and 88.2 g of sodium citrate in 800 mL of water. Adjust to p.H 7.0 with HCl, top up to 1 litre with water.

- 10X MAB: 116 g Maleic acid, 87 g NaCl, 60 g NaOH, 800 mL water, p.H to 7.5

- Fast Red Solution: SIGMA*FAST*^{TM} Fast Red TR/Naphthol AS-MX Tablets dissolved in 10 ml alkaline phosphatase buffer.

2.4.0 Statistical analysis

Chi-squared test for association was used to test phenotype yes or no categories for MO injected embryos processed by *in situ* hybridisation or Alcian blue, to see if there was a relationship between two categorical values. Excel was used to collate and tabulate data. SPSS v25 for Mac to carry out chi-squared test. When describing statistical significance; $p<0.05$ = *, $p<0.01$ = **, $p<0.001$ = ***, $p<0.0001$ = ****. Embryos and embryo phenotypes were counted and judged by self and blind counted by at least one other colleague to prevent unconscious bias.

2.5.0 Double whole mount *in situ* hybridisation

Embryos were rehydrated in graded methanol washes from 100%, 75%, 50% and 25% methanol DEPC-PBST for 5 mins each. Embryos were then washed twice for 5 mins in DEPC-PBST before proteinase K treatment (no rocking for proteinase K) and re-fixation in 3.7% formaldehyde. Embryos were rinsed in

hybridisation buffer then replaced with fresh and left in hybridisation for 1 hr at 60°C, after this, embryos underwent hybridisation with riboprobe overnight at 60°C. Riboprobe included 1 µg/ mL final concentration of two probes in a final volume of 1 mL, for example starting concentration of each probe was 2 µg/ mL and 500 µL of each probe was taken.

Probes were removed and saved for re-use, and embryos underwent a series of 2X SSC washes at 60°C. Embryos were then RNase treated (RNase A/T1-Thermo Scientific, EN0551) for 30 mins at 37 °C. Embryos were then washed in a series of SSC washes and then 1 X MAB wash before blocking at room temperature with rocking for 1 hr before incubation overnight with anti-DIG antibody (1:4,000) in blocking buffer, at 4°C. A series of MAB washes preceded alkaline phosphatase treatment and colour development with NBT/BCIP at 37°C until reached desired colour. Colour reaction was stopped by 3 x 5 min DEPC-PBST washes. Embryos were then heated up to 65^{o}C for 1 hr in MABT. Embryos were then re-blocked as previous before incubation with anti-fluorescein/DIG AP Fab fragments antibody (1:1,000; Roche, cat. no. 11426338910). Embryos underwent another series of MAB washes before FITC colour development with Fast Red or BCIP development. Colour reactions were stopped as before, and embryos were fixed in MEMFA and dehydrated in 100% Methanol or if FITC developed just PBS. FITC must be imaged under fluorescent lamp.

2.5.1 Imaging

Imaging of embryos was carried out on a 2% agarose plate (2 g agarose in 100 mL distilled water, 25 mL per plate). Light microscopy images were captured using Zeiss Axiovert Stemi SV 11, Jenoptik ProgRes C5 camera (Germany), ProgRes software version 2.7.6. Fluorescent images were captured using Leica MZ 16 F microscope, Leica DFC300 FX camera, Leica Kubler codix light source, Leica FireCam software version 3.4.1.

2.6.0 CRISPR/Cas9 in X. tropicalis for miRNAs

2.6.1 Method of CRISPR-Cas9

CRISPR/Cas was carried out with *X. tropicalis* embryos. SgRNAs with Cas9 protein were co-injected into 1 cell stage embryos. See Fig. 2.1 below for workflow.

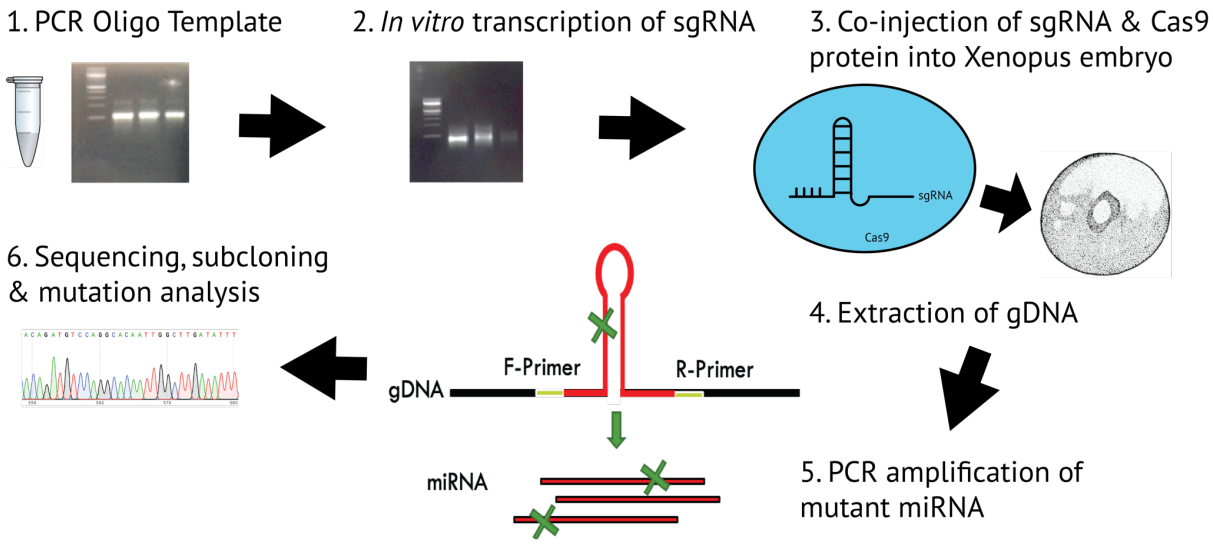

Figure *2.1*- CRISPR/Cas9 Workflow and pipeline.

2.6.2 SgRNA design

SgRNAs were designed to incorporate the T7 promoter, as in (Nakayama et al., 2013). Sequences for miRNAs were taken from Ensembl (ensembl.org/), miRNA sequences from *X. tropicalis* version 4.2 were found on Ensembl, for miR-196a: ENSXETG00000029181, for miR-219: ENSXETG00000029136.

The following online tools were used in the design of sgRNAs:

- Dharmacon: http://dharmacon.horizondiscovery.com/gene-editing/crispr-cas9/crispr-design-tool/
- CRISPOR: http://crispor.tefor.net
- CRISPRscan http://www.crisprscan.org/

Off-target effects were taken into consideration in the design process. T7 promoter was set as the chosen promoter for transcription and GG set as desired starting sequence for promoter binding, Cas9 used with protospacer

adjacent motif (PAM) sequences as any nucleotide GG (NGG). sgRNA sequences designed are listed in Table 2.6 below.

Table *2.6* - List of sgRNAs designed and trialled in *X. tropicalis*. sgRNAs with a "*" are successfully validated as a pair or individually "**", to "drop-out" miRNAs. Sg219-1-4 and sg1961-3 are guides designed to be used individually, sg219-5-10 and sg196-4-8 are designed to be used in pairs.

Guide RNA (sgRNA) Oligo	Sequence 5' to 3'
sg219-8	taatacgactcactataGGGTGTGTTGGGGGGGTTGGgttttagagctagaa
sg219-5*	taatacgactcactataGGTGAATTTTCCACAGCAATgttttagagctagaa
sg219-9*	taatacgactcactataGGGTCTTCAGAATCAGCGACgttttagagctagaa
sg219-10	taatacgactcactataGGAAAGATTGTAAGTCCAAGgttttagagctagaa
sg196-4*	taatacgactcactataGGGAGGCTTCTCAGAATATTgttttagagctagaa
sg196-5	taatacgactcactataGGAGCCCTTGTCCCCCTGGCgttttagagctagaa
sg196-7*	taatacgactcactataGGGAGCCTATGGAGCCATATgttttagagctagaa
sg196-8	taatacgactcactataGGGCTCCCATATGGCTCCATgttttagagctagaa
196aF1	taatacgactcactataGGGATTGCTTTTTCTTAACGgttttagagctagaa
196aF2	taatacgactcactataGGTTTAGGTAGTTTCATGTTGTgttttagagctagaaatagcaag
196aF3**	taatacgactcactataGGTTAGGTAGTTTCATGTTGTTgttttagagctagaaatagcaag
219F1	taatacgactcactataGGATTGCGTTTGGACAATCAgttttagagctagaa
219F2**	taatacgactcactataGGATGTCCAGGCACAATTCTgttttagagctagaa
219F3	taatacgactcactataGGATTGTGCCTGGACATCTGgttttagagctagaa
219F4	taatacgactcactataGGTGCCTGGACATCTGTGGCgttttagagctagaa

Table 2.7 - Table of primers and sequences. Primers used for sequencing and PCR of gDNA. Primers highlighted in green were used to generate the final data published in this thesis.

Primer	Sequence 5' to 3'
Common Reverse oligo for sgRNA synthesis	AAAAGCACCGACTCGGTGCCACTTTTTCAAGTTGATAACGGACTAGCC TTATTTTAACTTGCTATTTCTAGCTCTAAAAC
219 F	CGACCGGTCATATCTCCAGC
219 R	TACAATCTTTGCCCGTCGCT
219 F2	GGGTTGGTGGGGGTTCTATCG
219 R2	GCCCTGGCAATGCTGGAAATG
219 F3	GACGTAGAATCAGCGAGCGA
219 R3	GGTAGGCAACACACTCTTCAAC
219 F4	GGCACAGTGGGGGTAACCAT
219 R4	GAAGGCTGTATTTTAGCCCTGGC
219 F5	CCCTTTCCAGCCTATGACAAC
219 R5	ATCTTGCACCTGCACACTCT
219 6F	CCCAGTCTTGGAAGGAGTAGAC
219 8F	GGGGTGACAATATTGGGACGTAGC
219 9F	CCCTTGAGTAGAGTATCGGCTG
196 F	GAGGGGAGTTTTGGGCATGA
196 R	GTGGAAGAATGGCACCCAGA
196 F2	GGCTCATAGGAGGACGTTGG
196 R2	GGAGGGCTTCTTTTGTCTGCC
196 F3	GTGAGAATTGGGGAGGGGAG
196 R3	AGGAGTTCTGAAGGAGGGCTTC
196 F4	GGGCAGGAGCTCCCATATGG
196 R4	GCCCAATATTCTGAGAAGCCTC
196 F5	TTCAGGACACCTTGTCTGGC
196 R5	TGAGCTTTCCGGTTTAGGGG
196 F7	CAGCCCAGCACTTACAGGTT
196 R7	GGAGTTCTGAAGGAGGGCTT

Primers

Primers were designed using the online tool NCBI Primer3 and are listed above in Table 2.6 & 2.7. These primers were used to sequence DNA isolated from embryos injected with Cas9 protein (20 μM) and sgRNAs. The sequence data was analysed with the online tool tide: https://tide.deskgen.com/ . This revealed the point mutations in the sequence data chromatogram, revealing any differences in peaks.

2.6.3 SgRNA synthesis & CRISPR-Cas9 embryo injection

PCR of template

Template oligomers for the sgRNAs were generated by PCR with the following conditions: stage 1- 95°C for 5 mins x1, stage 2- 95°C for 20 secs, 66°C 20 secs (ramp) to 68°C for 15 secs x13, stage 3- 94°C 20 secs, 58°C 20 secs x30. Taking 1 hr 10 mins in total. PCR reaction mix included: 10 μL GoTaqGreen (Promega, M782A), 2 μL Forward primer (sgRNA oligomer template), 4 μL Reverse primer, 7.6 μL nuclease-free water. Products were run on 2% agarose gel.

Transcription of sgRNA guides

MegaSHORTScript kit (Applied Biosystems, AM1354, Ambion) was used according to manufacturer's instructions to transcribe RNA from oligo template with T7 polymerase. Transcription product was cleaned up with SigmaSpin Post-reaction clean-up columns, (Sigma, S5059), according to manufacturer's instructions, ran on a gel and quantified on a Nanodrop 1000.

Injection of sgRNAs & CRISPR

4.2 nL of 300 pg sgRNA and 0.8 μL of 20 μM Cas9 Protein plus GFP tracer capped RNA were co-injected into a 1 cell *X. tropicalis* embryo. Embryos were kept in 3% Ficoll until they reached 8 cell stage and transferred into 0.05 X MMR and incubated at 23^{o}C until embryos reached tailbud stage. Embryos were snap-frozen on dry ice before genomic DNA (gDNA) isolation. sgRNA was produced by digesting pDR274 plasmid with Dra I and transcribing with T7 RNA polymerase (Appendix 1 and Table 2.8). Method based on (Nakayama et al., 2013).

Table *2.8* - Oligos for tyrosinase mutagenesis by CRISPR-Cas9.

Oligo	Sequence 5' to 3'
sgRNA oligo for tyrosinase	5'-AACTGGCCCCTGCAAACA -3' PAM 5'-TGG-3'
Tyr-F primer	TGATGTAAGCCTGCACATGTGA
Tyr-R primer	CAGTCTGCACAGTTATAGCCCA

MiRNA CRISPR, single and double gRNA embryo injection

X. tropicalis embryos were injected with 300 ng of sgRNA for single sgRNA injections and 150 pg of each sgRNA when injecting pairs of sgRNAs. SgRNAs were diluted in nuclease free water and 0.8 µL Cas9 protein 20 µM (New England Biolabs, #M0646M, EnGen Cas9 NLS 20 µM) was added, flicked, and spun; left on ice for at least 30 min before injection to allow sgRNA to chelate with Cas9. 4.2 nL of CRISPR reagents plus GFP tracer capped RNA were co-injected into the 1/2 cell *X. tropicalis* embryo. Embryos were kept in 3% Ficoll until reached 8 cell stage and transferred into 0.05 X MMR and incubated at 23^{o}C until embryos reached tailbud stage. Embryos were snap-frozen on dry ice before gDNA isolation.

2.6.4 CRISPR Validation

Genomic DNA isolation

Embryos were homogenized in Eppendorf tubes with micropestles and brief vortexing. Genomic DNA was isolated using PureLink gDNA Mini Kit, K1820-00 (Invitrogen, California, USA), according to manufacturer's guidelines and then quantified using a Nanodrop 1000 before sequencing.

T7 Endonuclease Assay

T7 Endonuclease assay kit was supplied by New England Biolabs, EnGen Mutation detection kit, E3321S. Genomic DNA was PCR'd up with the recommended Q5 polymerase or another high-fidelity polymerase and Taq polymerase in the lab. If using high-fidelity polymerase, the annealing temperature of the primers for Tyrosinase PCR was 66-68^{o}C and for miRNA was 54^{o}C regardless of polymerase. PCR programme recommended by

manufacturer: Initial denaturation: 98°C 30 seconds, cycles: denaturation 98°C 5 seconds, Annealing: 50-72°C 10 seconds, Extension: 72°C for 20 seconds; final extension of 72°C for 2 mins.

TA cloning, Colony PCR & Sequence Analysis

CRISPR- embryos and corresponding control embryos had gDNA isolated which was then subcloned for sequence analysis. G-DNA was amplified by PCR with high-fidelity polymerase- Phusion (New England Biolabs, M0530), then incubated at 72°C for 15 mins with 1 µL of GoTaq (Promega, M7832) to produce "A" overhangs. miRNAs were amplified by PCR using the following programme from gDNA, for wild-type miRNA: initial denaturation of 95°C 5 mins, cycle: 95°C 20 seconds, 57°C 30 seconds, 72°C for 30 seconds, cycle 35 times, then final extension of 72°C 5 mins and store at 4°C. For miRNA mutant (KO): initial denaturation of 98°C 5 mins, cycle: 95°C 20 seconds, 57°C 30 seconds, 72°C for 10-30 seconds (dependent on size of amplicon, smaller amplicon shorter extension time to bias smaller fragment), cycle 35 times, then final extension of 72°C 5 mins and store at 4°C. PCR product was purified with PCR purification kit (Qiagen, 28104). If the PCR product was extracted from a gel, 15 µL of PCR product was run on a 2% agarose gel, 90 V 40 min, and cut out on a UV analyser and purified using GeneJet Gel extraction kit (Thermo Scientific, K0692).

TA cloning kit with pGEM-T-Easy vector (Fig. 2.2), was used (Promega, A1360) according to manufacturer guidelines. Ligated PCR/gel extraction products into pGEM T-easy were transformed into bacteria as in section 2.3.1. X-Gal and ampicillin resistance were used as selection markers. Blue, white screening with X-gal identified colonies for colony PCR, with white colonies expected to show successful cloning. Colony PCR was carried out with Biomix Red (Bioline, BIO-25006) master mix, with M13 primers and colony. Successful colonies were grown up into cultures and prepped as described in 2.3.2 Midi prep section.

5.D. pGEM®-T Easy Vector Map and Sequence Reference Points

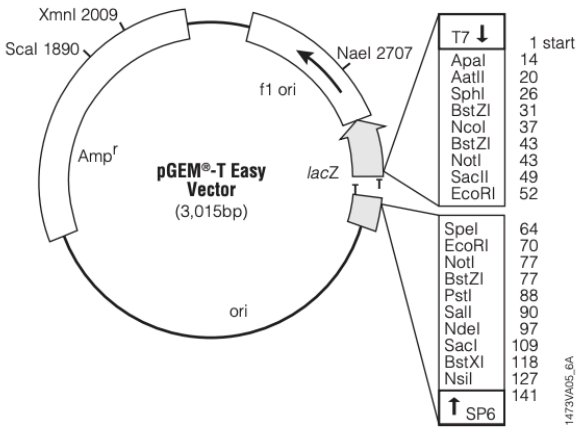

Figure- 2.2 pGEM T Easy Promega vector backbone and vector information.

Table *2.9* Generic primers and sequences

Name	Sequence 5' to 3'
M13 F	GTTTTCCCAGTCACGAC
M13 R	CAGGAAACAGCTATGAC
T7	TAATACGACTCACTATAGGG
SP6	ATTTAGGTGACACTATAG

Subclones were sequenced with M13 or T7/ SP6 primers (Table 2.9). Sequences were put through BLAST (https://blast.ncbi.nlm.nih.gov/Blast.cgi) to search for miRNAs and Snapgene software (www.snapgene.com/try-snapgene/) was used to align sequences and analyse for indel mutations.

2.6.5 MiRNA secondary structure prediction

MiRNA stem loop structures were predicted computationally using Vienna RNA fold tool: http://rna.tbi.univie.ac.at/forna/forna.html?id=RNAfold/vCiQTz5Wd4&file=cent_probs.json. Sequences for stem loops were sourced from miRbase http://www.mirbase.org/.

ImageJ craniofacial phenotype analysis

Image J v1.52p Mac was used to measure eye area, eye length and body length of mutant tadpoles. A measurement of pixels was taken as seen below in Fig. 2.3.

2.6.6 Alcian blue Cartilage staining
Alcian Blue

Embryos were fixed for 1.5 hour at room temperature (RT), then dehydrated with 5 washes of 100% ethanol (Sigma, UK) for 5 minutes each, all washes were at RT. Embryos were then left in Alcian blue (Fischer, UK) staining solution for 3 nights. After this they were washed 3 times for 15 minutes in 95% ethanol (Sigma, UK) then rehydrated in 2% KOH. This was done gradually using 10-minute washes of 75% EtoH in 2% KOH, 50% EtoH in 2% KOH, 25% EtoH in 2% KOH then 3 x 2% KOH washes. Embryos were then stored in glycerol to make embryos more transparent. This was done with 1 hr washes of 20% glycerol in 2%, 40% glycerol in 2% KOH, 60% glycerol in 2% KOH and finally stored in 80% glycerol in 2% KOH. Facial cartilage was then dissected out with forceps under the microscope before imaging.

Solutions:

• Alcian Blue solution: 20 mg Alcian blue, 15 mL acetic acid, 35 mL 100% ethanol

• 2% KOH: 10 g KOH tablets in 500 mL dH2O

To visualise craniofacial cartilage clearly, without pigmentation obscuring view and to reduce need for dissection, embryos underwent a modified bleaching and clearing process. Embryos were washed 3 x 5 mins in PBS before 20 min incubation in 10 mL pre-incubation solution (0.5 X SSC (150 mM NaCl, 15 mM sodium citrate, pH 7.2), 0.1% Tween-20), and then embryos were incubated in 10 mL of depigmentation solution (5% formamide, 0.5 X SSC, 3% H_2O_2). Embryos were then carefully dissected under a microscope using fine forceps to remove outermost membranes surrounding craniofacial cartilage. Method for bleaching the embryos in this section is modified from Affacticati and colleagues (Affaticati et al., 2018).

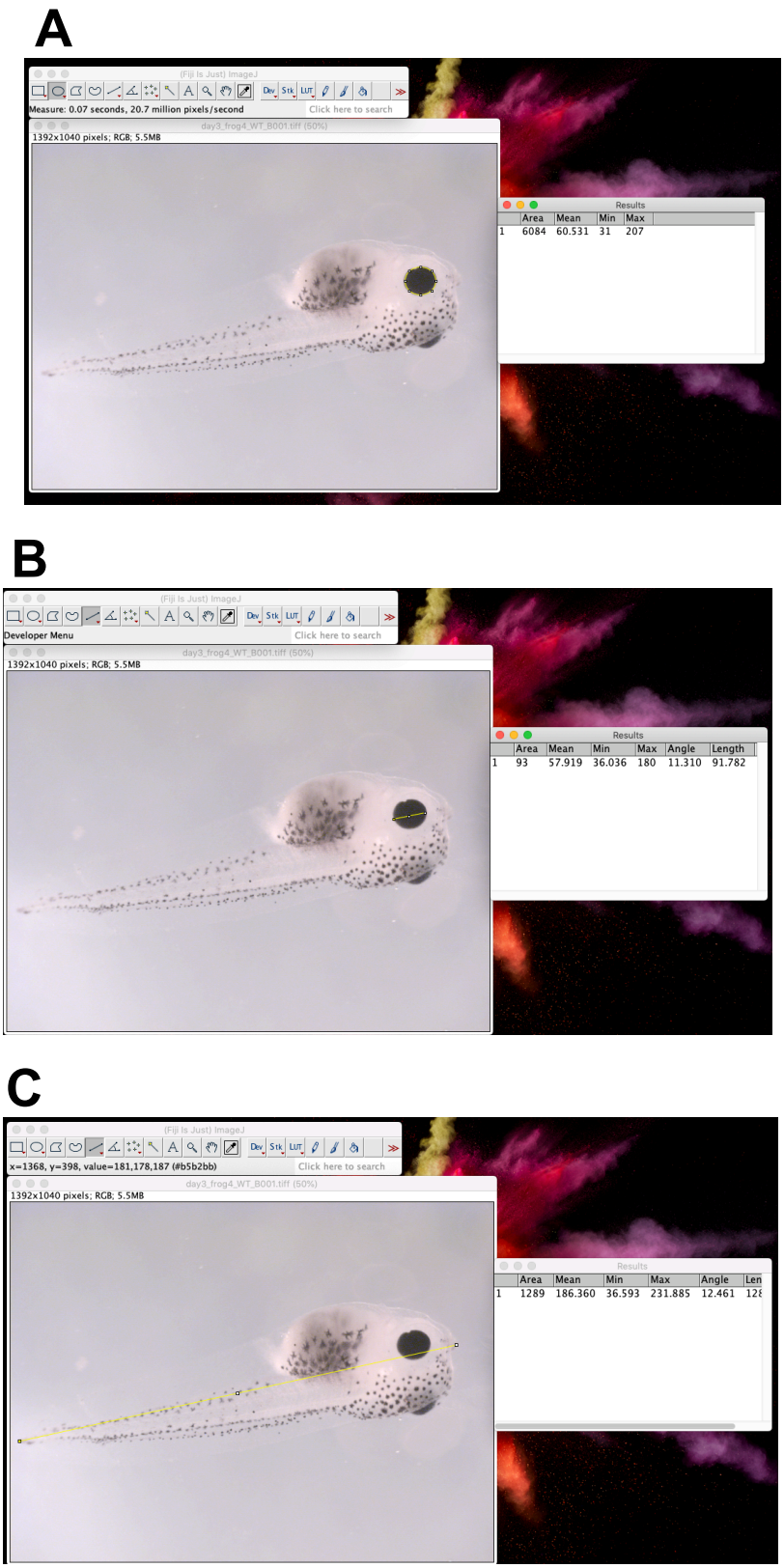

Figure- 2.3 – Measuring eye phenotypes in X. tropicalis tadpoles. WT embryo featured as an example tadpole. A) Eye area measurement. B) Eye length measurement. C) Body length measurement, all in pixels.

2.7.0 Chick whole mount *in situ* hybridisation

2.7.1 Chick & LNA whole mount in situ hybridisation

MiRCURY™ LNA (locked nucleic acid) probes (Table 2.10) were provided by Exiqon. Hybridisation temperature for all probes was 50^{o}C, probes were used at 1 ug/ mL and hybridised six times or more before use on Xenopus and chick embryos. Method for chick embryo whole mount *in situ* hybridisation was carried out according to (Sweetman, 2011; Sweetman et al., 2006). Chick embryos were staged according to Hamilton and Hamburger (HH) staging (Hamburger and Hamilton, 1992).

Chick embryos were fixed in 4% PFA at desired stage and dehydrated in methanol and kept at -20^{o}C. Embryos were rehydrated in 75%, 50% and 25% methanol/PBST and twice in PBST for 5 min each wash. Older embryos were treated with proteinase K (20 mg/ mL) for 30mins at RT. Embryos were washed in PBST then fixed in 4% PFA/ 0.1% Glutaraldehyde (20 mL PFA+80 µL 25% Glutaraldehyde) for 20 mins at RT rinsed and wash for 5mins in PBST. Embryos were hybridised at 54^{o}C for 2 hrs and left in LNA/DIG probe overnight at 54^{o}C/ 65^{o}C. Probe was removed and replaced with two rinses in hybridisation buffer at 54^{o}C, and then washed 3 times for 30 mins with hybridisation wash buffer. Embryos were then washed in 1:1 washing buffer: MABT at hybridisation temperature for 10 mins, rinsed 3 times in MABT and washed twice in MABT 30 mins before replacing with MABT/2% blocking reagent for 60 mins. Embryos were blocked with blocking solution (MABT/ 2% blocking reagent/ 10% goat serum) for a minimum 60 mins. Block buffer was removed and replaced with antibody solution 1:2000 dilution of Anti-Dig-AP Fab fragments (Roche 11093274910) in blocking solution and incubated with rocking at 4^{o}C overnight.

Antibody solution was removed and replaced with 3 x 5 min washes in MABT and 3x 1 hr washes in MABT at RT. Embryos were washed twice in NTMT for 10 mins each and placed in NBT + BCIP in NTMT until colour developed. Colour reaction was stopped with five TBST washes at 10 mins each and left in TBST overnight. Embryos were fixed in Na-Azide -5 µL per 10 mL of 20 mL PFA+ 80 µL glutaraldehyde.

Chick in situ solutions:

- MABT: 160 mL SDW + 40 mL MAB 5x + 2 mL Tween-20 (10%)
- MABT/2% Roche blocking reagent: 50 mL MABT + 1 g blocking reagent (possibly use half). Dissolve at 65^{o}C
- Blocking Solution (MABT/2% blocking reagent/20% goat serum): 40 mL MABT + 1 g blocking reagent + 10 mL goat serum
- Blocking solution (MABT/2% blocking reagent/10% goat serum) for a minimum 60mins
- Blocking solution containing 1:2000 dilution of Anti-Dig-AP Fab fragments (Roche 11093274910)
- Colour reaction NMTT (50 mL): 40.25ml SDW, 1 mL NaCL (5M), 2.5 mL Tris pH 9.5 (2M), 1.25ml $MgCl_2$ (2M) and 5 mL Tween-20 (10%) use formula 9 µL NBT + 7 µL BCIP / mL.

Table 2.10- miRCURY LNA Probe sequences. Supplied by Qiagen formerly Exiqon.

Name	*Sequence*	*Product code*
hsa-miR-219a-5p miR-219	5'UGAUUGUCCAAACGCAAUUCU	MIMAT0000276
Xtr-miR-196a miR-196a	5'UAGGUAGUUUCAUGUUGUUGG	MIMAT0003690
Gga-miR-133b miR-133b	5'UUGGUCCCCUUCAACCAGCUA	MIMAT0001138
Xtr-miR-302 miR-302	5'UAAGUGCUCCAAUGUUUUAGUGG	MIMAT0003636

2.8.0 MiRNA mimics and messenger rescue reagents

To rescue miRNA knockdowns, synthetic miRNA mimics from Qiagen were used. These LNA miRNA mimics are a unique, triple stranded RNA molecule. They have two passenger strands to take the miRNA mimic directly to the RISC complex to mimic natural miRNA function. This would also benefit the MO rescue experiments, as the miRNA is triple stranded the antisense MO oligonucleotide should not bind complementarily due to the passenger strands

on the LNA miRNA mimic. The structure of the miRNA mimic, and function are summarised in Fig.2.4.

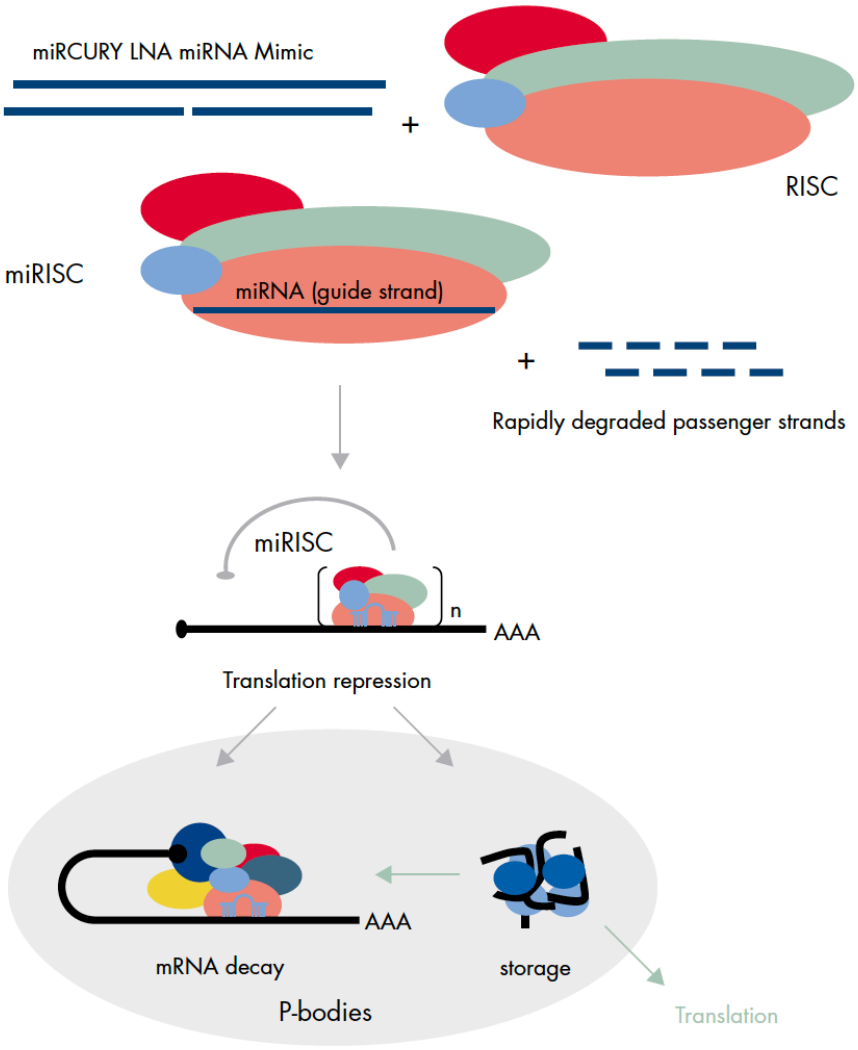

Figure- 2.4 – Triple-stranded design of Qiagen miRNA mimic. The miRNA is incorporated into the RISC complex, with the two LNA passenger strands degraded after displacement from miRNA. Figure supplied by Qiagen.

They were ordered at 5 nmol with no labelling and desalting. Before use they were diluted in 75 µL of nuclease free water to give a concentration of 66.7 µM and stored in small aliquots at -20^{o}C. Qiagen could not provide a molecular weight for the mimic. I estimated the approximate molecular weight using the following formula:

Molecular weight= 320.5 X Number of nucleotides of RNA
For the miR-219 mimic this equated to 6730.5 therefore:
66.7 µM = 448.9 ng / µL
6.67 µM = 44.9 ng / µL
1 µM = 6.73 ng / µL

MiRCURY LNA miRNA mimics were used to replace miRNA in MO miRNA knockdown rescue. miR-219 mimic was used from (Qiagen, 339173 YM0047076-ADA, MIMAT0000276); hsa-miR-219a-5p miRCURY LNA miRNA Mimic, compatible with xtr-miR-219 sequence: 5'UGAUUGUCCAAACGCAAUUCU. For miR-196a: (Qiagen, 339173 YM00470616-ADA, MIMAT0000226); hsa-miR-196a-5p compatible with xtr-miR-196a sequence: 5' UAGGUAGUUUCAUGUUGUUGGG. A negative control miRNA mimic recommended by Qiagen was used (Qiagen, 331973 YM00479902-ADA); Negative control (cel-miR-39-3p), sequence 5'UCACCGGGUGUAAAUCAGCUUG.

To rescue expanded Pax3 phenotypes Pax3 MO (Table 1.1) was optimized at 40 ng to provide a reduction in Pax3. This was co-injected with miR-219 MO 60 ng. As this isn't possible in one injection MOs were made up so Pax3 MO final concentration was 20 ng and miR-219 MO was 30 ng, two injections into the embryo at 4 cell stage into 2 blastomeres then gave a concentration of Pax3 MO 40 ng and miR-219 MO 60 ng. For miR-219 MM MO, two injections of 50 ng gave a final dose of 100 ng MO.

2.9.0 q-RT-PCR

RNA extraction

Embryos were frozen on dry ice for 30 mins and stored at -80^{o}C before RNA extraction. Total RNA was extracted from five st.14 X. tropicalis embryos, embryos were homogenised with a micropestle, and RNA was extracted according to manufacturer's guidance, Quick-RNA Mini prep plus kit (Zymo, Cat no. R1058). For q-RT-PCR on *X. laevis* embryos 10 *laevis* embryos were pooled for RNA extraction prior to cDNA, 5 embryos were pooled for *X.*

tropicalis cDNA synthesis. Samples were eluted in 25 µL of nuclease free water; RNA concentration and purity quantified on a Nanodrop 1000 and 1 µL was checked on a 2% agarose gel.

CDNA synthesis

CDNA synthesis for miRNA and mRNA q-RT-PCR used two different optimized protocols and kits. To produce cDNA for miRNA q-RT-PCR, miRCURY LNA RT kit (Qiagen, Cat No./ID: 339340). 50 ng of RNA was used and kit according to manufacturer's instructions. CDNA was produced on a thermocycler with the following programme: 42^{o}C for 60 min and 95^{o}C for 5 min. cDNA was diluted 1:40 for q-RT-PCR. cDNA can be stored at -20^{o}C. To produce cDNA for mRNA q-RT-PCR the following recipe was used: 500 ng of total RNA was added in 9 µL of nuclease free water, plus 2 µL of random primers (Promega, C1181). This was then incubated at 70^{o}C for 10 mins. A mastermix was prepared as follows per sample: 4 µL of 5X buffer, 2 µL of DTT, 1 µL of dNTPs, 1 µL of Superscript II (Invitrogen, 18064014), 1 µL of nuclease free water or RNasin (Promega, N2611).

Q-RT-PCR

For qRT-PCR, a primer master mix was prepared as described in Table 2.11 to give a final reaction volume of 10-11 µL. Primers used are listed in Table 2.12. U6 was used as internal reference control. Mastermix was pipetted into MicroAmp® Optical 96-Well Reaction Plate (Applied Biosystems, cat. no. N8010560), before adding cDNA to individual wells. The reaction plate was kept cool and protected from light in an ice box. The plate was briefly spun before running on a 7500 Standard PCR instrument (Applied Biosystems) following the cycling program [2 mins 50°C; 10 mins 95°C; 45 cycles (10 secs (for miRNA, 15 secs for mRNA) 95°C; 1 min 60°C); with melt curve analysis (15 secs 95°C; 1 min 60°C; 30 secs 95°C, ramp rate 1%; 15 secs 60°C). Raw CT values were downloaded onto an Excel spreadsheet for analysis to produce Delta Delta CT and fold change. EEF1 alpha for mRNA and U6 was used to normalise data, CT values were converted to relative gene expression by utilising delta delta ct method. Experiments were set up with triplicate

biological and technical repeats. No template controls for q-RT-PCR were also used.

Table *2.11*- qRT-PCR reaction mix.

Reagent	Volume per reaction
SYBR Green PCR Master mix (Applied Biosystems; cat. no. 4309155)	5 µL
miRNA-qPCR Primer	1 µL
cDNA template (1:40)	4 µL / well
mRNA qPCR Primer Forward (10 µM)	1 µL
mRNA qPCR Primer Reverse (10 µM)	1 µL

Primers for q-RT-PCR were found in the literature and some were designed using primer blast (https://www.ncbi.nlm.nih.gov/tools/primer-blast/), (Ye et al., 2012). Primers were designed to generate 100 bp products with a melting temperature of between 59-62^{o}C.

2.10.0 Embedding, Cryosectioning & Imaging slides

Embryos for sectioning were prepared as follows. Fix in MEMFA for up to 7 days to get best results, more important for younger embryos, or at least 2 hr at RT ideally overnight at 4^{o}C or longer. Embryos were then washed in 30% sucrose over night at 4^{o}C then 2 x PBS before 3 x 5 min washes in OCT media (Cellpath OCT Embedding Matrix, ThermoFisher; cat. no. 15212776). During those washes embedding moulds (TAAB Laboratory; cat. no. C094) were half-filled with OCT media, embryo was then added and carefully positioned under the microscope making marks and notes on the mould as to embryo location and orientation. Embryos in moulds were then left for 30 min on dry ice before storage at -20^{o}C. Embryos were sectioned at a thickness of 20-40 µM on a cryostat (Leica CM 1950 cryostat) and transferred onto Superfrost Plus microscope slides (Thermo Scientific cat no. J1800AMNZ). OCT was carefully washed off by placing them in a PBS bath for 5 minutes, drying slides on the bench. Slides were mounted with a few drops of pre-warmed 37^{o}C hydromount

and careful coverslip placement. Slides were left at 4°C to harden. Slides were imaged with a Zeiss Axioplan 2 Imaging microscope equipped with Zeiss AxioCam HRc. The software AxioVision with brightfield and default options were used.

Table *2.12* q-RT PCR Primers used for Xenopus tropicalis embryos. miRCURY LNA miRNA PCR primers, Qiagen. mRNA primers were ordered as standard oligos.

Primer name	Sequence 5' to 3'	Product code/ Accession number
xtr-miR-196a	UAGGUAGUUUCAUGUUGUUGG	YP02103491
xtr-miR-196b	UAGGUAGUUUUAUGUUGUUGG	YP02104328
ipu-miR-219a (for mature miR-219)	AGAAUUGUGCCUGGACAUCUGU	YP02101832
U6 snRNA	CTCGCTTCGGCAGCACA	YP00203907
hsa-miR-219a-5p (for mimic detection)	UGAUUGUCCAAACGCAAUUCU	YP00204780
EEF1Alpha F	CCCAACTGATAAGCCTCTGC	PMID 23559567
EEF1Alpha R	CATGCCTGGCTTAAGGACAC	PMID 23559567
Sox10 F	GATGGGTCCTCTGAAGCTGA	Self designed
Sox10 R	GGTAGGGGGTCCATGACTTT	NM_001100221.1 Self designed
Snail2 F	CCCCATTCCTGTATGAGCGG	NM_001100221.1 PMID: 32713114
Snail2 R	TGAAGCAGTCCTGTCCACAC	PMID: 32713114
Xhe2 F2	CGCCACCTCTTTTCCCATTCA	Self designed
Xhe2 R2	TTTGGGCCACAGACACTCCTT	NM_001044399.1 Self designed
Pax3 F	TACAGCATGGAGCCTGTCAC	NM_001044399.1 PMID: 24055059
Pax3 R	TCCTTTATGCAATATCTGGCTTC	PMID: 24055059

CHAPTER III

RESULTS:
SPATIAL AND TEMPORAL MICRO RNA EXPRESSION

3.0.0 Introduction

3.1.0 Characterizing Xenopus Neural Crest and miRNAs

The NC is a multipotent stem cell population that can give rise to many parts of the human body. MiRNAs have previously been shown to be expressed in and potentially have roles in the development of neural crest (Ahmed et al., 2015; Ward et al., 2018). MiRNAs are short non-coding RNAs that can affect post-transcriptional gene expression. This is seen with silencing of mRNAs through complementary seed-region binding of a miRNA that binds to the 3' UTR of the mRNA and ultimately labels it for destruction. Our lab has previously shown and short-listed candidate miRNAs; miR-196a and miR-219, that are strongly associated with the NC (Ward et al., 2018). The first objective of this project was to confirm if these miRNAs were expressed in the *Xenopus* embryo and if they are expressed in the NC regions.

3.1.1 MiRNAs in Neural crest

NC is an ectodermal-derived tissue (Mayor and Theveneau, 2013). Some work on miRNAs in *Xenopus* ectoderm has been recently conducted by the Sater group. The aim was to investigate miRNAs in GRNs in developmental specification events. Using next-generation sequencing strategies over 170 miRNAs were identified in *Xenopus* ectoderm, of which 125 were novel to *Xenopus*. It was thought that miRNAs were involved in the specification and reduced competency of ectodermal tissues through downregulation of *Oct4* networks and signalling (Shah et al., 2016; Shah et al., 2017).

MiRNAs are often conserved across species (Bartel, 2004). A miRNA can have a 5p and a 3p form. For example, in the pri-miRNA stem-loop structure, the 5p miRNA is on the forward strand, and the 3p miRNA is on the reverse strand, giving some miRNAs multiple forms (Kenyon et al., 2019). Whole mount *in-situ* hybridisation is a commonly used method for gene expression analysis in embryos. A database of miRNA expression profiles in *Xenopus laevis* was created by the Wheeler group using this method. This used synthetic LNA oligonucleotides as the *in situ* probe. These were designed to

detect the mature miRNA. The advantage of these miRCURY LNA probes by Exiqon (now Qiagen) is that they bind with high specificity to the mature miRNA. At the time this was the first use of whole mount *in situ* hybridisation to document miRNA expression profiles in *Xenopus* (Ahmed et al., 2015).

The spatial and temporal expression of miR-196a and miR-219 in the pri-miRNA and mature miRNA in *Xenopus* was not identified in this paper. This chapter will address the gap in knowledge surrounding the spatial and temporal expression of miRNAs, of miR-196a and miR-219, by development of modified *in situ* hybridisation protocols and q-RT-PCR. This section will also try to address if the miRNAs are expressed in neural crest tissue, and if miRNA-196a and miRNA-219 are potentially implicated in NC development.

3.2.0 Results

3.2.1 Spatial and temporal expression of miRNAs in developing Xenopus neural crest

MiRNAs can be found in the genome as independent genes or in intronic regions of other genes (Bartel, 2004). MiR-196a is located within a *HoxC* cluster and miR-219 is its own independent gene (Fig. 3.1). Both miR-196a and miR-219 are highly conserved across the animal kingdom, including: *X. tropicalis*, zebrafish, chick, human, gorilla, and mouse (Fig 3.1).

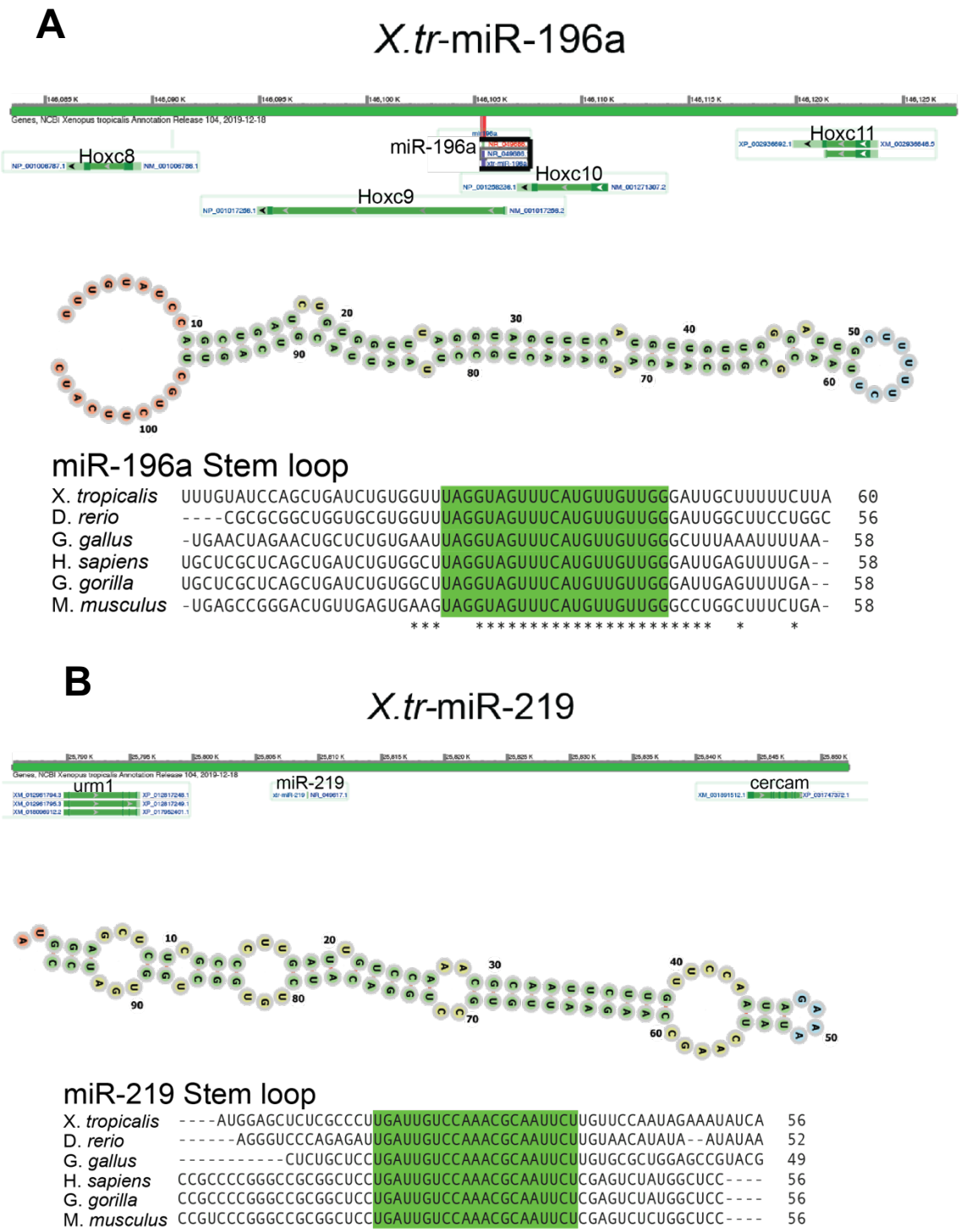

Figure 3.1- MiRNA structure and conservation. (A) Pri-miR-196a stem loop structure and location within the genome. (B) Pri-miR-219 stem loop structure and location within the genome. For (A) and (B) the stem loop sequence of miRNAs was accessed from miRbase and was aligned to *X. tropicalis* genome using BLAT on UCSC genome browser. miRNA stem loop structures as predicted using RNAfold Vienna http://rna.tbi.univie.ac.at/forna/forna.html?id=RNAfold/vCiQTz5Wd4&file=cent_probs.json. Sequence conservation of mature miRNA (green) in miRNA stem loops for miR-196a and miR-219. Sequences sourced from miRbase, correct as of November 2020 and aligned using Clustal omega multiple sequence alignment tool.

3.2.2 Q-RT-PCR

To ascertain a rapid temporal expression profile of miRNAs in *X. laevis* q-RT-PCR was performed. Both miRNAs have a very similar profile with early expression peaking at NF St.4 before dropping at gastrula stage of development and then rising at late-gastrula early neurula. Expression of miRNAs then peaks at St.25 before dropping at tadpole stages (Fig 3.2).

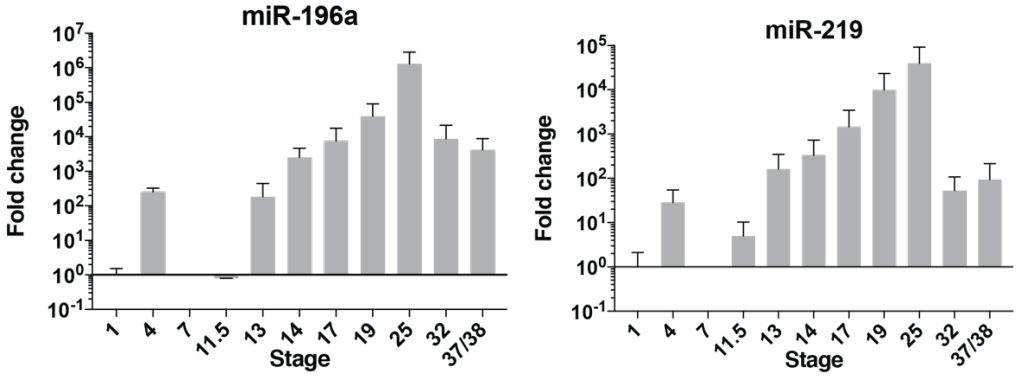

Figure 3.2- Q-RT-PCR showing temporal expression of miRNAs in *X. laevis* embryos. MiRNA expression peaks at tailbud development (St. 25) before reducing in tadpole development. Fold change is represented as mean +/- SD normalised to snU6. This data generated and analysed by master's student Michael van der Lee.

3.2.3 MiRNA probe synthesis

MiRNA expression can be detected for some miRNAs by whole mount *in situ* hybridisation. LNA probes have been previously used in the lab to visualize expression of miRNAs (Ahmed et al., 2015). Previously this had been used to visualise miR-196a and miR-219 but was unsuccessful. Therefore, careful optimization of hybridisation steps was carried out, according to (Sweetman, 2011; Sweetman et al., 2006). Although results improved, a pri-miRNA probe was trialled to see if clearer results could be achieved. A method had to be optimized to do this, but the key barrier to this was the development of a good RNA probe. Numerous primers were designed to amplify pri-miRNA from gDNA out of *X. tropicalis* embryos. miR-219 was generated by PCR of wild-type *X. tropicalis* gDNA with primer 219F4 and R2 to generate 626bp fragment. miR-196a was generated by PCR of WT *X. tropicalis* gDNA with primer 196 set 3 to produce a product of 666bp (Fig. 3.3A). The products were subsequently subcloned into pGEM T Easy (Fig 3.4). The plasmids generated then underwent further PCR with primers M13 to produce a miRNA template

(Fig 3.3B) for RNA transcription to produce a WISH antisense probe (Fig 3.3C). This probe could detect the pre-miRNA and pri-miRNA transcripts, but will be referred to as the pri-miRNA probe for simplicity.

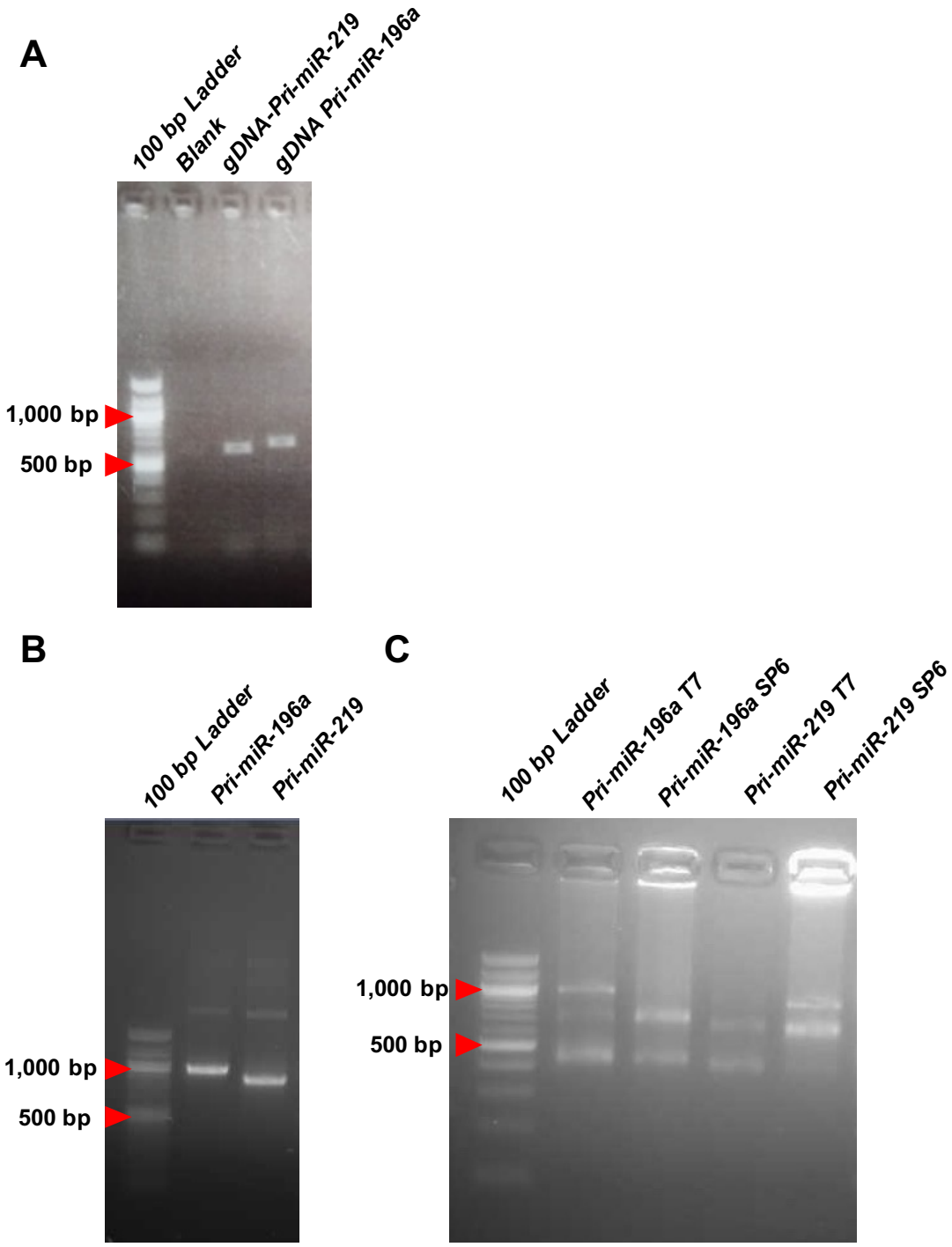

Figure 3.3 Generating pri-miRNA in situ probes. (A) PCR of gDNA from *X. tropicalis* to amplify pri-miR-219 with primer F4 and R2 to generate 626 bp amplicon, and to amplify pri-miR-196a with F3 and R3 to generate a 666 bp amplicon. (B) PCR of pri-miR-196a and pri-miR-219 plasmids with M13 primers to generate template for transcription. (C) Transcription of pri-miR probe template with T7/SP6 RNA polymerase to generate sense/antisense in situ hybridisation probes probes.

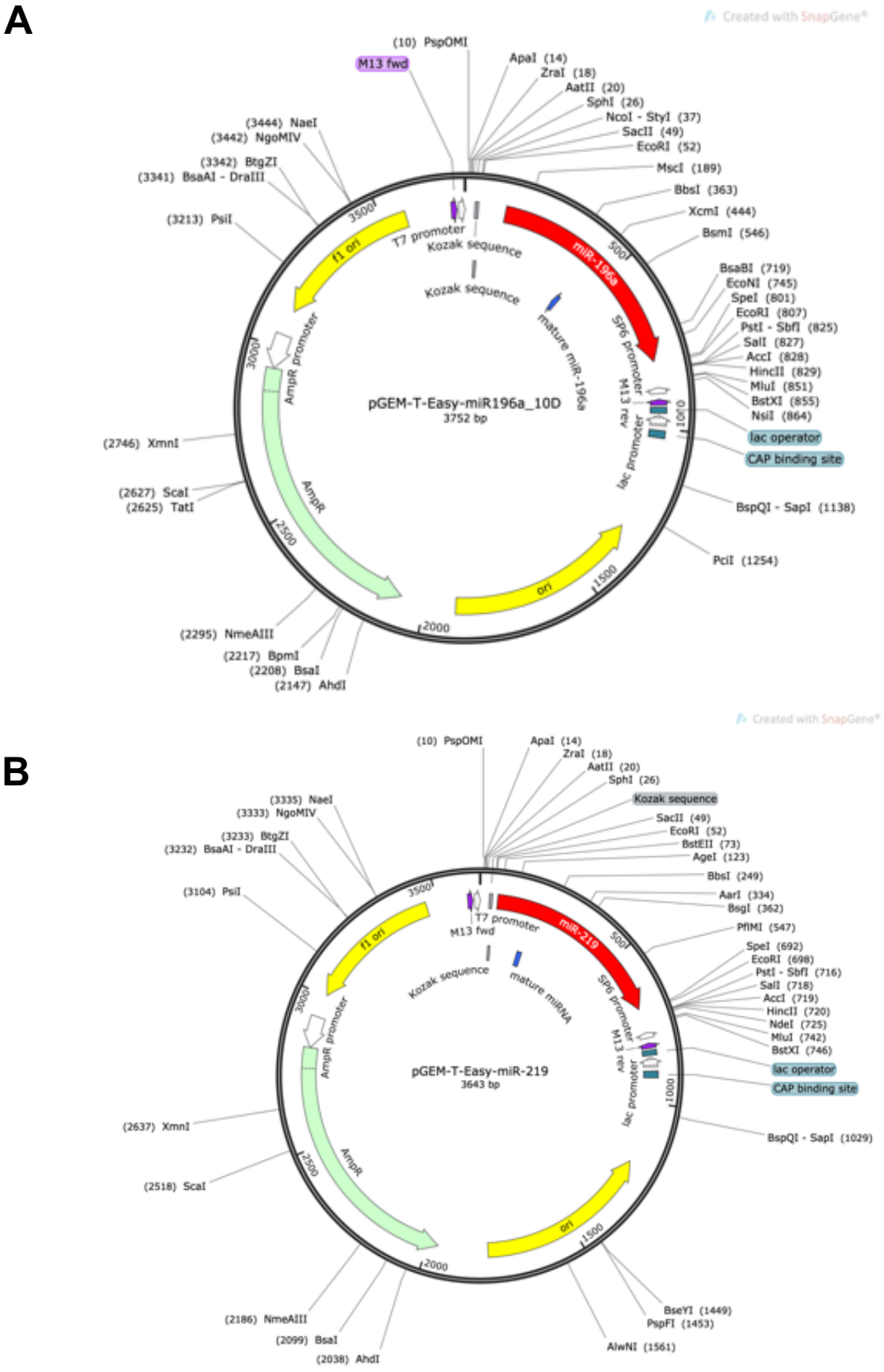

Figure 3.4 - Plasmids cloned from PCR of WT *X. tropicalis* genomic DNA. Plasmids contain pri-miR's for miR-196a (A) and miR-219 (B). Backbone vector is pGEM T Easy.

3.2.4 MiRNA expression in Xenopus

NC genes are first highly expressed in the neurula stage of *Xenopus* embryo development (Hong and Saint-Jeannet, 2007). Therefore, it was first decided to look at neurula miRNA expression and a later stage of development (Fig. 3.5). Both pri-miR-219 and pri-miR-196a share similar expression profiles at neurula stages. They were both highly expressed in the neural fold, neural plate and in the NC. At tadpole stage again the profile between the miRNAs is similar. Expression can be seen in the: eye, ventral branchial arches, the otic vesicle, the neural tissue running dorsally along the back of the tadpole. Looking at magnified panels regions of the brain, forebrain and hindbrain can also be seen to have miRNA expression. The sense probe used in the WISH of pri-miR-196a and pri-miR-219 shows no clear expression profile (Fig 3.5). The whole mount *in situ* hybridisation colour development of pri-miRNA took up to 48 hrs of development to get a clear profile. It was found that a clean profile was found if the colour development was conducted at room temperature or cooler over a longer period to reduce background signalling.

Mature miRNAs are short 20-22 nucleotides long (Bartel, 2004). Due to this they are too short to detect with a standard *in situ* hybridisation probe (Thompson et al., 2007). An optimal *in situ* probe is generally 500-700 bp in length. If the probe is longer, it can be difficult and take longer to hybridise, generating weaker profiles, if shorter it will give a lot of background signalling (Monsoro-Burq, 2007; Sive et al., 2007). Primers were designed to amplify the stem-loop pri-miRNA for miR-196a and miR-219 as outlined in section 3.2.2. These were then subcloned into pGEM-T-Easy to synthesise whole mount *in situ* hybridisation DIG-labelled antisense and sense probes.

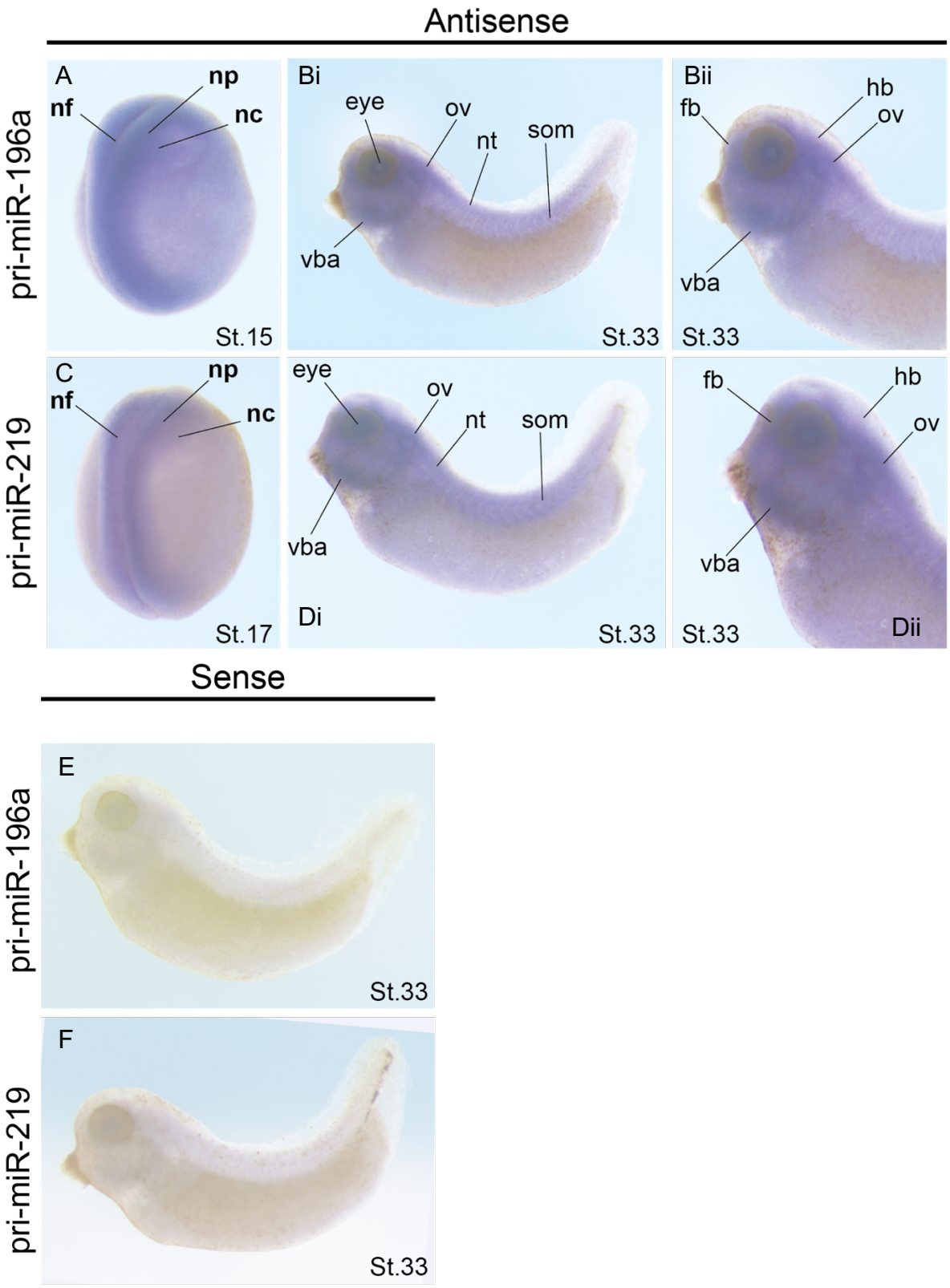

Figure 3.5 - Initial expression profile of pri-miR-196a and miR-219 in *X. tropicalis* neurula and tadpole embryos. MiRNAs are expressed in neural and NC tissues. Abbreviations: nf=neural fold, nc= neural crest, np= neural plate, br= brain, som= somites, vba= ventral branchial arches, op= otic placode. “AS” = antisense probe (A-D) “S”= sense probe (E-F).

Further whole mount *in situ* hybridisation experiments were carried out to see if pri-miRNAs were expressed in migratory NC populations by looking at expression in early tadpole and tailbud embryos. For pri-miR-196a the expression profile was similar to pri-miR-219. In the neurula stages, expression was seen in neural fold, neural plate, and NC. At St. 20 the NC expression was more diffuse (Fig. 3.6B). At early tailbud, St. 24 (Fig. 3.6C) the expression was more diffuse than miR-219, although expression in anterior structures like the eye and otic vesicle are discernible. At St. 26 (Fig. 3.6D & H) the branchial arches are clearly showing miRNA expression including the mandibular and hyoid arches (Fig 3.6). At the late neurula stages, 18 and 20, pri-miR-219 expression is highly expressed in the neural fold regions and neural plate, and somewhat expressed in NC (Fig. 3.6E, F). As the embryo developed into a tailbud tadpole at St. 24 the anterior most structures including the eye and otic vesicle showed some pri-miR-219 expression. At early tadpole stage, St. 26, expression can be seen across the craniofacial features, the branchial arches, the brain regions, and the eye as well as in the early spinal cord (Fig 3.6 G-H).

To further confirm spatial expression of miRNAs some *X. tropicalis* embryos were processed by cryosectioning. Neurula stage and tailbud stages were selected. The *in situ* processed embryos for sectioning were left to develop for extra time in colour reaction solution to give the best chance of seeing expression in these sections. Fig 3.7 showed less clear expression of pri-miR-196a. Fig. 3.7Aii and Bii show stronger neural than NC expression. At tailbud stage expression can be seen in some head structures such as the mesencephalic vesicle and less intensely in the lens placode (Fig. 3.7 Ai). Intense expression can be seen in Fig. 3.7Bi-Di in the notochord, and to a lesser extent the spinal cord and potentially in NC cells.

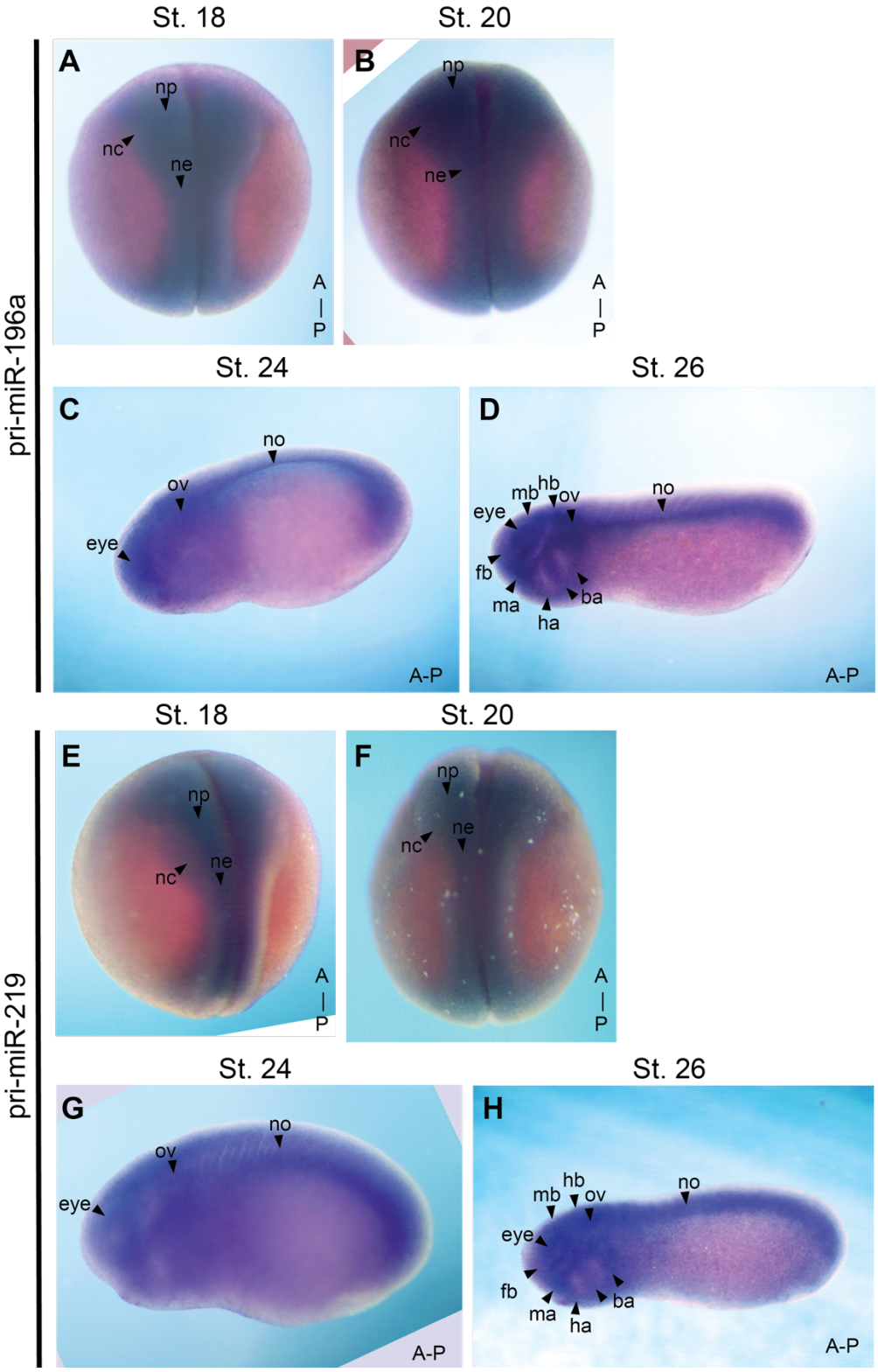

Figure 3.6 - Expression profile of pri-miR-196a and pri-miR-219 at neurula, tailbud and early *X. tropicalis* tadpole stages. (A-D) Pri-miR-196a, (E-H) Pri-miR-219 covering St 18, St 20, St 24 and St. 26. Neurula embryos are orientated anterior top and tailbud and tadpoles are orientated with anterior end of the embryo facing left. Pri-miRNAs can be seen to be expressed in neural and NC tissues. Abbreviations: eye= eye, ov= otic vesicle, ba= branchial arches, no= notochord, mb= midbrain, hb= hindbrain, fb= forebrain, ma= mandibular arch, ha= hyoid arch, np= neural plate, ne= neural ectoderm, nc= neural crest.

The expression of pri-miR-219 was also further assayed by cryosectioning embryos (Fig 3.8). Again, the whole-mount profile was cleaner for pri-miR-219 than for pri-miR-196a. Expression can be seen in NC, particularly in cranial NC regions in the bottom left area circled. Similarly, to pri-miR-196a, pri-miR-219 can be seen in spinal cord and notochord (Fig. 3.8Ai-Di). Fig. 3.8 Ei showed intense expression of pri-miR-219 in the medial portion of the spinal cord, likely in spinal ganglia. In Fig. 3.8 Fi expression can be weakly seen in the pronephric region of the embryo.

To confirm if the pri-miRNA and NC expression overlapped, a double whole mount *in situ* hybridisation experiment was used. To do this, Sox10 was used as a FITC labelled probe and pri-miRNA as a DIG labelled probe for red and purple/blue development respectively. There was some overlap between pri-miRNA-196a and pri-miRNA-219 and Sox10 expression, in the antero-dorsal region of the embryo (Fig. 3.9). This region of pri-miRNA expression covered the otic placode and craniofacial region and was also seen in sections in Fig. 3.7-3.8 in craniofacial tissues.

For analysing mature miRNA expression in developing embryos, LNA probes can be used. These are designed against the 20-mer mature miRNA (Ahmed et al., 2015; Sweetman et al., 2006). In Fig. 3.10, a range of miRNA expression profiles can be seen; miR-133b can be clearly and exclusively expressed in the somites (Fig. 3.10 A-B), miR-196a; can be seen in the NC, neural fold, and neural border (Fig. 3.10 B-C), miR-219 and has the same profile as miR-196a (Fig. 3.10 C-D, lastly miR-302 and can be seen in the neural tissue and neural plate (Fig. 3.10 F-G).

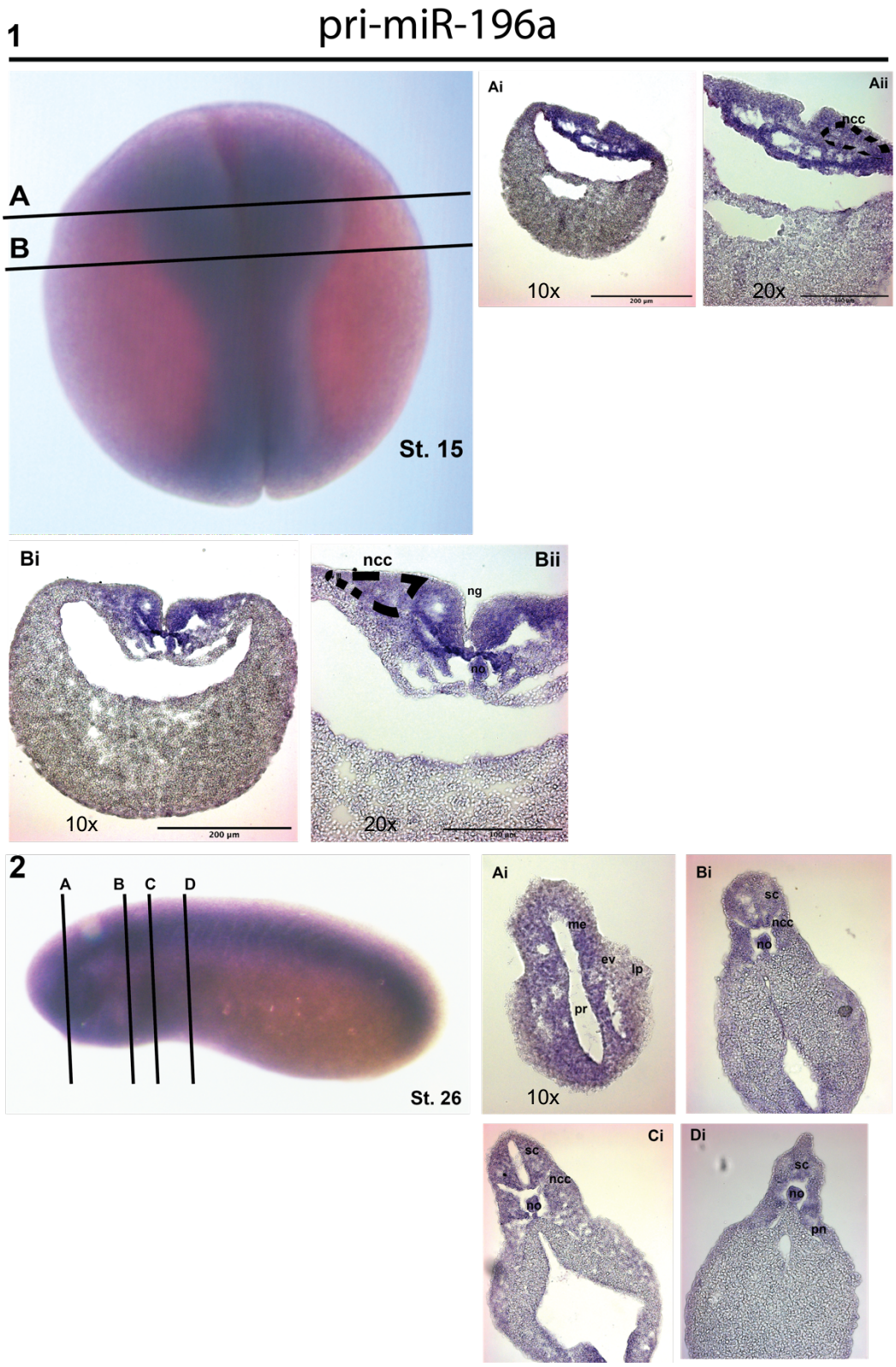

Figure 3.7 - Expression profile of pri-miR-196a in *X. tropicalis* embryos. 1- NF St.15 embryo with DIG-labelled pri-miR-196a antisense probe. 1A-B- sections of same embryo; A shows neural and NC at the edges in the outlined area with B showing further expression in the notochord. 2- NF St. 26 embryo A-D moving posteriorly through the embryo. Expression can be seen in the NC in Bi and Ci. Ncc- neural crest cell, ng- neural groove, me- mesencephalic vesicle, ev- eye vesicle, lp- lens placode, no- notochord, sc- spinal cord/ganglia, pr- prosencephalic vesicle.

1 pri-miR-219

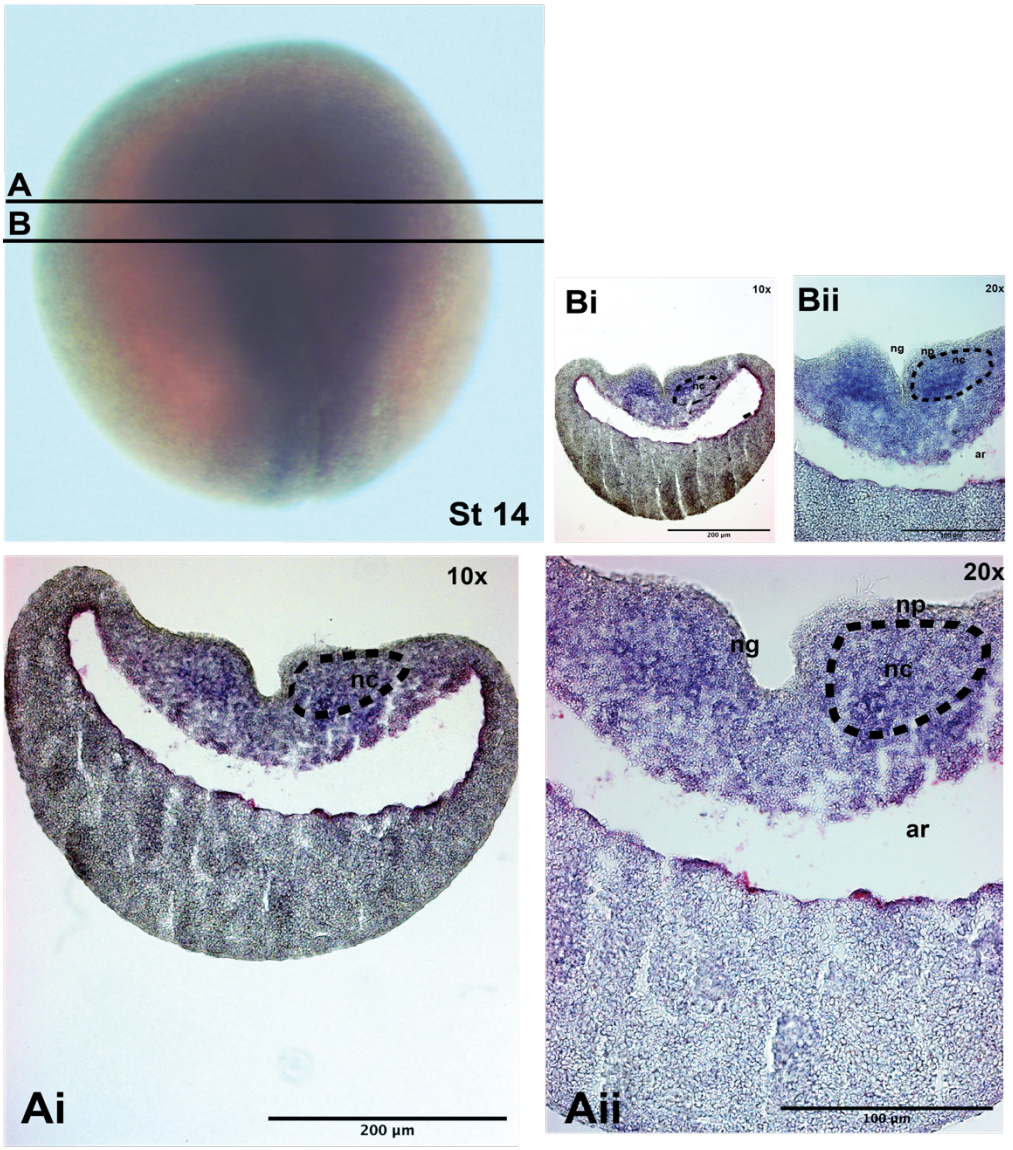

2

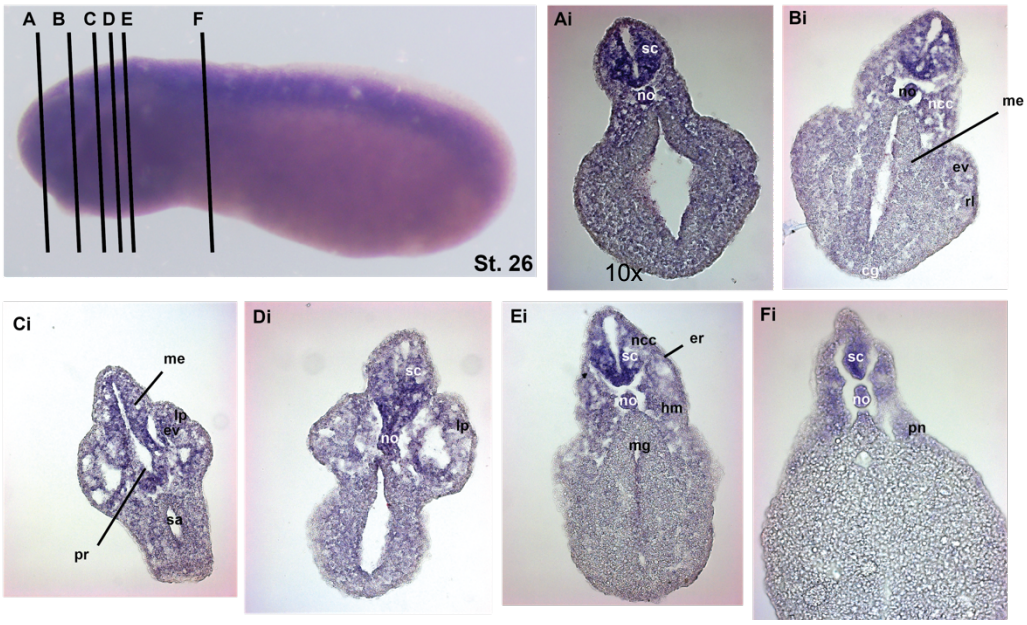

Figure 3.8 - Expression profile of pri-miR-219 in *X. tropicalis* embryos. 1- NF St.14 embryo with DIG-labelled pri-miR-219 antisense probe. 1A-1B Sections of same embryo, A shows neural crest in the outlined area with B showing stronger expression. 2- NF st. 26 embryo A-F moving posteriorly through the embryo. Expression can be seen in the neural crest in 2Bi and 2Ci. Ncc= neural crest cell, ng= neural groove, me= mesencephalic vesicle, ev= eye vesicle, lp= lens placode, no= notochord, sc= spinal cord/ganglia, pr= prosencephalic vesicle, pn= pronephric anlage, cg= cement gland, rl= prospective retinal layer, mg=midgut, sa= stromodeal anlage, er= ear vesicle, hm= head mesenchyme.

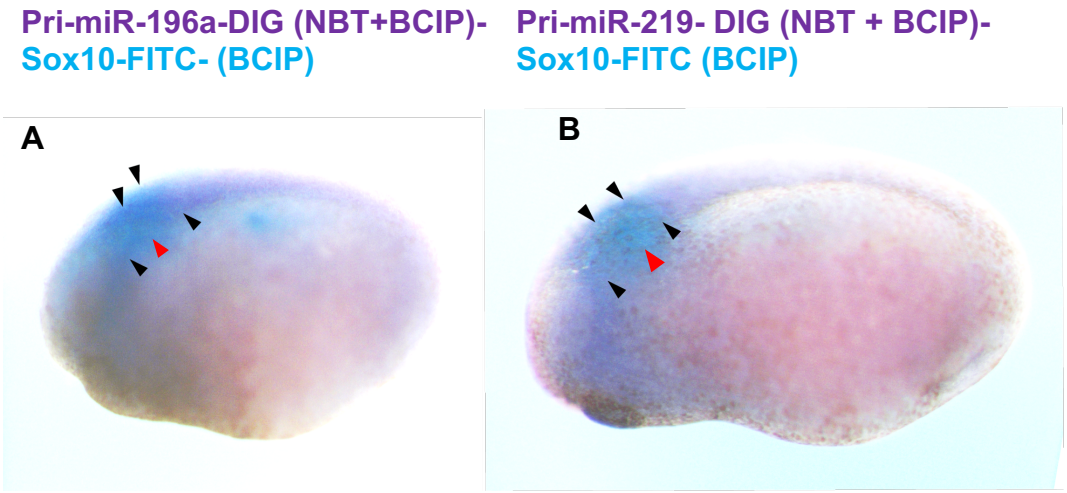

Figure 3.9 - Double WISH of pri-miR-196a and pri-miR-219 DIG and Sox10 BCIP. (A)Pri-miR-196a can be seen in purple in the anterior regions of the embryo and Sox10 in blue with overlap (black arrows) in the otic region (red arrow) . Embryo is St. 20. (B) Pri-miR-219 expression can be seen in purple in anterior regions of the embryos with overlap in the otic region of the embryo, denoted by black arrows. Embryo is St. 22. Both are *X. tropicalis embryos.* The anterior end of the embryo is left, posterior right, dorsal top, ventral bottom.

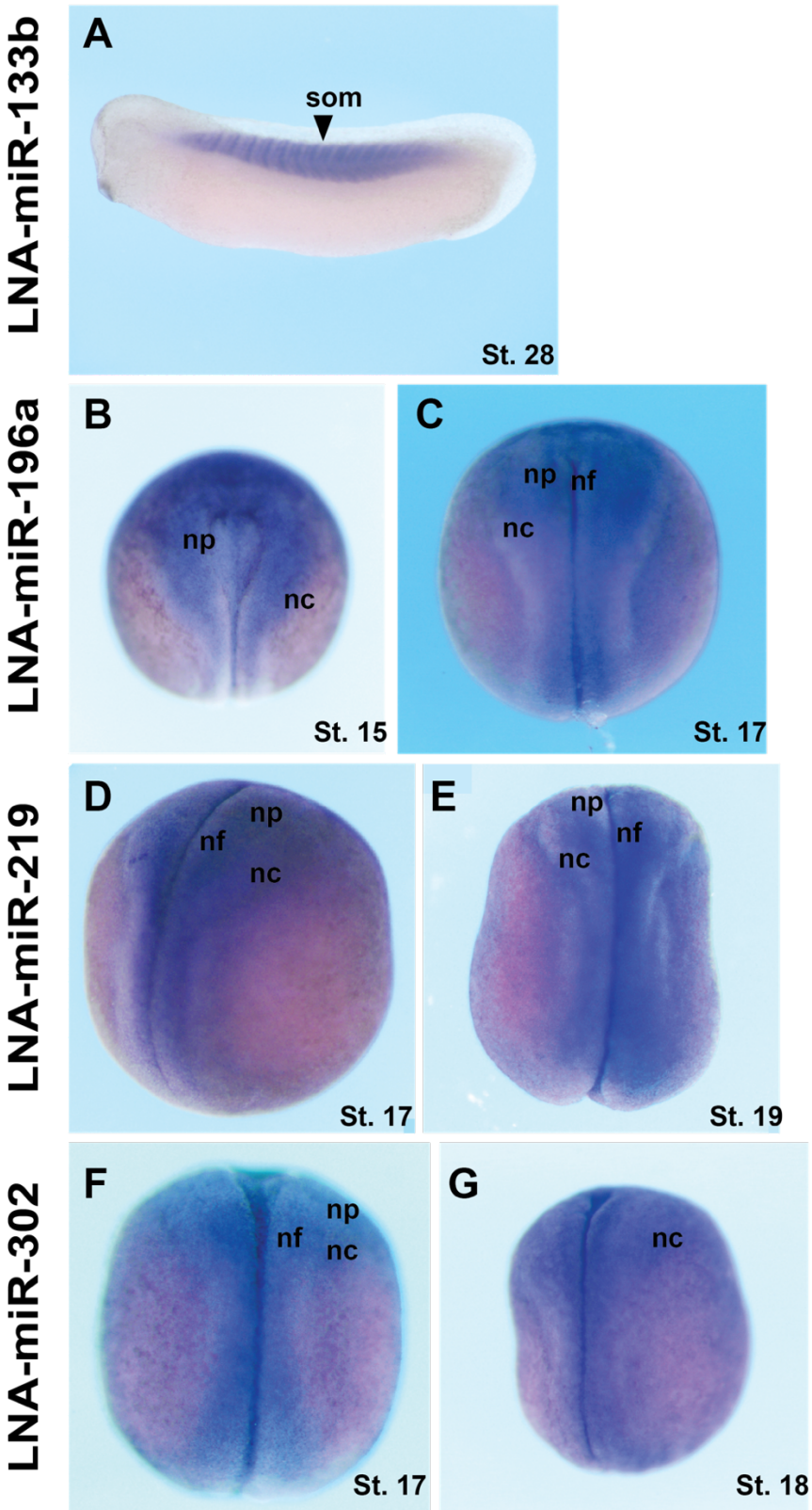

Figure 3.10 - *Xenopus laevis* LNA miR WISH expression profile. (A-B) LNA-miR133b, (B-C) LNA-miR-196a, (D-E) LNA-miR-219, (F-G) LNA-miR-302. miR-133b is expressed in somites, miR-196a and miR-219 are expressed in neural and NC tissues and miR-302 is seen in neural tissues. Abbreviations: som= somites, np= neural plate, nc= neural crest, nf= neural fold. Embryos orientated anterior top, posterior bottom, ventral facing. Embryo A is a tadpole St.28 and is anterior left, posterior right, dorsal top, ventral bottom. Stages as shown on panels.

3.2.5 MiRNA expression in chick

As shown in section 3.2.1 Fig. 3.1, miR-196a and miR-219 are highly conserved across the animal kingdom. I therefore decided to look at the expression of miR-196a and miR-219 in the chick embryo. The predicted mature miRNA sequence for chick and for *Xenopus* are identical for both miR-196a and miR-219 (Fig. 3.1) and therefore our LNA probe would work for both species.

As used above, miR-133b was used as a positive control LNA probe when looking at miRNA expression in developing chick embryos (Fig. 3.11 A). MiR-133b expression can be clearly seen in cardiac tissue and somites in developing chick embryos. Sox10 was used as a NC marker for cross-comparison and evaluation of NC expression (Fig. 3.11 B-E), (Hatch et al., 2016; Milet and Monsoro-Burq, 2012). Sox10 is expressed in NC and can be seen in head mesenchyme where there is migratory cranial NC, and in otic NC in the chick embryos.

MiRNA-196a (Fig. 3.11 F-L) and miR-219 expression (Fig. 3.11 M-U) can be seen from St HH8, the expression profile is more neural and in the anterior region of the embryo. At HH10-12 the expression then is found in the forebrain, midbrain, hindbrain, and neural tube/spinal cord. At HH12 migrating neural crest populations can be seen. At HH14 the spinal cord has miR-expression.

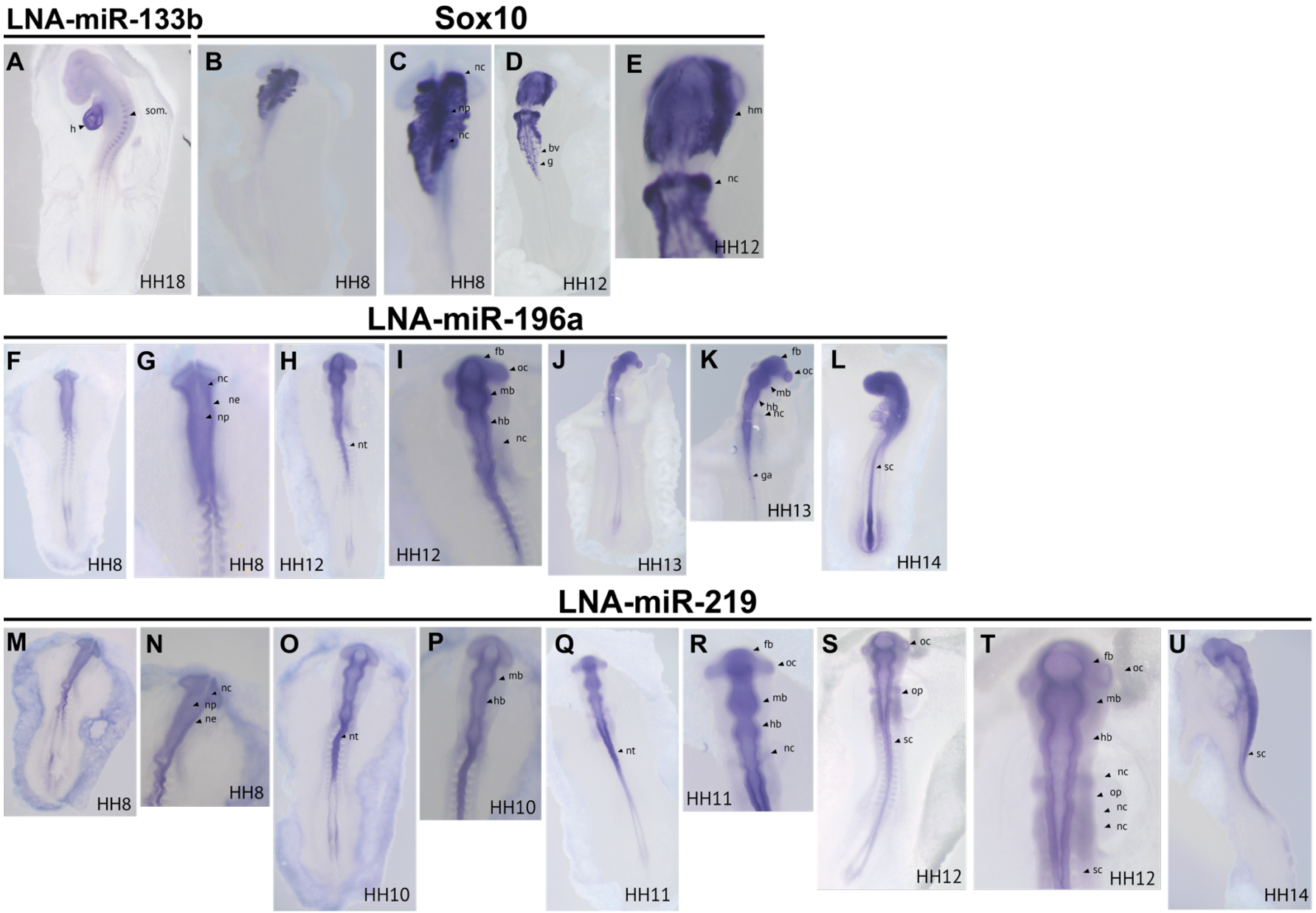
LNA-miR-133b
Sox10
A
som.
h
HH18
B
HH8
C
nc
np
nc
HH8
D
bv
g
HH12
E
hm
nc
HH12
LNA-miR-196a
F
HH8
G
nc
ne
np
HH8
H
nt
HH12
I
fb
oc
mb
hb
nc
HH12
J
HH13
K
fb
oc
mb
hb
nc
ga
HH13
L
sc
HH14
LNA-miR-219
M
HH8
N
nc
np
ne
HH8
O
nt
HH10
P
mb
hb
HH10
Q
nt
HH11
R
fb
oc
mb
hb
nc
HH11
S
oc
op
sc
HH12
T
fb
oc
mb
hb
nc
op
nc
nc
sc
HH12
U
sc
HH14

Figure 3*.11* - Chick embryo miRNA LNA and Sox10 expression profiling by whole mount in situ hybridisation. (A) LNA-miR-133b is expressed in somites and heart tissues. (B-E) Sox10 is expressed in the developing NC. (F-L) LNA- miR-196a and (M-U) LNA-miR-219 are expressed in NC and neural tissues. Hamilton and Hamburger stages (HH) denoted on individual panels. All panels imaged at 3.2 x magnification except: E, G, N, R and T which were imaged at 5 x magnification. Abbreviations: bv= blood vessels, fb= forebrain, h= heart, g= spinal ganglia, hb= hindbrain, hm= head mesenchyme, mb= midbrain, nc= neural crest, ne= neural, np= neural plate, nt= neural tube, oc= optic cup, op= otic placode, sc= spinal cord, som.=somites.

3.3.0 Discussion

The aim of this chapter was to investigate the spatial and temporal expression of miR-196a and miR-219 in *Xenopus* embryonic development as at the start of the project this was unclear. It was also hoped that miR-196a and miR-219 would be further validated as potentially being implicated in NC development. q-RT-PCR data showed that miRNA-196a and miR-219 were highly expressed from neurula stages of *Xenopus* embryo development through to tail bud stages before expression reduced (Fig. 3.2), this justified the use of neurula, and tail bud stage embryos used for visualising miRNA expression by whole mount *in situ* hybridisation experiments.

3.3.1 MiR WISH probe design & expression profile

The results seen in Figs 3.5-3.11, describing the spatial and temporal expression profile of pri-miR-196a and pri-miR-219, were significant as this was previously unknown.

3.3.2 LNA probe design and principles

The LNA miRNA probes were developing the profile of the mature miRNA. The turnover of a pri-miRNA is quite rapid, so this may explain why the pri-miRNA profiles were more diffuse than the mature miRNA experiments. Therefore, a whole mount *in situ* hybridisation experiment on the mature miRNA was optimal to cross-reference the miRNA profiles against each other and in relation to NC expression (Zhou et al., 2018).

Whole mount *in situ* hybridisation is a traditionally and widely used methodology to visualise gene expression in embryonic development (Darnell and Antin, 2014). Initially an antisense RNA *in situ* probe is designed and

synthesised. To do this, usually the cDNA template of the target mRNA of interest must be known and acquired. The design of an RNA antisense probe is limited in that it must be of at least 300 bp in length to have a chance of being effective and not degraded by RNases. This may be problematic if the user is looking at shorter transcripts, individual exons and importantly, miRNAs. To overcome this the design of LNA probes allows the user to target 12-24 nucleotide sequences and targets. An LNA probe consists of synthetic modified oligonucleotides that have a methylene bridge between the 2'O and the 4'C on the ribose ring structure that gives the oligo a stable and efficient binding affinity for the target of interest. One advantage of this is the increase in specificity and sensitivity of the probe (Darnell et al., 2010; Sweetman et al., 2006).

Previous work has utilised LNA miRNA *in situ* probes to detect spatial expression of miRNAs in developing *Xenopus* and chick embryos (Ahmed et al., 2015; Sweetman et al., 2006; Viaut et al., 2021). One limitation to using LNA probes is that the *in situs* can be very weak depending on the miRNA expression level (Fig. 3.10), (Ruegger and Grosshans, 2012).

By using LNA probes the spatial and temporal expression of miR-196a and miR-219 was revealed to be in neural and NC tissue at neurula, tailbud and tadpole stages. LNA probes were designed to the shorter mature miRNA sequence; (sequences can be seen in section 2.5.1). This is the portion of the miRNA that has an effect in post-transcriptional regulation of gene expression through seed-region binding to a complementary 3' UTR of a mRNA. This may explain the weaker staining and expression profile seen in Fig. 3.10 versus Fig. 3.5-3.9 which use pri-miRNA probes (Agarwal et al., 2015; Alberti and Cochella, 2017; Bartel, 2004; Inui et al., 2010). As *in situ* hybridisation experiments are not quantitative it was therefore important to have q-RT-PCR data generated in Fig. 3.2 where similar profiles of expression for both miR-196a and miR-219 is shown. Therefore, differences in the depth of signal shown by in situ experiments is limited.

Previous work in the lab with LNA probes had identified some anterior expression of miR-219 in *Xenopus* development, but this had no mention of NC and no supporting image. In addition, miR-196a did not generate any staining (Ahmed et al., 2015). After some temperature optimisation of hybridisation steps in the *in situ* protocol, as advised by (Sweetman, 2011; Sweetman et al., 2006), expression profiles were developed (Fig. 3.10) for *Xenopus*. MiR-302 is seen in neural and NC regions in developing *X. laevis* embryos. Hybridisation temperature steps were optimised to 54^{o}C for profiling miR-196a and miR-219 and were also used when looking at miR-133b and miR-302 (Fig. 3.10).

Other labs had used LNA probes to show expression in chick embryo development (Ritter et al., 2020; Viaut et al., 2021). Expression of miR-133b is clearly expressed in mesoderm tissue (heart, somites), (Chen et al., 2006). MiR-196a and miR-219 expression can be seen in the NC and neural plate regions. It is a significant finding to see that miR-196a and miR-219 are expressed not only in *Xenopus* NC, (Fig. 3.10) but also chick NC (Fig. 3.11). As previously shown, these miRNAs are highly conserved (Fig. 3.1), so this was to be expected. Due to the high turnover of mature miRNA's pri-miRNA probes were developed and trialled to see if a clearer profile could be obtained (Ruegger and Grosshans, 2012).

Overall, the pri-miRNA profiles for miR-219 and miR-196a (Fig. 3.5-3.9) in *X. tropicalis* are stronger than the LNA miRNA profiles (Fig. 3.10) and are most clearly seen in the anterior structures as described. This is not surprising as these miRNAs are thought to be implicated in the NC. The NC can give rise to many cranial structures not limited to: craniofacial skeleton, parts of the jaw, teeth and parts of the ear (Cordero et al., 2011; Simoes-Costa and Bronner, 2015). These populations of the NC are migratory from the trunk region of the embryo and migrate large distances. This may explain the unclear expression profiles of the embryos at St 24 where cranial NC populations are migrating from the trunk (Alfandari et al., 2010; Lukoseviciute et al., 2018; Mayor and Theveneau, 2013).

Other labs, like the Harland lab have previously taken a similar approach to visualize miRNA expression in the *X. tropicalis* embryonic development. They also generated a pri-miRNA by PCR from gDNA (Walker and Harland, 2008). Therefore, it was a significant finding to produce clean and functioning whole mount *in situ* hybridisation probes for our miRNAs.

To ascertain clearer expression profiles in craniofacial and other neural crest derivatives cryo-sectioning was used. Expression of NC in cranial arches is seen but the resolution and clarity as to which arches is less clear in the tail bud stage embryos (St. 24-26), (Fig. 3.7-3.8). At neurula stage both miRNAs can be seen weakly in NC. In the tail bud stage embryo sections both miRNAs can be seen in eye structures such as lens placode, although miR-219 is more highly expressed than miR-196a (Fig. 3.7-3.8). miR-196a has previously been shown to be implicated in eye development processes in *Xenopus*, it is therefore unsurprising that we saw expression here (Gessert et al., 2010; Qiu et al., 2009).

Previous work in the lab also profiled miRNA expression in NC animal explants. MiR-196a was found to be enriched in neural and NC tissue. Whereas miR-219 was found to be significantly and uniquely expressed in NC tissue (Ward et al., 2018). Therefore, it was expected that the LNA miRNA probe would show that miR-219 was cleanly expressed in NC, this was not the case, and neural expression was observed. Reasons for this are unclear but could be due to limitations of animal cap experiments which do not always account for neural induction and inductive signals so this may not have been picked up this time, (Linker et al., 2009). However, as expected miR-196a was seen in neural and NC tissue.

3.3.3 Double in situ

To reveal if miR-196a and miR-219 expression overlaps with NC expression a double whole mount *in situ* hybridisation experiment was carried out to show expression of a miRNA and Sox10 simultaneously in two different colours (Fig. 3.9). An antisense probe with a FITC-labelled Sox10 for NC and a DIG-labelled pri-miRNA was generated. When developing a double in situ in colour reaction

solution it is best to do the weakest staining first. To develop a colour reaction of a miRNA takes a few days at least, so this was prioritised and then Sox10 was developed. By the time the *Sox10* expression was developed the profile was weaker, and FITC probe development with Fast Red did not work effectively when used in double *in situ* hybridisation experiments, potentially due to the increased time taken to develop the miRNA profile the FITC development may not be stable enough to undergo lengthy processing steps (Fig. 3.9). Due to lack of time to investigate further owing to the first COVID-19 lockdown this work was adjusted to use the probes I had generated but to generate another colour, this time turquoise. The Sox10 probe was developed with BCIP to generate the turquoise colour. Due to the similarity in colour between the turquoise (Sox10) and miRNA (purple) where they overlap in expression it is a darker colour as indicated by arrows (Fig. 3.9). To confirm this fluorescent marker would be needed, FITC was developed with Fast-Red but was too weak to visualise after miRNA colour development. Sox10 GFP *Xenopus* lines have been generated by other labs. Future work could involve use of these to visualise co-expression of miRNAs in NC (Alkobtawi et al., 2018). Other work could utilise *in situ* hybridisation chain reaction. Hybridisation chain reaction offers high-resolution imaging of harder to detect mRNAs and transcripts. This would give higher resolution and reduce background signalling as upon probe binding the probe undergoes a chain reaction to give more sites for visualisation and thus a brighter and cleaner signal (Choi et al., 2018).

3.4.0 Conclusions

The aim of this chapter was to investigate the spatial and temporal expression of miR-196a and miR-219 and to determine if these miRNAs are implicated in NC developmental processes. Through extensive *in situ* hybridisation experiments the spatial expression of miRNAs was found to be in neural tissues including NC. Through q-RT-PCR analysis the temporal expression of miR-196a and miR-219 was found to initially be expressed at St.4, but reappear in neurula development (St. 13-19) before peaking at the tailbud stage of development (St. 26).

CHAPTER IV

RESULTS:

Loss of function analysis of miRNAs: Part I, morpholino knockdown

4.0 Introduction

MiRNAs are widely reported to be implicated in embryonic developmental processes (Ahmed et al., 2015; Goljanek-Whysall et al., 2014; Ward et al., 2018). MiRNAs were first found in the lab to be expressed in NC through small RNA-sequencing experiments on animal-cap tissue (Ward et al., 2018). MiRNAs are contained within intergenic, intronic and exonic regions of the genome (Olena and Patton, 2010). MiR-196a is located within a *Hoxc* cluster in the genome, and miR-219 is located downstream of the urm1 gene. Both miRNAs have a pri-miRNA stem-loop structure that is highly conserved in the animal kingdom (Chapter 3, Fig 3.1).

MOs have been used for over two decades in developmental biology research with many thousands of studies carried out (Blum et al., 2015; Heasman et al., 2000). MOs can be used to better understand signalling and regulatory pathways through stable KD of mRNAs (Bedell et al., 2011). MOs are antisense oligonucleotides, normally designed to target splice sites or translation start sites in mRNAs. When using MOs to target miRNAs, they can be designed to target Drosha and Dicer cleavage sites, binding complementarily, distorting the site, and preventing binding and cleavage by Drosha and Dicer (Fig. 4.1B-C). Additionally, a MO can be designed to be complementary to the mature miRNA (Fig. 4.1A), preventing the miRNA from exerting its affect. All these approaches should yield the same phenotype (Flynt et al., 2017). Our MOs targeted the mature miRNA (Fig. 4.1D). Careful control and validation experiments must be conducted when working with MOs, with rescue experiments viewed as the gold standard to decipher if the phenotypes generated following MO KD are specific (Eisen and Smith, 2008). MiR-196a and miR-219 have been shown in the previous chapter to be expressed at neurula stages of development, corroborating previous research in the lab that shortlisted these miRNAs as candidates of interest (Ward et al., 2018). In the first section of this chapter I will describe the optimisation of the MO KD and the optimization of the miRNA mimic rescue system I have designed. I shall also describe experiments related to the sequence homology of miRNA-196a and miR-296b. I will then describe the functional experiments in more detail in respect to their biological function.

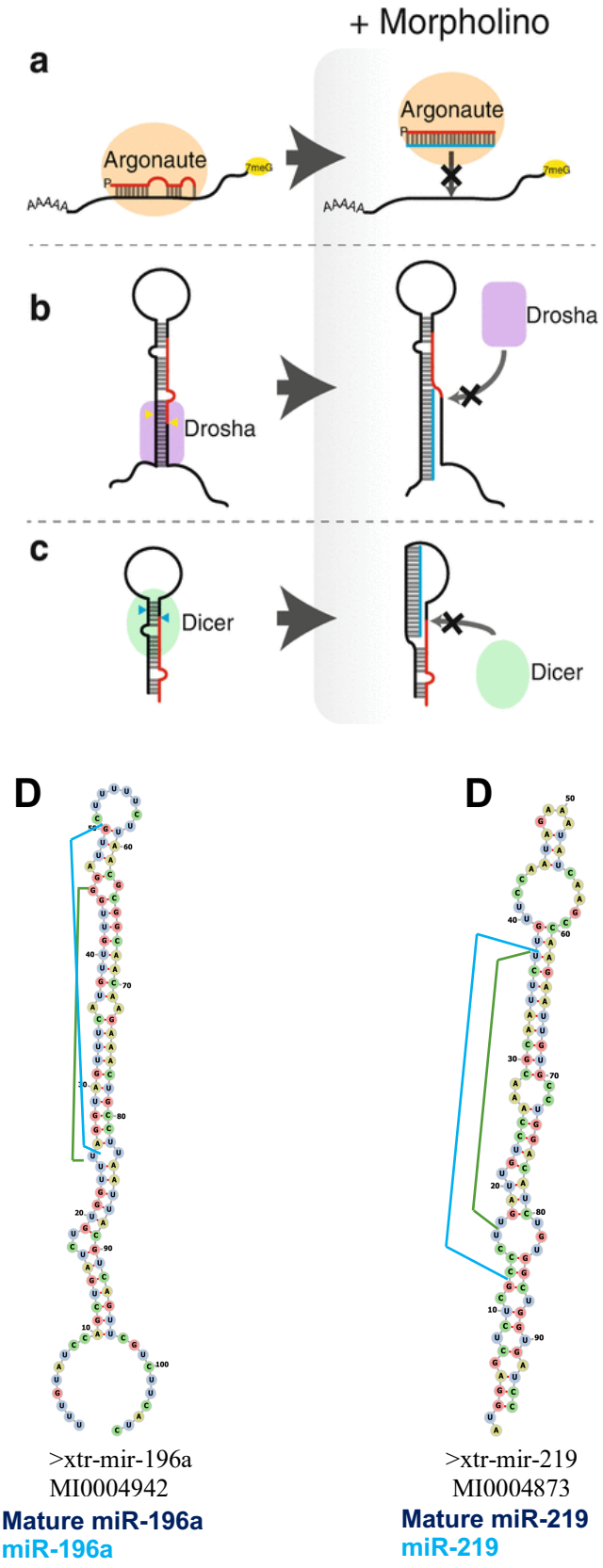

Figure 4.1 - Overview of morpholino design options to target miRNAs. (A) MO designed to target mature miRNA. (B) MO designed to perturb Drosha sites. (C) MO designed to target Dicer sites. (Di) MiR-196a MO design and (Dii) miR-219 MO design, both designed to target mature miRNA. miRNA sequences obtained from miRbase, accession numbers listed. Secondary structures of miRNAs visualised on rna.tbi.univie.ac.at/forna as described in methods.

4.1.0 Morpholino optimisation

To investigate the role of miRNAs in NC, MOs targeting miRNA-196a and miR-219 were designed (Fig. 4.1). A control MO denoted as “MM” was a mis-match control MO, it has five mismatches from the MO “MO” and is thus not expected to have an effect on the miRNA in development (Heasman, 2002). This project was started by a previous PhD student Nicole Ward, her thesis is referenced here (Ward, 2017). Dr. Ward generated some preliminary MO KD data and optimized the doses of MO’s used in this project at the beginning of my PhD with me. The dose response was validated by q-RT-PCR and for these reasons, I did not need to repeat this work.

X. laevis embryos were injected with various doses of MOs to create a dose-response and analysed by q-RT-PCR. It was found that micro injection of 60 ng of MO was optimal. To determine the impact of miRNA on NC development *X. laevis* embryos were injected at a 4 cell stage with 20, 40 and 60 ng of miR-219 MO along with lacZ tracer cRNA, into the right dorsal blastomere. The injected side is always shown in figures as the right side of the embryo. Impact on NC development after KD was analysed by whole mount *in situ* hybridisation experiments with NC marker Snail2 (Fig. 4.2). 40 ng and 60 ng of MO each led to 45% of embryos showing a decrease in Snail2 expression (Fig. 4.2B). MiR-196a MO dose response *in situ* experiments had also previously been conducted by Nicole Ward, so these were not repeated, they also showed 60 ng of MO was optimal.

4.2.0 MiRNA Rescue

4.2.1 MiRNA MO specificity

It was only discovered later in the thesis that miR-196a had a -*b* isoform, miR-196b (Table 4.1). Despite being on different chromosomes, the processed mature miRNA sequence of miR-196a, compared to miR-196b, is only one nucleotide different; and therefore, it was highly likely that the MO could target both miR-196 isoforms. To ascertain specificity of miRNA MO for targeting miR-196a q-RT-PCR was carried out to quantify this (Fig. 4.3).

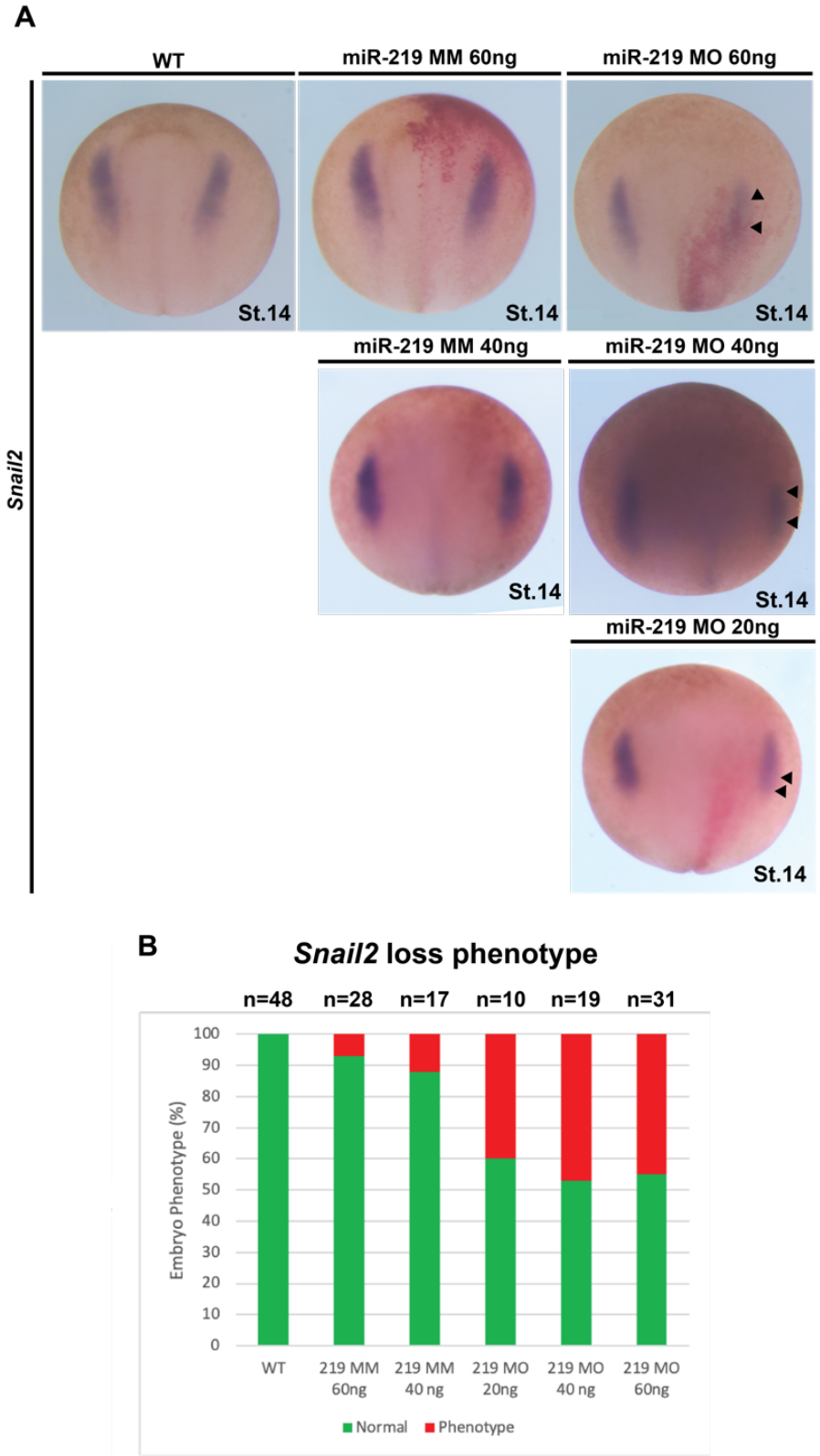

Figure 4.2 - miR-219 MO dose response. MO was injected into *X. laevis* embryos at 4 cell stage with 10 nL at a concentration of 20, 40 and 60ng MO with 300 pg lacZ cRNA tracer. Injected side of embryo is right side. Black arrows indicate region of phenotypic interest. Increasing MO dose reduces Snail2 expression. (A) shows Snail2 WISH phenotypes. First column WT embryos, then a mis-match control MO, then experimental MO KD. (B) The count data displaying the number of embryos exhibiting a loss of Snail2 phenotype.

Table 4.1 Comparison of miR-196a vs miR-196b sequences in relation to designed MO. Sequences obtained from miRbase (http://www.mirbase.org/). Green highlight is mature miRNA sequence.

MiRNA	MiRNA sequence 5'-3'	MO sequence 5'-3'	Genomic location
miR-196a Accession number: MI0004942	UAGGUAGUUUCAUG UUGUUGG	CAATCCCAACAAC ATGAAACTACCT	chr2: 142905363-142905468 [-]
miR-196b Accession number: MI0004943	UAGGUAGUUUUAUG UUGUUGG	N/A	chr6: 32896531-32896617 [+]

To quantify the impact of MO KD of miR-196a on miR-196b q-RT-PCR was carried out. Five neurula St.14 embryos were pooled to make one biological replicate, the q-RT-PCR was carried out with three biological and three technical replicates (Fig. 4.3). Embryos were treated with 60 ng of miR-196a MM MO, miR-196a MO 60 ng, or miR-196a MO 60 ng with miR-196a miRNA mimic 15 µM. MiRNA expression was normalised to snU6 housekeeping gene. Mismatch (MM) group was used as the experimental control group for delta delta ct analysis when analysing fold change. For miR-196a expression, following MO KD there is a significant 92% reduction in expression compared to the mismatch MO control group. This KD of miR-196a was significantly rescued with addition of a synthetic miR-196a miRNA mimic; with an 84% increase in miR-196a expression in the rescue group compared to the MO group. However, when looking at miR-196b expression on the same samples a significant 81% reduction in miR-196b expression is shown following miR-196a MO KD. This shows the MO for miR-196a is also targeting miR-196b. Despite this when adding miR-196a mimic with miR-196a MO no rescue is observed. This suggested the miRNA mimic at least is specific as the mimic was designed against the mature miRNA.

The intention of this body of work and the MO designed by previous lab members was to target miR-196a, therefore for simplicity all the figures denote

miR-196a with the caveat that the phenotype generated may not be specific and could target miR-196b. Despite this the miR-196a rescue is specific to miR-196a.

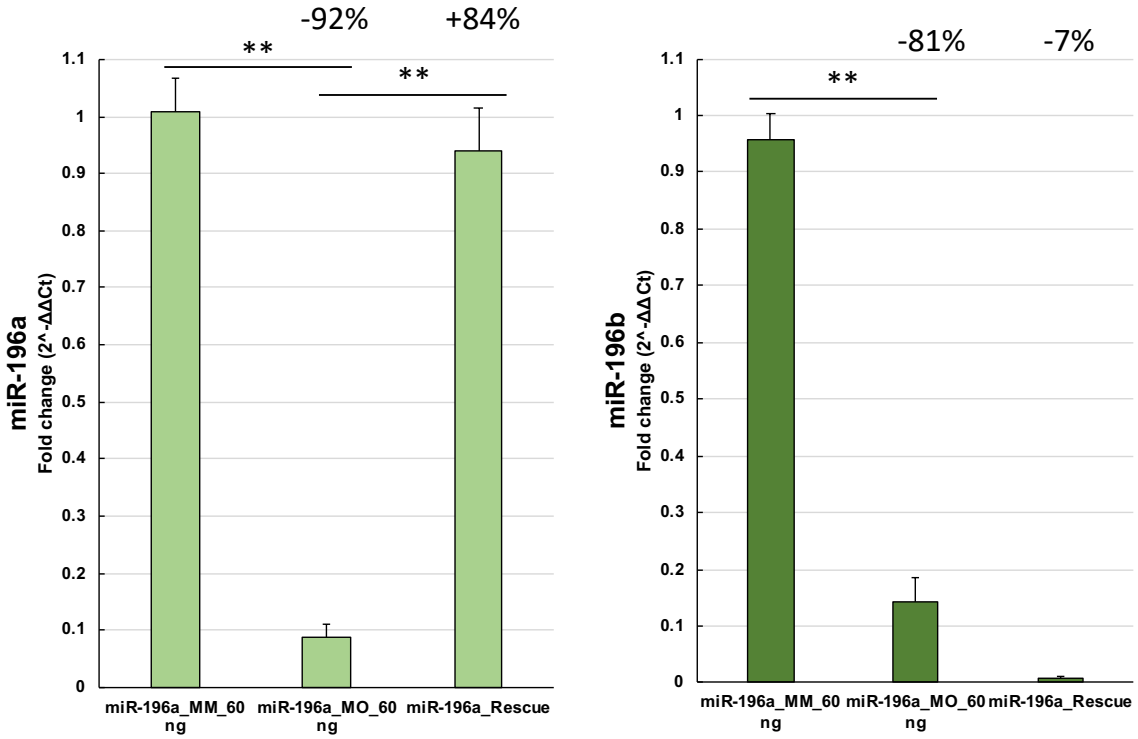

Figure 4.3 - Analysis of the specificity of miR-196a MO on the miR-196b isoform. MM= MM MO, MO= MO, rescue= MO 60 ng + miR-196a mimic 15 µM. miR-196a MO has capacity to KD both miR-196a and miR-196b but is more specific to miR-196a with a 92% reduction in expression compared to an 81% reduction in expression MM vs MO miR-196a vs miR-196b. Percentage's show MM vs MO above MO column, the MO vs rescue above the rescue column. Error bars show mean +/- S.E.M, statistical significance measured by T-test. P values: for miR-196a MM vs MO p=0.003, for MO vs rescue p=0.007. For miR-196b p values: miR-196b on miR-196a MM vs MO p=0.006, for MO vs rescue p=0.08. Carried out with three biological and three technical replicates. snU6 housekeeping gene was used for normalisation.

4.2.2 Characterising synthetic miRNA mimics to rescue miRNA knockdown

This section presents a novel approach to rescuing miRNA KD phenotypes through use of synthetic miRNA mimics, as supplied by Qiagen. These mimics are primarily designed to be transfected into cells and have been used in luciferase assays to ascertain miRNA-mRNA targeting (Viaut et al., 2021). At

time of writing, miRNA mimics have been previously used in a Zebrafish embryo experiment to overexpress a miRNA and observe a phenotype of VEGF-A (Madelaine et al., 2017). It is believed no miRNA mimic has been published for use in a rescue experiment to rescue loss of miRNAs in embryos before.

MiRNA mimics are available for different species, not all were available for our miRNAs for *Xenopus* specifically. However, due to the highly conserved nature of miRNAs, our miRNA mimics align to the *X. tropicalis* miRNA sequences (Fig. 4.4 A & C). To rescue the MO miRNA KDs efficiently, without giving excess miRNA mimic, a dose response experiment was performed from 0.1 µM to 15 µM. 15 µM of mimic was calculated to be equivalent to 60 ng of MO; to avoid non-specific and toxic effects dose was capped at 15 µM. The next step was to analyse miRNA mimic dose on impact on NC marker expression. This was achieved through whole mount *in situ* hybridisation experiments looking at Snail2 expression (Fig 4.4). Most embryos across miR-219 mimic doses showed no change in profile. As the amount of miR-219 mimic increased some loss of Snail2 phenotypes were seen. Control mimic (cel-miR-39-3p) had no effect on Snail2 expression (Fig. 4.5). This experiment was not repeated at a dose response for miR-196a mimic, instead was carried out at 15 µM dose and Snail2 by *in situ* hybridisation and gave no Snail2 phenotype. This dose experiment was omitted due to delays in acquiring the miR-196a mimic from Qiagen during the pandemic.

Preliminary experiments then proceeded to test miRNA mimic doses in conjunction with miR-219 MO addition to identify if loss of Snail2 phenotype was rescued with use of miRNA mimic. Increasing dose of miR-219 mimic with miR-219 MO led to an increased percentage of embryos with no phenotype (Fig. 4.6).

Q-RT-PCR experiments were performed to validate miRNA mimic experiments and quantify the dose response experiments to confirm if 15 µM dose of miRNA mimics was appropriate (Fig. 4.7). For this experiment, the whole embryo was targeted. Embryos were injected into both blastomeres at

2-cell stage of development with miRNA mimic 15 μM, mismatch MO 60 ng, MO 60 ng, MO 60 ng and miRNA mimic 15 μM, co-injected with GFP cRNA tracer. Embryos expressing GFP fluorescence on both sides of the developing embryo were selected, as this meant the whole embryo had been injected. Five neurulas were pooled into one biological sample. The experiment was performed with three biological repeats and triplicates. Addition of miRNA mimic for both miR-196a and miR-219 led to significant increases in miRNA expression (Fig. 4.7), mismatch MO had no impact, MO caused a significant decrease whilst rescue group (MO + miR mimic) for both miRNAs had significant rescue effect (Fig. 4.7).

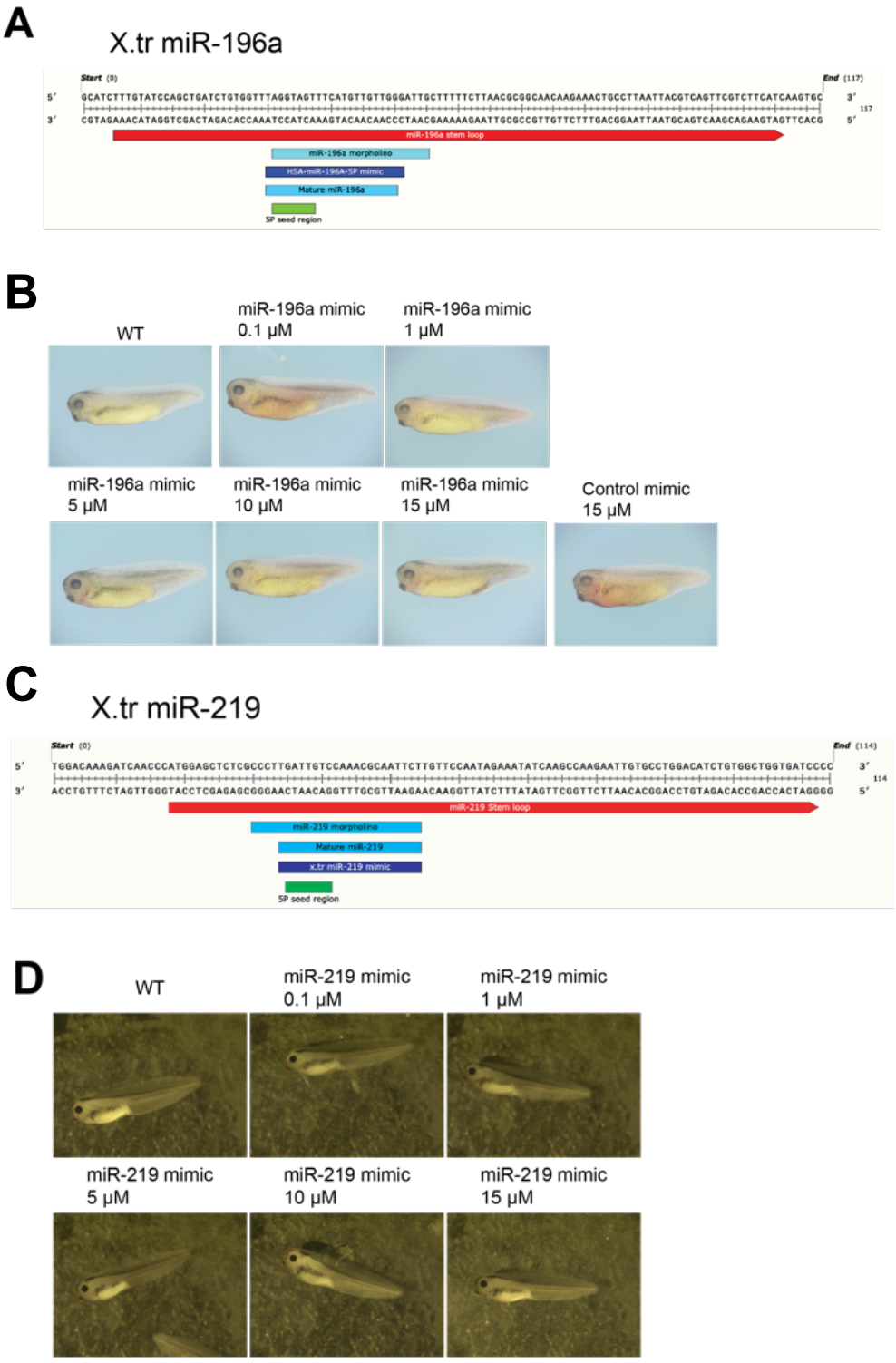

Figure 4.4 - MiRNA mimic sequence alignment and dose response in *X. laevis* experiments. miRNA mimics were injected at the 4 cells stage, using a 10 nL calibrated needle, into one dorsal blastomere with 300 pg tracer; lacZ cRNA for miR-196a and GFP cRNA for miR-219 experiment. Embryos were checked for fluorescence and GFP expression in miR-219 experiment. View is of the injected side of the embryos. Injected embryos show no phenotypes. (A & C) Sequence alignments of miRNAs in *X. tropicalis* with MO, mature miRNA, and miRNA mimic. For miR-196a the human mimic was selected as there was no *Xenopus* specific product available, however this is 100% compatible as seen in the alignment. (B & D)

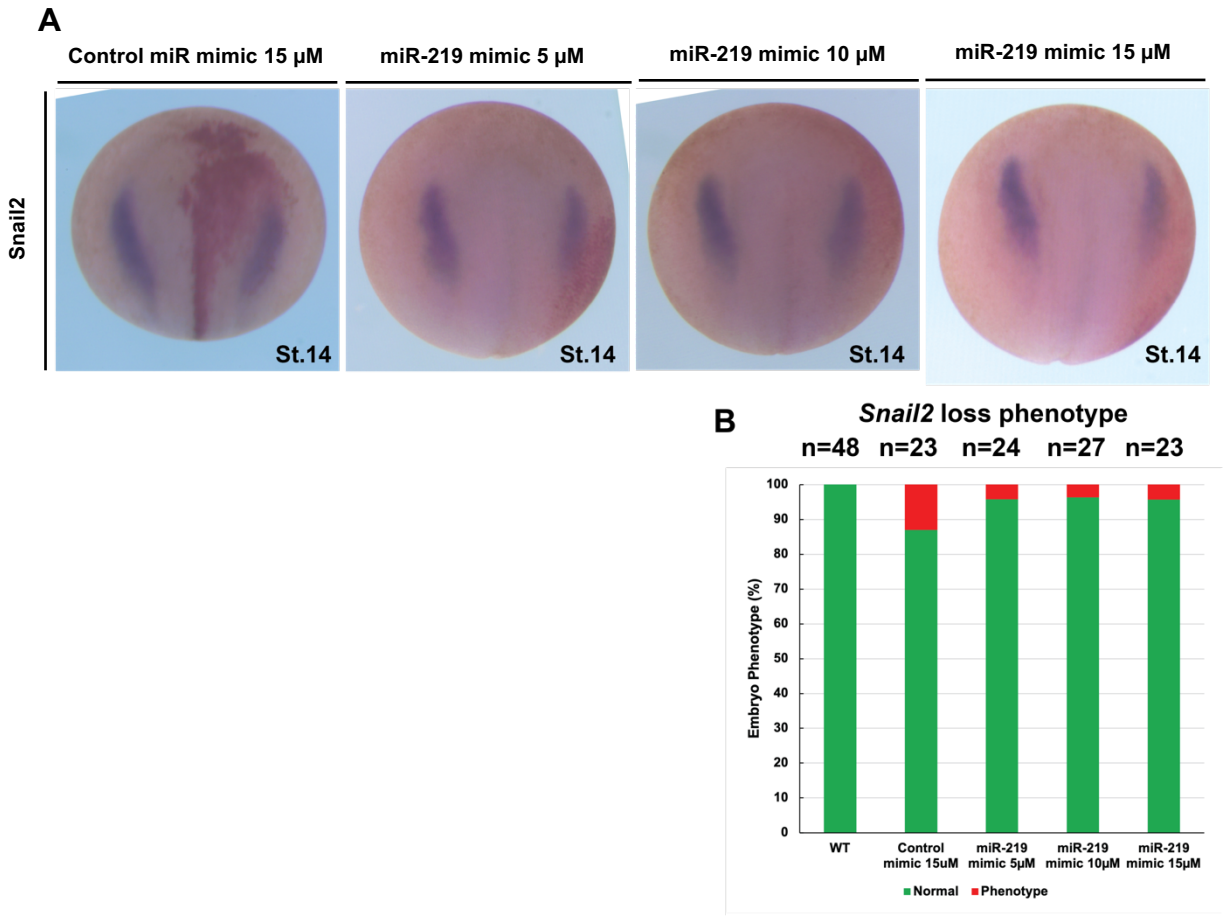

Figure 4.5 - MiR-219 mimic dose response. MiRNA mimic was injected in *X. laevis* embryos at 4 cell stage, using a 10 nL calibrated needle, into one dorsal blastomere with 300 pg of lacZ cRNA tracer. Injected side of embryo is right side. Embryos showed no real Snail2 phenotype after miR-mimic dose. (A) Snail2 WISH phenotypes. First column control mimic embryos, a negative control cel-miR-39-3p, at 15 µM. Then a dose response of miR-219 mimic at 5 µM, 10 µM and 15 µM. (B) shows the count data displaying the number of embryos exhibiting a loss of Snail2 phenotype.

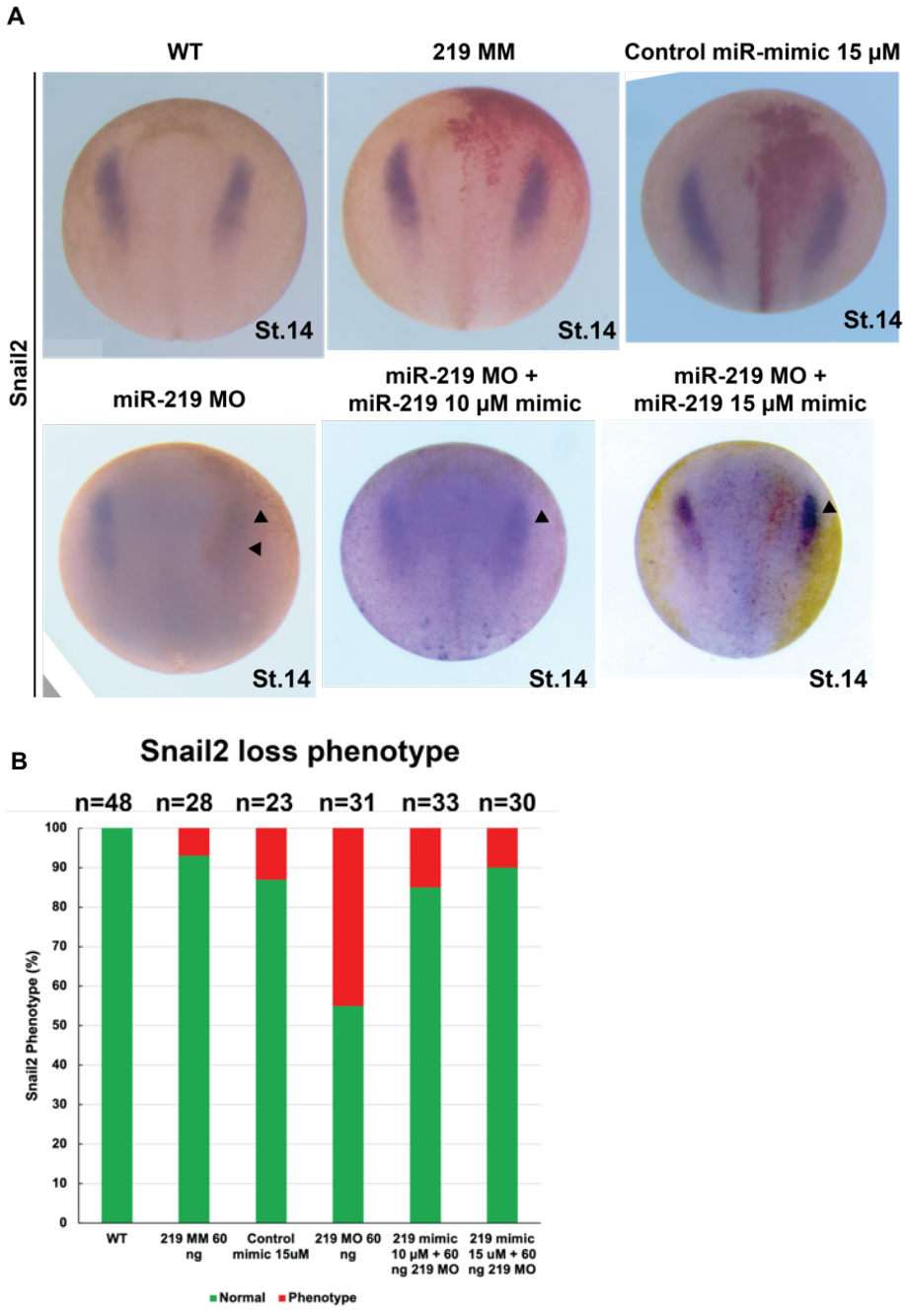

Figure 4.6 - MO KD rescue experiment on NC marker Snail2. Both MOs and mimics were injected into *X. laevis* embryos at 4 cell stage with a 10 nL calibrated needle to give a concentration of 60ng MO and 300 pg lacZ cRNA tracer. Injected side of embryo is right side. Black arrows indicate areas of phenotypic interest. miR-219 KD led to loss of Snail2 which was rescued by miR-219 mimic. (A) Snail2 whole mount *in situ* hybridisation phenotypes for miR-219 KD and rescue with miR-219 mimic doses. Top row left to right: WT, control MO, control mimic; bottom row left to right: miR-219 MO 60 ng KD, miR-219 MO KD 60 ng rescue with miR-219 mimic 10 µM and right with 15 µM. (B) miR-219 MO KD shows reduction in Snail2 expression, and rescue recovers this.

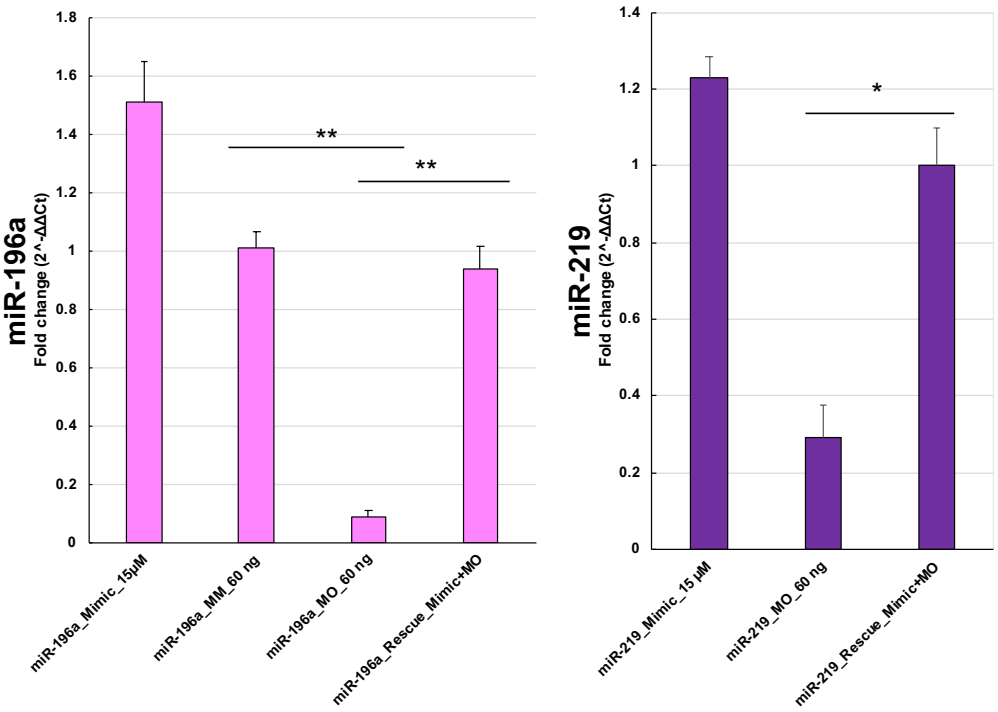

Figure 4.7 - Validation of miRNA mimic specificity and efficacy at rescuing MO-mediated KD of miRNA in *X. laevis* embryos. Embryos were injected into both blastomeres at 2-cell stage of development with miRNA mimic 15 μM, MM MO 60 ng, MO 60 ng, MO 60 ng and miRNA mimic 15 μM, co-injected with GFP cRNA tracer. MO KD led to loss of miRNA and mimic rescued and overexpressed miRNAs. Embryos expressing GFP fluorescence were selected. 5 neurulas were pooled into one biological sample. Experiment performed with three biological repeats and triplicates. miR-196a p values: MM vs MO p=0.0035, MO vs rescue p=0.0074. mir-219 p values: MO vs rescue p= 0.017. Bar charts show error bars depicting mean +/- SEM, statistical significance measured by T-test.

4.3.0 RNA-sequencing on miRNAs in NC

Previous work in the lab had identified miR-196a and miR-219 as being expressed in *Xenopus* NC (Ward et al., 2018). To see if key NC markers are potentially targeted directly or indirectly by our miRNAs, RNA-sequencing on miR-KD NC tissue samples was carried out. These samples were from embryos injected with morpholino for respective miRNA, left to develop to St.14 and then NC tissue was dissected out. This work was conducted by Dr. Nicole Ward (Wheeler lab) in collaboration with Dr. Méghanne Sittewelle with supervision from Prof. Anne-Hélène Monsoro-Burq (Orsay).

Overall following miR-196a KD 2,433 genes were differentially expressed with 1,099 enriched and 1,334 downregulated. Following miR-219 KD 2,039 genes were differentially expressed with 1,020 enriched and 1,019 downregulated.

Analysis of RNA-seq was performed to look at NC, neural plate and placodal markers (Fig. 4.8). The genes selected were chosen because of their key roles in the development of NPB, pre-placodal ectoderm and NC. The top 50 significantly enriched and downregulated genes following miR-196a and miR-219 KD are listed in Appendix 2. Not all the genes in top 50 lists are in Fig. 4.8; however, most of these genes were significantly differentially expressed and showed clear trends.

Differential expression of key genes showed some similarities between miRNAs miR-196a and miR-219 as summarised in Table 4.2. NC markers are downregulated, NPB, neural and placodal markers are generally enriched, ectodermal markers for miR-196a KD were mixed with Xhe2 enriched and Keratin (Krt19) downregulated, but both were downregulated for miR-219 KD.

Following miR-196a KD there was a larger decrease compared to miR-219 KD in expression of NC markers Ets1 (miR-196a only), Pdgfra, FoxD3, Twist1, Sox8, Sox9, Sox10 and Snail2 (Fig. 4.8). Neural plate markers Zic1 and Pax3 did not show significant enrichment. Placodal marker Eya1 also did not show significant enrichment for either miRNA KD. Placode marker Pax6 showed significant enrichment following miR-196a KD, more so for miR-219 KD. Neural markers Pou5f3.3L (Pou60), Sox2, Irx1 all show significant enrichment with extreme enrichment of Pou60 following miR-196a KD. Chrd.2.L showed enrichment following miRNA KD.

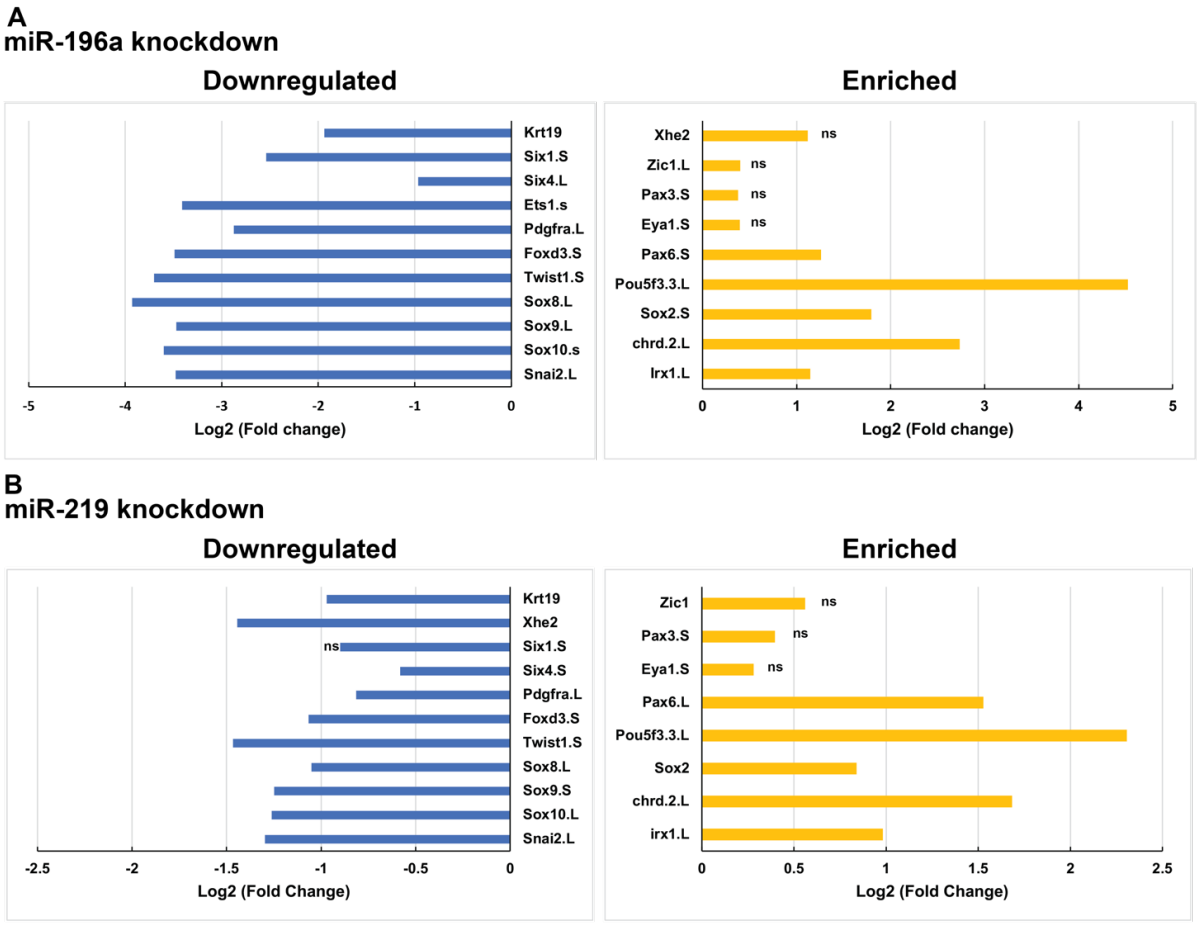

Figure 4.8 -RNA-sequencing on miRNA MO KD NC tissue samples. Differential expression is shown with blue bars showing decreased expression and yellow bars showing enriched expression. Ns= not significantly differentially expressed. A) miR-196a KD and B) miR-219 KD effect on key NC, NPB, neural, placodal and ectodermal markers. A MM MO for each miRNA was used as a control sample to calculate differential expression. The original experiments and data for this were generated by Nicole Ward and Méghane Sittewelle, with re-analysis done by Alice Godden.

4.4.0 Functional characterisation of miRNA KD and rescue

The next aim of the project was to functionally characterise the impact of miRNA KD on NC, neural plate, and HG development. To do this it was decided to focus on *Snail2* (Betancur et al., 2010; Hong and Saint-Jeannet, 2017b) and *Sox10* (Hatch et al., 2016; Milet and Monsoro-Burq, 2012), to characterise NC, *Pax3* to look at the neural plate (Monsoro-Burq et al., 2005) and Xhe2 to look at HG (Hong and Saint-Jeannet, 2007; Kurauchi et al., 2010).

Table 4.2 Summary of differential expression of NC (NC), NPB (NPB), neural, placodal and ectodermal markers following miRNA KD in NC tissue. Ns= not statistically significantly differentially expressed.

Markers	miR-196a MO-KD	miR-219 KD MO- KD
NC (Sox8,9,10, Snail2, Foxd3, Twist1, Ets1, Pdgfra)	Downregulated	Downregulated
NPB (Pax3, Zic1)	Enriched, ns	Enriched, ns
Neural (Pax6, Sox2, Irx1)	Enriched	Enriched
Placode (Eya1, Six1, Six4)	Six1, Six4 down, Eya1 up- ns	Six1 ns, Six4 down, Eya1 up- ns
Ectoderm (Xhe2, Krt19)	Enriched (Xhe2), Downregulated (Krt19)	Downregulated

To profile and investigate the role of miRNAs in the development of *Xenopus* NC whole mount *in situ* hybridisation experiments were carried out on embryos from the following experimental groups: Wild-type (WT- uninjected), control miRNA mimic 15 μM, mismatch miRNA MO 60 ng, miRNA MO 60 ng, miRNA mimic 15 μM, miRNA MO 60 ng and miRNA mimic 15 μM, miRNA MO 60 ng and control miRNA mimic 15 μM. All co-injected with 300 pg of lacZ cRNA tracer developed with Red-gal. Control mimic (cel-miR-39-3p), 15 μM had no impact on the expression of any of the WISH profiles for Snail2, Sox10, Pax3 or Xhe2. This result was as expected as this was a negative control suggested by Qiagen (Fig. 4. 9).

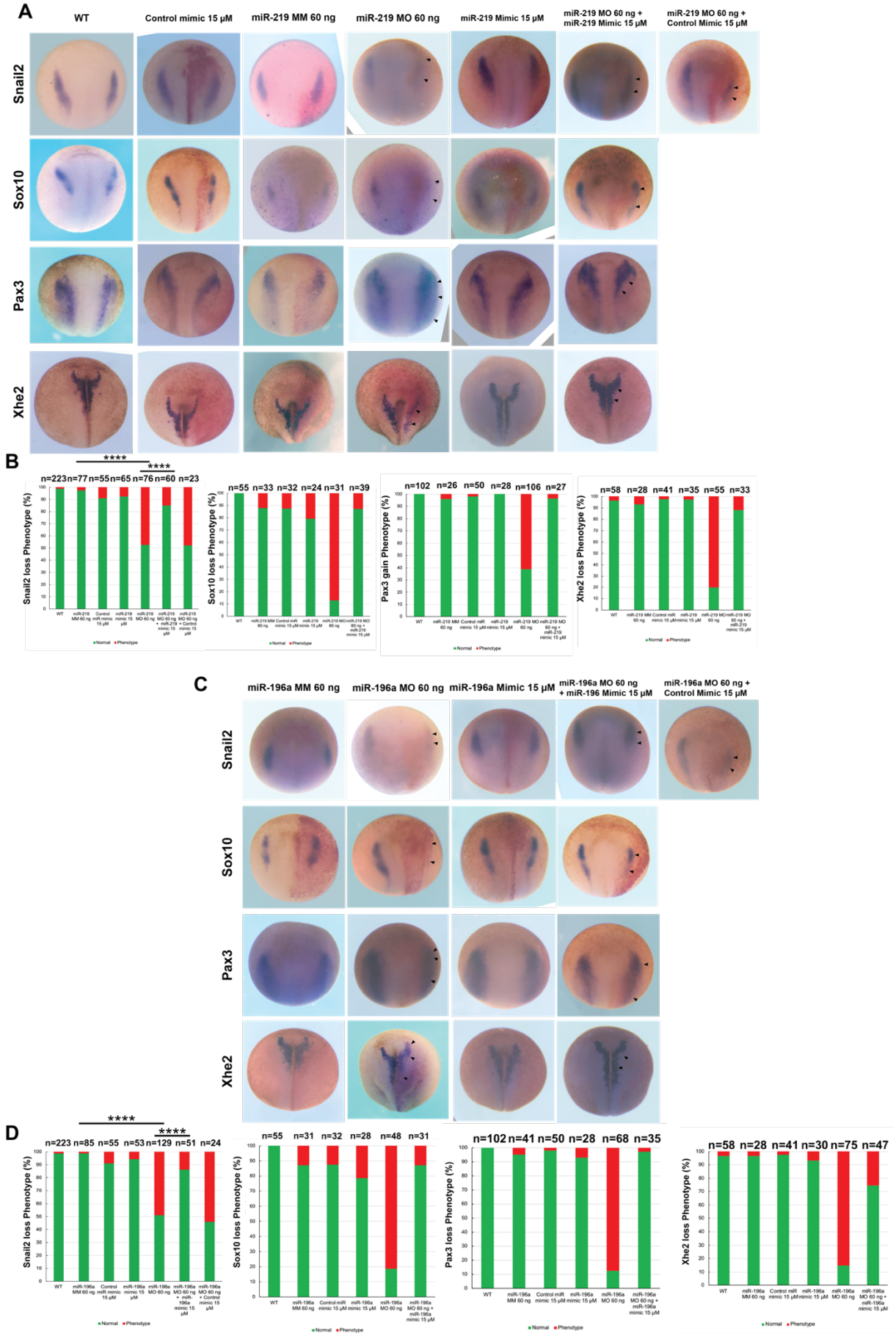
A
WT
Control mimic 15 µM
miR-219 MM 60 ng
miR-219 MO 60 ng
miR-219 Mimic 15 µM
miR-219 MO 60 ng + miR-219 Mimic 15 µM
miR-219 MO 60 ng + Control Mimic 15 µM
Snail2
Sox10
Pax3
Xhe2
B
****
****
n=223 n=77 n=55 n=65 n=76 n=60 n=23
Snail2 loss Phenotype (%)
n=55 n=33 n=32 n=24 n=31 n=39
Sox10 loss Phenotype (%)
n=102 n=26 n=50 n=28 n=106 n=27
Pax3 gain Phenotype (%)
n=58 n=28 n=41 n=35 n=55 n=33
Xhe2 loss Phenotype (%)
Normal
Phenotype
C
miR-196a MM 60 ng
miR-196a MO 60 ng
miR-196a Mimic 15 µM
miR-196a MO 60 ng + miR-196 Mimic 15 µM
miR-196a MO 60 ng + Control Mimic 15 µM
Snail2
Sox10
Pax3
Xhe2
D
****
****
n=223 n=85 n=55 n=53 n=129 n=51 n=24
Snail2 loss Phenotype (%)
n=55 n=31 n=32 n=28 n=48 n=31
Sox10 loss Phenotype (%)
n=102 n=41 n=50 n=28 n=68 n=35
Pax3 loss Phenotype (%)
n=58 n=28 n=41 n=30 n=75 n=47
Xhe2 loss Phenotype (%)
Normal
Phenotype

Figure 4.9 - Functional characterisation of MO mediated miRNA KD and rescue with synthetic miRNA on development of NC, NPB and HG in developing *X. laevis* embryos. MiRNA KD led to HG, NC and NPB phenotypes. Embryos were injected with a 10 nL calibrated needle into one dorsal blastomere at the 4-cell stage of development with 300 pg of lacZ cRNA as a tracer, developed with red-gal. Injected side is always right side. Black arrows indicate regions of phenotypic interest. (A) MiR-219 morpholino KD phenotypes for NC, NPB, and HG. (B) Count data for phenotype incidence. (C) MiR-196a morpholino KD phenotypes for NC, NPB, and HG. (D) Count data for phenotype incidence. Control miRNA mimic (cel-miR-39-3p. Chi squared statistical testing was carried out on Snail2 data, as three independent experiments were conducted covering 3 biological repeats and many technical repeats. between MM MO and MO and MO and rescue group. For miR-219 MM MO vs MO $p=1.47 \times 10^{-10}$, for miR-219 MO vs rescue p=0.000054. For miR-196a MM MO vs MO $p=4.72 \times 10^{-14}$, for miR-196a MO vs rescue p=0.000013.

Impact on NC development after miRNA KD was analysed by whole mount *in situ* hybridisation experiments with NC markers Sox10 and Snail2. The only injection groups to show strong loss NC phenotypes were the miRNA MO only groups. The rescue, with co-injection of MO plus mimic rescued the phenotypes successfully. It was clearly shown that when miRNAs were knocked-down, that Sox10 expression on the manipulated side of the embryo was strongly knocked down, with only very slight expression of Sox10 more anteriorly for miR-219 KD, and almost total KO for miR-196a KD (Fig 4. 9A, 9C). The Snail2 phenotypes generated after miRNA KD were weaker than Sox10, showing some loss of expression and a slight shift in expression with Snail2 expression more restricted to the medial region of the NC tissue. The Sox10 phenotype was more penetrant amongst the embryos, despite this Snail2 loss phenotype was still strongly seen in nearly half of the embryos (Fig 4.9B & D). Both Sox10 and Snail2 phenotypes were rescued with use of miRNA mimics (Fig. 4.9A & C).

To assess the impact of miRNA KD on the development of the neural border, it was decided to look at Pax3 expression as analysed by WISH (Monsoro-Burq et al., 2005). Following MO KD of miR-219 there is an expansion of Pax3 across neural plate and NC (Fig. 4.8A), through sectioning it was shown that the expansion is mainly in the superficial ectoderm (Fig. 4. 13). For miR-196a KD a reduction in expression intensity and spread can be seen across the neural plate region of Pax3 (Fig. 4.9C).

Pax3 is expressed in HG and its progenitors (Hong and Saint-Jeannet, 2007). The HG is a tissue that in *Xenopus* produces a proteolytic enzyme at the anterior end of the *Xenopus* embryo. This is important as this allows the young tadpole to release itself from the surrounding vitelline membrane and swim off. The HG has a fork-head shaped expression profile, Xhe2 (also known as UVS.2), encodes the HG enzyme (Katagiri et al., 1997; Schambony et al., 2003).

As shown, miR-219 KD had a strong impact on HG development, with a strong reduction in expression of Xhe2 (Fig. 4.9A). The reduction of Xhe2 is in the most anterior regions of the embryo (the top right of the fork-head structure), however moving dorsally along the embryo (bottom of the fork-head) the expression profile looks weaker and slightly expanded. Upon KD of miR-196a the phenotype exhibited by Xhe2 whole mount *in situ* hybridisation was distinctly altered, with a shift and subtle anterior expansion (Fig. 4.9C).

4.5.0 Investigating the Pax3 phenotypes

Pax3 phenotypes were examined to identify changes in NPB development at different stages. In early neurula development, Pax3 expression following miR-196a KD was reduced in the NPB region. Moving through to later, St.17 of neurula development the loss is still prevalent, the expression is more disorganised. Moving to even later neurula, St.19 there appears to be a recovery, as the expression looks more equal compared to the non-injected side of the embryo (Fig. 4.10). In addition, the HG population at the later neurula stage St. 19 (Fig. 4.10A), appears subtly expanded in the anterior-most regions, as indicated by black arrows. This agrees with the work in Fig. 4.9 that specifically looks at HG marker Xhe2 which showed a shifted and expanded HG phenotype (Fig. 4.9).

In early neurula development Pax3 development upon miR-219 KD was greatly expanded in the NPB region. The expression was also more intense across the embryo, anteriorly and posteriorly and laterally (Fig 4.11A). Moving to late neurula, St.19 there again appears to show some disorganisation but a

more normal phenotype, that is highly penetrant (Fig 4.11C). The *Pax3* profile is marginally expanded in the HG population in the anterior end of the embryo and is denoted by the black arrows. All phenotypes were highly penetrant and significantly common (Fig. 11B-C).

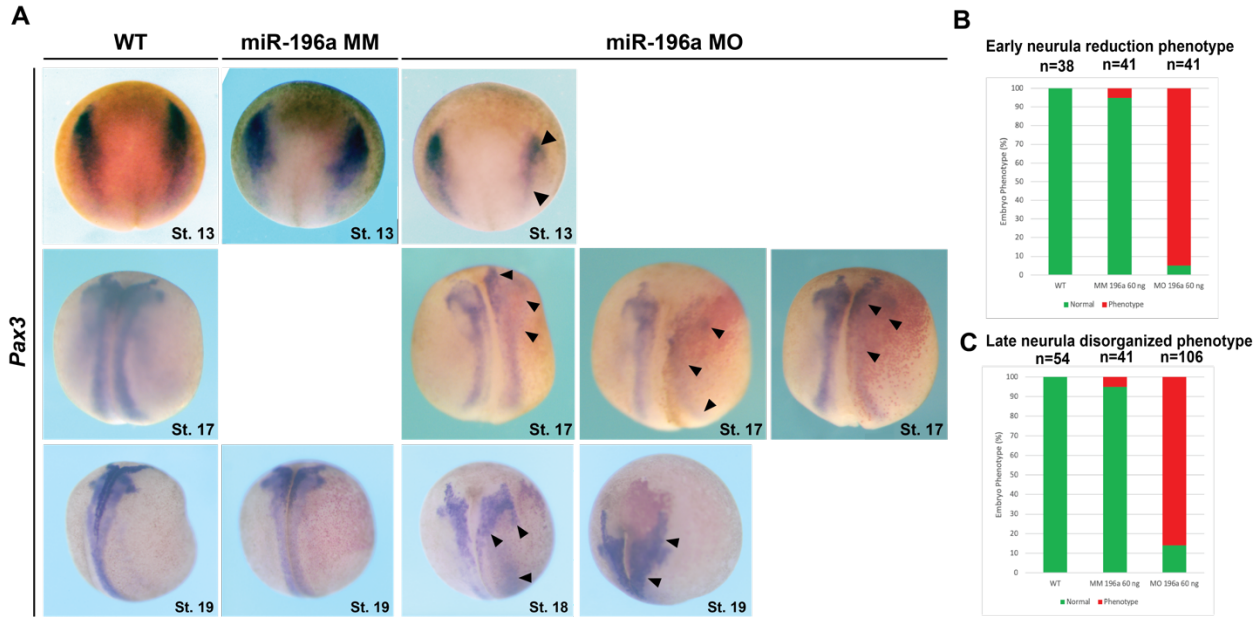

Figure 4.10 - miR-196a MO KD effect on NPB marker Pax3. MiR-196a KD in later neurula development perturbs Pax3 expression. *X. laevis* embryos were injected with 60 ng of MM MO or MO into one dorsal blastomere at 4 cell stage, using a 10 nL calibrated needle. Embryos were coinjected with 300 pg of lacZ cRNA tracer. Black arrows indicate regions of phenotypic interest. MO-injected embryos show changing Pax3 phenotypes through neurula development. (A) Pax3 WISH phenotypes for miR-196a KD. Pax3 shows expanded phenotype at early neurula, which becomes disorganised at St. 17 before some recovery at late neurula as indicated by the black arrows. (B-C) Shows the count data, the number of embryos with expansion and disorganized Pax3 phenotypes after miR-196a KD.

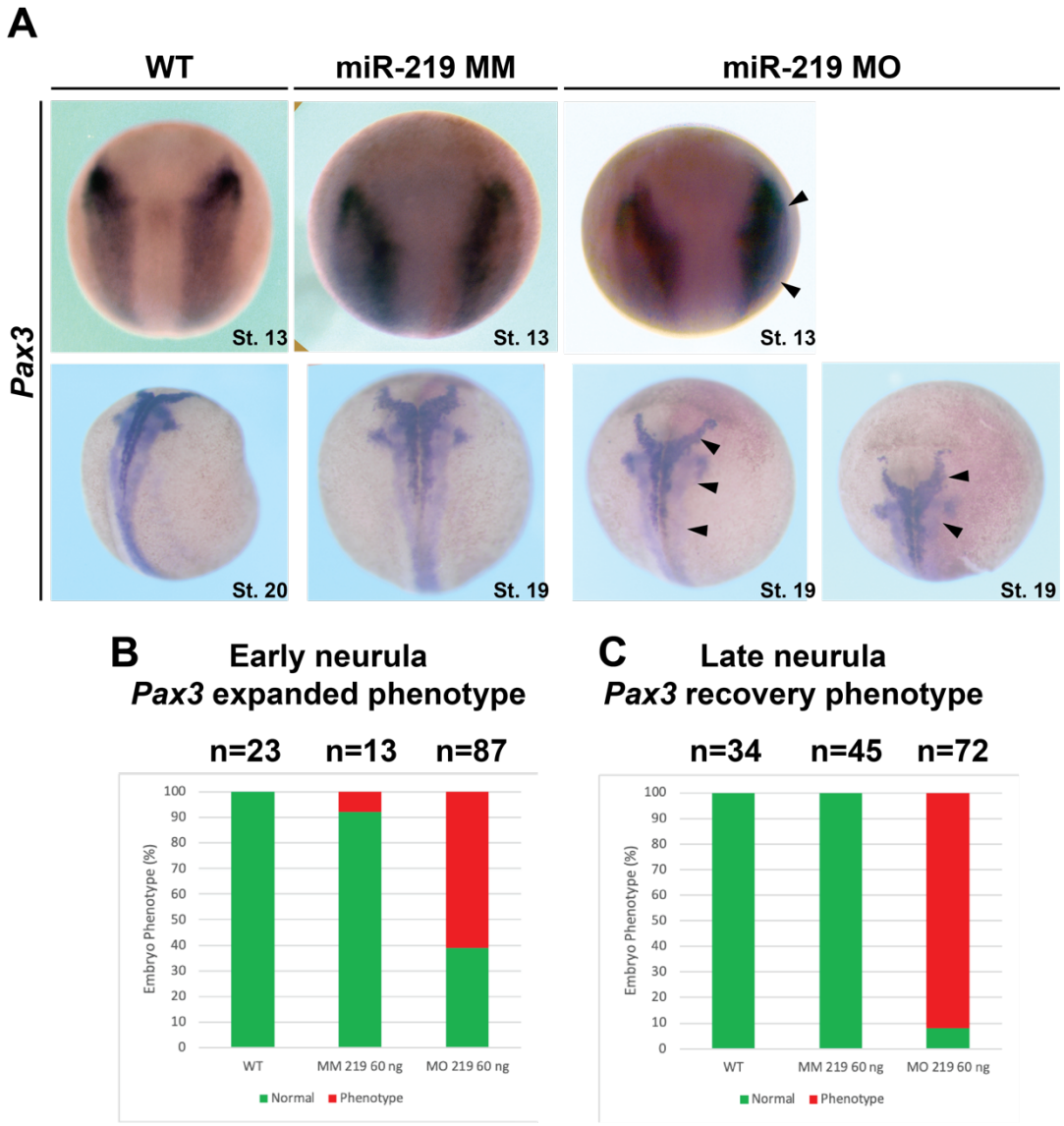

Figure 4.11 - miR-219 MO KD effect on neural plate marker Pax3. miR-219 KD in later neurula development led to some Pax3 expression recovery with reduced expansion phenotype. *X. laevis* embryos were injected with 60 ng of MM MO or MO into one dorsal blastomere at 4 cell stage, using a 10 nL calibrated needle. Embryos were coinjected with 300 pg of lacZ cRNA tracer. Black arrows indicate regions of phenotypic interest. MO-injected embryos show changing Pax3 phenotypes through neurula development. (A) Pax3 whole mount in situ hybridisation phenotypes for miR-219 KD. Injected side right side of embryo. First column WT embryos, then a mis-match control MO, then experimental MO KD. Pax3 shows expanded phenotype at early neurula, which shows some recovery at late neurula as indicated by the black arrows. B & C show the count data, the number of embryos showingexpansion and disorganized Pax3 phenotypes after miR-219 KD.

4.5.1 Pax3 Phenotype rescue

The Pax3 phenotypes which were in Fig 4.9 warranted further research and investigation. This was because we wanted to know if Pax3 was an indirect

target of miR-219. It was decided to see if the phenotypes of Pax3 expansion following miR-219 KD could be rescued. To do this a Pax3 MO was chosen as the method to KD the expanded Pax3 expression. To do this, a published MO from the Monsoro-Burq lab was used against Pax3 to reduce *Pax3* expression (Monsoro-Burq et al., 2005). To test the MO was working as expected I replicated the dose-response experiments performed in (Monsoro-Burq et al., 2005). Concordant with Monsoro-Burq et al., (2005), it was found that at 30 and 40 ng of Pax3 MO, Snail2 expression as tested by whole mount *in situ* hybridisation, was shifted and very slightly downregulated (Fig. 4.11). This phenotype was observed in approximately 75% of embryos, like Monsoro-Burq et al., (2005) who found this phenotype in 80% of embryos. In addition, I carried out the same 10-40 ng dose response of Pax3 MO out on embryos and developed whole mount *in situ* hybridisation for Pax3; it was found that as the dose increased, Pax3 expression decreased (Fig. 4.12), again similar to that shown in (Monsoro-Burq et al., 2005).

As shown in Fig.4.9, miR-219 KD had a strong impact on neural plate development and a strong Pax3 phenotype, with Pax3 expression expanded across the embryo. With the Pax3 MO optimized as above, it was decided to use a 40 ng Pax3 MO dose to rescue the expanded Pax3, as this gave a distinct reduction in *Pax3* expression (Fig. 4.12). To do this Pax3 and miR-219 MOs were injected into the embryo at the 4-cell stage into the right dorsal blastomere along with lacZ as a tracer. Pax3 MO was injected at 40 ng, and miR-219 MO at 60 ng dose, therefore 100 ng of MM MO for miR-219 was used as a suitable negative control. To achieve these doses two injections were used, with the doses being the final concentration put into the embryo (Fig. 4.14).

Embryos were injected with MO and gene expression assayed by WISH. For Pax3, WT and miR-219 MM MO embryo groups appeared normal. For Pax3 MO group, *Pax3* expression was downregulated as indicated by black arrows (Fig. 4.14). MiR-219 MO embryos showed the expanded Pax3 expression phenotype, but the Pax3 MO and miR-219 MO group (Pax3 rescue) showed significant rescue of this phenotype, with embryo appearing to have a normal

phenotype (Fig 4.14A). To take this further, I then compared miR-219 MO against the Pax3 rescue on *Snail2, Sox10, Xhe2*. For each of these markers miR-219 MO reduces expression of all these markers. However, when the Pax3 MO is applied this further reduces the expression of these markers with Snail2, Sox10 and Xhe2 barely visible on the manipulated side (indicated by black arrows), (Fig 4.14. A). These phenotypes were highly penetrant, with a statistically significant incidence as seen in Fig. 4.14 B. This suggests that Pax3 is an indirect target of miR-219 and will be discussed later.

To further examine the function of the Pax3 MO, embryos were cryosectioned (Fig. 4.13). Pax3 MO embryos showed loss of Pax3 in superficial ectoderm and medially in the section. This is less obvious in the whole-mount embryo image (Fig. 4.13A). Next, to interrogate the expanded Pax3 phenotype following miR-219 KD, these embryos were sectioned. This revealed expansion of Pax3 in the superficial ectoderm and neural plate (Fig. 4.13B). To assay if Pax3 was indirect target of miR-219 and if the expanded Pax3 phenotype could be rescued, the Pax3 MO and miR-219 MO were used, and embryos were sectioned (Fig. 4.13C). This revealed rescue of the expanded phenotype.

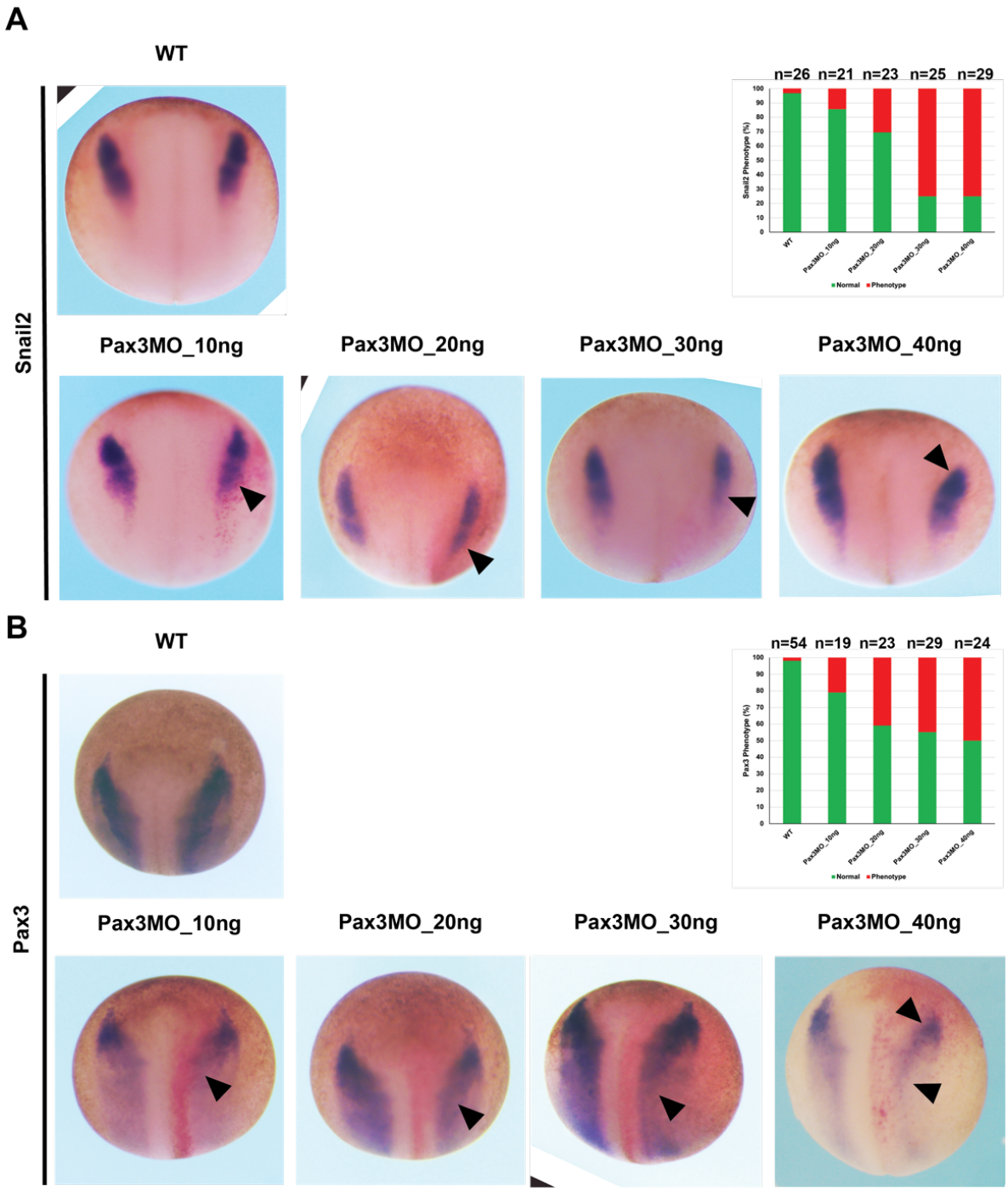

Figure 4.12 - Snail2 and Pax3 MO phenotypes in Pax3 MO dose response. *X. laevis* embryos were injected at the 4 cell stage, using a 10 nL calibrated needle, into one dorsal blastomere. Injected side of embryo is always right side. Black arrows indicate region of phenotypic interest. (A) Increasing doses of Pax3 MO perturbed Snail2 expression. (B) Increasing Pax3 MO dose led to increasing loss of Pax3 expression. Pax3 MO based on published MO in: (Monsoro-Burq et al., 2005).

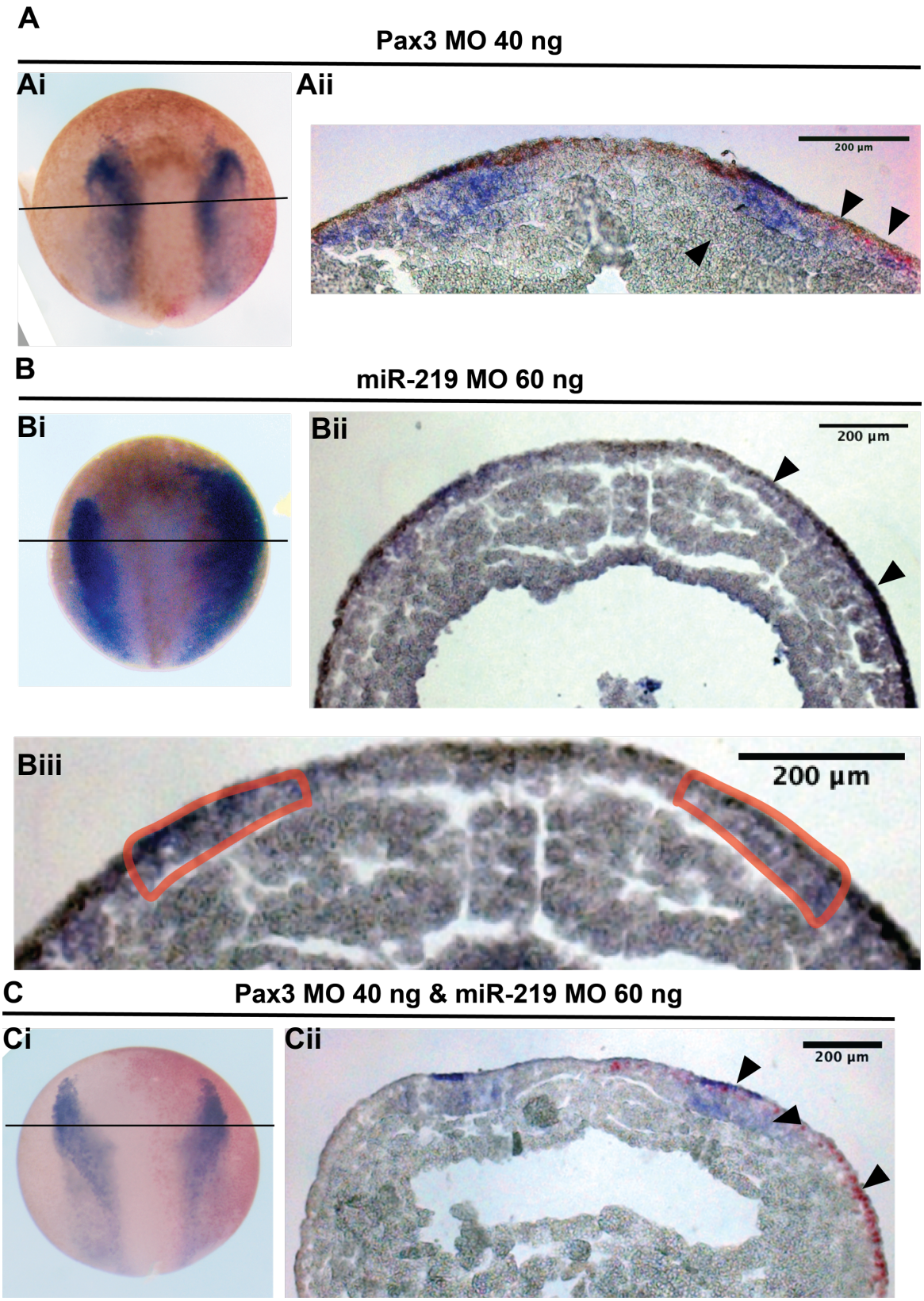
A
Pax3 MO 40 ng
Ai
Aii
200 µm
B
miR-219 MO 60 ng
Bi
Bii
200 µm
Biii
200 µm
C
Pax3 MO 40 ng & miR-219 MO 60 ng
Ci
Cii
200 µm

Figure 4.13 - Cryosectioning of Pax3 phenotypes. *X. laevis* embryos were co-injected with 300pg lacZ tracer, using a 10 nL calibrated needle. Injected side of the embryo is the right side. Embryos were injected at the 4 cell stage of development into 1 dorsal blastomere. (A) Embryos were injected with 40 ng of Pax3 MO. (Ai) Whole mount view, (Aii) Cross-section showing loss of Pax3 in NC and NP regions. (B) Embryos were injected with 60 ng of miR-219 MO. (Bi) Whole mount view. (Bii) Cross section showing expansion of Pax3 in superficial ectoderm and loss in NC area, (Biii) Close up view of Biii, red boxes highlight areas of interest, right side showing area where Pax3 expression is loss in NC and NP regions. (C) Embryos were injected with 40 ng of Pax3 MO and 60 ng of miR-219 MO. (Ci) Whole-mount view. (Cii) Cross section showing a rescue of Pax3 expression in NC, NP and superficial ectoderm regions. Black lines through Ai, Bi and Ci show the plane and region of the embryo sectioned. Sections Aii, Bii, Cii imaged at 5x magnification and Biii at 10 x magnification. Black arrows indicate areas of phenotypic interest.

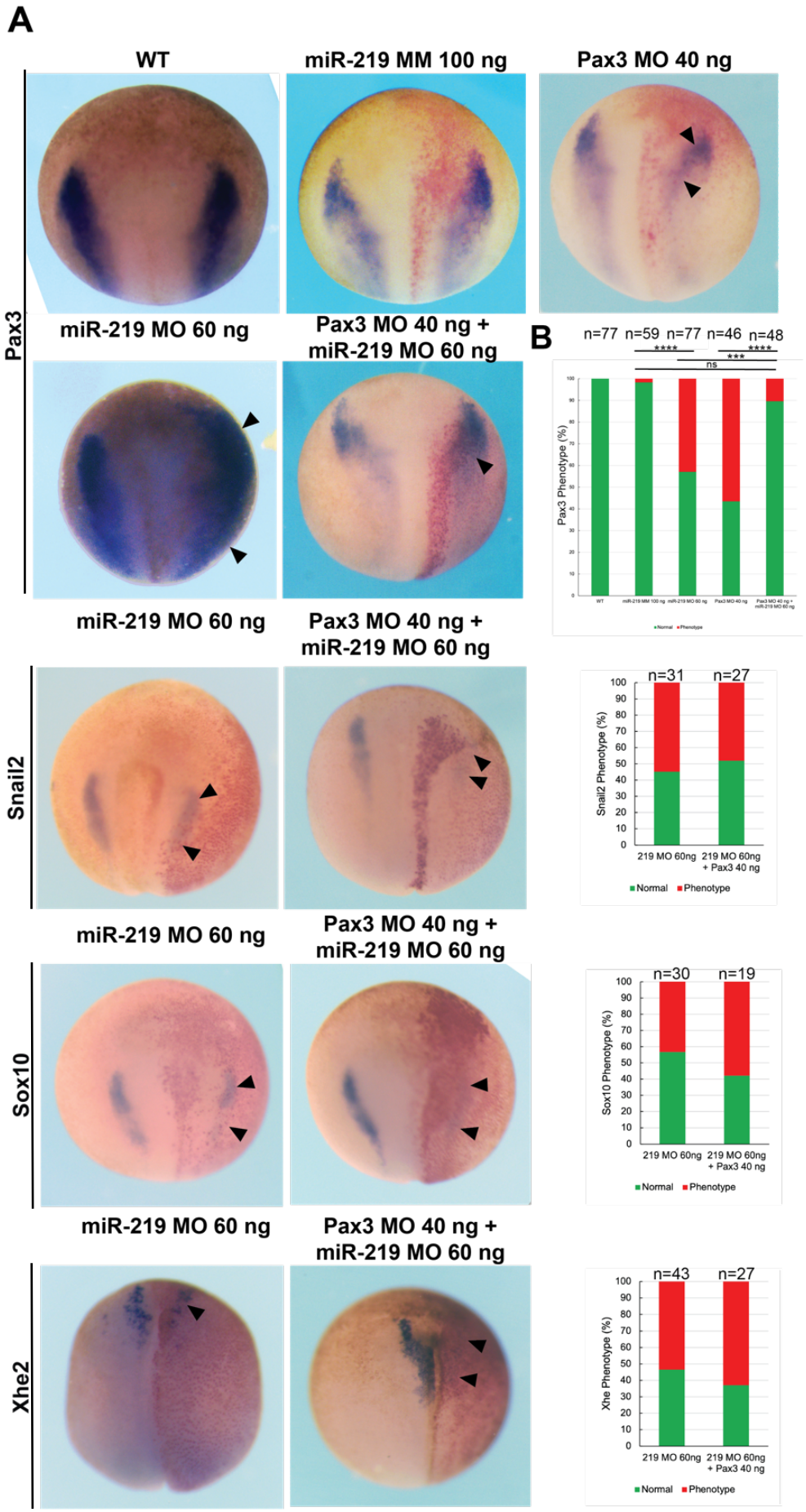
A
WT
miR-219 MM 100 ng
Pax3 MO 40 ng
Pax3
miR-219 MO 60 ng
Pax3 MO 40 ng +
miR-219 MO 60 ng
B
n=77 n=59 n=77 n=46 n=48
****
****
***
ns
Pax3 Phenotype (%)
WT
miR-219 MM 100 ng
miR-219 MO 60 ng
Pax3 MO 40 ng
Pax3 MO 40 ng + miR-219 MO 60 ng
Normal
Phenotype
miR-219 MO 60 ng
Pax3 MO 40 ng +
miR-219 MO 60 ng
Snail2
n=31 n=27
Snail2 Phenotype (%)
219 MO 60ng
219 MO 60ng + Pax3 40 ng
Normal
Phenotype
miR-219 MO 60 ng
Pax3 MO 40 ng +
miR-219 MO 60 ng
Sox10
n=30 n=19
Sox10 Phenotype (%)
219 MO 60ng
219 MO 60ng + Pax3 40 ng
Normal
Phenotype
miR-219 MO 60 ng
Pax3 MO 40 ng +
miR-219 MO 60 ng
Xhe2
n=43 n=27
Xhe Phenotype (%)
219 MO 60ng
219 MO 60ng + Pax3 40 ng
Normal
Phenotype

Figure 4.14 - Rescuing miR-219 phenotypes with Pax3 MO. Embryos were double injected, the total dose of MO is indicated. Embryos were injected at the 2 cell stage of development into one blastomere, twice with 300 pg of lacz cRNA as a tracer. Right side of embryos is always injected side. Pax3 MO and miR-219 MO rescued expanded Pax3, but Pax3 MO led to further loss of Xhe2, Snail2 and Sox10 expression. Black arrows indicate regions of phenotypic interest. (A) Pax3, Xhe2, Sox10 and Snail2 whole-mount *in situ* hybridisation following MO KD with miR-219 MM MO, miR-219 MO, Pax3 MO, miR-219 MO with Pax3 MO or WT control. (B) Blind score phenotype counts. For Pax3 group three individual biological experiments were carried out, Chi-squared statistical testing was performed. 219 MM vs 219 MO p= 3.9×10^{-8}, 219 MM vs 219 MO + Pax3 MO p=0.051, 219 MO vs 219 MO + Pax3 MO p=0.00013, Pax3 MO vs 219 MO + Pax3 MO p= 2×10^{-6}. miR-219 MO phenotype was only rescued with Pax3 MO for Pax3 group.

4.6.0 MiRNA impact on neural and placodal development

As previous sections showed, miRNA KD leads to NC phenotypes. To investigate more specifically what the miRNAs may be targeting, and to assay other tissue types, the genes assayed were expanded. I decided to analyse En2 for neural and anterior-posterior patterning (Dur et al., 2020; Hemmati-Brivanlou et al., 1991), Sox2 for neural development (Munoz et al., 2015), Pax6 for eye and placodal development (Grocott et al., 2020; Schlosser and Ahrens, 2004) and finally Zic1 to further understand the role of miRNAs in the development of neural and neural plate tissue (Hong and Saint-Jeannet, 2017a) following miRNA KD (Fig. 4.15).

It was decided to look at neural markers including Sox2 and En2 as previous work had shown alterations in expression of neural markers following miRNA KD (Dur et al., 2020; Hemmati-Brivanlou et al., 1991; Munoz et al., 2015). Following miR-196 KD En2 was shown to have a significant reduction in expression, whereas miR-219 KD led to a subtle posterior shift in En2 expression, as seen in 40% embryos. This shift was also seen following miR-219 KD when looking at Sox2 expression, but in only 20% of embryos, and no expansion of the neural plate. Following miR-196a KD Sox2 expression in the lateral region appeared expanded, this was seen in roughly 35% of embryos, contrastingly, En2 expression following miR-196a KD was markedly reduced. This was seen in half the embryos tested (Fig. 4.15A-B).

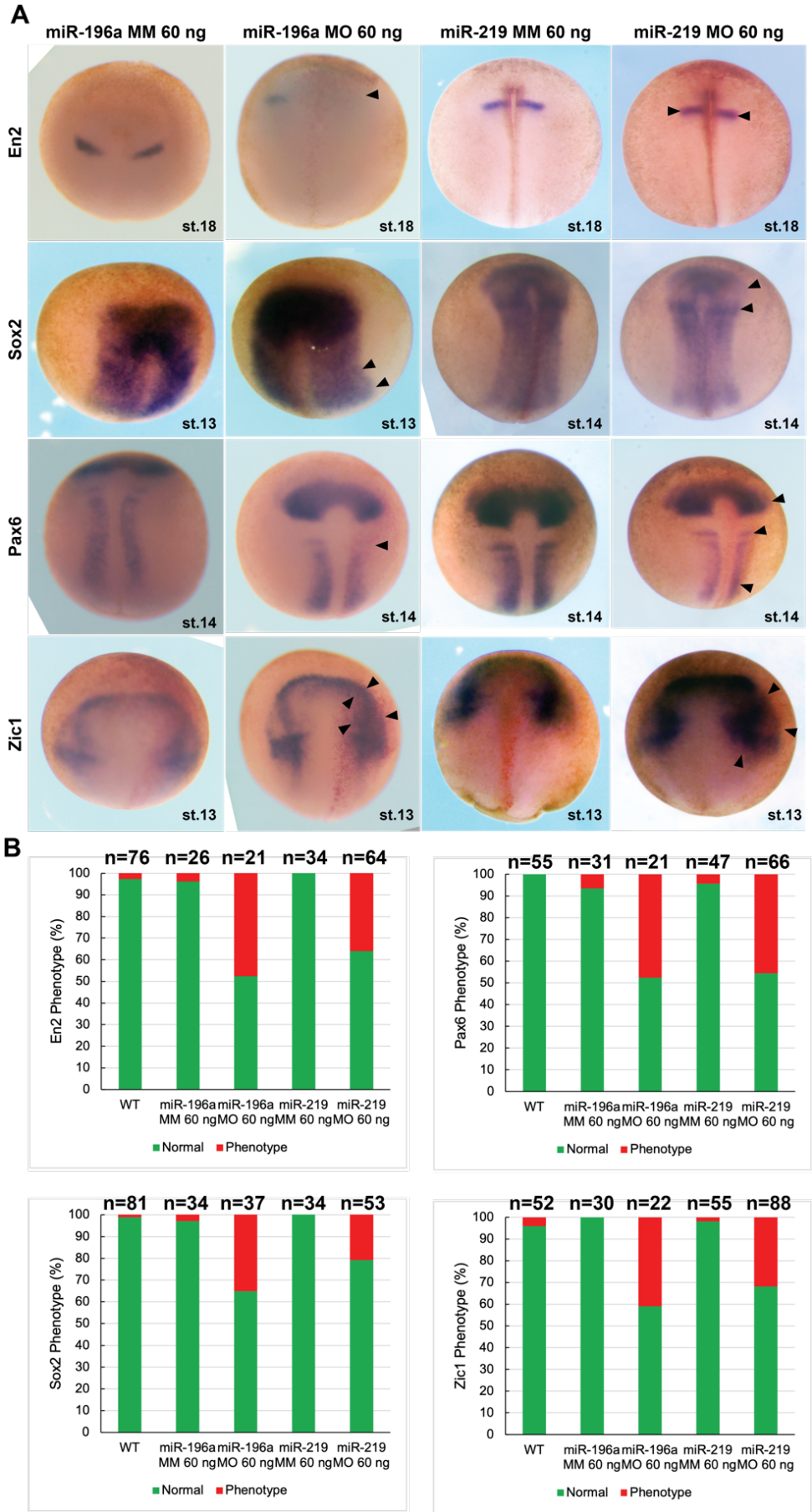
A
miR-196a MM 60 ng
miR-196a MO 60 ng
miR-219 MM 60 ng
miR-219 MO 60 ng
En2
Sox2
Pax6
Zic1
st.18
st.13
st.14
B
n=76 n=26 n=21 n=34 n=64
En2 Phenotype (%)
n=55 n=31 n=21 n=47 n=66
Pax6 Phenotype (%)
n=81 n=34 n=37 n=34 n=53
Sox2 Phenotype (%)
n=52 n=30 n=22 n=55 n=88
Zic1 Phenotype (%)
WT
miR-196a MM 60 ng
miR-196a MO 60 ng
miR-219 MM 60 ng
miR-219 MO 60 ng
Normal
Phenotype

Figure 4.15 - Assessment of neural, neural plate and placodal development following MO mediated miRNA-KD. MO was injected into *X. laevis* embryos into one dorsal blastomere at the 4-cell stage of development with MO and 300 pg of lacZ cRNA as a tracer. Right side of embryo is always injected side. miR-196a KD led to loss of neural markers and expansion of neural plate, whereas miR-219 KD led to shift of neural expression and expansion of neural plate. Black arrows indicate regions of phenotypic interest. (A) Whole mount in situ hybridisation of En2, Sox2, Pax6 and Zic1 following MO mediated miRNA KD. (B) Blind score phenotype counts. En2 and Pax6 loss of expression was observed after miR-196a KD with Sox2 and Zic1 expanded. MiR-219 MO KD exhibited a shift in anterior-posterior patterning with shifts in En2, Sox2 and Pax6 midbrain profiles and a subtle expansion of Zic1. MM= MM, MO= MO.

Looking downstream of the NPB would require analysis of placodal markers in development. Placodes give rise to sensory organs and structures (Schlosser and Ahrens, 2004). Pax6 is regarded as the master control gene in visual organ development and implicated in lens placode formation (Ashery-Padan et al., 2000; Grocott et al., 2020). Due to this, Pax6 was chosen as one marker to analyse the impact of miRNA KD. MiRNAs have been previously shown to be expressed in placodal tissues in *Xenopus*; including miR-19 and miR-200a which are expressed in brain and olfactory placodes (Ahmed et al., 2015). Therefore, it was predicted to see phenotypes in placodal expression following miRNA KD. Following miR-196a KD Pax6 is knocked down in the medial neural plate as indicated by the black arrow (Fig. 4.15A). miR-219 KD shows a subtle expansion in the lens placode region (top black arrow), a slight loss in the midbrain boundary (middle arrow), and a slight expansion in more posterior neural tube (bottom arrow), (Fig. 4.15A).

To further assess the impact of miRNA-219 in the development of the NPB, following the expanded Pax3 phenotype, another significant neural plate marker was analysed, Zic1 (Hong and Saint-Jeannet, 2017a). On the miR-219 MO injected side the Zic1 expression in the anterior end of the embryo is expanded and disorganized. The expression is spread out more posteriorly and medially. The expression spreads across the embryo throughout the neural plate region (Fig. 4.15A). Following miR-196a KD a similar expansion of Zic1 is also seen, albeit it the expansion is more anterior in a more placodal region. These phenotypes were seen in approximately 45% of the embryos tested (Fig. 4.15B). Interestingly all phenotypes were highly prevalent for En2,

Sox2, Pax6 and Zic1, however Sox2 phenotypes were less clear and present in 20-30% of embryos (Fig. 4.13B).

4.7.0 MiRNA KD effect on craniofacial development

NC cell populations give rise to parts of the craniofacial skeleton and broadly affect craniofacial development (Cordero et al., 2011; Simoes-Costa and Bronner, 2015). To investigate miRNA KD in craniofacial development it was decided to push the embryo development further into later tadpole stages (St. 42). Embryos this time were injected at the 2-cell stage into one blastomere with control/experimental MO and GFP cRNA as a tracer. Instead of stopping embryos at neurula stages of development, embryos were grown until they had reached St. 42 of development. The tadpoles do not look like they were significantly affected but when looking closely at some anterior head structures there are some very subtle differences in the craniofacial structures. When comparing WT and MM against the MO (see black arrows), there was a small bulge in the cheek region, medial to the cement gland region of the miRNA MO KD tadpoles (Fig 4.16).

Taking this a step further, it was decided to look at the developing cartilage of the head. The tadpoles (Fig. 4.16B) were allowed to develop until st.42. These tadpoles were then fixed, and carefully stained in Alcian blue. This stains craniofacial cartilage. Tadpoles were then carefully bleached to remove pigment and cartilage was dissected out before imaging. The small bulge in the cheek region of the MO injected embryo above (Fig. 4.16A), may be representative of the disorganised branchial arches seen on the MO injected side of the embryo below in (Fig. 4.16 B-C). Other parts of the craniofacial cartilage appear mostly normal, with some disorganisation in the palatoquadrate and Meckel's cartilage region. Using chi-squared statistical analysis on the count data, counting the number of embryos exhibiting craniofacial cartilage disfigured phenotypes, the MO injected set were significantly different from WT (Fig. 4.16 B&C).

The small bulge in the cheek region of the MO injected embryo above (Fig. 4.16A), may be representative of the disorganised branchial arches seen on

the MO injected side of the tadpole (Fig. 4.14B-C). Some parts of the craniofacial cartilage for miR-219 KD appear mostly normal, but with some disorganisation in the palatoquadrate, ceratohyale, basibranchiale and Meckel's cartilage region. Using chi-squared statistical analysis on the count data, counting the number of embryos exhibiting craniofacial cartilage disfigured phenotypes, the MO injected set were highly significantly different, $p<0.001$ (Fig. 4.14B- C).

4.8.0 Discussion

4.8.1 Optimization and experimental design

MO use for developmental biology has been prevalent for many years, however recent discussions have questioned the use of MOs, and guidance for carefully controlled experiments to generate meaningful data have been determined (Blum et al., 2015; Heasman, 2002). Dose response data can also be useful where subtle effects could be missed in total loss-of-function experiments (Blum et al., 2015). Control experiments such as use of mismatched MO's are widely used and recommended in *Xenopus* research. Gold-standard controls include rescue experiments with mRNAs to rescue phenotypes (Blum et al., 2015; Heasman, 2002; Heasman et al., 2000; Stainier et al., 2015). MiRNAs have been previously knocked down with MOs and were thus used and appropriate for this project (Flynt et al., 2017).

MOs were initially used to KD miRNAs -196a and miR-219 and the results on gene expression of common markers analysed. Early experiments were needed to validate which dose of MO would be appropriate to induce phenotypes, without inducing toxicity. As seen in Fig. 4.2 for miR-219 KD, as MO dose increased so did incidence of *Snail2* loss of expression phenotype, with 60 ng dose giving the highest number of embryos exhibiting loss of *Snail2* expression. The 60 ng was decided as an optimal dose as between 40 ng and 60 ng the number of embryos exhibiting phenotype began to and then peaked at 60 ng, we chose not to use higher than 60 ng as it is well-known that increasing dose of MO can increase risk of non-specific abnormalities in the embryos (Heasman, 2002).

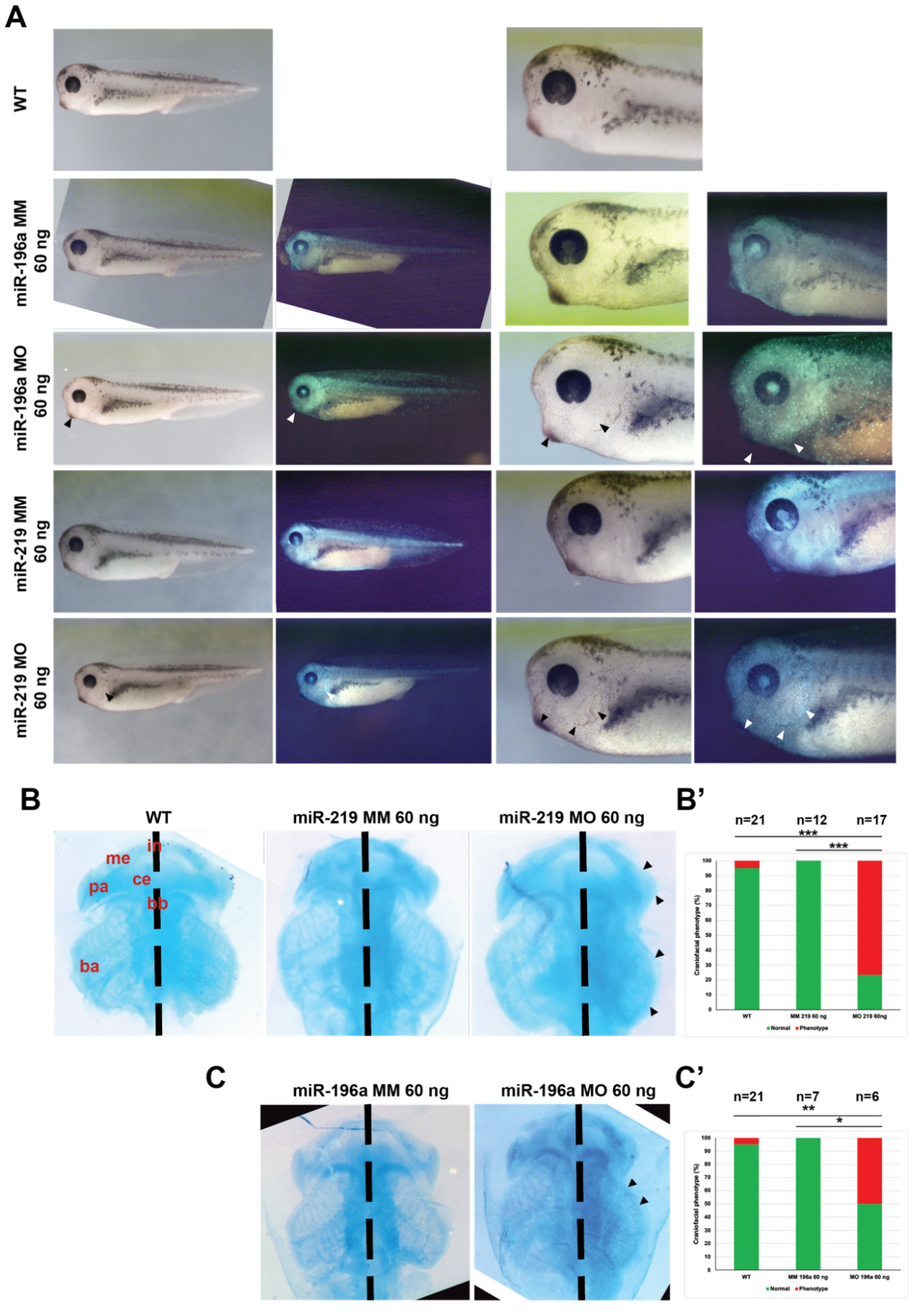
A
WT
miR-196a MM 60 ng
miR-196a MO 60 ng
miR-219 MM 60 ng
miR-219 MO 60 ng
B
WT
miR-219 MM 60 ng
miR-219 MO 60 ng
me
in
ce
pa
bb
ba
B'
n=21
n=12
n=17
***
***
Craniofacial phenotype (%)
WT
MM 219 60 ng
MO 219 60ng
Normal
Phenotype
C
miR-196a MM 60 ng
miR-196a MO 60 ng
C'
n=21
n=7
n=6
**
*
Craniofacial phenotype (%)
WT
MM 196a 60 ng
MO 196a 60 ng
Normal
Phenotype

Figure 4.16 - Assessment of craniofacial and craniofacial cartilage development after MO mediated miRNA KD in *X. laevis* embryo development. Embryos were injected into one dorsal blastomere at the 4-cell stage of development with a 10 nL calibrated needle and co-injected with 5 ng GFP cRNA. Right side of embryo is always injected side, black and white arrows indicate regions of phenotypic interest. miRNA KD led to craniofacial phenotypes. (A) Subtle craniofacial phenotypes seen in tadpoles are indicated by arrows. (B-C) Alcian blue cartilage preparations show clear branchial arch and cartilage phenotypes following miRNA KD. (B'-C') Blind count phenotype data. Test used for statistical analysis is Chi-squared on independent repeats. WT vs miR-196a MO p=0.006, miR-196a MM vs MO p=0.033, WT vs miR-219 MO p=<0.001, miR-219 MM vs MO p=<0.001. Key: ba= branchial arches, me= Meckel's cartilage, pa= palatoquadrate, ce= ceratohyale, bb= basibranchiale, in= infrastrole.

4.8.2 RNA-sequencing data analysis

RNA-sequencing was conducted on dissected NC tissue from embryos that had undergone miRNA KD on one side of the embryo. The NC of the injected and manipulated side was used for dissection (Fig. 4.8, Table 4.2). NC in situs were used to prove appropriate tissue had been dissected (Ward, 2017).

Following miRNA KD of miR-196a and miR-219 there were very clear reductions in NC marker expression. MiRNAs are negative regulators of gene expression, and post-transcriptionally down regulate gene expression upon complementary binding (Alberti and Cochella, 2017). Following KD of miRNA it is expected that a direct mRNA target of that miRNA would show enriched expression (Cheng and Li, 2008; Krutzfeldt et al., 2005). It could therefore be possible, as we see downregulation of NC genes, that miRNAs are targeting genes that are thus negatively regulating the expression of NC markers. Therefore, our miRNAs are likely to be indirectly affected along with development of NC; potentially targeting molecules that are upstream in the development of the neural plate or placodal development.

Overexpression of miR-196a has been shown to exhibit eye defects in *Xenopus* embryos (Qiu et al., 2009). Work aiming to investigate miR-196a further identified anterior neural development phenotypes (Gessert et al., 2010). Therefore, it was expected that following misexpression of miR-196a with MO or miRNA mimic that there would be phenotypes generated on eye markers and neural markers. As expected, the neural marker Pax6, responsible in eye development, is enriched after miR-196a KD (Grocott et al.,

2020). Interestingly the skeletal preparations for miR-196a KD tadpoles showed craniofacial defects, indicative of abnormal NC specification, this has also been seen in previous work by Gessert and colleagues (Gessert et al., 2010).

Previous unpublished data in the lab shows that Eya1 is a direct target of miR-219. Eya1 is implicated in early placodal development (Ward, 2017). The placodal tissue largely gives rise to sensory organs (Schlosser, 2014b; Schlosser and Ahrens, 2004). The RNA-seq data shows Eya1 is enriched following miR-219 KD but not significantly. The reason behind this enrichment not being significant could be due to the design of the experiment, in that NC tissue was dissected, and could be variable between dissections. This may mean that loss of tissues and expression within those is limiting the results. Therefore, it is unsurprising that genes that are highly expressed in neural plate or placode which are located anteriorly to NC, are not statistically significantly differentially expressed.

Recent research in developing chick has shown that the *Pax-Six-Eya-Dach* (PSED) network is regulated by miRNAs in the context of myogenesis, this provides strong evidence for miRNA role and function in regulation of PSED network in early embryonic development, and could also be implicated in the NC PSED network (Viaut et al., 2021). Given that *Eya1* is a cofactor for *Six1*, it is unsurprising that an upregulation of Eya1 led to a decrease in *Six* gene expression following KD of each miRNA in NC tissue (Fig. 4.8, Table 4.2), (Riddiford and Schlosser, 2017).

Six1 and *Irx1* are reciprocally linked in their expression and regulation of each other. The loss of *Six1* and expansion of *Irx1* is indicative of neural border signature which may mean that a fraction of neural border tissue was dissected when removing the NC tissue for RNA-seq (Sullivan et al., 2019). Some work has previously shown that *Eya1* and *Six1* interact with SWI/SNF chromatin re-modellers to drive neurogenesis. This may also go some way to explaining the dramatic enrichment of neural markers (Ahmed et al., 2012). KD of Six1 has previously shown a loss of PPE and an expansion of neural

plate (Brugmann et al., 2004). This may explain the upregulation of Pax3 and *Zic1* expression, as these are neural plate markers (Hong and Saint-Jeannet, 2007; Hong and Saint-Jeannet, 2017a; Milet and Monsoro-Burq, 2012).

4.8.3 MiRNA mimic rescue experiments

MiRNA mimics are used in experiments usually to rescue luciferase assay experiments (Wang, 2011). As previously mentioned, at time of writing a miRNA mimic has not been used to rescue a phenotype generated in a miRNA KD. However, a miRNA mimic had been used to overexpress miR-9 in Zebrafish to observe impact on *VEGFA* expression (Madelaine et al., 2017).

It was discovered late in this project that miR-196 in *Xenopus* has two isoforms, miR-196a and miR-196b. Therefore, it was essential to assess to what extent our miR-196a MO was targeting miR-196b. MOs are highly specific but can also bind complementarily to a target with a few mismatches in sequence matching (Heasman, 2002). In this case miR-196a mature miRNA is only one nucleotide different in its sequence as compared to miR-196b (Table 4.1). Therefore, it should have been expected that miR-196a MO could target and KD miR-196b. This can clearly be seen in Fig.4.3 where the miR-196a MO treated groups show a decrease in miR-196a expression -92% and decrease in miR-196b -81%. This is despite the fact the miRNAs are in separate parts of the genome. This is something to bear in mind for the next chapter where I present CRISPR-Cas9 data to KO miR-196a. Despite this, the rescue experiments performed in this chapter are likely to be specifically rescuing miR-196a, this is because in Fig.4.3 the addition of miR-196a mimic to miR-196a MO samples appears to significantly rescue miR-196a expression and not miR-196b. According to manufacturer (Qiagen) the LNA high binding affinity properties of the miRNA mimic means that the one MM between miR-196a and miR-196b can be detected and distinguished specifically by the q-RT-PCR primers used in this experiment (Grunweller and Hartmann, 2007). Therefore, it is thought that we are theoretically rescuing the expression of miR-196a at a transcript level when using the miRNA mimic in combination with miR-196a MO. This is because the miR-196b mimic would not rescue miR-196a at the transcript level. However, it is possible that the

miR-196b mimic, with miR-196b being so like miR-196a could still be targeting miR-196a target-mRNAs, and we may be overexpressing this miRNA. Therefore, at a functional level the miR-196b rescue following miR-196a MO KD may also rescue miR-196a KD phenotypes.

Looking at previous sRNA-seq on miRNAs in *Xenopus* NC tissue and other tissue explants, miR-196a and miR-196b both have significant expression in the NC (Ward et al., 2018). It is unclear at this stage if this could be the case without in situ hybridisation validation. Despite these concerns, q-RT-PCR is listed as a valid validation strategy when using miRNA mimics (Wang, 2011), as miRNAs do not produce proteins, a functional *in situ* hybridisation experiment may be the only option to analyse miRNA redundancy. Perhaps if we had known mRNA targets for miR-196a and -b we could analyse the expression profile of these by q-RT-PCR to identify if these are affected. Despite these concerns I believe the miR-196a mimic is rescuing miR-196a KD specifically. This is discussed further when I present CRISPR-Cas9 methodology to specifically KO miR-196.

MiRNAs are highly conserved across species, including our candidates miR-196a and miR-219 (See Chapter 3). Due to this, synthetic miRNA mimics for a variety of species are widely available (Jin et al., 2015; Wang, 2011). Figure 4.4 shows that human miR-196a mimic is 100% complementary to the Xenopus miR-196a. Use of miRNA mimics in cells have come under recent scrutiny, with the delivery of miRNA mimics affecting the expression level of the miRNA delivered (Wang, 2011). The research from this group conclude that considered and controlled concentrations of miRNA mimics are imperative. Dose response of miRNA mimics in *Xenopus* embryos were performed (Fig. 4.5 & 4.6). Optimal dose was selected at 15 μM (Fig. 4.5) as this would replicate the 60 ng dose of MO administered and would avoid non-specific toxicity, especially when co-injected with MO (Fig. 4.7), (Jin et al., 2015; Wang, 2011). For further information on miRNA mimic 15 μM to 60 ng morpholino please see materials and methods section for calculations and justification.

Using q-RT-PCR to evaluate the expression of miR-196a and miR-219 in MO control experiments and MO KD experiments were important to evaluate the efficiency of our miRNA mimic rescue at the transcript level (Fig. 4.7). As expected, when miRNA mimic was injected into embryos alone, this was enough to create an overexpression of the miRNA (fig. 4.7). Also, when control mismatch MOs were used for miR-196 no change in expression of miR-196a was seen at all. However, when MO for respective miRNAs were used significant reductions in miRNA expression were observed. As predicted, when respective MO and miRNA mimic was injected into the embryo the expression of miRNA is significantly rescued, and near normal levels of expression. This is the only published work that has used synthetic miRNA mimic in embryo research (Madelaine et al., 2017). In this research by Madelaine and colleagues, miRNA-9 mimic was used to overexpress miR-9, this was with the view that if you overexpress a miRNA, then more of the mRNA targets are being post-transcriptionally repressed, thus changing gene expression (Madelaine et al., 2017). Therefore, it was important in this project to see if overexpression of the miRNA mimics would affect expression of our mRNAs of interest such as *Snail2*, even though it is not a direct target of our miRNAs. In this case we do not see significant changes (Fig. 4.5 & 4.6). This presents another use of miRNA mimics in embryonic research to better understand miRNA targeting. For instance, if you are visualising the spatial expression of an mRNA that is a direct target of the candidate miRNA, and you overexpress the miRNA through use of a mimic it would be expected that to you would see less of the mRNA of interest if it is a direct target, and post-transcriptionally regulated by your miRNA. It is hypothesised that miRNA mimic will bind to the complementary MO to prevent MO binding to 3' UTR of an mRNA, and rescue gene and miRNA expression. However, it could also be possible that surplus mature miRNA copies can target the mRNA and post-transcriptionally function normally by repressing gene expression (Madelaine et al., 2017; Wang, 2011).

4.8.4 Functional characterisation of miRNA MOs and mimics

After demonstrating that miRNA mimics can rescue miRNA KD it was important to include the use of a control miRNA mimic, for this work this was

a miRNA mimic cel-miR-39-3p, as recommended by Qiagen (Fig. 4.9A). For all markers assayed by whole mount *in situ* hybridisation no significant phenotypes were observed (Fig. 4.9B). This was important as overexpression of a miRNA, could have unwanted effects as miRNAs are involved in almost every cellular process (Fan et al., 2020). The overexpression of miRNA-196a and miRNA-219 mimic had no significant impact either. Perhaps this is because of the low optimal dosing, and if doses were higher, then phenotypes would be observed. In Madelaine et al., (2017), a 2 μM dose of miR-9 mimic was used to overexpress miR-9 in zebrafish embryos, leading to reduction in VEGF-A expression. It is expected that the amount of mimic required would vary between miRNAs and embryos (Madelaine et al., 2017). Our q-RT-PCR data Fig.4.7 show that 15 μM of mimic leads to approximately 50% increase of miR-196a but a 25% increase in miR-219 expression (Madelaine et al., 2017).

Snail2 and *Sox10* are implicated in the induction, development, specification, and migration of NC, as well as anti-apoptotic regulation. Previous work has shown Sox10 loss leads to NC cell apoptosis and that Snail2 is anti-apoptotic (Honore et al., 2003; Klymkowsky et al., 2010; Shi et al., 2011). Following miR-219 and miR-196a MO KD, *Snail2* expression was reduced, with *Sox10* even more reduced in expression profile. This could be indicative that miR-219 is indirectly affecting the development of NC (Fig. 4.9A). Further work on Pax3 showed that NC expression may be affected by miR-219 at the NPB level, as *Pax3* is a key NPB marker (Milet and Monsoro-Burq, 2012). Cryosectioning of embryos following miR-219 KD was showed Pax3 upregulation was in the superficial ectoderm of the embryo (Fig. 4.13). This could then show that miR-219 is affecting NC development at the PPE and neural plate level through interaction with Eya1, Six3; but also, through altering Wnt, FGF or BMP signalling (Pla and Monsoro-Burq, 2018).

Other previous work in the Wheeler lab has shown that Eya1 is a direct target of miR-219, this agrees with the data presented on miRNA mRNA target prediction algorithm TargetScan (Agarwal et al., 2015). Eya1 is a marker of the pre-placodal ectoderm (Schlosser, 2014b). Interestingly, one of the other

mRNAs listed as a top target include Six3. This is significant as Six genes are also implicated in the development of PPE (Schlosser and Ahrens, 2004).

Pax3 is also expressed in HG and *Xhe2* is expressed in the HG (Hong and Saint-Jeannet, 2007), therefore it was decided to assay *Xhe2* expression following miR-KD. It has previously been reported that decreases in *Pax3* lead to a reduction in *Xhe2* expression with overexpression of Pax3 leading to an increase in *Xhe2* expression (Hong and Saint-Jeannet, 2014). In Fig.9 the opposite is seen, where *Pax3* is expanded and *Xhe2* is lost. Possible reasons for this include that *Xhe2* expression was assayed at St.18 later in neurula development than *Pax3* where the expansion was seen, and it would be useful to look at Pax3 expression later in neurula development for better comparison. This will be discussed in upcoming paragraphs. This suggests that there could be a fine balance of Pax3 required for Xhe2 expression. To see if embryo hatching is affected, it would be interesting to target the whole embryo with miRNA-MO and see if the expanded Xhe2 phenotype following miR-196a KD and the loss of Xhe2 phenotype has an effect on embryo hatching rate, as previous work has shown overexpression of hatching enzymes can lead to early hatching events (Schambony et al., 2003).

Following miR-196a KD, *Snail2* showed a similar loss of expression profile to miR-219 KD, but Sox10 following miR-196a KD shows an even stronger loss compared to miR-219 KD. This difference in expression profile may be indicating that our miRNAs are acting differently and are affecting the eventual development of NC differently.

Pax3 expression is expanded following miR-219 KD but reduced following miR-196a KD (Fig. 4.9). It could be possible that miR-196a is also acting upstream of the NPB and it would be important to look at other markers like Zic1 (discussed later). Misexpression of *Pax3* has previously been shown to lead to a loss of Snail2 expression (Hong and Saint-Jeannet, 2007).

Xhe2 was slightly expanded following miR-196 KD in the anterior forkhead region, but more posteriorly is slightly reduced (Fig. 4.9C). Previously, it has

been shown that when *Pax3* expression has been reduced, *Xhe2* expression is also reduced (Hong and Saint-Jeannet, 2014). This may explain the posterior phenotype where it looks slightly reduced in expression but does not explain the shift and expansion in the anterior region. Pax3 progenitors are responsible for expression of Xhe2, suggesting miR-196a KD has disrupted these same progenitors to affect Xhe2 expression.

To examine the impact of miR-KD on neurula development it was important to also look at later neurula development and the expression profile of Pax3 following miR-KD. For miR-196a KD (Fig.4.10) at early neurula, (St. 13), we see a loss of *Pax3*, for mid-late neurula (St. 17) a loss in the neural plate region can still be seen, but by later neurula (St. 18-19) the expression of *Pax3* is more normal. The HG progenitors of Pax3 following miR-196 KD at St. 17 show varied phenotypes, with expanded hatching progenitors in the anterior-most regions (Fig. 4.10).

The HG is found in the ectodermal region of anterior neural folds with Xhe2 expressing the hatching enzyme in the superficial ectoderm (Hong and Saint-Jeannet, 2007). *Pax3* overexpression leads to expansion of *Xhe* in the posterior and neural plate region of the embryo, and Pax3 KD leads to loss of Xhe expression in the forkhead anterior domains (Park et al., 2009). Our results show a small loss of Pax3 following miR-196a KD. It could be possible that Zic1 overexpression (Fig. 4.15) is compensating to maintain HG progenitor expression as loss of Pax3 and increase in Zic1 are hypothesised to generate HG fate (Hong and Saint-Jeannet, 2007). The same experiment was carried out following miR- 219 KD to examine *Pax3* expression later in neurula development (Fig. 4.11). The early neurula *Pax3* expansion phenotype following miR-219 KD is reduced later in neurula development (St. 17-19) and shows reduction in expression in the neural plate region. Reasons for Pax3 expansion will be discussed later.

Our RNA-seq data shows upregulation of neural pluripotency genes, *Pou*, following miR-196a and miR-219 KD, therefore it may be possible that genes that affect both Pax3 and neural differentiation are affected following miR-KD,

but are affected transiently affected in neurula developmental stages. This suggests a critical time point for miRNA regulation of NC induction and specification.

4.8.5 Further exploration of the miR-219 KD Pax3 phenotype

To investigate Pax3's role further, and to see if we could rescue expanded Pax3 phenotypes following miR-219 KD, a Pax3 MO approach was used (Fig. 4.11). The doses were in accordance with work published by Monsoro-Burq and colleagues (Monsoro-Burq et al., 2005). Increasing dose of Pax3 MO leads to altered *Snail2* expression, and loss of *Pax3* expression as reported previously (Monsoro-Burq et al., 2005). Pax3 has previously been reported to be regulated by miRNAs in myogenesis (Goljanek-Whysall et al., 2011). Human Pax3 is a direct target of miR-219 (hsa-miR-219a-1) according to miRDB miRNA mRNA target prediction database (Wong and Wang, 2015). This is significant as the mature miR-219 produced from this isoform is conserved within *Xenopus,* however, Pax3 is not listed as a target of miR-219 in Targetscan searches for Xenopus genomes. Potential future work may involve confirming if Pax3 is a direct target of miR-219 in *Xenopus*. This could be tested by luciferase assay (Viaut et al., 2021).

The Pax3 MO dose that had been optimised in (Fig. 4.11), was used to perform rescue Pax3 MO and miR-219 MO were injected into one dorsal blastomere at 4-cell stage (Fig. 4.12). When used this experiment recovered the expanded Pax3 phenotypes seen following miR-219 KD. This provides some evidence that miR-219 is interacting directly or indirectly with Pax3. Snail2, Sox10 and Xhe phenotypes following miR-219 KD were all loss of expression phenotypes (Fig. 4.12). When miR-219 MO and Pax3 MO rescue was performed this further reduced the expression of these genes with very little expression on the injected side of the embryo. This is to be expected as Pax3 is central to NC induction and Xhe2 development (Hong and Saint-Jeannet, 2007; Milet et al., 2013).

Loss of Pax3 would have a negative impact on the development of the NC GRN and is reported to be significant for the induction of NC (Pla and

Monsoro-Burq, 2018). Therefore, loss of *Snail2* and *Sox10* expression was to be expected when Pax3 MO was used in conjunction with miR-219 MO which also reduced expression of *Snail2* and *Sox10* (Fig. 4.12). With Pax3 expressed in HG progenitors, the further loss of *Xhe2* expression seen with Pax3 and miR-219 MO use was also predictable (Hong and Saint-Jeannet, 2007).

4.8.6 Exploring miRNA targets beyond NC

To further investigate at what level the miRNAs, miR-219 and miR-196a are implicating the development of NC, it was decided to look at other neural, neural plate and placodal markers, En2, Sox2, Zic1 and Pax6 respectively (Fig. 4.15). *En2* was chosen to examine for phenotypes as it was possible that the miRNAs may be affecting positional and anterior-posterior patterning in the developing embryos. *En2* is part of the Engrailed family of genes and are a group of highly conserved Hox genes expressed at the mid-hindbrain boundary (Dur et al., 2020; Hemmati-Brivanlou et al., 1991). Disruption to Hox expression can affect NC differentiation as Hox gene expression corresponds to the different rhombomeres and allow the NC to migrate in streams (Parker et al., 2018; Trainor and Krumlauf, 2000).

Other work has indicated that *Pou* genes are pluripotency mediators and have a role in NC differentiation. RNA-seq data presented in Fig. 4.8 shows that following miR-219 KD *Pou5f3.3* was enriched; and following miR-196a KD *Pou5f3.3* and *Pou5f3.2* are both also significantly enriched. Tien and colleagues show that *Pou5f3.2* must be repressed to allow for differentiation of NC (Tien et al., 2021). Therefore, it could be concluded that our miRNAs are once knocked down are preventing the differentiation and induction of NC at an upstream level, potentially through de-repression of *Pou* genes. The posterior shift in En2 expression may be further supported by other work that shows RALDH activity can lead to posterior shift in profile of *En2* expression (Chen et al., 2001). This posterior shift was also observed following miR-219 KD for *Sox2* and *Pax6* at the midbrain hindbrain boundary region. Following miR-196a KD, *En2* expression is lost. Changes in *En2* expression could be indicative of alterations in the Wnt signalling pathways, this is because En2 is

a direct target of Wnt signalling and works with BMP signals in order to pattern the nervous system in *Xenopus* (Lou et al., 2006; McGrew et al., 1999).

To be speculative and think beyond NC, it is possible *Pou* gene expression is impacted directly by miRNA KD (Fig. 4.8). *Pou* genes are pluripotency and stem cell factors. Pou60 (Pou5f3.3) has been shown to be upregulated following KD of Sall4 (Young et al., 2014). Sall4 KD shows inhibition of induction of induced pluripotent stem cells (Tsubooka et al., 2009). Repression of Pou60 allows for induction of neural fates and it is thought that Sall4 regulates Pou60 expression (Young et al., 2014). Young and colleagues show that Sall4 morphants (KD) have a shift in Pax2 expression just as seen in En2 phenotype following miR-219 KD (Fig. 13). Young and colleagues propose that Pou5f3 inhibits hindbrain patterning through disruption of FGF signalling in the isthmus (Young et al., 2014). This may explain the posterior shift in En2 expression shown in Fig. 4.15 following miR-219 KD. This may suggest anterior migration of forebrain and midbrain tissues, it would be beneficial to examine expression of other anterior posterior markers like Hox genes (Dressler and Gruss, 1989; McNulty et al., 2005).

Following miR-196a KD *Sox2* expression was expanded in the lateral neural plate regions. Sox2 is a neural marker and regulates the development of the peripheral nervous system (Wakamatsu et al., 2004). Previous work carried out in avian models show that Sox2 misexpression inhibits the formation of NC (Wakamatsu et al., 2004). This may explain the loss of Sox10 seen in Fig. 4.8 following miR-196a and miR-219 KD. In mouse it has been shown that Sox2 can affect the regulation of EMT processes which are important in the development of cranial features (Mandalos et al., 2014).

Pax6 is a placodal expressed gene and is a master gene in eye development (Grocott et al., 2020). NC cells are important in the development of the lens and eye (Grocott et al., 2011; Grocott et al., 2020). Following miR-219 MO KD the lens field, as indicated by the top arrow in Fig. 4.15A, has reduced expression on Pax6. The neural Pax6 expression in the medial region of the embryo appears expanded for miR-196a and miR-219 KD, potentially

indicative of perturbed neural development as Pax6 is initially expressed after neural tube closure (Manuel et al., 2015). Dicer is integral to miRNA biogenesis and Dicer MO KD experiments also show a reduction of Pax6 expression in lens placode tissue (Gessert et al., 2010). This supports the hypothesis of this project that miRNAs are implicated in the development of NC and NC-related tissues by suggesting that at least one miRNA must be influencing Pax6 development.

Zic1 is expressed in the NPB region and is implicated in the specification of NC (Hong and Saint-Jeannet, 2017a). Following miR-196a and miR-219 KD Zic1 is expanded, as indicated by the black arrows (Fig. 4.15). Zic1 overexpression work has previously been shown to affect Pax3 expression (Hong and Saint-Jeannet, 2007). This work supports previous research that shows a balance of Zic1 and Pax3 is required for NC fates (Hong and Saint-Jeannet, 2007; Milet et al., 2013).

4.8.7 Modelling miRNA KD effect on cranial NC development

Xenopus are a useful model system for studying human craniofacial disorders, particularly neurocristopathies. The use of Alcian blue cartilage staining is a useful method for visualizing craniofacial cartilage development in tadpoles (Dubey and Saint-Jeannet, 2017; Gouignard et al., 2016). Cranial NC originates from the dorsal neural tube (Gilmour et al., 2002). Sox9 contributes to chrondrogenesis and thus affects the development of craniofacial cartilage, Sox9 morphant tadpoles show abnormal pharyngeal arches and cranial skeleton (Spokony et al., 2002). It could be hypothesised that miRNA KD is affecting Sox gene expression, as we see strong loss of *Sox10* in early embryo development, and abnormal craniofacial phenotypes associated with Sox9 misexpression, in the future it would be interesting to examine Sox9 expression following miRNA KD.

With the loss of NC marker expression, it was important to look at later stages of embryonic development in tadpole stages to assay for craniofacial phenotypes (Fig. 4. 14). To do this MO miRNA KD's were performed as before but embryos were then left to develop until late tadpole stages (Fig. 4.13A).

Morphologically only subtle craniofacial phenotypes could be seen in whole embryos (see white arrows). Dissection of Alcian blue stained craniofacial cartilage revealed much clearer phenotypes. The miR-219 KD shows branchial arch phenotypes and reduced anterior craniofacial cartilaginous structures. MiR-196a showed more of a phenotype in the branchial arches. These phenotypes could be potentially indicative of changes in Wnt signalling, as this is important for the development and migration of NC (Borday et al., 2018).

Similar Alcian blue staining showed disruption of the craniofacial skeleton following miR-196a KD in (Gessert et al., 2010). Additionally, Gessert and colleagues used a MO to KD Dicer expression. The results showed strong craniofacial phenotypes showing similar branchial arch perturbations. In addition, morphologically their tadpoles have eye phenotypes, with very little eye pigment visible and loss of eyes (Gessert et al., 2010). We did not see this in our experiments, our morpholino sequences both target the mature miRNA, so our approach from this perspective was similar, the only technical explanation for this difference could be in concentration and volume of morpholino used, and that they performed 8-cell injections, whereas I performed 2-cell injections, making my MO potentially less concentrated. Despite this, loss of positional identity and patterning could explain the craniofacial phenotypes observed.

4.9.0 Conclusions & future work

The hypothesis for this chapter was that miR-196a and miR-219 would likely influence NC development. This was investigated through carefully controlled and validated miRNA MO KD experiments. Results showed clear NC phenotypes and indicated that at some level miR-196a and miR-219 are implicated in the development of NC. In addition, phenotypes were seen implicating the miRNAs in neural patterning, NPB development and the HG. The novelty of this chapter lies with the innovative approaches used. Use of miRNA mimics to rescue miRNA KD experiments in embryos had not been done before. Therefore, the careful validation experiments used, help set this

up as a routine method for future experimentation. Furthermore, the data presented helps support the claim that our miRNA candidates are implicated NC development.

This chapter, although showed clear evidence NC development is greatly impacted by miRNAs, it does not present the exact targets of miRNAs miR-196a or miR-219. This could be rectified through luciferase assay experiments but due to time constraints imposed by the COVID-19 crisis this work was not pursued. As discussed earlier, MOs only KD targets, the next chapter will investigate the use of CRISPR-Cas9 to KO miR-196a and miR-219. Further work will elucidate the impact and role of miR-196a and miR-219 in the gene regulatory network of NC development.

CHAPTER V

RESULTS

Functional characterisation of miRNAs: Part II
CRISPR Knockouts

5.1.0 Introduction

5.1.1 CRISPR-Cas9 and use in embryo development

CRISPR-Cas9 is the disruptor technology of my cohort of molecular biologists. It is a powerful tool with big promise but the core technology behind it was overlooked for over three decades. CRISPR was initially discovered in bacteria. In 1987 a small article published from Japanese researchers showed an obscure bacterial gene that encoded for an alkaline phosphatase that was juxtaposed between short repetitive sequences; these sequences function and purpose were to be left unknown until 2013 where they were revealed to be part of the CRISPR-Cas system (Charpentier and Doudna, 2013; Cho et al., 2013; Cong et al., 2013; Hwang et al., 2013; Ishino et al., 1987; Jiang et al., 2013; Mali et al., 2013). These short bacterial sequences were found to match DNA sequences from plasmids and viruses and led to speculation that this bacterial system was part of an adaptive immune response armoury to detect and protect bacteria from foreign DNA (Charpentier and Doudna, 2013).

The targeted genome editing works by using sgRNAs to target Cas9 nucleases to induce genomic cleavage (Cong et al., 2013). SgRNAs are part of the CRISPR RNA (crRNA); sgRNAs are the region that is complementary to the gDNA that is being targeted. The sgRNA will bind to the genomic target region if it has a protospacer adjacent motif (PAM), nGG sequence, any nucleotide, guanine guanine present. This helps guide the Cas9 endonuclease. Additionally, crRNA pairs with a trans-activating CRISPR RNA (tracrRNA), and recruits the Cas9 endonuclease to the target site for mutagenesis (Hwang et al., 2013; Nakayama et al., 2013).

In bacteria, the naturally occurring CRISPR complex is known as the type II CRISPR-Cas9 system. This system requires the uptake of foreign DNA into CRISPR loci to produce crRNAs, which anneal to tracrRNAs to direct Cas9 endonuclease mediated cleavage of target DNA (Hwang et al., 2013).

CRISPR can be used to target mutagenesis in a few different ways. The CRISPR Cas9 approach can induce double strand breaks in the genome. These can then be repaired by non-homologous end-joining (NHEJ), or

homology-directed repair (HDR). NHEJ processes lead to the formation of insertion-deletion mutations (INDELs), (Jang et al., 2020). To insert a transgene homology-directed repair (HDR) can be used to knock-in genes. An overview of CRISPR can be seen in Fig.1.

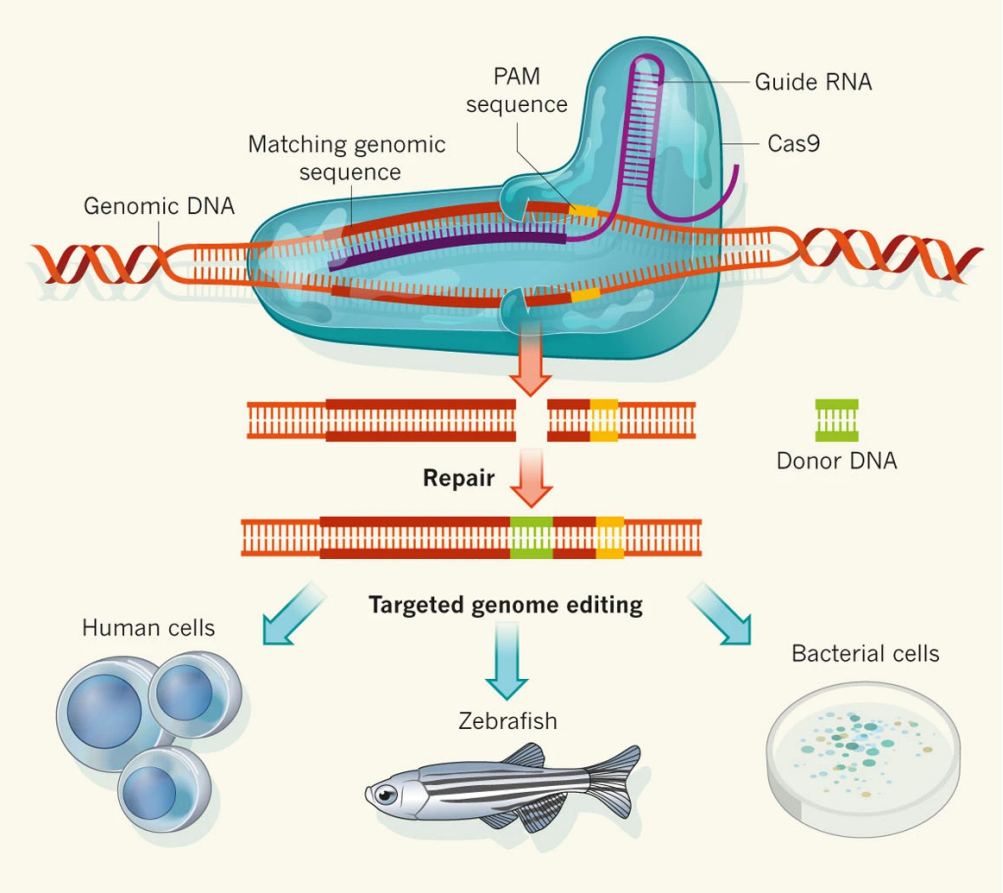

Figure 5.1 - Overview of CRISPR-Cas9 sgRNA targeted mutagenesis and genome editing strategies. Figure taken from: (Charpentier and Doudna, 2013).

CRISPR reports initially showed and demonstrated function in cell culture systems, however Hwang and colleagues were first to report efficient genome editing in zebrafish embryos (Hwang et al., 2013). It showed up to 50% efficiency of CRISPR in mutating the genes *tial1* and *gsk3b*. They also reported use of a plasmid based customisable approach. First a Cas9 expressing T7 promoter vector was generated and a separate vector with the sgRNA sequence with the tracrRNA sequence at the 3' end of the sgRNA sequence. For validation, gDNA was isolated and PCR was used to amplify region of interest. Sequencing was then used to identify presence of INDELs

(Hwang et al., 2013). T7 endonuclease assays were also employed to detect mutation events through detection of heteroduplexes (Hwang et al., 2013; Sentmanat et al., 2018). The method reported shows how phenotypes can be screened in founder fish but these fish would be mosaic, so stable KO lines were generated (Hwang et al., 2013).

In recent years CRISPR has become increasingly popular for manipulating gene expression in model organisms. CRISPR-Cas9 utilizes a highly specific targeted nuclease to induce genomic editing by NHEJ or HDR. CRISPR therefore is an efficient method that can rapidly generate KO *Xenopus* embryos for phenotype and genotype analysis (Nakayama et al., 2013; Ran et al., 2013).

X. tropicalis are a diploid species of *Xenopus* and so are the optimal *Xenopus* model for this project using targeted mutagenesis techniques such as CRISPR/Cas9 (Grainger, 2012; Nakayama et al., 2013). Transient knockouts and generation of stable lines can be achieved with this approach.

Hypotheses and Aims

This chapter will address the following gaps in knowledge: development of a CRISPR-Cas9 pipeline to KO miRNAs efficiently in *Xenopus* embryos if miRNA KO embryos are viable and how to generate stable miRNA knockout *Xenopus* lines. It is hypothesised that CRISPR can be used to generate miRNA KO F0 and eventually, lines of miRNA-KO *Xenopus*. Therefore, the aim of this chapter was to generate a novel CRISPR-Cas9 approach to KO miRNA-196a and miR-219 in *X. tropicalis* embryos, validate this technique, and functionally characterise the impact on NC, NPB and HG development. It is expected that NC, NPB and HG expression will show strong phenotypes similar to those observed in chapter 4 following morpholino-mediated miRNA-KD.

5.2.0 Results

5.2.1 Optimization of CRISPR-Cas9 and control development

To optimize CRISPR-Cas9 and to determine if the technique was viable with the system implemented here, a positive control experiment was developed. Reference sgRNAs and approach used by Nakayama et al., to mutate the pigment gene *tyrosinase*, by disrupting the start codon and generating a frameshift mutation were used (Nakayama et al., 2013).

To do this, gDNA was taken from *X. tropicalis* tadpoles at St. 35 and PCR was carried out with primers targeted to amplify tyrosinase region. WT embryos as well as mutants were processed, keeping WT as a control. The raw sequence can be seen in Fig. 5.2. When comparing the sequences, with WT, both mutants are not only very different to the WT but also each other with a variety of INDELs. The chromatogram for the mutant sequences supports this by showing that the position of the mutations is different within the cloned mutant PCR amplicon.

To further validate the presence of indel mutations, a T7 endonuclease assay was carried out. A T7 endonuclease assay is a PCR based assay used for the identification of INDELs. The target of interest needs to be amplified from gDNA by a high-fidelity PCR. This PCR then undergoes heating and graded cooling to allow sites of mismatches, heteroduplexes, to form. The final step involves the addition of T7 endonuclease, which cleaves these heteroduplex sites, and generates multiple amplicons which can be visualised on an agarose gel (Sentmanat et al., 2018).

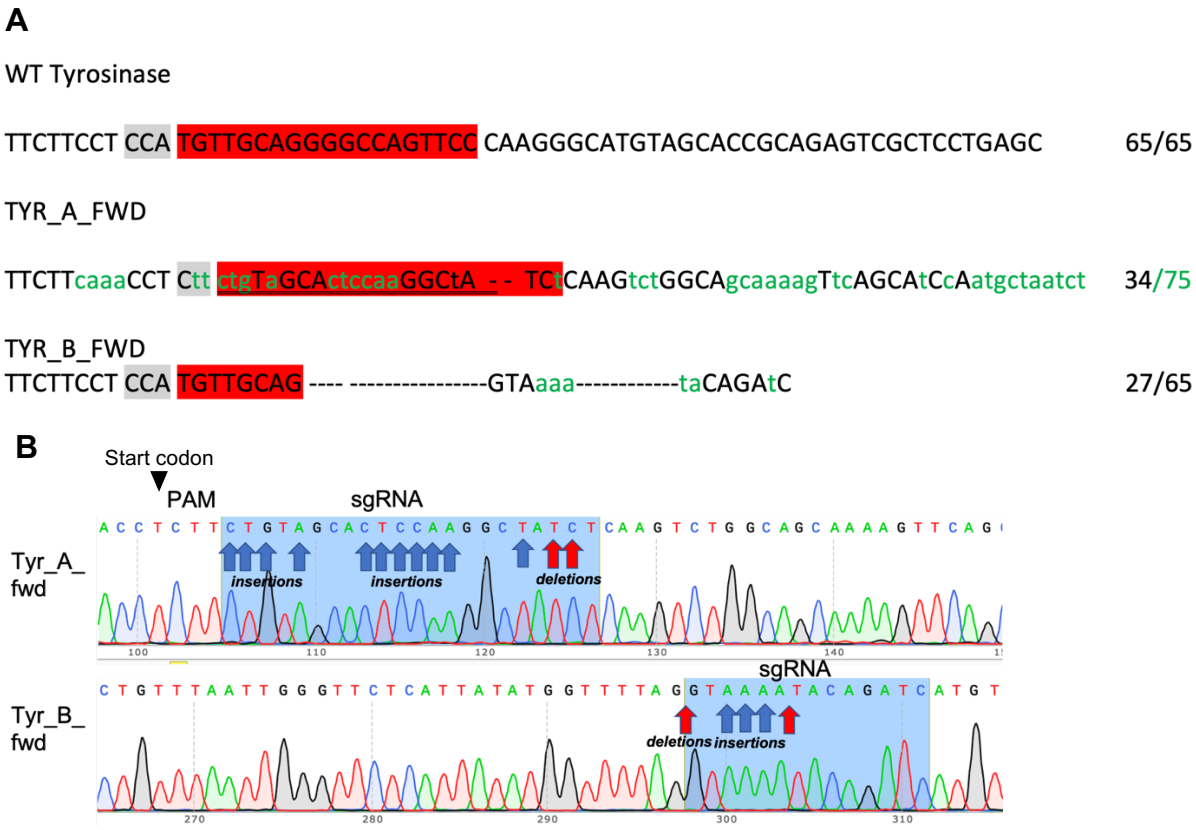

Figure 5.2 – Sequence analysis of CRISPR-Cas9 mutant tyrosinase embryos. (A) Raw sequence data, WT sequence, then two different mutant embryo sequences. The highlighted grey region indicates the PAM region for the Cas9, the red highlight signifies the sgRNA sequence, -'s indicate deletions, and lower case green letters indicate mismatch or insertion mutations. (B) Mutant chromatogram sequence data, blue arrows indicate insertion mutations, and red deletions. Highlighted blue regions show where the sgRNA complementary sequence would have been.

It was decided to assess the efficacy of sgRNAs, using the T7 endonuclease assay. In Fig. 5.3 WT and mutant tyrosinase embryo samples were used to trial this method. PCR was carried out and a WT and mutant sample were selected for the assay. As expected, control samples, (WT and Cas9), yielded a single amplicon, indicating no CRISPR events had occurred. The mutant tyrosinase samples yielded multiple bands, as did the positive control sample, indicative of CRISPR cleavage events in these embryos. These additional bands were generated from the T7 endonuclease cleaving mismatches induced by INDEL mutation CRISPR events.

Tyrosinase is a key molecule in the development of pigment (Kumasaka et al., 2003; Zuasti et al., 1998). Pigment is a NC derivative with *Sox10* and *Mitf* critical in the development of the melanocyte lineage (Aoto et al., 2015; Cheung and Briscoe, 2003; Sauka-Spengler and Bronner-Fraser, 2008). Therefore, it would not be surprising that if tyrosinase was mutated that a pigment and melanocyte phenotype would be generated.

To observe pigment phenotypes induced via CRISPR, embryos were left to develop into tadpoles as this is when most pigment can be seen, particularly in the eye and above the abdomen and running dorsally along the embryo (Tomlinson et al., 2009). As seen in Fig. 5.4, WT and Cas9 treated groups of tadpoles have round pigmented eyes, pigment running along the dorsal side of the tadpole and above the abdomen in a dense patch. In stark contrast to this the tyrosinase mutant tadpoles saw a large reduction in the amount of pigment. The red arrows denote regions most highly affected; these include the eye where most of the pigment in the retina is completely absent. This phenotype was extremely penetrant and was observed in every tadpole in the CRISPR treated group.

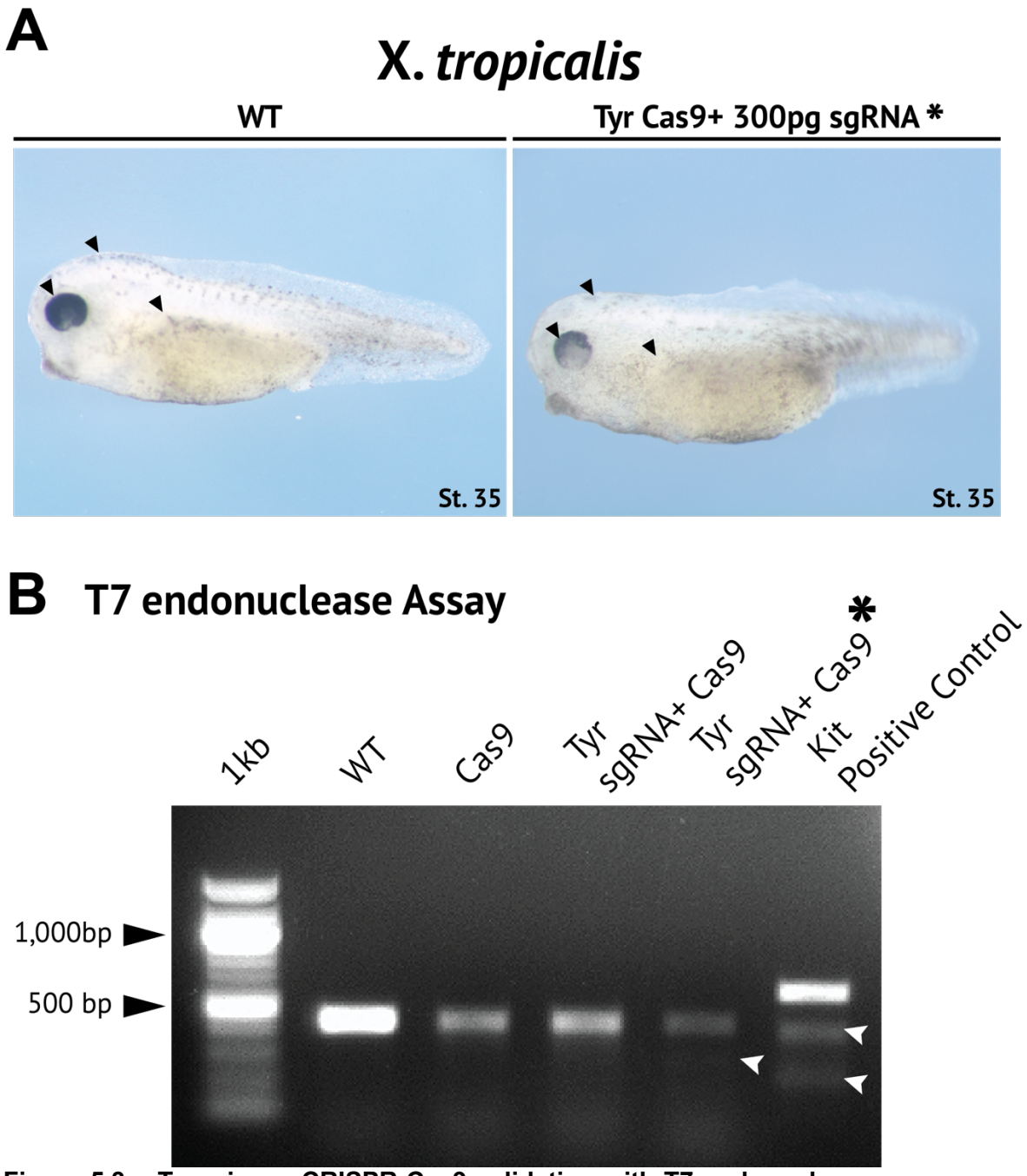

Figure 5.3 – Tyrosinase CRISPR-Cas9 validation with T7 endonuclease assay with PCR digest of genomic DNA amplified with tyrosinase primers. *X. tropicalis* embryos were injected at 2-cell stage into one blastomere with a 4.2 nL calibrated needle. Black arrows indicate regions of phenotypic interest, with loss of pigment in mutants. (A) Phenotype of embryos used for T7 endonuclease assay; loss of pigment phenotype observed in crispant tadpole. (B) T7 endonuclease assay. Expected band size is approximately 450 bp. Lane 1 kb NEB ladder, lane 2- WT genomic sample, lane 3= Cas9 control injected embryo genomic sample, lane 4 & 5- tyrosinase crispant embryo genomic samples, lane 6= positive control sample from the kit (unknown orgin). Mutant lane 5 and positive control lane 6 show multiple bands indicative of CRISPR INDEL mutation events.

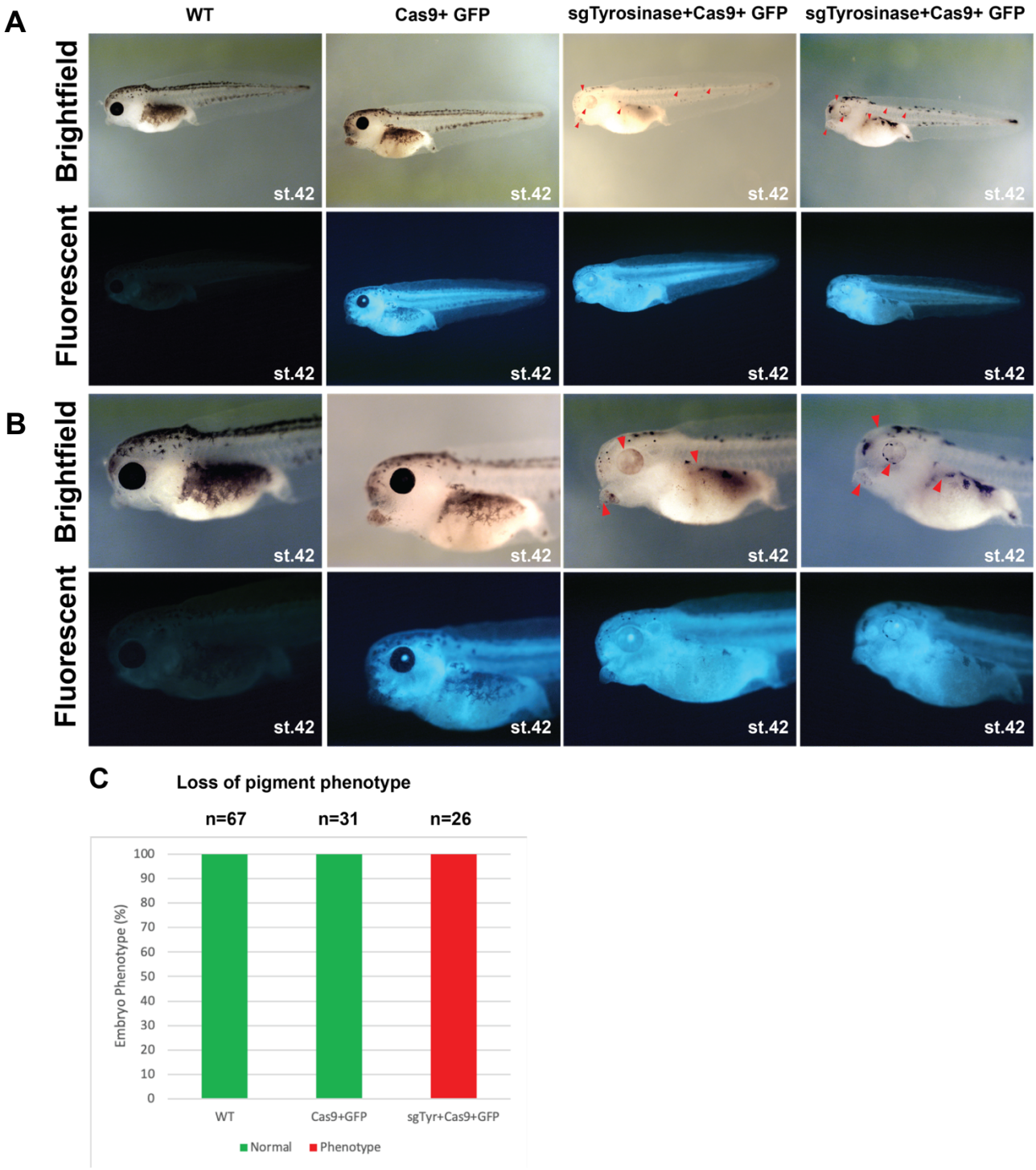

Figure 5.4 – Phenotype analysis of CRISPR-Cas9 mutant tyrosinase *X. tropicalis* tadpoles. Tyrosinase crispant embryos show strong loss of pigment phenotypes. Embryos were: uninjected WT, injected with Cas9 protein and GFP cRNA tracer (negative control) or injected with 4.2 nL with 300 pg of sgRNA, Cas9 and GFP cRNA tracer (experimental). Red arrows indicate pigment loss phenotype. A) Whole-tadpole view, 5 x magnification. B) 10 x magnification view of anterior half of tadpole. Phenotypes in mutants are highlighted by red arrows. C) Count data showing 100% loss of pigment phenotype in mutant tadpoles.

5.3.0 CRISPR Optimization to mutate miRNA-196a

As the CRISPR method was now working in the lab I began to develop a method for knocking out miR-196a and miR-219 in *X. tropicalis*.

5.3.1 Using single sgRNA injection to mutate miR-196a

The first step to mutate the miRNAs with CRISPR-Cas9 was to design efficient sgRNAs. MiRNAs are processed during their development; they are first transcribed in the cell nucleus and undergo processing and cleavage to form a mature miRNA. At first, they can appear as a pri-miRNA stem loop structure. The ends of the stem-loop are trimmed off by DROSHA and DICER enzymes. This then leaves the mature miRNA. This can then elicit disruption to gene expression via post transcriptional silencing. The miRNA does this through complementary binding of its internal seed region with the 3' UTR of a messenger RNA. Upon binding the messenger RNA is targeted for destruction (Agarwal et al., 2015; Inui et al., 2010). Therefore, when designing sgRNAs to silence and knockout a miRNA the seed region was the first target of interest, and if this was not possible the next most desirable region was to target the mature miRNA region.

In Fig. 5.5 the designs for sgRNAs made using CRISPR scan were modelled to see where within the stem-loop the miRNA would be targeted. The large red arrows indicate probable sites of potential CRISPR events. Guide 196a-1 would have potentially targeted the end of the mature miRNA. Guide 196a-2 and 196a-3 targeted the mature miRNA more centrally.

A **196a**

FORWARD

1. 5′ TAATACGACTCACTATAGGGATTGCTTTTTCTTAACGGTTTTAGAGCTAGAA 3′ + STRAND PAM: CGG
2. 5′ TAATACGACTCACTATA*GG*TTTAGGTAGTTTCATGTTGTGTTTTAGAGCTAGAAATAGCAAG 3′ + STRAND PAM: TGG
3. 5′ TAATACGACTCACTATA***GG*** TTAGGTAGTTTCATGTTGTTGTTTTAGAGCTAGAAATAGCAAG 3′ + STRAND PAM: GGG

REVERSE

3′ AAAAGCACCGACTCGGTGCCACTTTTTCAAGTTGATAACGGACTAGCCTTATTTTAACTTGCTATTTCTAGCTCTAAAAC 5′

B

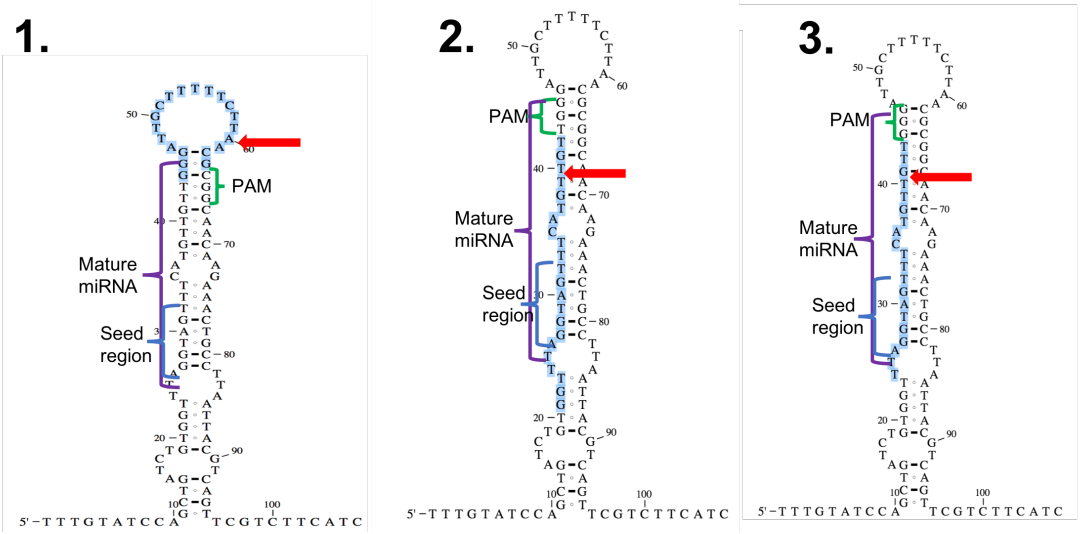

Figure 5.5 - Guide RNA designs for miR-196a using sequence data from Xenopus tropicalis version JGI 4.2, for T7 promoter design using CRISPRScan. (A) Sequence of sgRNAs to target miR-196a. Key- yellow- T7 promoter sequence, blue- sgRNA, bold italic- extra guanine residue, purple- complementary reverse primer sequence region. (B) SgRNA designs. Grey bar highlights the seed region, purple bar highlights the mature miRNA, PAM highlighted by green bar and expected site of CRISPR mutation is highlighted by a red arrow. The sequences annotated are: Mature miRNA-TAGGTAGTTTCATGTTGTTGG and Seed 5P- AGGTAGT. Red arrow indicates forecast cutting site of Cas9.

To quickly evaluate the efficacy of the candidate sgRNAs above, and their ability to create indels, a T7 endonuclease assay was deployed (Sentmanat et al., 2018). In Fig 5.6 candidate 196-2 and 196-3 showed promise, however an erroneous extra amplicon was faintly seen in the WT control.

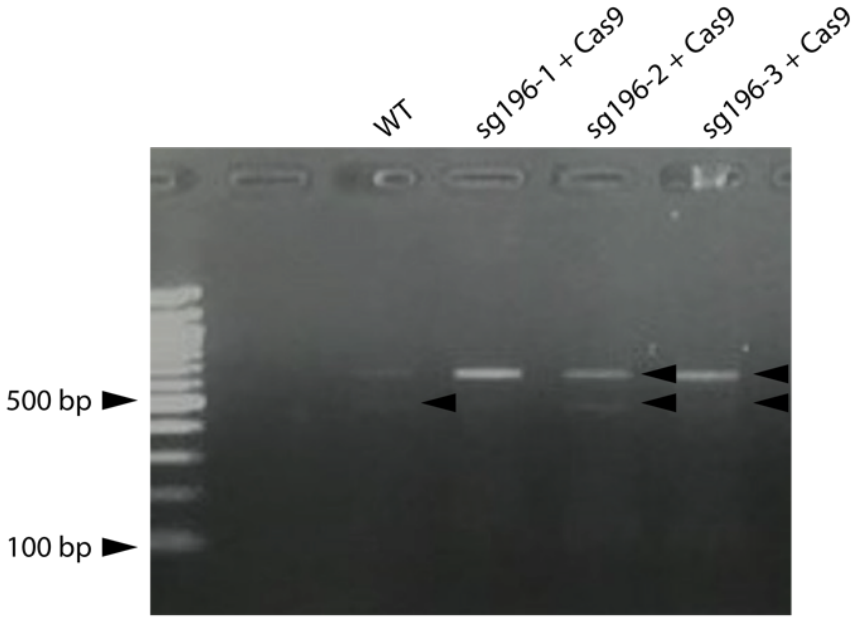

Figure 5.6 - T7 Endonuclease assay of mutant miR-196a. Genomic DNA was taken from X. tropicalis embryos and PCR amplified miRNA region *of 558 bp with miR-196a F and R primer*. This went through T7EI assay. miR-196a WT products are in lane 3, mutant miR-196a products can be seen in lane 4-6. Lane 5 embryo was injected with sgRNA 196-1. Lane 6 embryo was injected with sgRNA 196-2. Lane 7 was injected with sgRNA 196-3.

The sgRNAs designed were synthesised and prepared with the Cas9 and a tracer GFP cRNA. SgRNAs were injected into a *X. tropicalis* embryo at a 1 cell stage to target the whole embryo and hopefully see more CRISPR events as a result. The gDNA was then extracted from these individual embryos for genetic analysis. This was achieved using PCR of gDNA for miR-196a, which produced amplicons that were then subcloned into pGEM-T-easy and sequenced by Sanger sequencing. The sgRNA region was located within these sequences, both for controls: WT uninjected samples and Cas9 injected only samples, as well as potential mutants. The WT and Cas9 sequences showed 100% match of the sgRNA sequence, showing that a CRISPR event, an INDEL mutation had occurred in the expected region in the mutant sample. The chromatogram results can be seen below in Fig. 5.7. The WT and Cas9 samples have the WT sequence for miR-196a, and the sgRNA and PAM regions have been annotated by green and blue bars. This was indicated by black arrows. The INDEL mutation showed a point mutation, a change from thymine to adenine nucleotide.

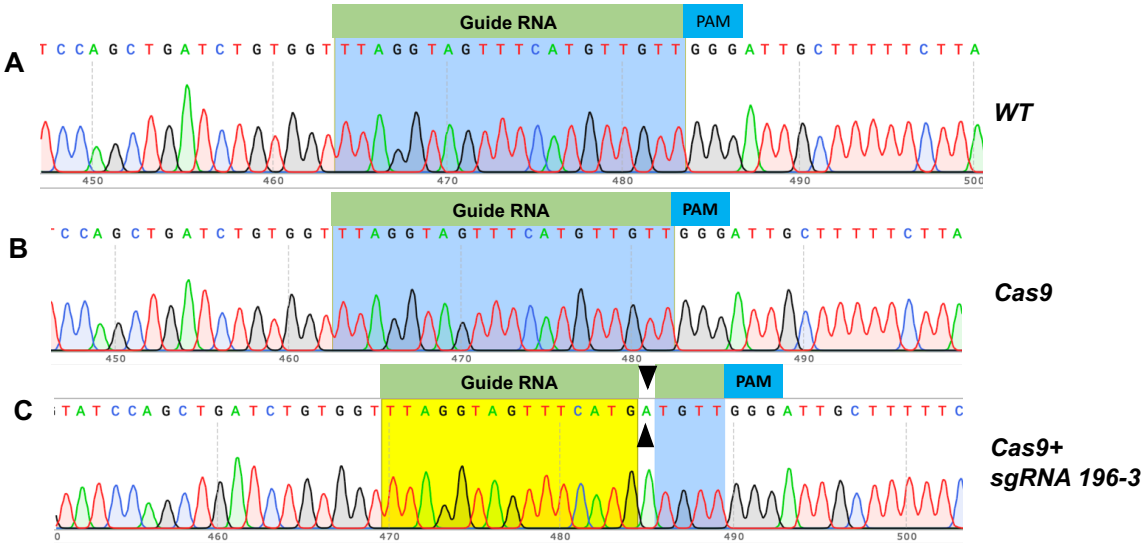

Figure 5.7 – Chromatogram sequence data for single guide RNA mutation of miR-196a. Guide RNA sequence highlighted in green and PAM sequence in blue. Genomic DNA was PCR amplified and subcloned into pGEM-T-Easy and sequenced with M13 primers. A) WT control embryo miR-196a sequence. B) Cas9 injected only control embryo miR-196a sequence. C) Cas9 + sgRNA 196-3 mutant "CRISPR" embryo miR-196a sequence with mutation T to A nucleotide indicated by the black arrows.

To observe the significance of the single point mutation the raw sequence data was modelled. The pri-miRNA stem-loop structure was predicted by online bioinformatics tool RNA Vienna fold. This gave a visual output of the miRNA structure. The WT structure for miR-196a shown in A, and the mutant in B (Fig. 5.8). The mature miRNA is indicated by a blue bar and the seed region is highlighted in green. The shift from GTT to GAT in the mutant generated a small extra bulge within the miRNA (Fig 5.8), and could still have a normal or novel function (Bhattacharya and Cui, 2017).

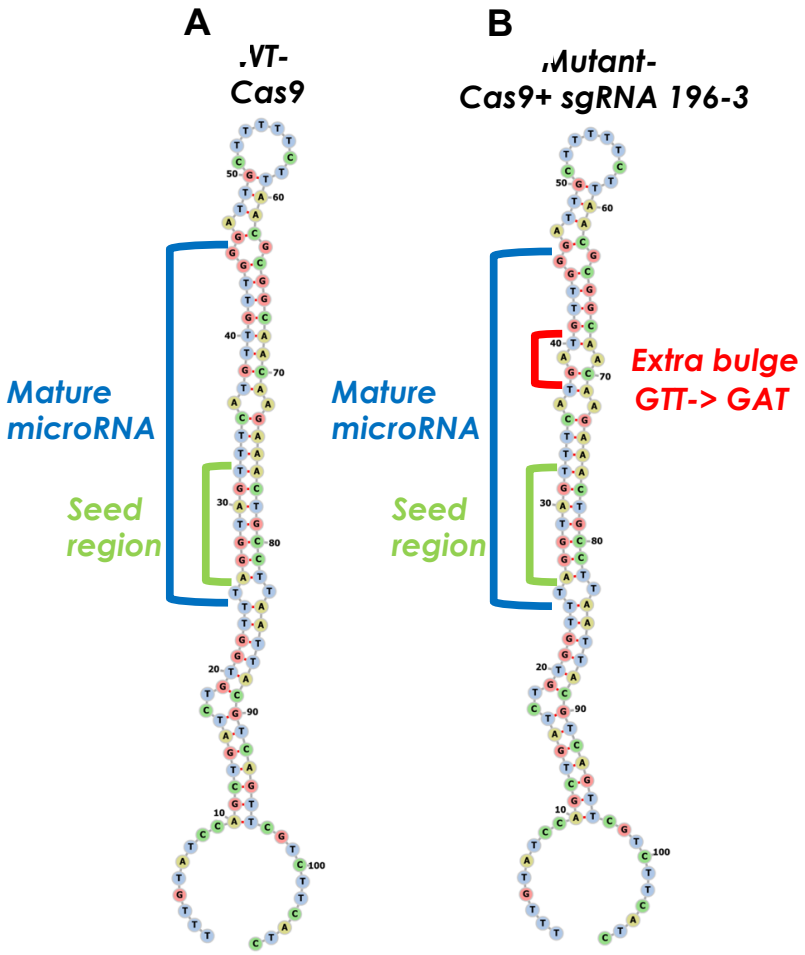

Figure 5.8 – Modelling miRNA stem-loop predicted structures after CRISPR mutagenesis of miRNA. Sequence information taken from sequences described in Fig.7. Blue bar indicates where the mature miRNA sequence would be, the green bar indicates where the miRNA seed region would be and red bar denotes any areas of change. Left- WT Cas9 injected only embryo genomic sequence subcloned into pGEM T Easy. Right- Mutated miRNA-196a model miRNA stem loop structure. 3 bp change in mutation from GTT to GAT. Modelled by RNA fold vienna.

Before freezing embryos for gDNA extraction and genotyping analysis, embryos were tracked during development to observe for any abnormalities. Some abnormal phenotypes were observed. In Fig.5.9 mutant embryos look underdeveloped and have some craniofacial impairments. These defects are more readily seen at later stages of development in the early tadpole. This is reflected by the number of embryos counted with phenotype (Fig. 5.9B).

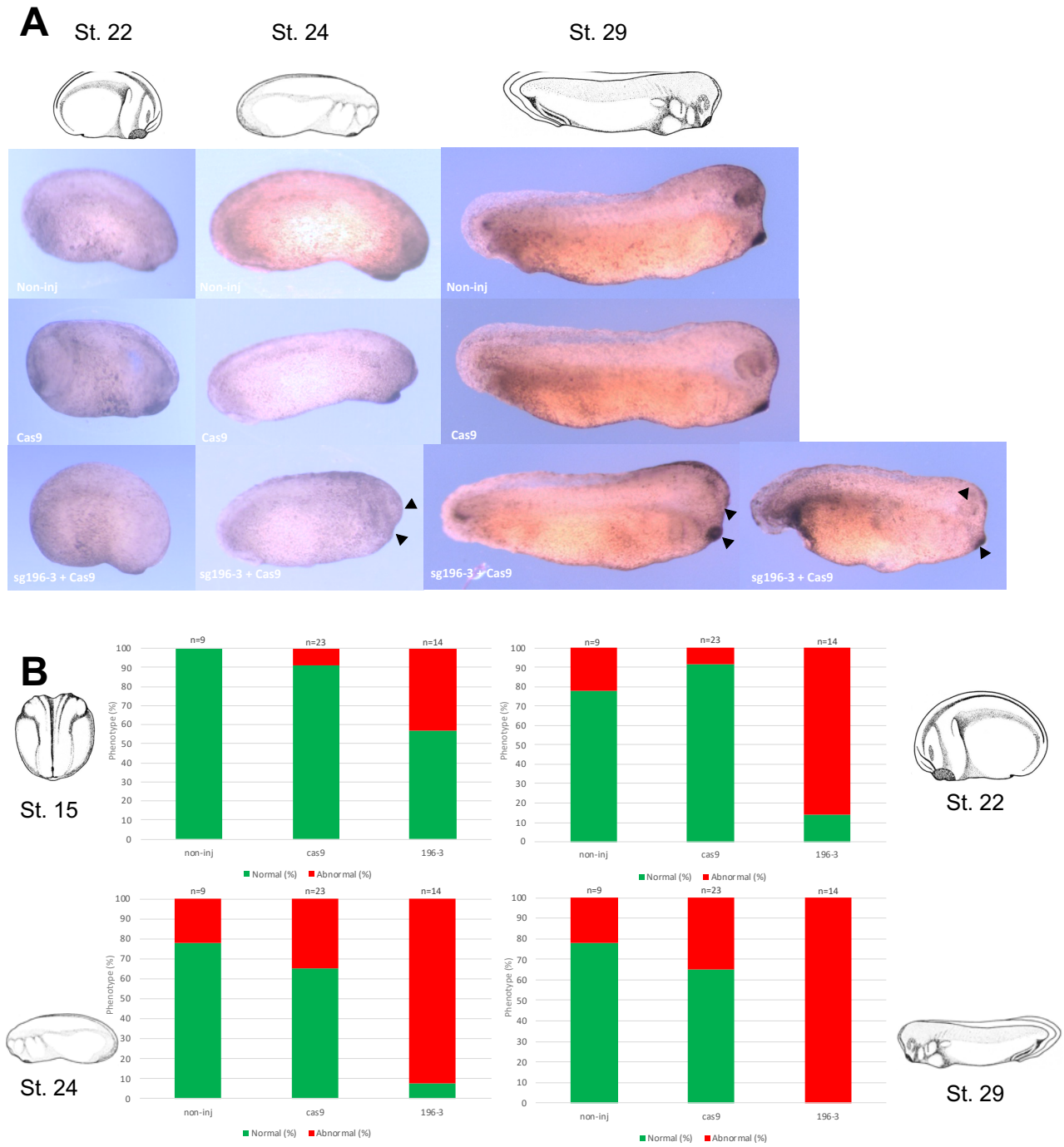

Figure 5.9 – MiR-196a mutant embryo phenotype analysis. *X. tropicalis* embryos were injected into one blastomere at 1 cell stage using a 4 nL calibrated needle containing 300 pg sgRNA, Cas9 protein and 5 ng of GFP cRNA tracer. Injected side of embryo facing viewer. Black arrows indicate craniofacial phenotypes. (A) Early tadpole development starts to show craniofacial phenotype in miR-196a mutants from St. 24 onwards, with eye and cement gland phenotypes visable. (B) Count data to score prevalance of phenotypes in developing embryos from neurula through to tadpole stages.

The same clutch of *X. tropicalis* mutant embryos were used from the above experiment to conduct whole mount *in situ* hybridisation gene expression analysis to see if there would be any phenotype in NC or neural plate border derivatives because of miR-196a KO. As the embryos were at tadpole stages

it was decided to perform whole mount *in situ* hybridisation for Xhe2, a HG marker, as this marker is highly expressed at this stage (Hong and Saint-Jeannet, 2014; Katagiri et al., 1997).

Xhe2 has a fork head HG profile. This can be seen in Fig. 5.10 by the WT and Cas9 treated embryo groups. The mutant miR-196a group however had alteration on one side of the embryo, the injected side of the embryo, as shown by the black arrows. Parts of the fork head are missing or severely disrupted in over 70% of the embryos (Fig. 5.10B).

5.4.0 CRISPR Optimization to mutate miRNA-219

MiR-219 was previously identified in the lab to be highly enriched in NC tissue, and was a strong candidate to investigate the role of miRNAs in the development of NC (Ward et al., 2018).

5.4.1 Using single sgRNA injection to mutate miR-219

The first step to mutate the miRNAs with CRISPR-Cas9 was to design sufficient sgRNAs against miR-219. As mentioned before to silence and KO a miRNA the seed region was the first target of interest, and if this was not possible the next most desirable region was to target the mature miRNA region.

The design of the sgRNAs generated to knockout miR-219 are described in Fig. 5.11. Candidates 1 and 3 would potentially target the seed region of the miRNA, candidate 2 would target the mature miRNA and candidate 4 would target the stem loop.

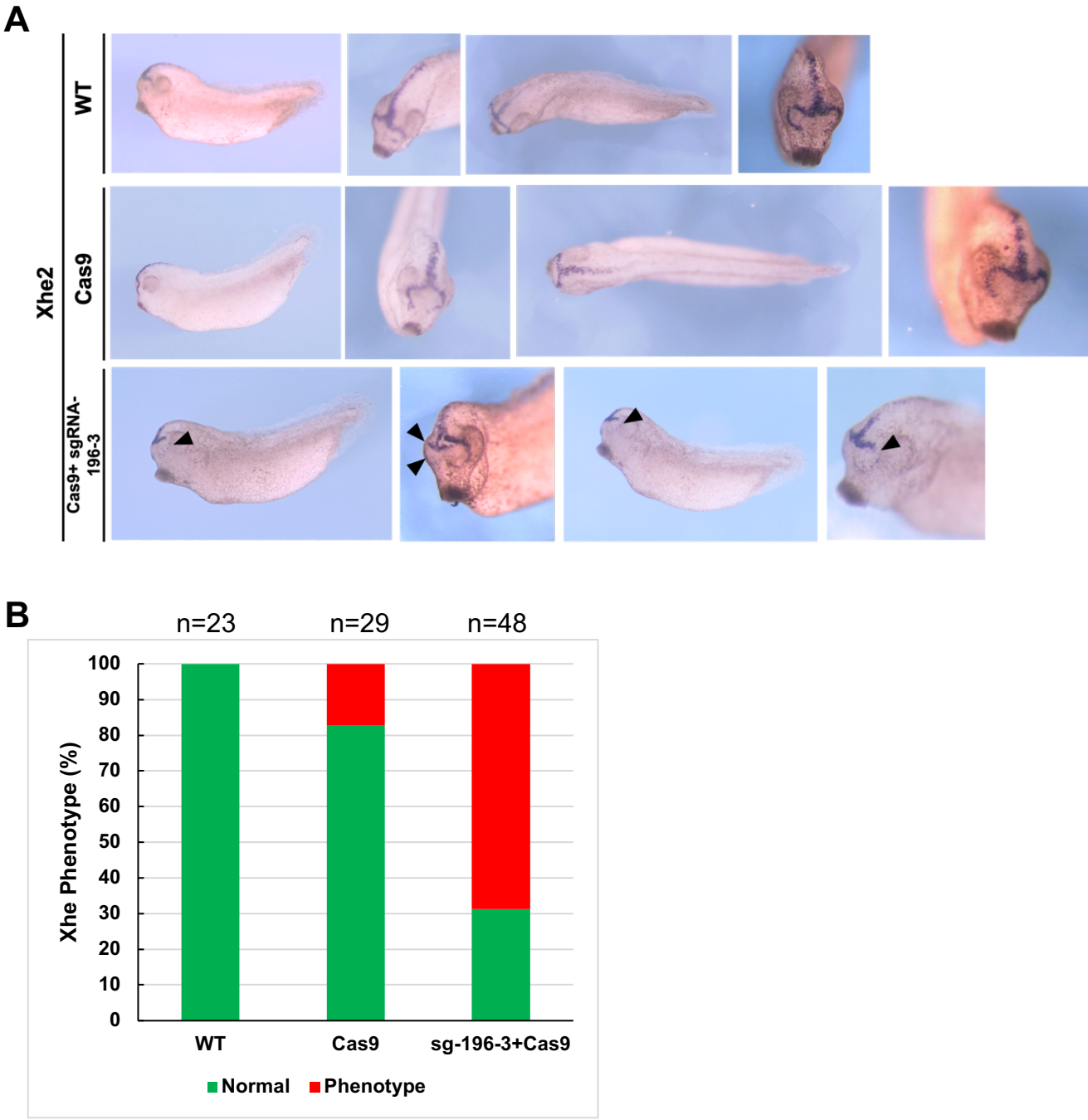

Figure 5.10 - Hatching gland phenotype analysis of CRISPR miR-196a mutant *X. tropicalis* embryos by WISH with marker Xhe2. Embryos were injected at the 2 cell stage into one blastomere with 300 pg of sgRNA 196-3 plus Cas9 protein and GFP cRNA tracer. All embryos are St. 33. Injected side of embryo is facing viewer. Black arrows indicate Xhe2 loss phenotypes. (A) Parts of the fork head expression profile are missing on one side of the *X. tropicalis* miR-196a mutant embryos as indicated by the black arrows. (B) Xhe2 loss phenotype count data, one biological repeat; all tadpoles are sister embryos.

A **miR- 219 Guide RNAs**

Forward oligos

1. 5′ TAATACGACTCACTATA***GG***ATTGCGTTTGGACAATCAGTTTTAGAGCTAGAA 3′ - STRAND PAM: AGG
2. 5′ TAATACGACTCACTATA***GG***ATGTCCAGGCACAATTCTGTTTTAGAGCTAGAA 3′ -STRAND PAM: TGG
3. 5′ TAATACGACTCACTATA***GG***ATTGTGCCTGGACATCTGGTTTTAGAGCTAGAA 3′ + STRAND PAM: TGG
4. 5′ TAATACGACTCACTATA***GG***TGCCTGGACATCTGTGGCGTTTTAGAGCTAGAA 3′ + STRAND PAM: TGG

Reverse oligo

3′ AAAAGCACCGACTCGGTGCCACTTTTTCAAGTTGATAACGGACTAGCCTTATTTTAACTTGCTATTTCTAGCTCTAAAAC 5′

B

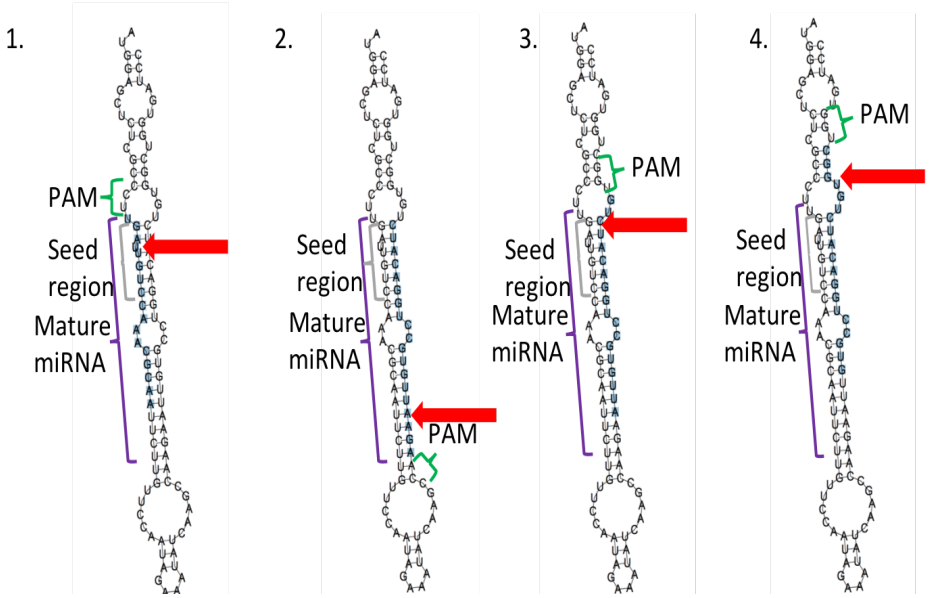

Figure 5.11 Guide RNA designs for miR-219 using sequence data from Xenopus tropicalis version JGI 4.2, for T7 promoter design using CRISPRScan. (A) Sequence of sgRNAs to target miR-219. Key- yellow- T7 promoter sequence, blue- sgRNA, bold italic- extra guanine residue, purple- complementary reverse primer sequence region. (B) SgRNA designs. Grey bar highlights the seed region, purple bar highlights the mature miRNA, PAM highlighted by green bar and expected site of CRISPR mutation is highlighted by a red arrow. The sequences annotated are: Mature miRNA: TGATTGTCCAAACGCAATTCT and Seed 5P- GATTGTC. Red arrow indicates forecast cutting site of Cas9.

Again, to rapidly evaluate the efficacy of the candidate sgRNAs the T7 endonuclease assay was deployed to find an effective sgRNA. In Fig. 5.12 the WT lanes give a clean band for miR-219 at the expected size. For the mutant lanes in the gel 5-7, sgRNA-219-1 did not give an extra band so appears as though it is not highly efficient. However, sgRNA-219-2 and sgRNA-219-3 yielded an extra band, suggestive of good CRISPR events and indels. As sgRNA-219-2 gave the brightest band it was decided to focus on using this sgRNA for further evaluation and validation.

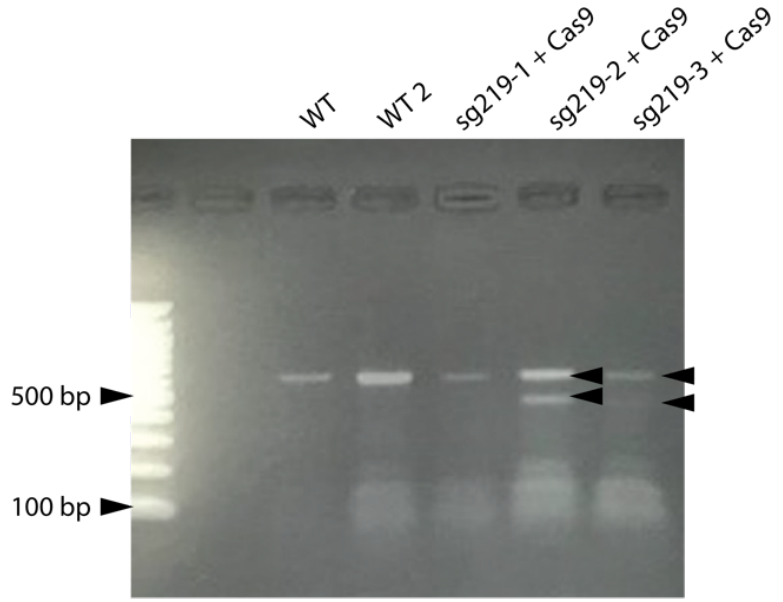

Figure 5.12 - T7 Endonuclease assay of mutant miR-219. Genomic DNA was taken from *X. tropicalis* embryos and PCR amplified miRNA region. This went through T7EI assay. Primers miR-219 F2 and R2 were used to generate an amplicon of 586 bp. miR-219 WT products are in lane 3 and 4, mutant miR-219 products can be seen in lane 5-7. Lane 5 embryo was injected with sgRNA 219-1. Lane 6 embryo was injected with sgRNA 219-2. Lane 7 was injected with sgRNA 219-3.

GDNA was isolated from injected embryos, miR-219 was amplified by PCR and subcloned into pGEM-T-Easy for sequencing. Fig. 5.13 shows the chromatogram sequence output from this experiment. The green bars denotes the region where the sgRNA is, blue-turquoise bars highlight the PAM region. It is expected that the indels would be a few base pairs upstream of the PAM site. Fig 5.13 C shows the mutant sequence from a CRISPR sample, the black arrows denote the site of indel mutation. A -3bp deletion of -CTT can be seen.

To model the impact of the -3bp deletion seen in Fig. 5.13 C by sgRNA-219-2 RNA fold Vienna tool was used. The WT sequence was also modelled for miR-219 and can be seen below in Fig. 5.14. The mature miRNA region is highlighted in green and the seed region in dark blue. For the mutant model the site of mutation is denoted by a red arrow. This mutation of -3bp -CTT, led to the formation of a small bulge in the mature miRNA.

sgRNA 219-2 on minus strand 5′-***G***GATGTCCAGGCACAATTCT-3′ PAM: TGG

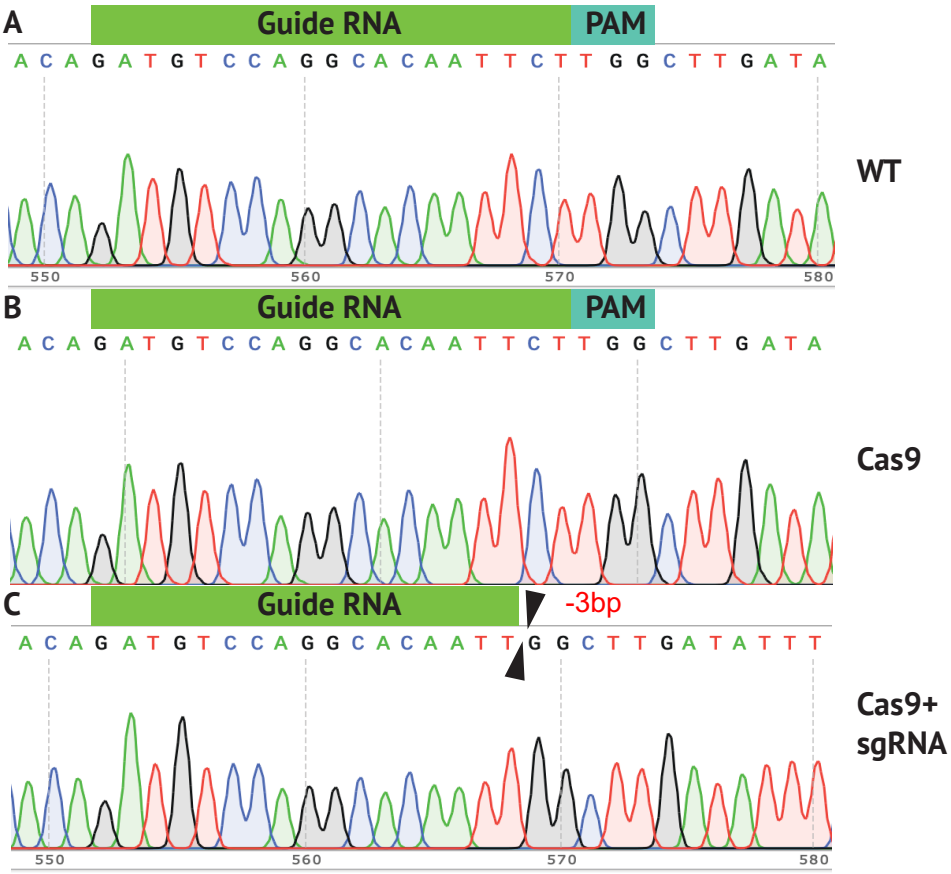

Figure 5.13 - Chromatogram sequence data for single guide RNA mutation of miR-219. Guide RNA sequence highlighted in green and PAM sequence in blue. Genomic DNA was PCR amplified and subcloned into pGEM-T-Easy and sequenced with M13 primers. A) WT control embryo miR-196a sequence. B) Cas9 injected only control embryo miR-219 sequence. C) Cas9 + sgRNA-219-2 mutant "CRISPR" embryo miR-219 sequence with -3bp deletion, -CTT, indicated by the black arrows.

It was uncertain if this mutation will have had the desired effect to generate a stable miR-219 KO. Instead, it may have generated a different miRNA. If we had targeted the seed region it could also have generated a new miRNA with novel and undesired effects (Bhattacharya and Cui, 2017).

The embryos injected with the miR-219 sgRNA candidates underwent phenotype analysis (Fig. 5.15). Embryos were left to develop to tadpole stage 33. It is not surprising that as sgRNA-219-2 and sgRNA-219-3 were thought to be efficient in creating indels as assayed by T7 endonuclease assay (Sentmanat et al., 2018), these embryos had the most extreme phenotypes. Some of the embryos are missing key anterior structures such as cement

gland, eye, and most of the head. SgRNA 219-2 had the highest percentage of mis formed embryos with craniofacial phenotypes (Fig. 5.15J). SgRNA-219-1 and -4 still created phenotypes, although these were less extreme and targeted the fore-region of the anterior structures.

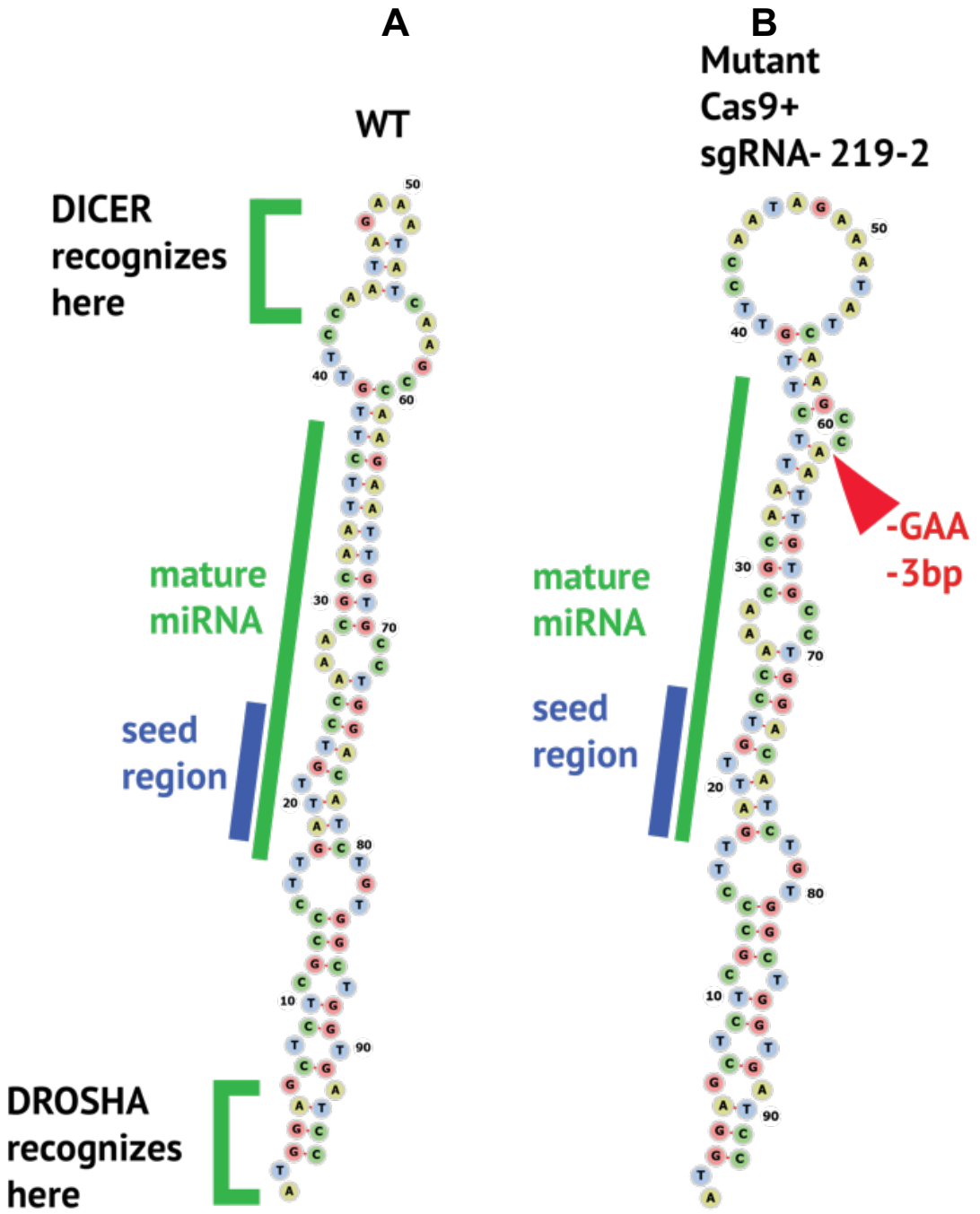

Figure 5.14 - Modelling miRNA-*219* stem-loop predicted structures after CRISPR mutagenesis of miRNA. Sequence information taken from sequences described in Fig.5. Blue bar indicates where the mature miRNA sequence would be, the green bar indicates where the miRNA seed region would be and red bar denotes any areas of change. Left- WT embryo genomic sequence subcloned into pGEM T Easy. Right- Mutated miRNA-219 model miRNA stem loop structure. -3 bp change - CTT deletion mutation. Modelled by RNA fold Vienna.

SgRNA, sg219-2 was thought to be most effective at this stage, so whole mount *in situ* hybridisation phenotype analysis was conducted. To see if the effects of this miRNA mutation Xhe2 HG marker was used again to compare to the previous result for single sgRNA miR-196a 3 above in Fig. 5.10. For miR-219 CRISPR the phenotype observed in the Xhe2 expression was like that seen in Fig. 5.10. Lower portions of the fork head were missing or greatly disturbed in over 70% of the embryos (Fig. 5.16B). The loss of *Xhe2* expression following CRISPR was also seen following MO KD of miR-219, but not miR-196a (Chapter 4, Fig. 4.9).

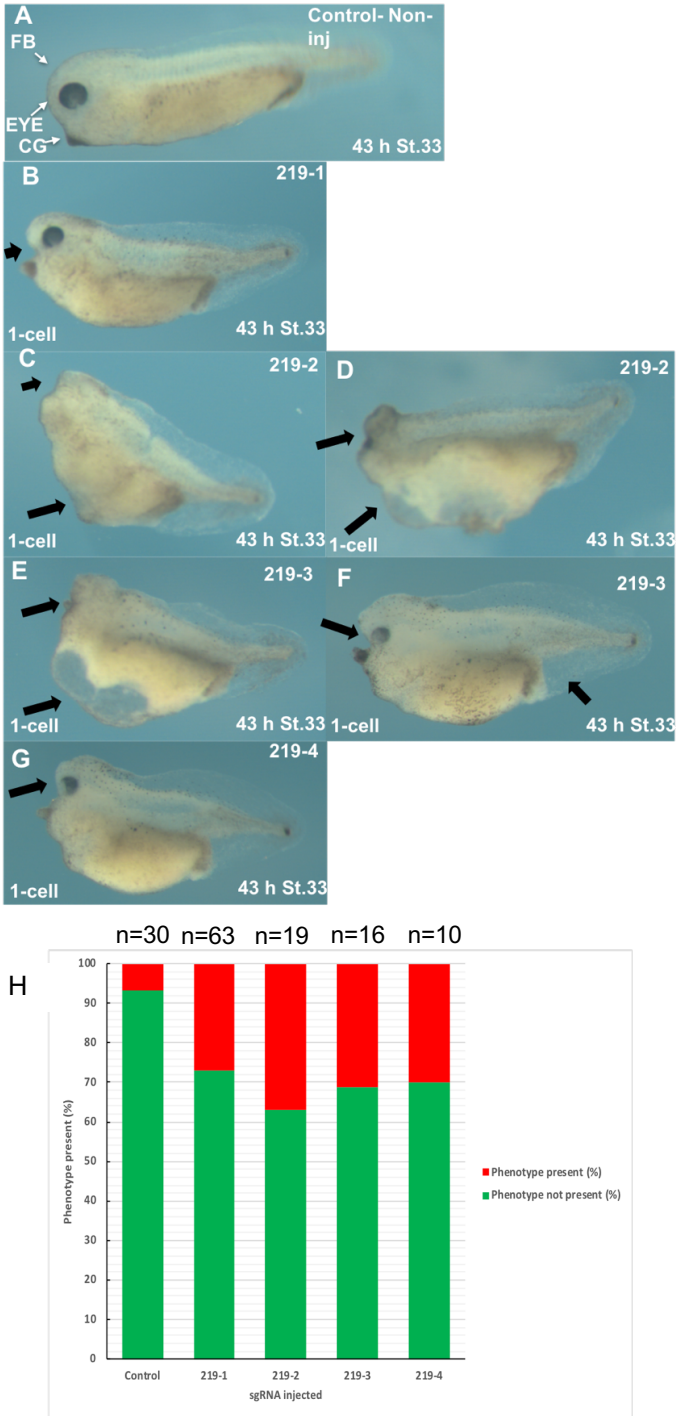

Figure 5.15 – Preliminary phenotype CRISPR/Cas9 results for miR-219 KO. *X. tropicalis* embryos were injected at the 1 cell stage with 4nL 300 pg sgRNA, Cas9 protein and 5 ng of GFP cRNA as a tracer. Crispant embryos show gross craniofacial impairments. Black arrows show areas of craniofacial and other gross phenotypes. (A) Control non-injected embryo. (B) Embryo injected with sgRNA 219-1. (C) Embryo injected with sgRNA 219-2. (D) Embryo injected with sgRNA 219-2. (E) Embryo injected with sgRNA 219-3. (F) Embryo injected with sgRNA 219-3. (G) Embryo injected with sgRNA 219-4. (H) Count data to display amount of embryos displaying a disfigured craniofacial phenotype. Black arrows indicate areas of change (B-G). FB= forebrain, CG= cement gland. Embryos were left to develop for 43 h to St.33.

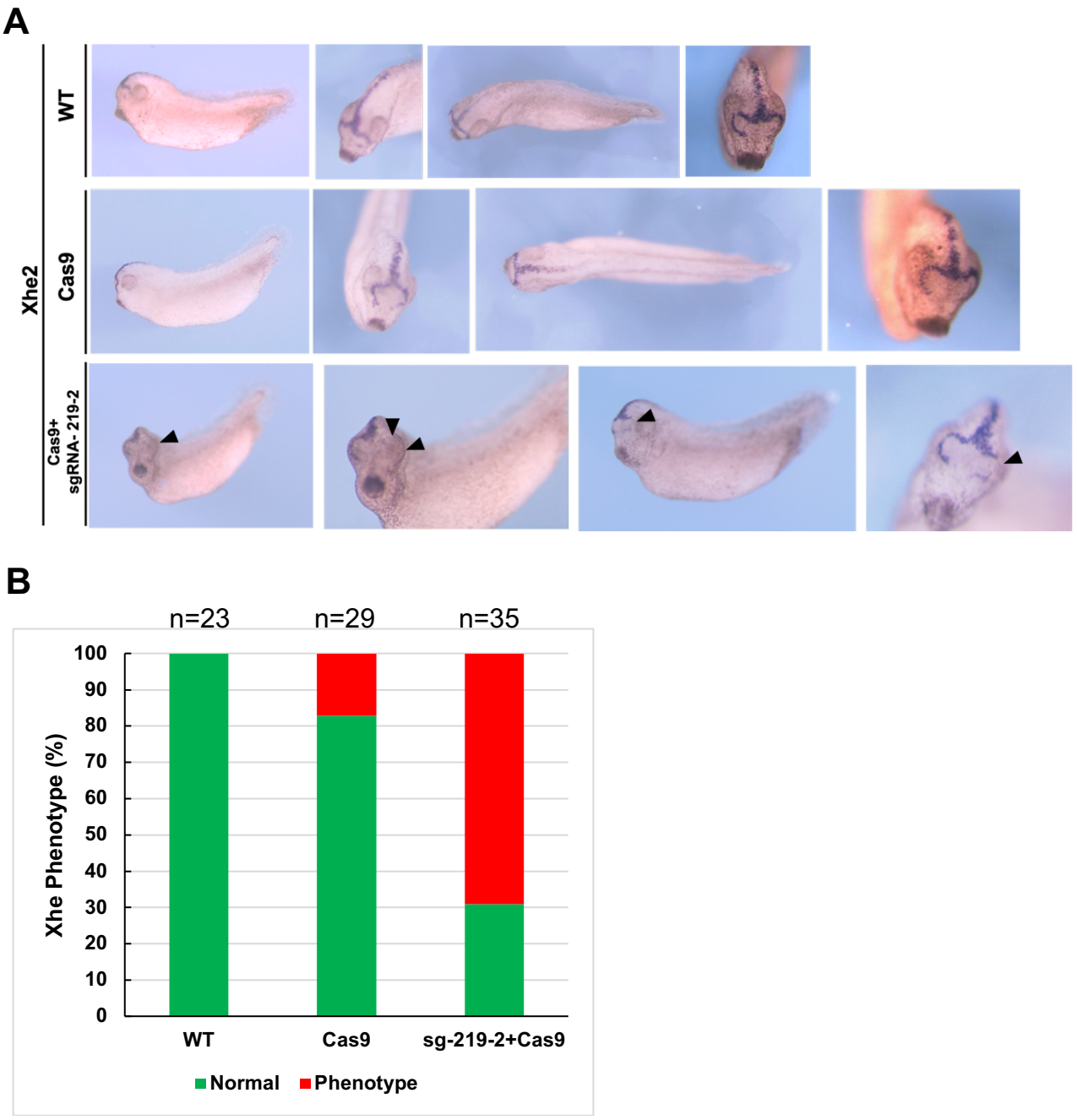

Figure 5.16 – Hatching gland phenotype analysis of CRISPR miR-219 mutant X. tropicalis embryos by WISH with marker Xhe2. Embryos were injected at the 2 cell stage into one blastomere with 300 pg of sgRNA plus Cas9 protein and 5 ng GFP cRNA tracer using a 4 nL calibrated needle. Injected side facing viewer. Crispant embryos show loss of Xhe2. Black arrows show regions of loss of Xhe2 expression. (A) Parts of the forkhead expression profile are missing on one side of the *X. tropicalis* miR-219 mutant embryos as indicated by the black arrows. (B) Xhe2 loss phenotype count data, one biological repeat- sister embryos.

5.5.0 CRISPR Optimization to drop-out miRNA-196a

Use of single sgRNA to KO miRNA-196a may not have generated a clean KO as previously discussed. To overcome this, it was decided to try another CRISPR approach. Instead of just injecting one sgRNA, two sgRNAs designed to be complementary to either side of the miRNA stem-loop, were co-injected to simultaneously to "drop-out" and delete the miRNA. This gave us a larger amount of genomic sequence to target, and thus more sgRNA designs to choose from and would possibly lead to a more consistent phenotype.

5.5.1 Using double sgRNA injection to mutate miRNAs

Using a single, sgRNA works well when the guide RNA targets the start codon or exon if you are targeting an mRNA, and worked with the tyrosinase gene (Nakayama et al., 2013), which has been used as a positive control for the early CRISPR experiments in this chapter. Using two sgRNAs to disrupt miRNAs has been published since we began this work. The approach adopted was very similar, whereby two sgRNAs were designed between miRNAs, and use of individual or pairs of sgRNAs were used to knockout or disrupt the miRNA in Zebrafish embryos (Kretov et al., 2020). However, using CRISPR to do this for a miRNA at time of starting had not been done before.

No one had yet tried to KO a miRNA in *Xenopus*, so the approach highlighted in Fig. 5.17 was trialled with different pairs of sgRNAs. Individual sgRNAs were tested to begin with but this was quite time consuming, so all sgRNAs and combinations were also trialled to accelerate development of a pair of sgRNAs that both work well to simultaneously create double strand breaks and INDELs in the gDNA.

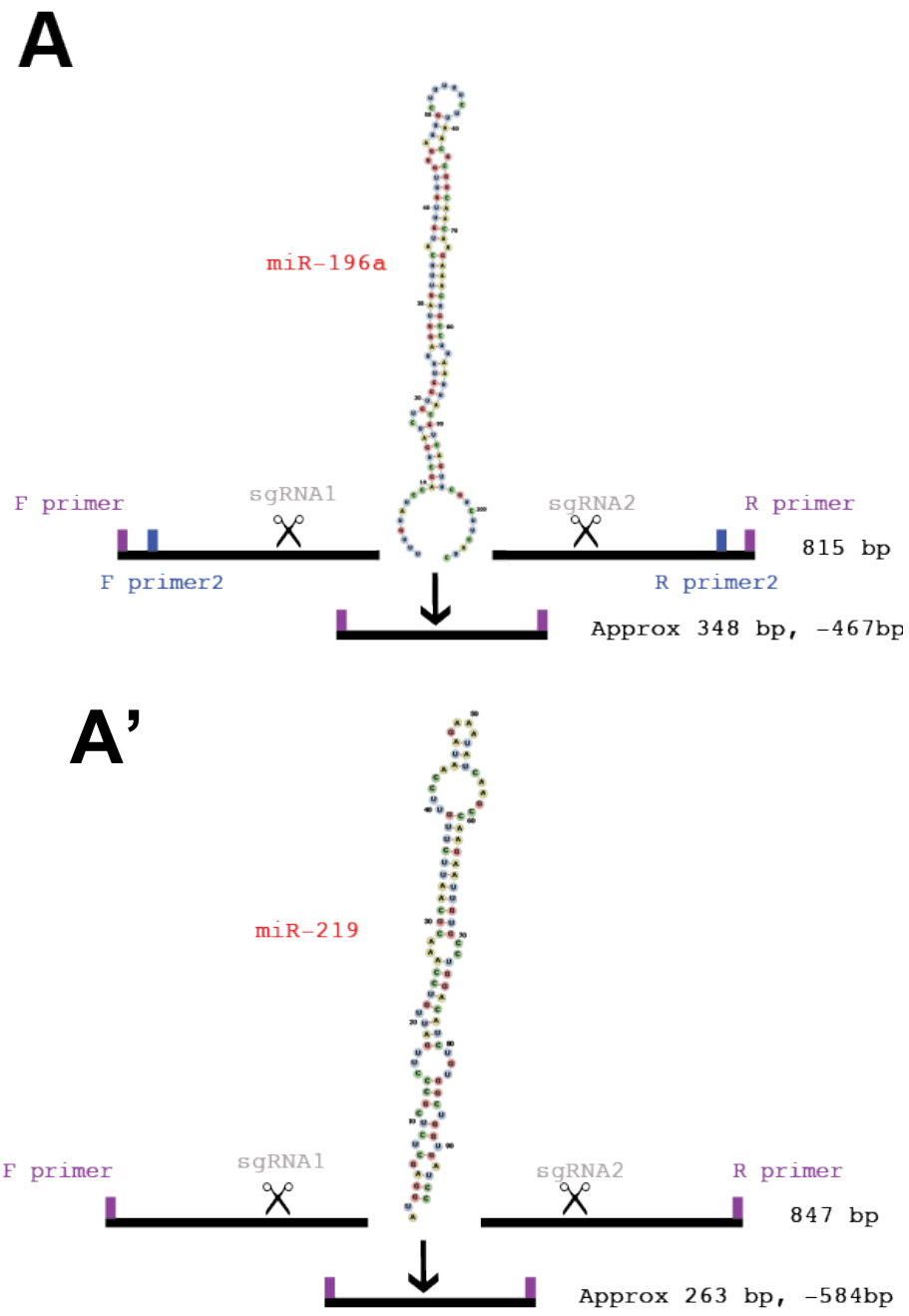

Figure 5.17 - Schematic representation of CRISPR-Cas9 approach to drop out the miRNA stem loop. Use of a pair of sgRNAs to simultaneously create double strand breaks to drop-out miR-196 and miR-219. Primers listed in figure are representative examples, some nested PCRs were used to generate different amplicon sizes.

5.5.2 Using double sgRNA injection to mutate miR-196a

To evaluate the efficacy of the pairs of sgRNAs injected into *X. tropicalis* embryos to KO miR-196a, genotype and phenotype analysis was carried out. GDNA was taken from these phenotyped embryos and the miRNA-196a was amplified by PCR with primer set 5 to yield a miR-196a amplicon of 947 bp

(Fig. 5.19 A). The mutant set of tadpoles had been injected with sgRNAs 196-4 and 196-7. If both sgRNAs create double strand breaks in the gDNA simultaneously, this would delete the pri-miRNA stem-loop, creating a drop out; this mutant sequence would then yield a PCR fragment of less than 480 bp and be much shorter than WT miR-196a gDNA. As embryos were injected at the 2-cell stage all embryos and all lanes should have a WT copy of miR-196a and thus an amplicon of 947 bp. This can be clearly seen across all lanes. In the mutant lane an extra smaller amplicon of 350 bp can be clearly seen. These bands were gel extracted and subcloned and sequenced. The WT, Cas9 and mutant bands were then sequenced (Fig. 5.19A'). The mutant sequence is approximately 600 bp shorter than the WT original amplicon. This strongly suggests that both sgRNAs in this instance created double strand breaks and dropped out our miRNA, miR-196a. q-RT-PCR validation of miR-196a expression levels following miR-196a KO showed a 67% reduction in expression of miR-196a in crispant embryos (Fig. 5. 19B).

Embryos were split into three experimental groups, WT, Cas9 protein injected + GFP tracer, and finally, pair of sgRNAs + Cas9 protein + GFP tracer and left to develop for phenotype analysis. WT and Cas9 control groups appear normal in phenotype at St. 39 (Fig. 5.20A). The mutant group, injected with sgRNA 196-4 and 196-7 pair, has a strong craniofacial phenotype (Fig. 5. 21), and a pigment loss phenotype (Fig. 5. 20A). The tadpole below has a smaller eye, and craniofacial deformities in the cement gland and forebrain regions. Pigment is lost along the dorsal side of the embryo from the head all the way down to the tip of the tail (Fig. 5.20A).

In chapter 4 it was shown that miR-196a MO was also targeting miR-196b. It was strongly believed that our miR-196a CRISPR sgRNAs would only target miR-196a, however a validation q-RT-PCR experiment was performed on Cas9 injected control embryos, and miR-196a KO samples to analyse miR-196b expression. No significant change in miR-196b expression was observed, as expected (Fig. 5.18).

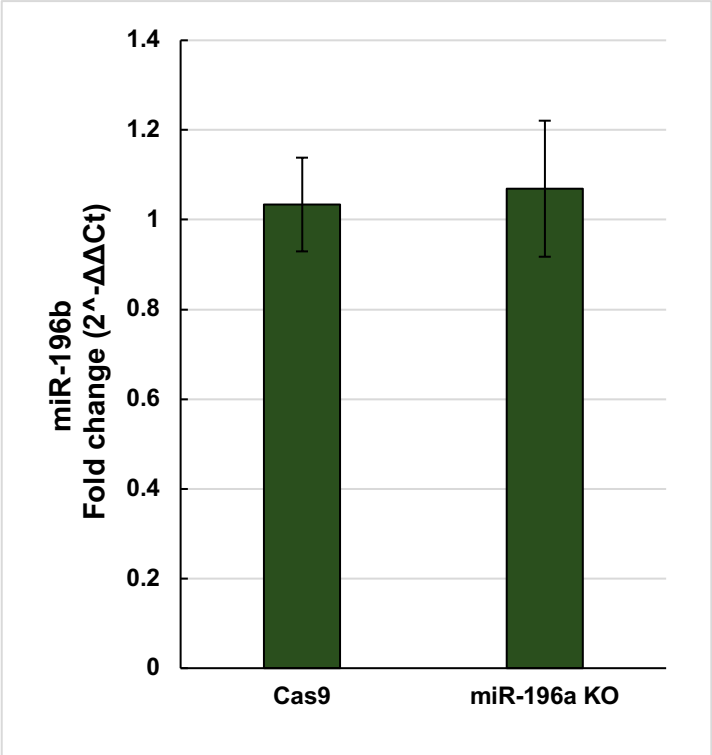

Figure 5.18 - q-RT-PCR analysis of miR-196b expression on miR-196a KO *X. tropicalis* embryos. miR-196b not significantly reduced in miR-196a KO, p= 0.91. Embryos were injected at the 1 cell stage with 150 pg of each sgRNA, Cas9 protein and 5 ng of GFP cRNA. 5 St. 14 embryos were pooled for RNA extraction, miR-196a expression was normalised to housekeeping gene U6. Three biological repeats and three technical repeats were conducted. Statistical significance measured by T-test, error bars show mean+/- SEM.

Following miR-196a KO it was important to let the embryos develop and determine if there were any NC-associated phenotypes (Fig. 5. 20). Embryos were injected into one cell at the 2-cell stage of embryonic development. WT and negative control Cas9+ GFP cRNA were used for comparison, as well as the opposite side of the injected embryo as an internal bilateral control. Embryos were left to develop to St.42 and imaged. At this stage the miR-196a KO tadpoles show clear pigment phenotypes, with much fewer pigment cells, as indicated by the red arrows. With tadpoles being transparent along the dorsal fin at this stage the pigment you are seeing is from the opposite side of the embryo and is such out of focus (Fig. 5. 20 A). This phenotype was seen in over 50% of tadpoles (Fig. 5. 20B). Aberrant pigmentation in the anterior craniofacial region can also be seen.

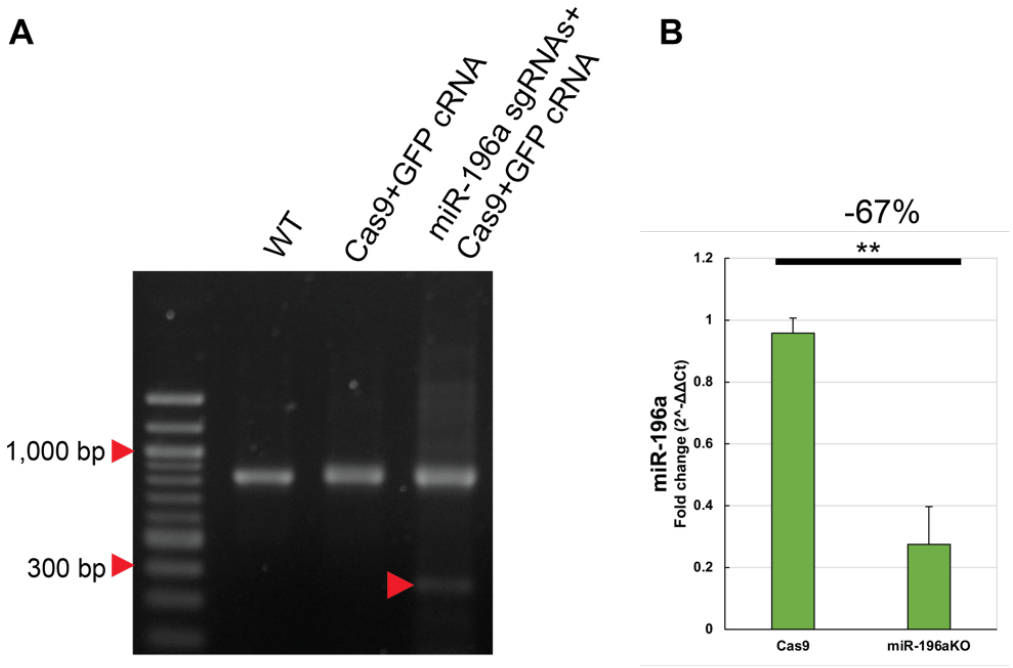

A'

miR-196a WT

GTAGAATTGGGGAGGGGAGTTTTGGGCATGAGCACATCCCATCTCCTTAATCAGGATTTCTA
AGTGAAAGAGATGAAAATCTGTAGTGATTGAGAGGCGCTGTGCAGAGGCTGTAGGAGCAGGG
AGGTATCCCCCAGTGTGGTGCAGCTGGCACAGGGGCTGGAGCTCCCATATGGCTCCATAGGC
TCCATAGGCTCATAGGCTCCATAGGCTCATAGGCTCCATAGGCTCATAGGAGGACGTTGGTG
GCGCATTCTGTGCATTATTGTTGTTTCCCCTCTTTTTTGCTCGCTTTCCTTCTCTTCTGTAT
CTGACAAGGAATTGTGGATGTTGCATCTTTGTATCCAGCTGATCTGTGGTTTAGGTAGTTTC
ATGTTGTTGGGATTGCTTTTTCTTAACGCGGCAACAAGAAACTGCCTTAATTACGTCAGTTC
GTCTTCATCAAGTGCAACGATTTCCGTTAAACCCAGCAGGTTCTGCAAGGGGCTCCCCAGCA
AGTGAGAGGCAACATGGCAGCATCCCGGCCAGGGGGACAAGGGCTTCCTCACATCTGGGTGC
CATTCTTCCACAGCCACTTTTAGTGCCTCTCCTTGCTATTGTCTCTGGCCAGAAGGAGGCTT
CTCAGAATATTGGGCAGACAAAAGAAGCCCTCCTTCAGAACTCC — 664bp

miR-196a Cas9

GTGAGAATTGGGGAGGGGAGTTTTGGGCATGAGCACATCCCATCTCCTTAATCAGGATTTCT
AAGTGAAAGAGATGAAAATCTGTAGTGATTGAGAGGCGCTGTGCAGAGGCTGTAGGAGCAGG
GAGGTATCCCCCAGTGTGGTGCAGCTGGCACAGGGGCTGGAGCTCCCATATGGCTCCATAGG
CTCCATAGGCTCCATAGGCTCATAGGCTCCATAGGCTCATAGGCTCCATAGGCTCCATAGGC
TCATAGGAGGACGTTGGTGGCGCATTCTGTGCATTATTGTTGTTTCCCCTCTTTTTTGCTCG
CTTTCCTTCTCTTCTGTATCTGACAAGGAATTGTGGATGTTGCATCTTTGTATCCAGCTGAT
CTGTGGTTTAGGTAGTTTCATGTTGTTGGGATTGCTTTTTCTTAACGCGGCAACAAGAAACT
GCCTTAATTACGTCAGTTCGTCTTCATCAAGTGCAACGATTTCCGTTAAACCCAGCAGGTTC
TGCAAGGGGCTCCCCAGCAAGTGAGAGGCAACATGGCAGCATCCCGGCCAGGGGGACAAGGG
CTTCCTCACATCTGGGTGCCATTCTTCCACAGCCACTTTTAGTGCCTCTCCTTGCTATTGTC
TCTGGCCAGAAGGAGGCTTCTCAGAATATTGGGCAGACAAAAGAAGCCCTCCTTCAGAACTC
C — 683 bp

miR-196a Cas9+ SgRNAs 1 *Gel image

TGAGAATTGGGGAGGGGAGTCACGTGACACTGAGAGCTGTCACTGAAGTGTTGTTTCAGTGA
GCACAGCGCACAGAAGTGAGACACAGAGAGTCTTTAGCTCTATTTCTCACCCTAGGCTTATA
CGCGAGTCAATAAGTTTTCCCAGTTTTTGTAGGTAAAATTAGGTACCTCGGCTTATACACGG
GTCGGCTTATACACGAGTATATACGGTACCTAACTGGCCACCATTCAATCCCACTGTATAAA
CAGCATCTTTAGTCCACAGAACTGTGTGAAGCCCTCCTTCAGAACTCC 296bp. -370bp

miR-196a Cas9 + SgRNAs 2

GTGAGAATTGGGGAGGGGAGTTTTGGGCATGAGCACATCCCATCTCCTTAATCAGGATTTCT
AAGTGAAAGAGATGAAAATCTGTAGTGATTGAGAGGCGCTGTGCAGAGGCTGTAGGAGCAGG
GAGGTATCCCCCAGTGTGGTGCAGCTGGCACAGGGGCTGGAGCTCCCATATATTGGGCAGAC
AAAAGAAGCCCTCCTTCAGAACTCC 211bp. -455bp

miR-196a Cas9 + SgRNAs 3

GTGAGAATTGGGGAGGGGAGTTTTGGGCATGAGCACATCCCATCTCCTTAATCAGGATTTCT
AAGTGAAAGAGATGAAAATCTGTAGTGATTGAGAGGCGCTGTGCAGAGGCTGTAGGAGCAGG
GAGGTATCCCCCAGTGTGGTGCAGCTGGCACAGGGGCTGGAGCTCCCATATGGCTCCATAGG
CTATTGGGCAGACAAAAGAAGCCCTCCTTCAGAACTCC 224bp. -442bp

4/4 Sequences contained drop out mutation

Figure 5.19 –Genotype analysis of miRNA knock out double guide RNA approach in *X. tropicalis*. Embryos were split into three groups, a WT control group (uninjected), Cas9 protein + GFP cRNA tracer and 150 pg of each sgRNA plus Cas9 protein and GFP tracer. Reagents were injected at 2 cell stage into one blastomere using a 4 nL calibrated needle. A) Genotype analysis, gDNA was isolated from above tadpoles and miR-196a region was PCR amplified. WT miR-196a is 815 bp in size, if both sgRNAs have cut the expected size of amplicon should be 348 bp. Bands were excised in gel extraction and subcloned A') Sequence analysis of subcloned PCR amplicons. Scissor icons and black arrows indicate where the sgRNAs are believed to have created double strand breaks and indel mutations In the WT the miR-196a stem loop is highlighted by a red bar, and sgRNAs in grey bars, both up and down-stream of the miRNA stem loop. B) q-RT-PCR validation of miR-196a knockout. miR-196a expression was 67% reduced in knockout compared to Cas9 injected group, p=0.006, statistical significance measured by T-test. Bar charts show error bars depicting mean +/- SEM. Embryos were injected at the 1 cell stage. 5 St. 14 embryos were pooled for RNA extraction, miR-196a expression was normalised to housekeeping gene U6. Three biological repeats and three technical repeats were conducted.

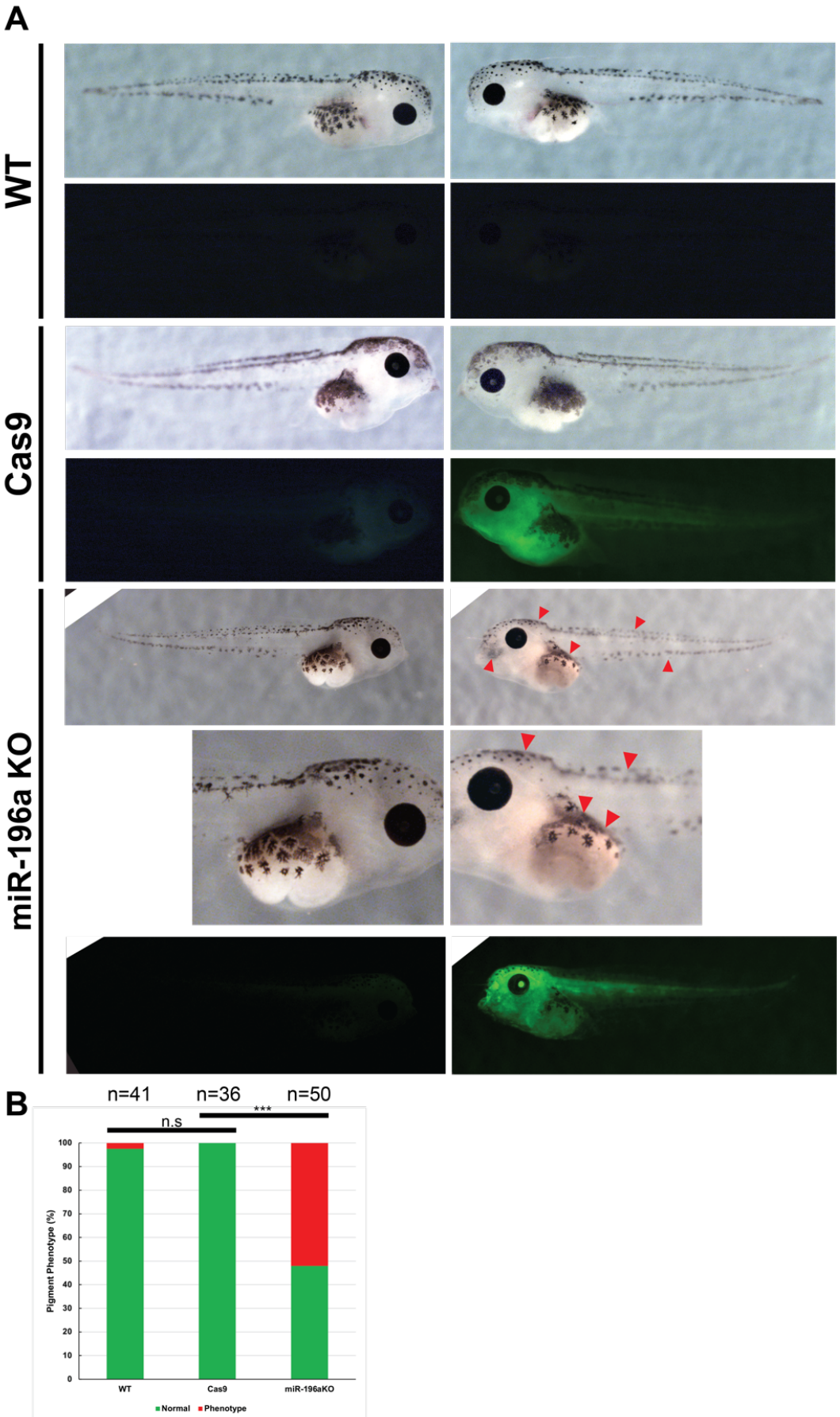
A
WT
Cas9
miR-196a KO
B
n=41
n=36
n=50
n.s
***
Pigment Phenotype (%)
100
90
80
70
60
50
40
30
20
10
0
WT
Cas9
miR-196aKO
Normal
Phenotype

Figure 5.20 - Phenotype analysis of miR-196a knock out double guide RNA approach in *X. tropicalis*. Embryos were split into three groups, a WT control group (uninjected), Cas9 protein and GFP cRNA tracer and 150 pg of each sgRNA plus Cas9 protein and GFP tracer. Reagents were injected at 2 cell stage into one blastomere using a 4 nL calibrated needle. miR-196a KO leads to loss of pigmentation in tadpoles. A) Phenotype analysis of *X. tropicalis* tadpoles at st. 42, and magnified in view of craniofacial region. WT and Cas9 groups appear normal whereas miRNA knockout tadpoles have pigment phenotypes as indicated by the red arrows. (B) Count data showing proportion of embryos exhibiting craniofacial phenotypes and disfigurements. Embryo phenotype was blind counted verified. There is a significant difference between and Cas9 and mir-196a knockout groups $p=2.22x10^{-7}$.

To analyse for craniofacial phenotypes from miR-196a CRISPR was repeated, and embryos were allowed to develop to St. 45 (Fig. 5.21). The WT and Cas9 groups appear normal, all anterior structures are formed and presently correct, as well as much pigment throughout the embryo. This is in stark contrast to the miR-196a KO tadpoles. The tadpole has a huge reduction in the amount of pigment expressed throughout. The craniofacial structures are greatly impacted, for example the eye is reduced in size and there appeared to be structures missing in the cranium (Fig. 5 21A). Due to this it was decided to let a few tadpoles develop to St. 45 and process them with Alcian blue staining to investigate further and look at their developing cartilage in the head. In Fig. 5. 21B the WT tadpole has all the cranial features present, with the eye, cement gland and branchial arches visible. For the miR-196a KO, the whole anterior end of the embryo appeared reduced in size with structures present like the branchial arches and the eye, which were very disorganised and shrunken in appearance.

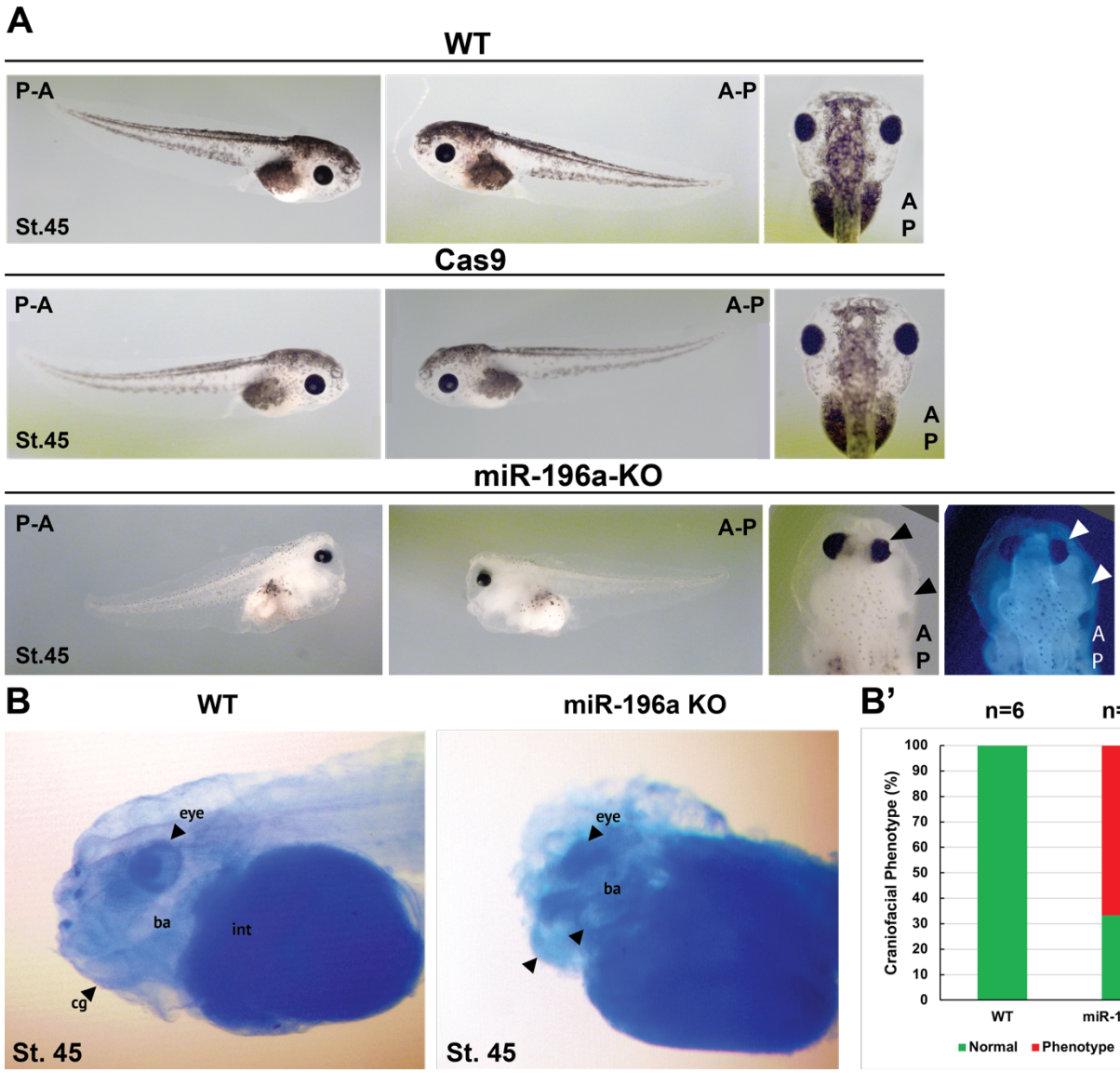

Figure 5.21 – Craniofacial phenotype analysis after miR-196a KO. Embryos were split into three groups, a WT control group (uninjected), Cas9 protein and GFP cRNA tracer and 150 pg of each sgRNA plus Cas9 protein and GFP tracer. Reagents were injected at 2 cell stage into one blastomere using a 4 nL calibrated needle. Injected side of embryo is always right side of embryo. MiR-196a KO leads to craniofacial pheontypes. Black and white arrows indicate regions of phenotypic interest and craniofacial disfigurement *(*A) Phenotype analysis of *X. tropicalis* tadpoles at st. 45. WT and Cas9 groups appear normal whereas miRNA KO tadpoles have some craniofacial and pigment phenotypes. Embryos were processed and stained by alcian blue and craniofacial cartilage were dissected. (B) Strong craniofacial disfigurements can be seen in miR-196a KO tadpole.

5.6.0 CRISPR Optimization to drop-out miRNA-219

The same two-sgRNA approach that was used to KO miR-196a, was used to KO miR-219.

5.6.1 Using double sgRNA injection to mutate miR-219

To evaluate the efficacy of the pairs of sgRNAs injected into *X. tropicalis* embryos to KO miR-219, genotype and phenotype analysis was carried out. Embryos were split into three experimental groups, WT, Cas9 protein injected + GFP tracer, and pair of sgRNAs + Cas9 protein + GFP tracer.

To validate the genotype of the tadpole's, gDNA was isolated and the miR-219 region was amplified by PCR (Fig. 5.22 A). MiR-219 was amplified with primer 6F and R2, and then gel extracted and nested PCR carried out with primers 6F and R3 to yield a product of 835 bp for WT miR-219. This can be seen in all the lanes in Fig.21 A, as the embryos were injected at 2 cell stages, only half the genome will be mutant, and thus should still contain copies for miR-219. If both sgRNAs sg-219-5 and 9 have dropped out miR-219 this would delete approximately 588 bp to yield a mutant miR-219 KO product of less than 247 bp. These products were then gel extracted, subcloned and sequenced (Fig. 5. 22C') The WT sequence is 835 bp, the mutant miR-219 knockout band sequence is much shorter by -608bp and is only 227 bp long. It also does not align to miR-219 sequence at all. The proposed site of miR-219 deletion is highlighted by two scissor icons. This evidence strongly suggests that sgRNAs 219-5 and 219-9 have dropped out miR-219. q-RT-PCR validation of miR-219 knockout was used and showed a highly significant 93% reduction in miR-219 expression in crispant miR-219 KO group (Fig. 5. 22B).

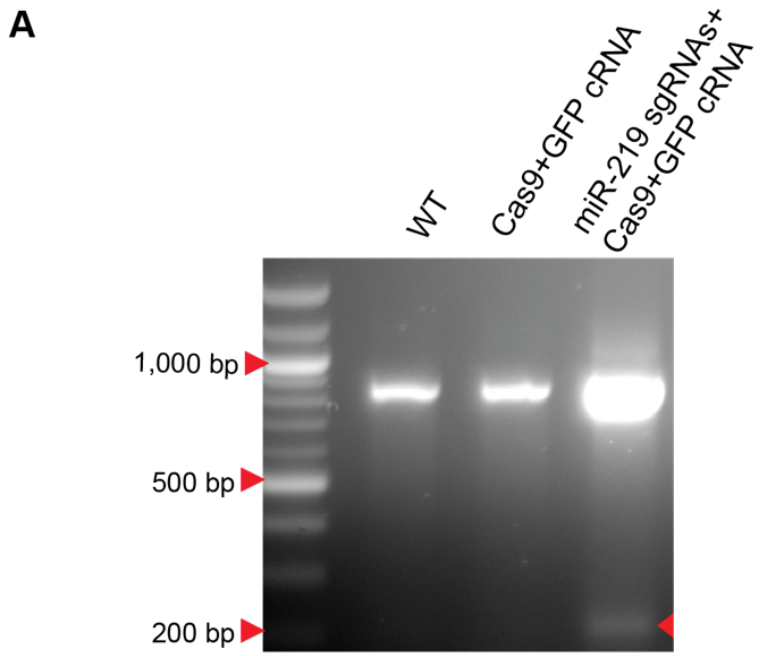

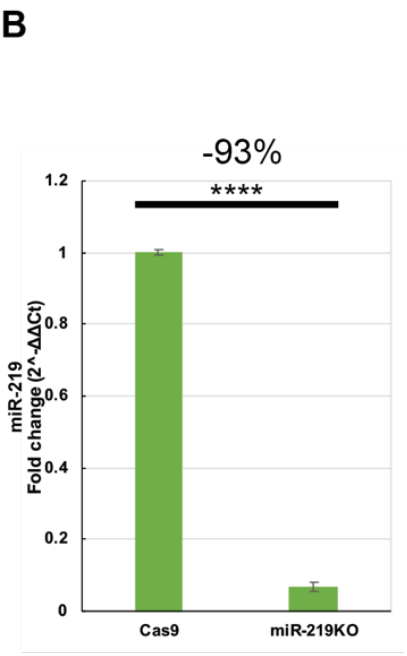

A'

miR-219 WT
GAATTCGATTCCCAGTCTTGGAAGGAGTAGACCTTCAGAATAAGGAATTCTATGTAATTGTG
CGAATTGAATTTGCTGTGAATTTTCCACAGCAATGGGTTTTGGCCAAATGAGAGTTATCCAG
GTATAGATATATACATACTTTTTTATGTGTCTGTAAATATGTTATATCGTATTTCGTTTATA
TGATGGTAGGTTAAGGCATGGAAGAGAACTGATGGCAATGACTGCAGGCTGCAGGTATAATT
CTCTATGTTGGGAAAAAAAGCCTATCCTTTGCCAAGACATCATTGCAGGAGGAGATGAATAC
AATGAATACCGGATAGGATTTAACCCTTTCCAGCCTATGACAACATTCACCCAGTGCCTGTG
GCAGGGAGTGGGTTGCGCTTGAAGGCGACGTAGAATCAGCGAGCGAATCTGAACTTGCTGTC
GCTGCACAACTGGTTGTGTTATTGTCAGCACTGGCACAGTGGGGGTAACCATGCTGTGTGTG
TGTGTTGGGGGGGTTGGTGGGGGTTCTATCGACCGGTCATATCTCCAGCTGGACAAAGATCA
ACCCATGGAGCTCTCGCCCTTGATTGTCCAAACGCAATTCTTGTTCCAATAGAAATATCAAG
CCAAGAATTGTGCCTGGACATCTGTGGCTGGTGATCCCCGGTCTTCAGAATCAGCGACGGGC
AAAGATTGTAAGTCCAAGAGGCAGAGGATCTTTCTTTAAAACCAGAGATGGAGAGTAAAGAG
TGTGCAGGTGCAAGATATATATATTGTCATAATATAAAGACAAAAGTGTAAGGATACTAACC
TATGTATGTATAAACTGAAATTCACTTATGTTGAAGAGTGTGTTGCCTACCAATCACTAGTG
AATTC - 847bp

miR-219 Cas9
GAATTCGATTCCCAGTCTTGGAAGGAGTAGACCTTCAGAATAAGGAATTCTATGTAATTGTG
CGAATTGAATTTGCTGTGAATTTTCCACAGCAATGGGTTTTGGCCAAATGAGAGTTATCCAG
GTATAGATATATACATACTTTTTTATGTGTCTGTAAATATGTTATATCGTATTTCGTTTATA
TGATGGTAGGTTAAGGCATGGAAGAGAACTGATGGCAATGACTGCAGGCTGCAGGTATAATT
CTCTATGTTGGGAAAAAAAGCCTATCCTTTGCCAAGACATCATTGCAGGAGGAGATGAATAC
AATGAATACCGGATAGGATTTAACCCTTTCCAGCCTATGACAACATTCACCCAGTGCCTGTG
GCAGGGAGTGGGTTGCGCTTGAAGGCGACGTAGAATCAGCGAGCGAATCTGAACTTGCTGTC
GCTGCACAACTGGTTGTGTTATTGTCAGCACTGGCACAGTGGGGGTAACCATGCTGTGTGTG
TGTGTTGGGGGGGTTGGTGGGGGTTCTATCGACCGGTCATATCTCCAGCTGGACAAAGATCA
ACCCATGGAGCTCTCGCCCTTGATTGTCCAAACGCAATTCTTGTTCCAATAGAAATATCAAG
CCAAGAATTGTGCCTGGACATCTGTGGCTGGTGATCCCCGGTCTTCAGAATCAGCGACGGGC
AAAGATTGTAAGTCCAAGAGGCAGAGGATCTTTCTTTAAAACCAGAGATGGAGAGTAAAGAG
TGTGCAGGTGCAAGATATATATATTGTCATAATATAAAGACAAAAGTGTAAGGATACTAACC
TATGTATGTATAAACTGAAATTCACTTATGTTGAAGAGTGTGTTGCCTACCAATCACTAGTG
AATTC - 847bp

miR-219 Cas9 + SgRNAs 1 **Gel image
GAATTCACTAGTGATTCCCAGTCTTGGAAGGAGTAGACGGGCAAAGATTGTAAGTCCAAGAG
GCAGAGGATCTTTCTTTAAAACCAGAGATGGAGAGTAAAGAGTGTGCAGGTGCAAGATATAT
ATATTGTCACAATATAAAGACAAAAGTGTAAGGATACTAACCTATGTATGTATAAACTGAAA
TTCACTTATGTTGAAGAGTGTGTTGCCTACCAATCGAATTCC 201bp. -646bp

miR-219 Cas9 + SgRNAs 2
CCCAGTCTTGGAAGGAGTAGACCTTCAGAATAAGGAATTCTATGTAATTGTGCGAATTGAAT
TTGCTGTGAATTTTCCACAGCAATGGGTTTTGGCCAAATGAGGGCAAAGATTGTAAGTCCAA
GAGGCAGAGGATCTTTCTTTAAAACCAGAGATGGAGAGTAAAGAGTGTGCAGGTGCAAGATA
TATATATTGTCATAATATAAAGACAAAAGTGTAAGGATACTAACCTATGTATGTATAAACTG
AAATTCACTTATGTTGAAGAGTGTGTTGCCTACC 282bp. -565bp

miR-219 Cas9 + SgRNAs 3
GAATTCGATTCCCAGTCTTGGAAGGAGTAGACCTGAGTTATACAAGCTGGTACAGAAATGAC
CCTTCTATCTGTAAGTAAATCAAAGAGCATTCTTGGGACAGTGGTTGAAGAGTGTGTTGCCT
ACCAATCACTAGTGAATTC 117bp. -730bp

8/8 Sequences contained drop out mutation

Figure 5.22 -Genotype analysis of miRNA-219 knock out double guide RNA approach in *X. tropicalis*. Embryos were split into three groups, a WT control group (uninjected), Cas9 protein + GFP cRNA tracer and 150 pg of each sgRNA plus Cas9 protein and GFP tracer. Reagents were injected at 2 cell stage into one blastomere using a 4 nL calibrated needle. A) Genotype analysis, gDNA was isolated from above tadpoles and miR-219 region was PCR amplified and then nested PCR was performed to enrich for knockout amplicon. WT miR-219 is 1,081 bp in size initially (6F R2 primer) then after nested PCR (6F R3) 846 bp, if both sgRNAs have cut the expected size of amplicon should be approximately 200 bp. A') Sequence analysis of subcloned PCR amplicons, contains the WT miR-219 sequence from WT sample and miR-219 knockout sample which is a much shorter sequence, 220 bp in size. Scissor icons and black arrows indicate where the sgRNAs are believed to have created double strand breaks and indel mutations. B) q-RT-PCR validation of miR-219 knockout. miR-219 expression was 93% reduced in knockout compared to Cas9 injected group, $p= 5.29 \times 10^{-7}$, statistical significance measured by T-test. Bar charts show error bars depicting mean +/- SEM. Embryos were injected at the 1 cell stage. 5 St. 14 embryos were pooled for RNA extraction, miR-219 expression was normalised to housekeeping gene U6. Three biological repeats and three technical repeats were conducted.

Following miR-219 KO it was important to let the embryos develop and determine if there were any NC-associated phenotypes (Fig. 5. 23). Embryos were injected into one cell at the 2-cell stage of embryonic development. WT and negative control Cas9+ GFP cRNA were used to compare, as well as the opposite side of the injected embryo as an internal bilateral control. Embryos were left to develop to St.41 and imaged. At this stage, the miR-219 KO tadpoles show clear craniofacial and eye phenotypes, with smaller eye, and a compressed fronto-nasal region as indicated by the red arrows. This phenotype was seen in nearly 60% of tadpoles and was highly penetrant.

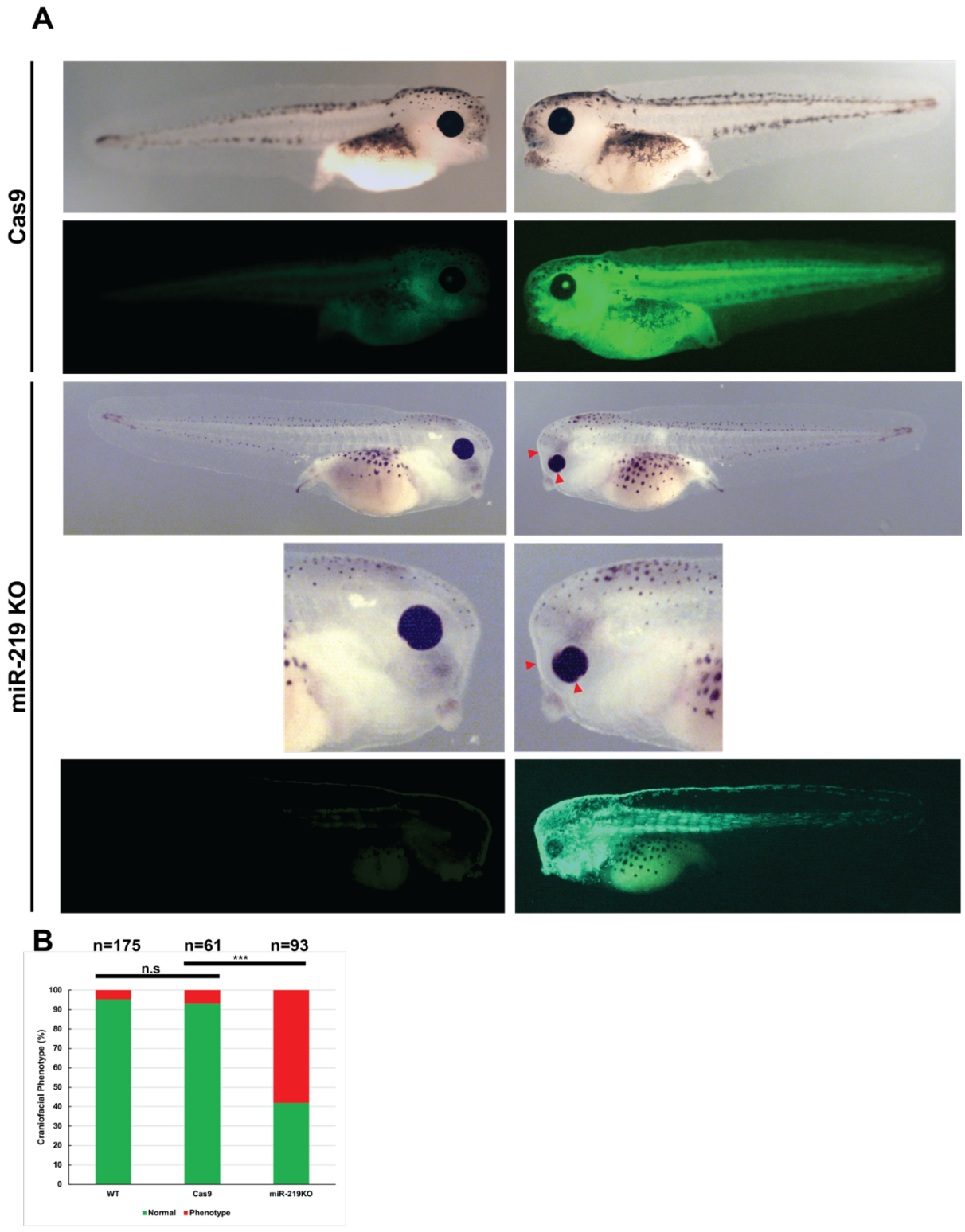
A
Cas9
miR-219 KO
B
n=175
n=61
n=93
n.s
***
Craniofacial Phenotype (%)
100
90
80
70
60
50
40
30
20
10
0
WT
Cas9
miR-219KO
Normal
Phenotype

Figure 5.23 –Phenotype analysis of miR-219 KO double sgRNA approach in *X. tropicalis*. Embryos were split into three groups, a WT control group (uninjected), Cas9 protein + GFP cRNA tracer and 150 pg of each sgRNA plus Cas9 protein and GFP tracer. Reagents were injected at 2 cell stage into one blastomere using a 4 nL calibrated needle. miR-219 KO leads to craniofacial phenotypes. Injected side is always right side of embryo and red arrows show regions of phenotypic interest.. (A) Phenotype analysis of *X. tropicalis* tadpoles at st. 41, and zoomed in view of craniofacial region. WT and Cas9 groups appear normal whereas miRNA knockout tadpoles have some craniofacial and phenotypes as indicated by the red arrows. (B) Count data showing proportion of embryos exhibiting craniofacial phenotypes and disfigurements. Embryo phenotype was blind counted verified. There is a significant difference between and Cas9 and miR-219 KO groups $p=1.1x10^{-10}$.

To further evaluate the craniofacial phenotype, embryos were injected with the sgRNAs sg-219-5 and 219-9 and left to develop to St. 45 and were processed with Alcian blue staining. Fig. 5.24A showed WT and Cas9 control group tadpoles looking normal, with symmetry between both sides of the embryo. For the miR-219 KO tadpole on the injected side the eye appears reduced in size, when magnified on the anterior view there is also some asymmetry. In Fig. 5. 24B the WT tadpole had a normal craniofacial phenotype whereas the miR-219 KO has craniofacial features, they are shrunken in size and misshaped in places. The eye is smaller in size, and the branchial arches appear disorganised.

To validate if eye size was relative to tadpole size, it was questioned that the small eye was present because the tadpole was smaller; measurements of tadpole's body length, eye size and eye area were taken from tadpoles that had been randomly sampled and imaged at the same magnification. These measurements were taken using ImageJ looking at eye area, eye length and body length. Three random individual WT, Cas9 and miR-219 knockout embryos were measured. The measurement taken was in pixels (number). Embryos that had miR-219 knocked out did appear slightly shorter in length (Fig. 5. 25A). However, there was no significant difference in body length of tadpoles between WT, Cas9 or mutant groups, and the body length remained constant. Eye area was very significantly reduced between WT and mutant and C9 and mutant groups, as well as eye length (Fig. 5. 25 B). More work would be needed to elucidate if the embryos are developmentally delayed, use

of a Cas9 negative control group does not indicate this, so would be dependent on whether miR-219 KO is impacting rate of embryo development.

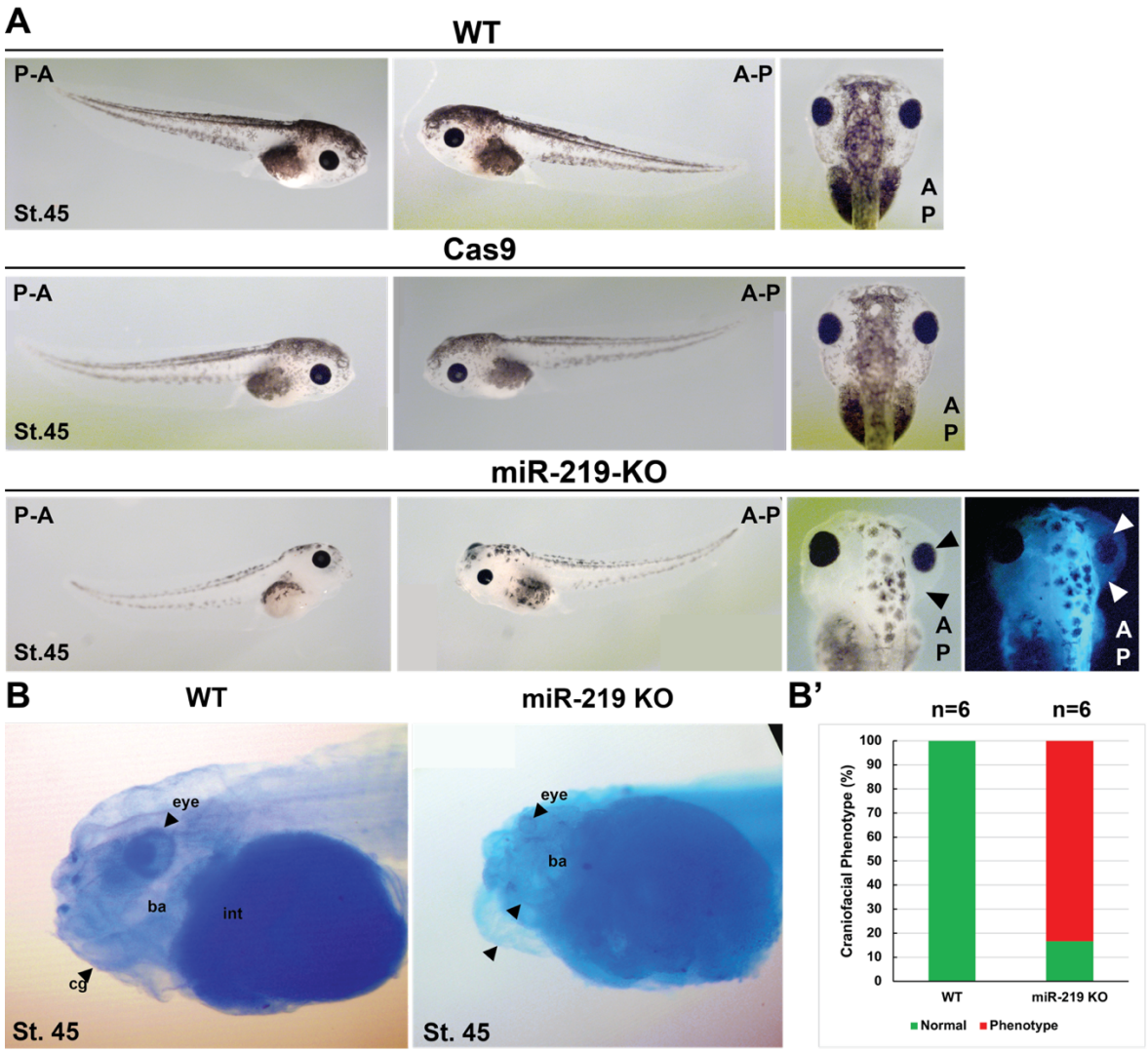

Figure 5.24 - Craniofacial phenotype analysis after miR-219 KO. Embryos were split into three groups, a WT control group (uninjected), Cas9 protein + GFP cRNA tracer and 150 pg of each sgRNA plus Cas9 protein and GFP tracer. Reagents were injected at 2 cell stage into one blastomere using a 4 nL calibrated needle. Injected side of embryos always right side. miR-219 KO leads to craniofacial phenotypes and microcephaly phenotypes. Black and white arrows denote craniofacial tissue and phenotypes in mutants. (A) Phenotype analysis of X. *tropicalis* tadpoles at st. 45. WT and Cas9 groups appear normal whereas miRNA knockout tadpoles have some craniofacial phenotypes. Embryos were processed and stained by alcian blue and craniofacial cartilage were dissected. Strong craniofacial disfigurements can be seen in miR-219 knockout tadpole (B). This phenotype was highly penetrant and can be seen in the count data (B'). Embryo orientation: A-P= anterior- posterior, P-A= posterior-anterior. Black arrowheads denote areas of phenotype interest.

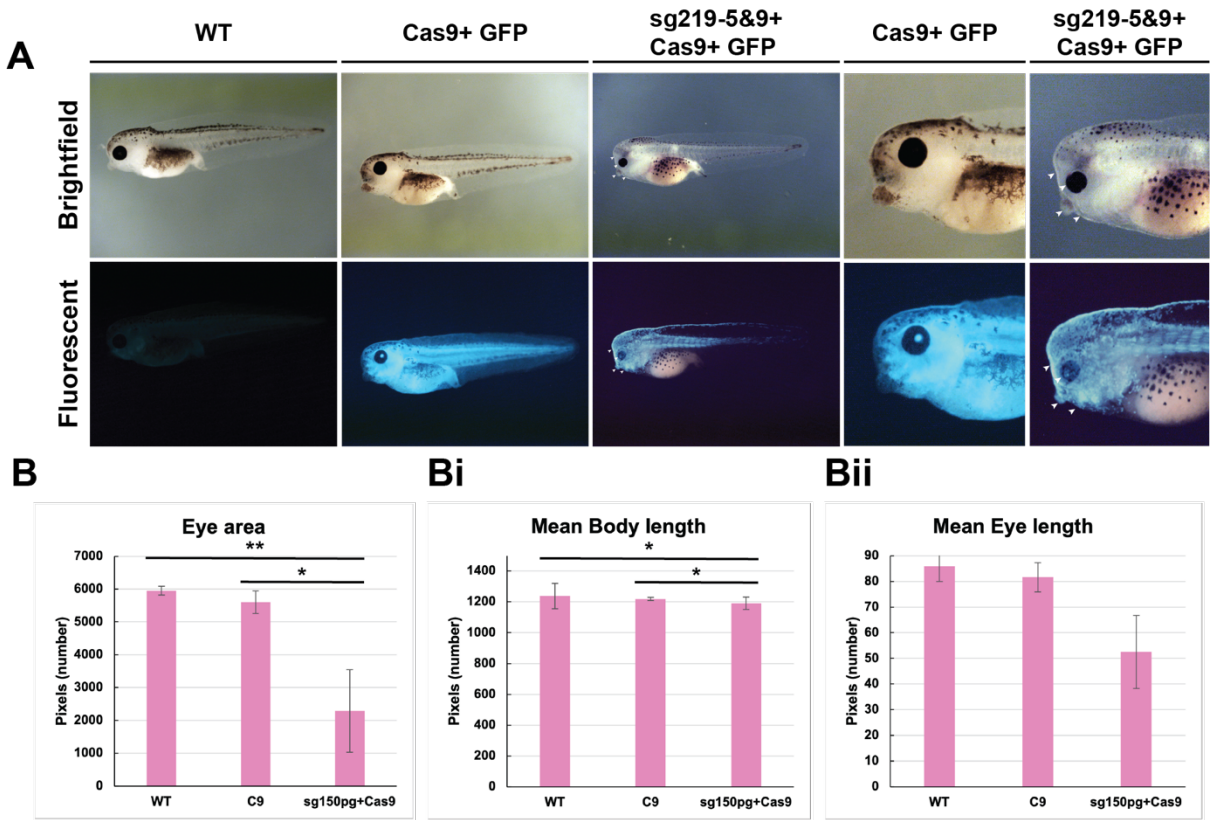

Figure 5.25 - Validating if eye size was small in relation to the size of the tadpole. *X. tropicalis* embryos were injected at the 2 cell stage into one blastomere with a 4 nL calibrated needle. White arrows show craniofacial phenotypes. Embryos were split into three groups: WT (uninjected), Cas9 (C9), (Cas9 protein only + GFP cRNA tracer) and miR-219 KO (sgRNAs 150pg each, Cas9 protein and GFP cRNA tracer). Eye area and eye length was reduced in mutant tadpole group, whereas there was no significant difference in body length between WT, Cas9 injected and Cas9+ sgRNAs + GFP group. For eye area WT vs sg150pg each + Cas9 (mutant) p=0.007, Cas9 vs mutant p=0.012. For eye length WT vs mutant p=0.014, Cas9 vs mutant p=0.021. There was a strong reduction in eye size phenotype in mutant tadpoles. (A) Phenotype of tadpoles with whole tadpole (5x magnification) and craniofacial region (10x magnification). (B) Measurements of eye area show reduced eye size. (Bi) Measurements of body length show no significant change. (Bii) Measurements showed no significant change in eye length.

5.7.0 MiRNA-KO neural crest phenotypes

Since our miRNA KO model was successful and working, it was important to next analyse the F0 embryos further. As with the MO KDs, it was decided to conduct whole mount *in situ* hybridisation phenotype analysis on CRISPR F0 generation embryos at neurula stage to analyse for any NC phenotypes with NC markers Sox10 and Snail2.

5.7.1 Analysis of neural crest, neural plate and hatching gland markers

NC marker *Sox10* was chosen to make direct comparison from the results seen after MO KD. Previously it was seen that miRNA-KD led to a reduction in expression of Sox10 on the manipulated side of the embryo. In Fig. 5. 26 the WT and Cas9 control neurulas embryos have equal and bilateral expression of *Sox10*. The miR-196a and miR-219 KO embryos have a significant loss in expression of *Sox10*. MiR-196a KO only has a small expression of the most posterior portion of Sox10 expression, and this is also perturbed. For miR-219 KO, there was almost total KO of Sox10 expression on the manipulated side of the embryo. These phenotypes were present in nearly 40-60% of the miR-196a KO embryos and 60% of the miR-219 KO embryos (Fig 5.26 B-C). q-RT-PCR was used to further quantify the loss of Sox10 and Snail2 expression observed following miR-KO. Following miR-196 KO Sox10 expression was reduced by 94% and following miR-219 KO Sox10 expression was reduced by 65%. Following miR-196a KO Snail2 expression was reduced by 87% and following miR-219 KO Snail2 expression was reduced by 52% (Fig. 5. 26 D-E).

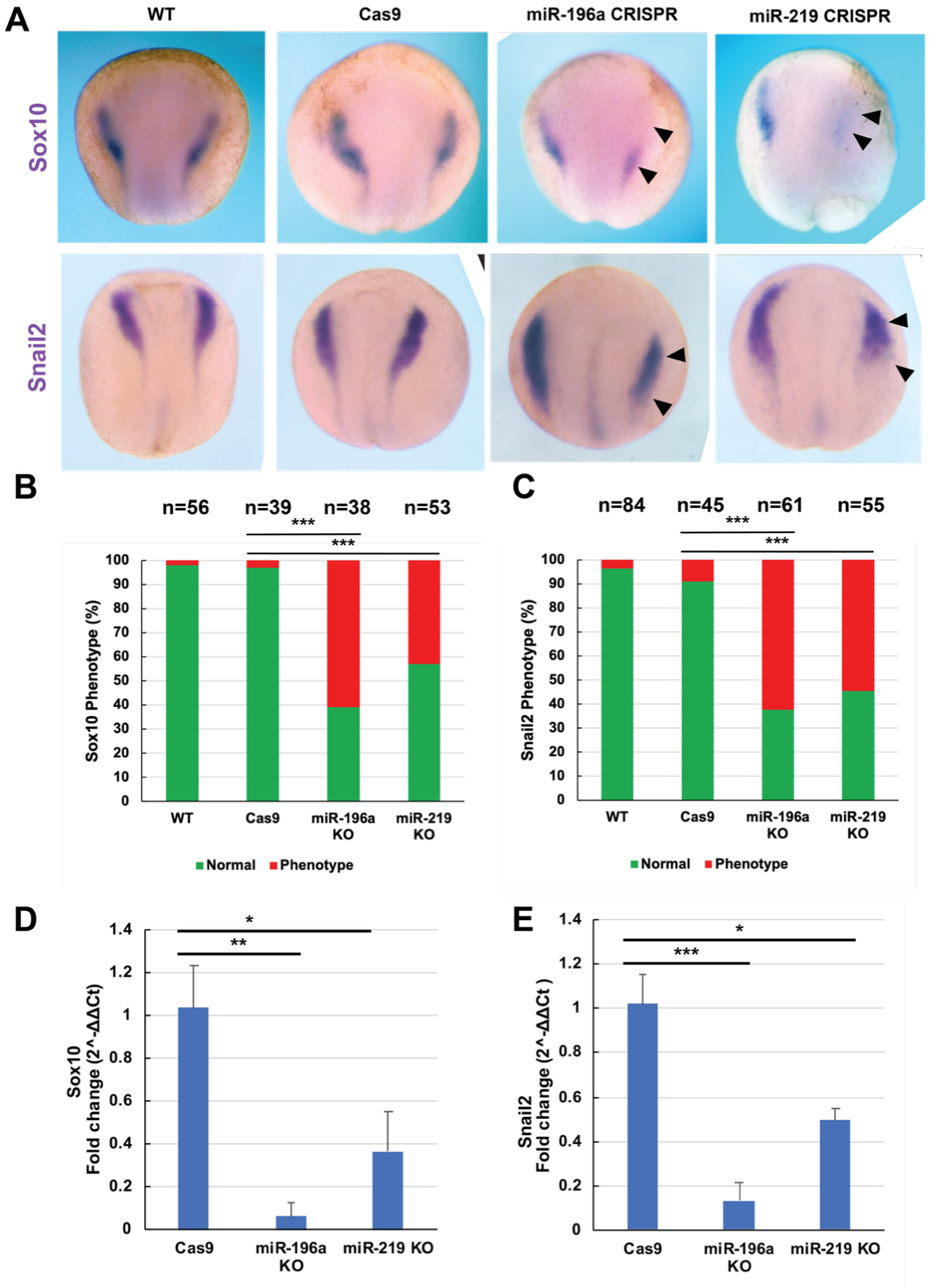
A
WT
Cas9
miR-196a CRISPR
miR-219 CRISPR
Sox10
Snail2
B
n=56
n=39
n=38
n=53
***
***
Sox10 Phenotype (%)
WT
Cas9
miR-196a KO
miR-219 KO
Normal
Phenotype
C
n=84
n=45
n=61
n=55
***
***
Snail2 Phenotype (%)
WT
Cas9
miR-196a KO
miR-219 KO
Normal
Phenotype
D
*
**
Sox10 Fold change (2^-ΔΔCt)
Cas9
miR-196a KO
miR-219 KO
E
*
***
Snail2 Fold change (2^-ΔΔCt)
Cas9
miR-196a KO
miR-219 KO

Figure 5.26 - Analysing neural crest phenotypes in CRISPR miR-KO *X. tropicalis* embryos at neurula stage of development. miRNA KO led to loss of NC expression. Embryos were injected at 2 cell stage into one blastomere using a 4 nL calibrated needle. Right side of embryo injected side. Black arrows show loss of NC marker expression. Embryos were split into three groups: WT (uninjected), Cas9 (Cas9 protein only + GFP cRNA tracer) and miR-knockout (sgRNAs 150pg each, Cas9 protein and GFP cRNA tracer). A) NC phenotypes shown by WISH for Sox10 and Snail2, phenotypes shown by black arrows. B-C) Count data of embryos exhibiting Sox10 and Snail2 loss phenotype. Sox10: Cas9 vs miR-196a KO $p=4.02x10^{-8}$, Cas9 vs miR-219 KO $p=1.04x10^{-5}$. Snail2: Cas9 vs miR-196a KO $p=6.15x10^{-9}$, Cas9 vs miR-219 KO $p=4.07x10^{-7}$. D-E) q-RT-PCR data on miR-KO groups show significant decrease in Sox10 and Snail2 expression. Bar charts show error bars depicting mean +/- SEM, statistical significance measured by T-test.

Again, to make direct comparison with MO KD data and phenotypes, Pax3 and Xhe2 expression was analysed by whole mount *in situ* hybridisation (Fig. 5. 27A). Following miR-196 KO, Pax3 expression appears slightly reduced and shifted anteriorly, for miR-219 KO, Pax3 expression was expanded. Following miR-196a KO Xhe2 expression appears expanded, whereas miR-219 KO leads to a reduction in Xhe2 expression. These phenotypes were highly penetrant and observed in over half of the embryos assayed (Fig. 5. 27 B-C9. The q-RT-PCR data supported these trends, although Xhe2 expression by q-RT-PCR was assayed on St.14 embryos whereas in situ data presented shows St. 18 embryos (Fig. 5. 27 D-E). A summary of all the q-RT-PCR data can be seen in Table 5.1.

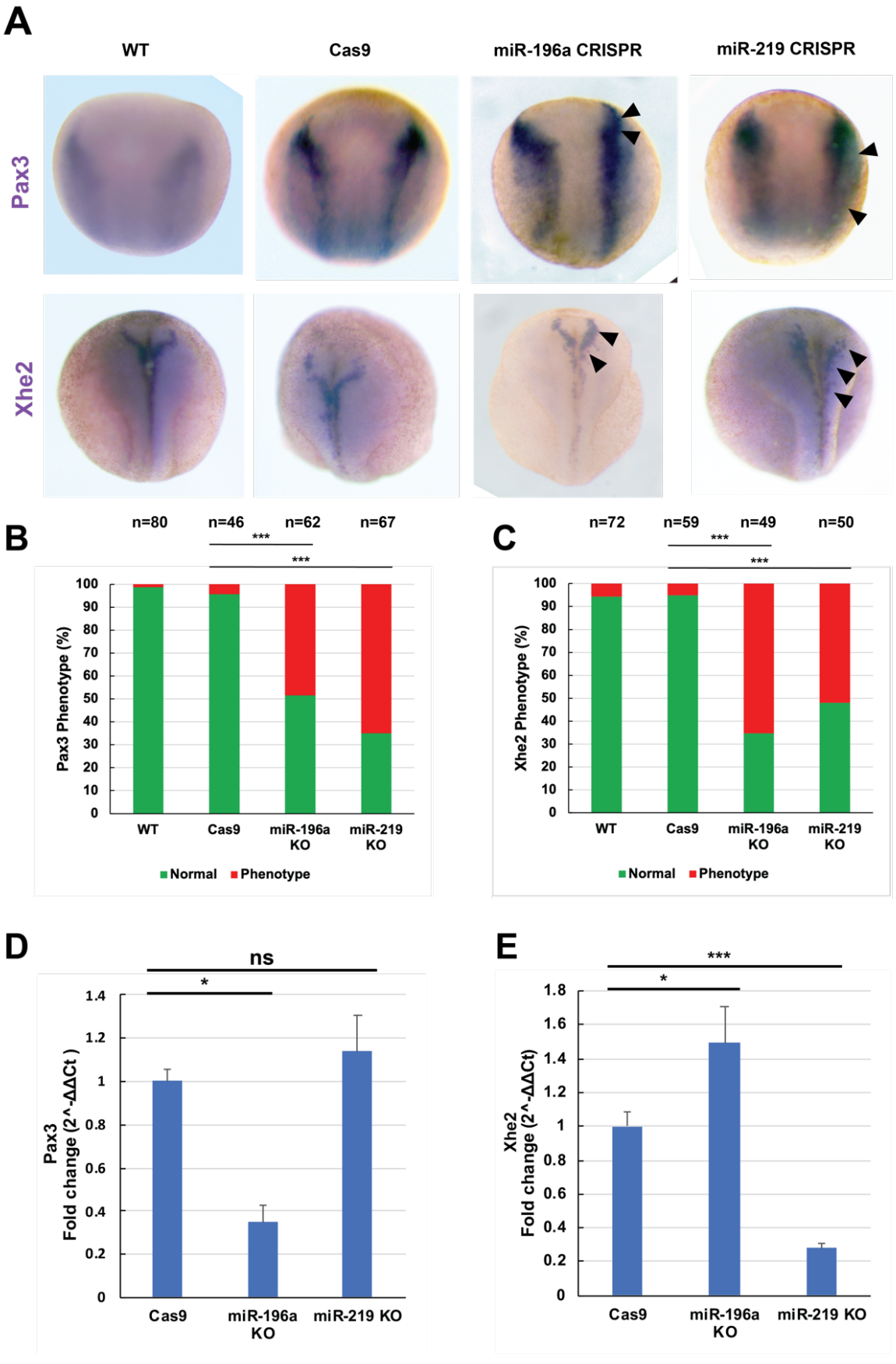
A
WT
Cas9
miR-196a CRISPR
miR-219 CRISPR
Pax3
Xhe2
B
n=80
n=46
n=62
n=67
***
***
Pax3 Phenotype (%)
100
90
80
70
60
50
40
30
20
10
0
WT
Cas9
miR-196a KO
miR-219 KO
Normal
Phenotype
C
n=72
n=59
n=49
n=50
***
***
Xhe2 Phenotype (%)
100
90
80
70
60
50
40
30
20
10
0
WT
Cas9
miR-196a KO
miR-219 KO
Normal
Phenotype
D
ns
*
Pax3 Fold change (2^-ΔΔCt)
1.4
1.2
1
0.8
0.6
0.4
0.2
0
Cas9
miR-196a KO
miR-219 KO
E
***
*
Xhe2 Fold change (2^-ΔΔCt)
1.8
1.6
1.4
1.2
1
0.8
0.6
0.4
0.2
0
Cas9
miR-196a KO
miR-219 KO

Figure 5.27 - Analysing neural plate and hatching gland phenotypes in CRISPR miR-knockout *X. tropicalis* embryos at neurula stage of development. miRNA KO led to perturbation of NPB and HG expression. Embryos were injected at 2 cell stage into one blastomere using a 4 nL calibrated needle. Injected side of embryo right side. Black arrows show neural plate and HG phenotypes. Embryos were split into three groups: WT (uninjected), Cas9 (Cas9 protein only + GFP cRNA tracer) and miR-knockout (sgRNAs 150pg each, Cas9 protein and GFP cRNA tracer). A) Neural crest phenotypes shown by WISH for Pax3 and Xhe2, phenotypes shown by black arrows. B-C) Count data of embryos exhibiting Pax3 and Xhe2 loss phenotype. Pax3: Cas9 vs miR-196a KO $p=7.19x10^{-7}$, Cas9 vs miR-219 KO $p=2.29x10^{-8}$. Xhe2: Cas9 vs miR-196a KO $p=3.32x10^{-8}$, Cas9 vs miR-219 KO $p=3.33x10^{-8}$. D-E) q-RT-PCR data on miR-KO groups show significant decrease in Pax3 and Xhe2 expression. Bar charts show error bars depicting mean +/- SEM, statistical significance measured by T-test.

Table 5.1 - Summary of CRISPR miR-196a and miR-219 KO neural crest, neural plate and hatching gland gene expression reduction and significance.

Gene	miR-196a KO		miR-219 KO	
Sox10	-93%	P=0.0047	-65%	P=0.033
Snail2	-87%	P=0.0022	-52%	P=0.030
Pax3	-65%	P=0.0131	+14%	P=0.238 (n.s)
Xhe2	+40%	P=0.05	-73%	P=0.0005

It was possible that NC cells were dying and undergoing apoptosis but unfortunately time did not permit the study of this. Analysis of apoptosis could have been achieved via the use of a TUNEL assay which detects DNA degradation indicative of apoptotic events (Tseng et al., 2007). Instead, the expression of *C-myc* and *Snail2* following miRNA-KO was analysed using whole mount *in situ* hybridisation experiments (Fig. 5.28 & 5.29). This is because *C-myc* and *Snail2* are both implicated in NC cell survival, proliferation, and induction (Kerosuo and Bronner, 2016; Li et al., 2019; Tribulo et al., 2004). Control groups; WT and Cas9 injected embryos appeared normal for c-myc and Snail2 expression. MiR-196a and miR-219 KO embryos both showed a subtle shift and reduction in *C-myc* expression in half the embryos analysed (Fig. 5. 28B).

Snail2 expression was greatly reduced at early neurula stages of development, therefore it was decided to look at later stages of neurula development to determine if this phenotype was transient, and if it would

recover (Fig. 5. 29A). Following KO of both miR-196a and miR-219 embryos showed

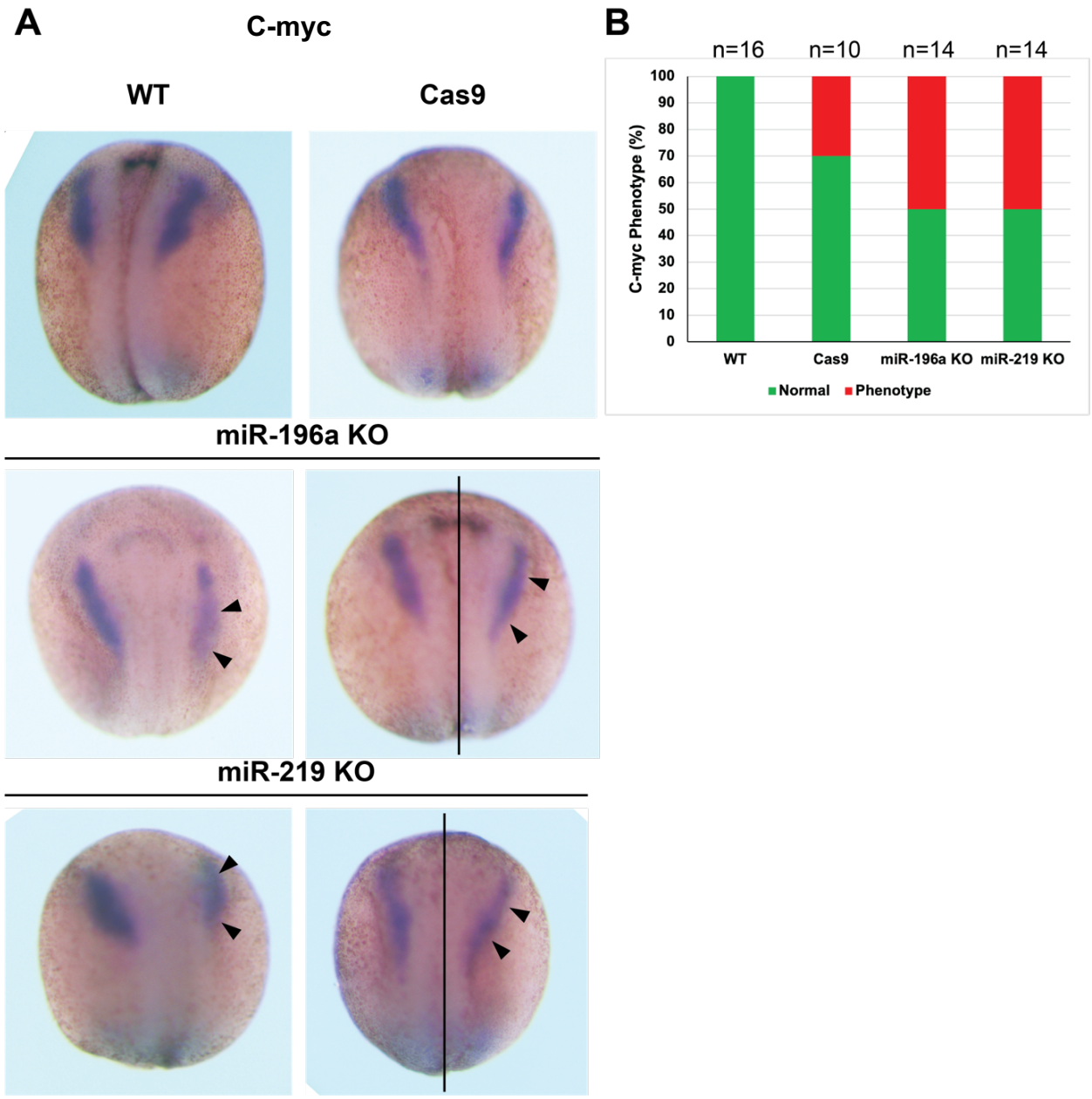

Figure 5.28 - Expression profile of C-myc following miR-196a and miR-219 KO by CRISPR-Cas9 in *X. tropicalis* embryos. miRNA-KO led to subtle loss of c-myc expression. Embryos were injected with Cas9 + GFP tracer, or Cas9 + GFP+ sgRNAs 150 pg ea, into right dorsal blastomere at 4-cell stage of development with a 4 nL calibrated needle and left to develop to St. 17. Right side of embryo injected side. Black arrows show shifted c-myc expression. (A) Expression of C-myc is perturbed in miR-196a and miR-219 KO's, as indicated by black arrows. Injected side of the embryo is the right-hand-side. (B) Count data of phenotypes observed, with miR-196a and miR-219 KO showing 50% incidence of perturbed c-myc phenotype.

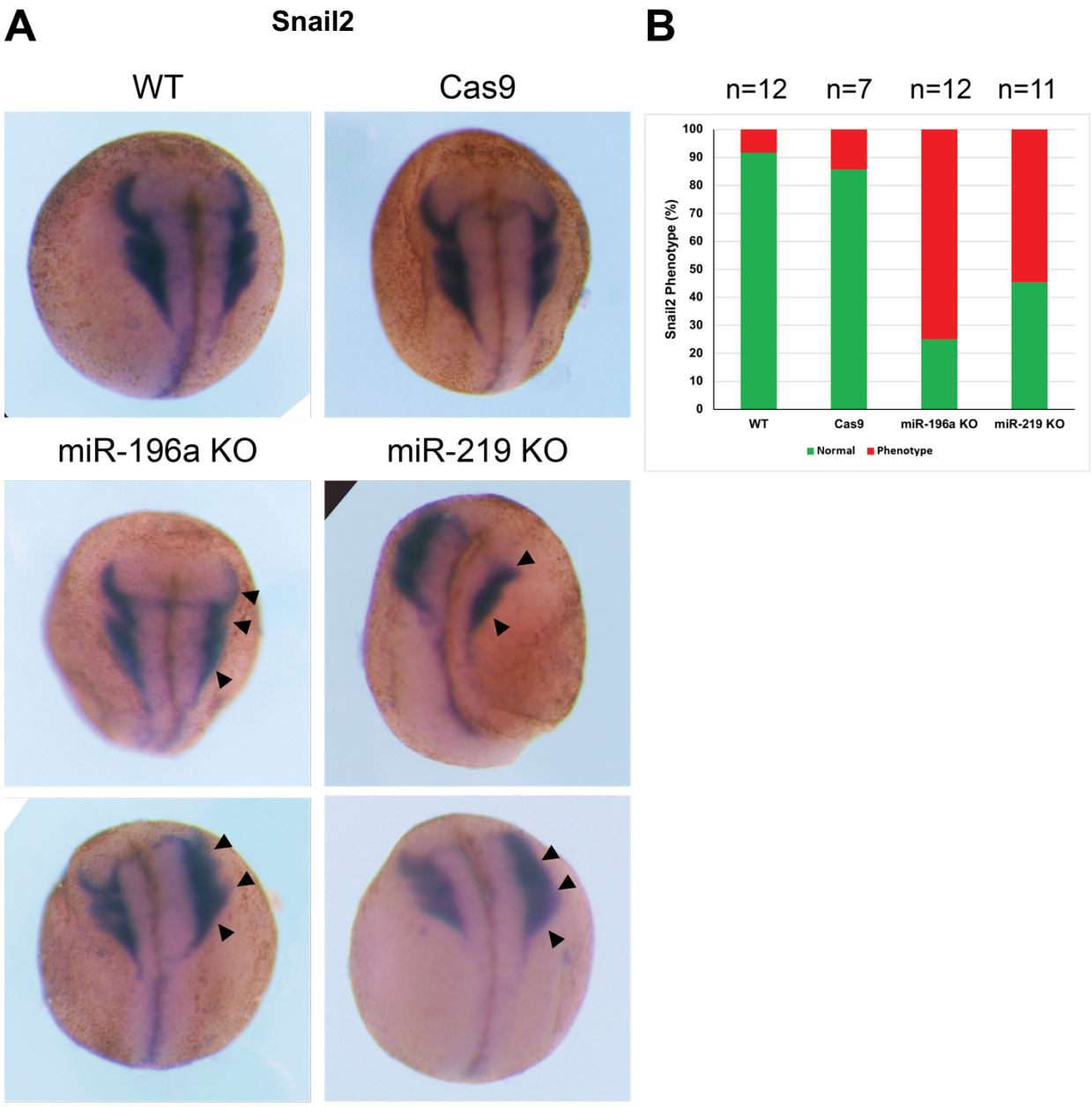

Figure 5.29 - Expression profile of Snail2 on later stage neurulas following miRNA KO in *X. tropicalis* embryos. miRNA-KO led to shifted Snail2 expression. Embryos were injected with Cas9 + GFP tracer, or Cas9 + GFP+ sgRNAs 150 pg ea, into right dorsal blastomere at 4-cell stage of development with a 4 nL calibrated needle and left to develop to St. 18. Right side of embryo injected side. (A) Expression of Snail2 is perturbed in miR-196a and miR-219 KO's, as indicated by black arrows. Injected side of the embryo is the right-hand side. (B) Count data of phenotypes is observed, with miR-196a showing over 70% incidence of phenotype and miR-219 KO showing over 50% incidence of perturbed Snail2 phenotype.

shifted and expanded Snail2 phenotypes in a significant number of embryos (Fig. 5. 29 B). Given the loss of *Snail2* expression and the shift in expression profile, it would be better to look at tailbud and tadpole stages to analyse for NC migration. This could be achieved by using a Snail2:eGFP transgenic and time lapse imaging to support this work (Li et al., 2019).

5.8.0 Making lines of miRNA KO *X. tropicalis*

To globally analyse the effect of miR-196a or miR-219 KO and conduct more complex experiments for miRNA target validation, a line of miRNA KO *X. tropicalis* would be useful and work towards this is ongoing due to delays caused by the COVID-19 pandemic. Experiments to contribute to miRNA target prediction and validation involve analysis of the global genome and RNA-sequencing on miRNA KO embryos.

5.8.1 Using dose sgRNAs

To produce a line of miRNA KO *X. tropicalis*, embryonic lethality from induced mutations needed to be avoided. To overcome this issue, a dose response of pairs of sgRNAs was trialled to see if the craniofacial phenotype could be titrated out. Even at low doses of 37.5 pg of each pair of sgRNAs, a weak phenotype was still visible. The phenotype got more extreme with an increasing dose of sgRNAs (Fig 5. 30A-B).

5.8.2 Making miR-KO lines of X. tropicalis

To overcome embryonic lethality another method was used to generate a line of frogs (Fig. 5. 31D). The primordial germ cells of the developing embryo was targeted, that way the tadpole would survive into adulthood and be able to reproduce for line generation. To target germ cells the CRISPR experiment was carried out at the 32-cell stage. 1 nL of CRISPR reagents (sgRNA pair + Cas9 protein) was injected into four of the most vegetal cells. Fig. 5. 31 shows how this overcomes the craniofacial phenotype normally obtained when targeting the embryo more globally. In the 32-cell injection group no tadpoles had craniofacial impairments or phenotypes.

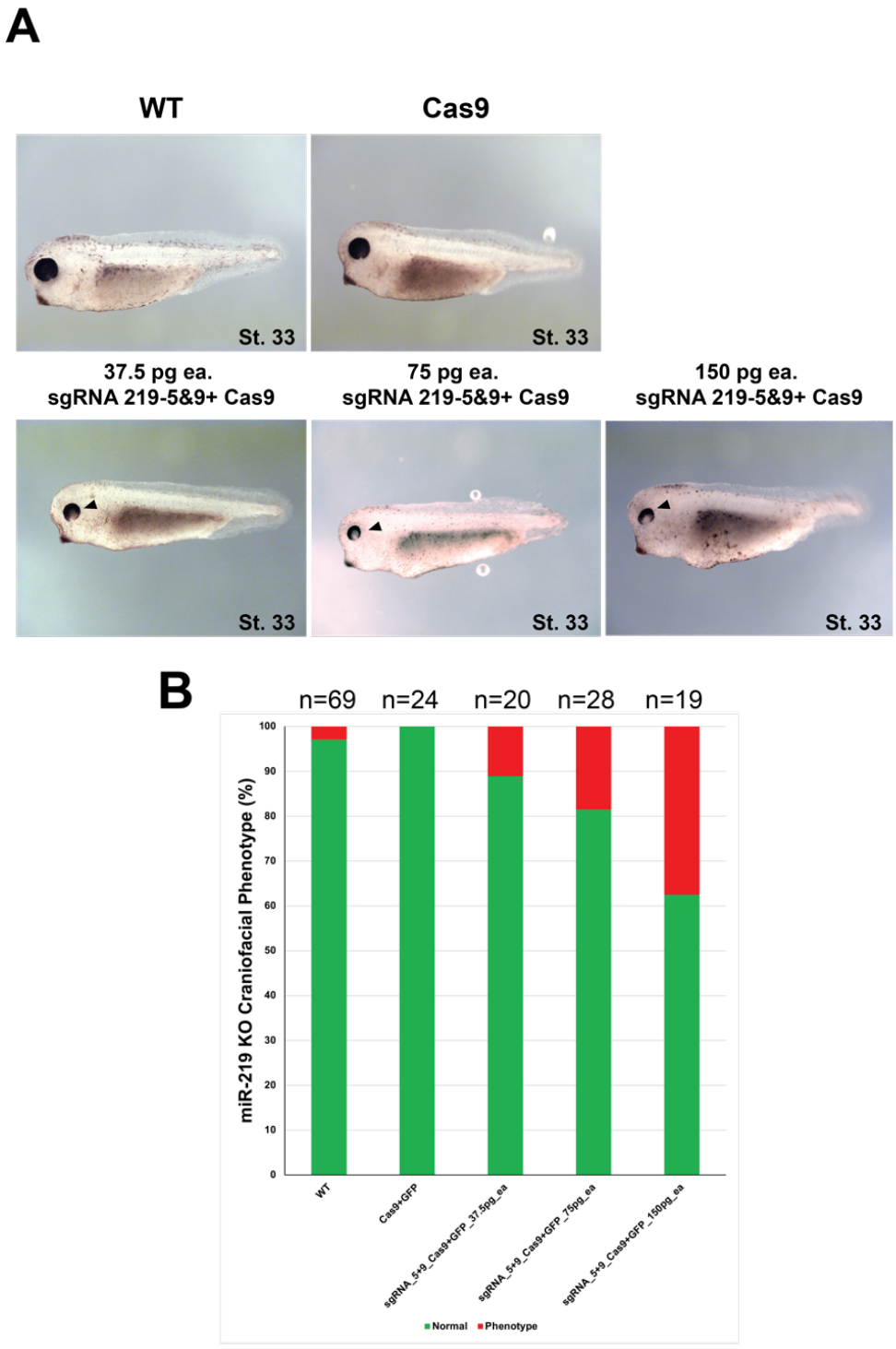

Figure 5.30 - Dose response testing of guide RNAs to titrate the craniofacial phenotype. *X. tropicalis* embryos injected with CRISPR reagents sgRNAs + Cas9 protein + GFP cRNA tracer. SgRNA pairs were injected with sgRNAs at an individual concentration of: 37.5 pg, 75 pg and 150 pg. As dose of CRISPR reagents increases the phenotype of the embryos becomes more extreme, regions showing phenotype indicated by black arrows. (A) Phenotype analysis of St. 33 tadpoles with control (WT, Cas9) groups and increasing concentration of sgRNAs for miR-219 KO. (B) Incidence of craniofacial phenotypes observed in count data, increasing dose of sgRNAs leads to increasing incidence of craniofacial phenotypes.

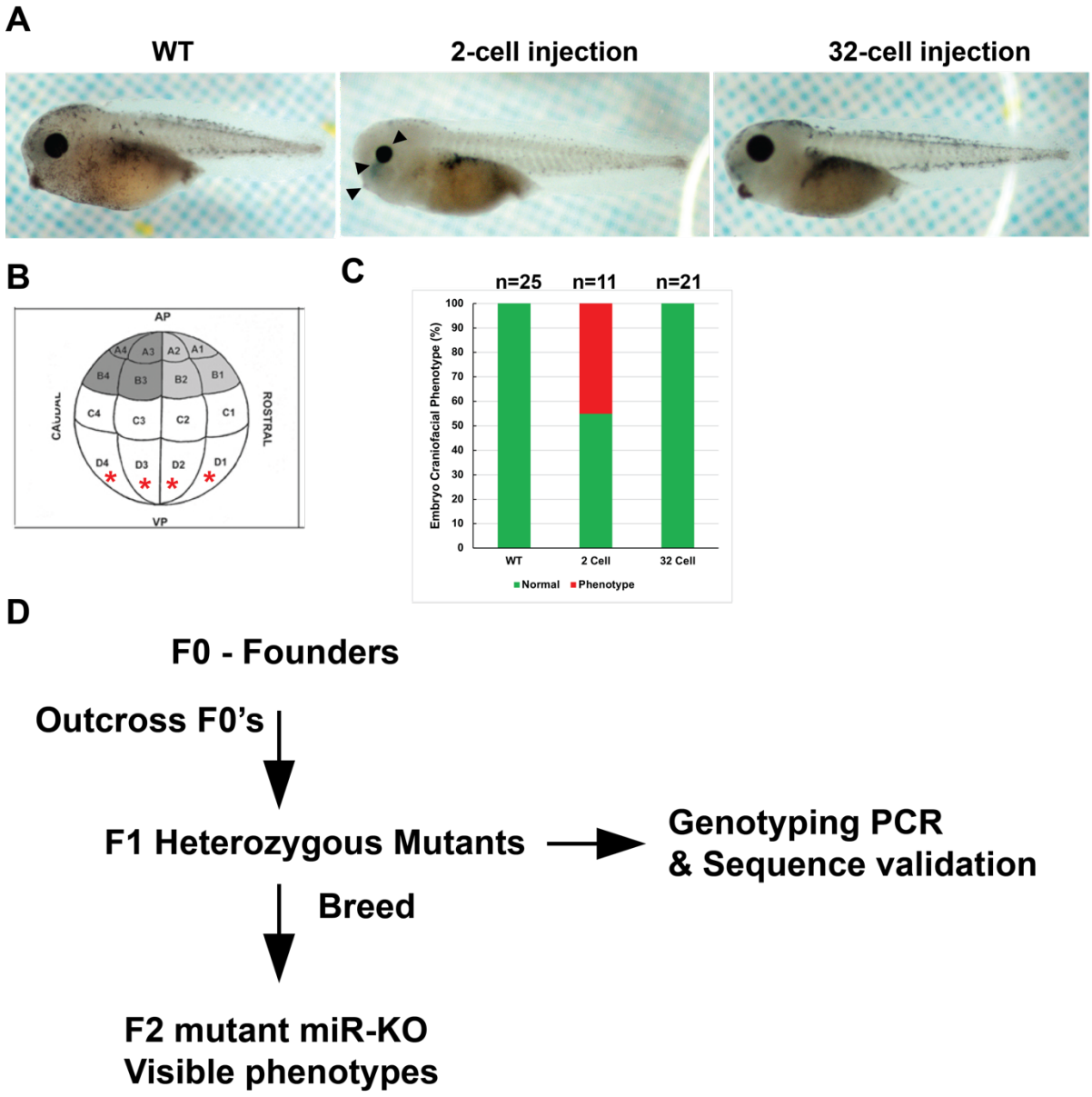

Figure 5.31 - Making a line of *X. tropicalis* miR-219 knockout frogs by targeting the germ cells. (A) Embryos were injected with 4 nL of sgRNAs at 150 pg each into one cell of a 2 cell embryo. For the 32 cell injection, sgRNAs were kept at the same 150 pg each concentration. Black arrows show craniofacial phenotypes. (B) 1 nL was injected into 4 of the most vegetal cells at the 32-cell stage. (C) Count data showed that the 2 cell injection gave a high percentage of embryos with craniofacial phenotype compared to WT and 32-cell injection groups. (D) A flow diagram outlining how a line is generated. The F0's are only mutant in their germ cells, so are crossed in the F1 to produce heterozygous mutants. These can then bred to produce miR-KO frogs.

As we were targeting the germ cells, the F0 founders would not have global miRNA-KO. They would need to be left to develop to adulthood. Once viable, these frogs (F0), would need to be crossed to generate an F1 generation. This generation would then be heterozygous mutant. At this stage sequence validation could be carried out to determine if they carry a mutation. To then generate mutant miRNA-KO frogs, the F1 generation would be bred, and their offspring would be mutant and miRNA KO (Fig. 5. 31D). These would likely be non-viable and would have the extreme craniofacial and pigment phenotypes described above. Five froglets (F0) from a short residence at the EXRC were generated, but due to COVID-19 shutdowns these have not currently been fully analysed, therefore this work is still ongoing.

5.9.0 Discussion

MOs have been successfully used for over 20 years in developmental biology research with many thousands of studies carried out (Bedell et al., 2011; Blum et al., 2015; Heasman et al., 2000). More recently CRISPR has been used as a convenient way to KO gene expression (Naert and Vleminckx, 2018). Phenotypes generated by MO KDs (morphants) are not always recapitulated by CRISPR (crispants), (Kok et al., 2015; Stainier et al., 2015). This raises concerns about phenotype interpretation when they are not concordant. It has been postulated that morpholinos could have off-target effects and thus be responsible for the extra phenotypes (Stainier et al., 2015). Therefore careful control and validation experiments must be conducted, with controlled rescue experiments viewed as the best means of validation (Eisen and Smith, 2008).

CRISPR-Cas9 utilizes a highly specific targeted nuclease to induce genomic editing by non-homologous end joining or homology-directed repair. CRISPR is an efficient technology that can rapidly generate knockout samples for analysis (Ran et al., 2013). Recent studies have shown CRISPR can be used to analyse gene function and can generate mutant lines in *Xenopus* embryos (Nakayama et al., 2013).

Having a short target sequence to induce CRISPR mutations in, limits the number of sgRNAs that one can design due to technical limitations due to PAM site incidence (Jinek et al., 2012; Kim et al., 2020; Wilson et al., 2018). This may mean that the end-user has less choice of, and less efficient sgRNAs to work with (Najah et al., 2019). However, with the advent of more Cas9 nucleases with broader PAM recognition sequences it is hoped this will be alleviated to generate more sgRNA candidates that are predicted to be efficient (Kim et al., 2020). Furthermore, new sgRNA design tools are making sgRNA design easier and more robust (Hsu et al., 2021).

5.9.1 CRISPR optimization

For this chapter, optimization of CRISPR experiments were required, not only because CRISPR was new to the lab, but also because new approaches for miRNA targeting needed to be developed. To accompany this, and as part of training purposes a positive control experiment was carried out. This involved inducing a mutation in the start codon of tyrosinase as based on the work by Nakayama and colleagues (2013); by targeting the start codon of an mRNA by using CRISPR to introduce mutations, it is expected that insertion-deletion mutations will disrupt the start codon, causing frameshift mutations that prevent transcription of the mRNA and thus KO the gene expression (Nakayama et al., 2013; Prykhozhij et al., 2017).

In Fig. 5.2, sgRNA was designed to disrupt the start codon of the tyrosinase gene. Tyrosinase is a vertebrate gene encoding a melanogenic enzyme, involved in production of melanin (Kumasaka et al., 2003).The tyrosinase crispant phenotype shows reduced pigmentation in tadpoles from St. 35 (Fig.3A), which become clearer as tadpoles continue to develop (Fig. 4A-B), where there is a strong decrease in pigmentation in the tyrosinase tadpoles, particularly in the eye, dorsal fin and abdomen. This phenotype is indicative of lack of pigment differentiation and development (Kumasaka et al., 2005). Our results show that although the start codon was not always directly disrupted by an INDEL. For gene disruption to occur, so long as the mutations are near the transcription start site, it is thought that this will still disrupt gene expression (Mohr et al., 2016).

To further validate the sgRNA efficiency, a T7 assay was performed. This assay involved a PCR of gDNA to amplify the region of the genome where the sgRNA was targeting. Through a combination of heating and cooling cycles, if there are insertion-deletion mutations, mismatch nucleotides will form heteroduplexes which are then cut by T7 endonuclease to produce bands of multiple sizes on an agarose gel (Sentmanat et al., 2018). This was be weakly seen in Fig. 5.3B but strongly in the positive control lane of the gel. T7 assays are limited in proving if an sgRNA is effective, as it will only pick up substantial and complex insertion-deletion mutations, although there are formulas for calculating the amount of non-homologous end joining events generated by CRISPR (Sentmanat et al., 2018). To elucidate the extent of the genetic aberration being induced, sequencing of the targeted sites was required (Sentmanat et al., 2018). We used a Cas9 which recognised this PAM sequence N-GG and cut the gDNA 3bp upstream of this PAM region (Jinek et al., 2012; Wilson et al., 2018). Therefore, primers were designed to amplify this region of the tyrosinase gene by PCR, and amplicons were sequenced (Fig. 5. 2). These experiments showed CRISPR was working efficiently to KO gene expression in *Xenopus* using this system.

5.9.2 Initial miRNA knockout experiments with CRISPR: miR-196a

To disrupt the expression of miRNAs, the initial plan was set to disrupt the mature miRNA sequence or the seed region of the miRNA. To do this sgRNAs were designed to target these regions in the genome (Fig. 5. 5). The main limitation of designed sgRNAs is the PAM sequence which depends on the Cas9 nuclease being used, the fact the targeted miRNA is a very short sequence, this limits the potential targets available to us (Wilson et al., 2018). The efficiency of sgRNAs vary depending on sequence, it is reported that if a guanine residue is next to your PAM motif this will support binding of your sgRNA to target genomic sequence and aid CRISPR efficiency (Moreno-Mateos et al., 2015). Some of my sgRNA designs were designed with this in mind, but due to lack of options this was not always achievable due to the short target input sequence as mature miRNAs are only 20-22 nucleotides in length (Agarwal et al., 2015). With the PAM limitations this greatly reduced the

length of sequence that could be a candidate for a sgRNA design. This meant that it wasn't always possible to design a sgRNA that would confidently target the seed region. However, it was decided it would still be beneficial to proceed as we had candidates that would target the mature miRNA and potentially disrupt the function of miRNA-196a.

To validate the efficiency of the miR-196a sgRNAs, a T7 endonuclease assay was performed (Fig. 5.6). Unfortunately, this wasn't a valid result, as our WT lane with WT gDNA also showed a spurious extra amplicon, potentially indicative of non-specific primer binding, making the extra bands in the crispant lanes untrustworthy, therefore sequencing was used to verify the CRISPR events (Fig.5.7), (Sentmanat et al., 2018). Sequencing of the mutant miR-196a gDNA samples revealed poor efficiency of insertion-deletion mutations, with just a single mismatch mutation in the expected region (Fig. 5.7). To see how this would impact the function of the miRNA, the structure of the miRNA stem loop was modelled to determine if this mismatch mutation would be sufficient to change the function of the miRNA (Fig. 5.8). The mismatch mutation only introduced an extra bulge in the mature miRNA region, and not the seed region. It was theorised that as the mature miRNA was not significantly disrupted it is unlikely that the miRNA stem-loop would be processed differently and thus may not have had a significant effect on the miRNA function (Alberti and Cochella, 2017).

Embryos injected with miR-196a sgRNA were left to develop to observe for any phenotype (Fig. 5.9). Embryos were imaged at multiple stages throughout development, and embryos were screened for those expressing GFP signal as this would show expression of tracer and successful injection of CRISPR reagents. As embryonic development progresses, mutant embryos show delayed and disrupted craniofacial development from St. 22 onwards. This could be evidence to support the argument that miR-196a is implicated in the development of NC and is disrupting cranial NC (Minoux and Rijli, 2010; Ward et al., 2018). As cranial NC takes time to develop, and is part of migratory NC (Simoes-Costa and Bronner, 2015), this supports the increasing incidence of phenotype observed through embryonic development (Fig. 8B).

To identify if gene expression was affected by the small insertion mutations generated by sgRNA-196-3, a whole mount *in situ* hybridisation experiment was performed (Fig. 5.10). HG marker, Xhe2 was used as this was a good probe for rapid in situ colour development so any disruption in gene expression would be easily detected. MiR-196a crispant embryos show loss and changes in *Xhe2* expression. Xhe2 is expressed in the superficial ectoderm and is co-expressed with *Pax3*. With disruption to Pax3 also observed following miR-196a KO, it is possible that the loss of Pax3 is causing the disruption to Xhe2 expression (Hong and Saint-Jeannet, 2007).

5.9.3 Initial miRNA knockout experiments with CRISPR: miR-219

As with miR-196a CRISPR, sgRNAs were designed to target the mature miRNA, or preferably, the seed region of the miRNA of miR-219 (Fig. 5.11). The position of the PAM sites allowed us to target the seed region and the mature miRNA sequence (Fig. 5.11B). All were then injected individually into *X*. *tropicalis* embryos for validation. To validate efficacy of sgRNA's, a T7 endonuclease assay was performed (Fig. 5.11). G-DNA was amplified by PCR and the experiment showed that sgRNA design 2 and 3 both generated INDEL mutations by showing an extra amplicon on the PCR of the T7 endonuclease assay, sgRNA 4 embryos did not survive. This time the WT lanes show one clear amplicon indicative of a clean PCR of the WT miRNA. Crispant lanes for sg-219-2 and 219-3 show a smaller amplicon in each lane respectively, this is indicative of deletion mutations as the band is smaller, indicating that the sgRNAs have cleaved out and released a smaller amplicon, a "drop-out" from the miRNA.

To further validate the successful CRISPR events, and to characterise further, sequencing was performed on PCR amplicons of the WT, Cas9 only control and crispant samples (Fig. 5.13). For crispant sample, a -3bp deletion, -CTT can be seen in the chromatogram sequence alignment (Fig. 12C). This is indicative of a deletion mutation induced by the CRISPR, showing the sgRNA sgRNA-219-2 was working. To visualise if this small deletion mutation was enough to impact the function of miR-219 in silico modelling of the miR-219 stem loop was performed (Fig. 5.14). As with the miR-196a crispant, (Fig. 5.8)

a small bulge was present in the apical stem of the miR-stem loop. This may not be enough to impact the expression and function of miR-219 as the recognition sites for DICER are intact; however, as the apical stem is affected, DROSHA recognition may be impacted. This could have affected the processing of miR-219 (Burke et al., 2014). However due to the low efficiency of the sgRNAs, and mosaicism of the CRISPR, this may not be reliable enough for our work. To validate the efficiency of mutations to disrupt expression of miRNA, q-RT-PCR could have been used (Falabella et al., 2017). Therefore, another approach was needed and will be discussed later in this chapter.

To further characterise the phenotype of the single sgRNAs embryos injected with CRISPR reagents, and control embryos were allowed to develop to analyse for any phenotypes. Sg-219-2, 219-3 and 219-4 were analysed and all show gross craniofacial phenotypes (Fig. 5.15-B-G). It was unclear if this was due to RNA toxicity or miR-KO at this stage as the previous data show we may not have knocked out miR-219. In addition, we did not have a negative control other than WT to compare to, so going forward experiments involved a WT, and a Cas9+GFP tracer negative control to account for injection stress on embryo development. Furthermore, we may have generated a novel miRNA with novel interactions binding to a different set of complementary 3' UTR's in mRNAs (Bhattacharya and Cui, 2017). These potential miR-219 KO embryos (Fig. 5.15), had gross phenotypes and did not survive well, whereas the control WT embryos survived normally, potentially indicating the CRISPR has caused genomic disruption (Wilson et al., 2018).

As with miR-196a crispants, embryos injected with sgRNA-miR-219-2 to KO miR-219 were processed by whole-mount *in situ* hybridisation to assess impact on *Xhe2* expression (Fig. 5.16). Xhe2 expression relies on a balanced level of Pax3 expression, as Pax3 expression is expanded following miR-219 KO, this may impact the Pax3 expression level, and a consequent effect could be disruption to Xhe2 expression (Hong and Saint-Jeannet, 2014). In Fig. 5.16 a reduction in Xhe2 expression was seen, therefore miR-219 KO could be indirectly affecting Pax3 expression leading to loss of Xhe2 (Hong and Saint-Jeannet, 2007; Hong and Saint-Jeannet, 2014).

The single sgRNA approach may have knocked-out our miRNAs of interest, miR-196a and miR-219, however doubts remained as to how efficient the sgRNAs were, and if they were true KO's. Another concern was that they might be creating novel miRNAs due to a change in sequence, with undesired effects (Bhattacharya and Cui, 2017). Therefore, it was decided to implement a novel approach and to generate a double sgRNA method (Fig. 5.17), to remove the pri-miRNA entirely, and KO the miRNAs individually, with the view of generating miRNA KO *X. tropicalis* lines. This approach was validated and tested, with the addition of q-RT-PCR validation steps in addition to genotyping and phenotype analysis on samples.

miR-196a MO approach in Chapter 4 highlights how miR-196a MO can KD both miR-196a and miR-196b. Due to these concerns, it was thought to be important to test that our CRISPR miRNA KO approach was not affecting the expression of miR-196b (Fig. 5.18). The sgRNAs for miR-196a KO were designed specifically for targeting miR-196a. As expected, sgRNAs to target and KO miR-196a, did not target miR-196b, as miR-196b expression remains constant in Cas9 control samples and miR-196a KO samples based on q-RT-PCR expression analysis of miR-196b on miR-196a KO samples (Fig. 5.18).

Genotyping validation of miR-196a KO involved PCR of gDNA from individual X. *tropicalis* embryos (Fig. 5.19). The embryos had been injected with CRISPR reagents into one blastomere of the embryo at the 2-cell stage of development, thus targeting half the embryo with CRISPR reagents, to let the other half the embryo develop as a WT embryo as an internal control. This strategy for genotyping is also known as a *DSP* assay, *direct sequencing of the PCR-amplified targeted genome region* (Nakayama et al., 2013). In Fig. 5.19A, the PCR gDNA from embryos can be seen, with the mutant lane showing a released extra amplicon, indicative of a CRISPR event. Through sequencing, the extra amplicon was confirmed as miR-196a KO (Fig. 5.19 A'). Further validation by q-RT-PCR showed sgRNAs crispant group led to 67% reduction in miR-196a expression, showing the sgRNAs were efficient (Fig. 5.19 B). This is a significant KO for F0 generation as these embryos would have a high degree of mosaicism (Mehravar et al., 2019). Using q-RT-PCR is a valid

approach for quantifying efficiency and specificity of sgRNAs used in CRISPR experiments and shows how much of your transcript is still being expressed (Ren et al., 2016). Efficiency of sgRNAs can vary depending on what and where the target is and may explain the difference in efficiency of our sgRNAs for each miRNA (Yang et al., 2017). We could therefore be more confident that these paired sgRNAs are reducing miR-196a expression in comparison to the individual sgRNA approach. This is because single sgRNA may be limited as the small INDEL mutations may not have been enough to disrupt the miR-196a expression, and as previously discussed may have generated novel miRNAs (Bhattacharya and Cui, 2017). It would have been best to have also performed q-RT-PCR on this individual sgRNA approach to be sure of this.

CRISPR miR-196a KO embryos and control groups were left to develop until St. 42 of embryonic development. It was discovered that at this stage the tadpoles for miR-196 KO, targeted with CRISPR reagents, exhibited a loss of pigment phenotype on one side. This is significant as pigment is a NC derivative (Aoto et al., 2015; Cheung and Briscoe, 2003; Collazo et al., 1993; Milet et al., 2013; Tomlinson et al., 2009). Therefore, this is further evidence that miR-196a is involved in the development of NC in the developing *Xenopus*.

Pigment cells or melanophores, are a derivative of the NC (Ohsugi and Ide, 1983; Tomlinson et al., 2009). Melanophores are seen as black spider shaped cells, this is the normal dendritic morphology (Tomlinson et al., 2009). On the untargeted side of the miR-196a KO tadpoles the melanophores appear normal in terms of cell number and morphology. On the injected side of the embryo, the cells appeared slightly reduced in size, and reduced in number. This may be indicative of a lack of melanophore differentiation, as Sox10 which is depleted in miR-196a KO's is required for melanophores to differentiate (Aoki et al., 2003). *Sox10*, *Mitf* and *Pax3* all interact together and are implicated in the development of Waardenburg syndrome. This is a neurocristopathy which has a pigmentation phenotype in patients (Bondurand et al., 2000). Therefore, with perturbed Sox10 and Pax3 phenotypes following miR-196a KO, it is unsurprising that we see pigment phenotypes. Mitf is

another regulator of melanophore development (Kumasaka et al., 2005), it would be interesting to analyse how Mitf expression is changed following miR-196a KO to get a better understanding of the pigment phenotypes observed.

Tadpoles targeted with CRISPR reagents were allowed to develop until St.45 for Alcian blue analysis to investigate for craniofacial phenotypes (Simoes-Costa and Bronner, 2015), (Fig. 5.21 B). MiR-196a KO embryos did not externally exhibit craniofacial phenotypes at St. 42, (Fig. 5.20), only pigment phenotypes, in accordance with Chapter 4 when miR-196a was knocked down with MO. Perhaps if MO KD embryos were pushed to develop to St. 45, they may have started to externally exhibit craniofacial phenotypes like Fig. 5.21A with CRISPR miR-196a KO. There is also an eye phenotype in these embryos, with smaller eyes on the crispant side of the tadpole. Due to the pigment phenotypes seen in Fig. 5.20, this may indicate that the pigment in the retinal pigment epithelium cells are affected (Tomlinson et al., 2009), this is not a NC-derived melanophore population (Bharti et al., 2011). Although this is difficult to be sure of as the opposing side of this tadpole is also exhibiting craniofacial phenotypes and is showing some GFP fluorescence, this is not unusual as tadpoles are transparent and GFP signal can bleed through the whole embryo.

Previous reports for miR-196a KD experiments show eye phenotypes. With smaller eyes observed following morpholino mediated miR-196a KD (Gessert et al., 2010). Other reports show that overexpression of miR-196a in *X. laevis* can also lead to eye anomalies (Qiu et al., 2009). This may explain the eye phenotypes following miR-196a KO in Fig.20 later in tadpole development at St.45, and may suggest that a fine balance of miR-196a is required for normal eye development, as overexpression (Qiu et al., 2009) leads to eye anomalies and miR-196a KD leads to smaller eye phenotypes (Gessert et al., 2010). We did not test embryos following miR-196a KD by morpholinos at St. 45, we tested at St. 42 therefore it may be worth letting the embryos develop to older stages to determine if we also see eye phenotypes following morpholino KD. We did however see eye anomalies at St.45 when miR-196a was knocked out by CRISPR, with micropthalmia phenotypes. This may warrant further investigation.

5.9.4 MiR-219 KO validation and analysis

The same approaches to validate miR-196a KO were used to validate miR-219 KO. Genotyping PCRs were conducted and indicate that the pair of sgRNAs designed to KO miR-219 release a smaller amplicon, indicative of CRISPR events. The sequencing of these amplicons shows clear deletion of the miR-219 stem-loop (Fig. 5.22 A'). The q-RT-PCR (Fig. 5.22 B) further indicates the sgRNAs are not only efficient but specifically targeting miR-219. As the sgRNAs were 93% efficient and sequence analysis showed loss of miR-219 it is unlikely these sgRNAs have off-target amplicons (Clement et al., 2020). To account for off-target effects a rescue experiment as with the MO experiments in chapter 4, could be carried out, although we expect off-target effects to be minimal as sgRNAs were chosen with no predicted off-target mutation (Moreno-Mateos et al., 2015).

It was decided to analyse the phenotype of the *X. tropicalis* crispant miR-219 KO embryos, with control samples included. Embryos were left to develop until St.41, these tadpoles showed craniofacial abnormalities (Fig. 5.23). Alcian blue experiments were carried out to assess for any craniofacial cartilage changes and abnormalities (Fig. 5.24). After Alcian blue staining it was revealed that the small eye phenotype was more striking, and a microcephaly phenotype was revealed. These craniofacial phenotypes could be indicative of miR-219 affecting the development of cranial NC development which is important in development of craniofacial features (Minoux and Rijli, 2010). The most prominent craniofacial phenotype is the anterior shift of the eye and craniofacial changes (Fig. 5. 23A), this is reminiscent of the phenotypes seen in Treacher Collins syndrome and Nager syndrome which have hypoplastic craniofacial cartilage with patients having cleft lip and palette and eyelid phenotypes (Devotta et al., 2016; Sakai and Trainor, 2009). It could be speculated that miR-219 is targeting directly or indirectly, pathways implicated in the development of these pathologies. *Xenopus* embryos have been used to model Nager syndrome through MO-mediated KD of Sf3b4 experiments. This leads to characteristic hypoplastic craniofacial cartilage in morphants, like in the Nager syndrome patients. This is significant as *Sf3b4* mutations lead to Nager syndrome in human patients. In the morphant embryos a loss of Sox10

expression is clearly seen, which we also see following miR-219 KO, which also leads to craniofacial phenotypes (Fig. 5.23), (Devotta et al., 2016). More work could be done to investigate the role miR-219 is playing in craniofacial development to understand if migration, development, or differentiation of cranial NC is being affected. Simple migration assays with live imaging to track NC development could be conducted. This could involve use of Sox10 GFP transgenics generated by the Monsoro-Burq lab, embryos could be knocked down for miR-219 and time-lapse imaging could be carried out (Alkobtawi et al., 2018). Or experiments involved NC explants to culture NC cells could be cultured (Usami et al., 2014) and transfected with miR-219 morpholino or use explants from miR-219 KO embryos from CRISPR generated lines.

It was questioned whether the miR-219 KO tadpoles may have smaller eyes because the embryos themselves are smaller or shorter in length. Eye size, eye area and body length were all measured (Fig. 5.25). It was found that eye area and eye length, measured horizontally across the eye, was reduced, with eye area significantly reduced. This is further evidence that miR-219 is implicating the development of craniofacial features. The NC cell make a small contribution to eye development, although that are some rare eye diseases where NC are implicated, such as branchio-oculo-facial syndrome, which also presents with craniofacial defects and micropthalmia (Akula et al., 2019). It would therefore be interesting to investigate further if miR-219 KO has impact on markers of optic cup and periocular mesenchyme, such as *Pitx2* and *Tfap2a* (Akula et al., 2019; Sivak et al., 2004).

In chapter 4, miRNA MO KD embryos underwent whole mount *in situ* hybridisation experiments for NC markers: Sox10 and Snail2, NP marker Pax3, and HG marker Xhe2. To make direct comparison with the CRISPR KO's, the same *in situ* hybridisation experiments were performed on CRISPANT embryos. WT and Cas9 injected only embryos were used as negative controls, just as with MO experiments where WT and mismatch MO negative controls were used. Following miR-196a and miR-219 KO Sox10 was significantly reduced in expression (Fig.5.26 A, B & D). *Snail2* was reduced in expression and shifted laterally for miR-196a and miR-219 KO (Fig. 5.26 A, C

& E). Sox10 is expressed in pre-migratory and migratory NC as seen in Sox10 GFP transgenic *Xenopus* (Alkobtawi et al., 2018). Snail2, also known as Slug, has anti-apoptotic activity in the development of NC (Tribulo et al., 2004). Snail2 is required for induction and specification of the cranial NC populations (Li et al., 2019). Combined, loss of *Sox10* and *Snail2* expression may be indicative of loss of migration and differentiation of NC populations that are then leading to craniofacial phenotypes (Alkobtawi et al., 2018; Li et al., 2019; Tribulo et al., 2003).

Sox10 and Snail2 in morphant (Fig. 4.9) and crispant (Fig. 5.26) embryos following miR-196a and miR-219 KD and KO were both reduced. Sox10 is more significantly reduced for morphant and crispant groups. However, Snail2, in morphant embryos showed a loss phenotype, but in crispant showed a loss phenotype in miR-196a KO, and a more disorganised phenotype, with a small in miR-219 crispant embryos. This difference could be due to the difference in KO versus KD experimental design. Kok and colleagues conclude that differences in phenotype between MO and CRISPR or other gene editing mutations could be due to off-target effects of the MO (Kok et al., 2015). This could be indicative of effects of our miR-196a MO targeting both miR-196a and miR-196b (Fig.4.3), which is not seen in crispant embryos (Fig. 5.18). Therefore, validated crispant embryos could be more trustworthy and less likely to have off-target effects if proven to be specific. Thus, the novel miRNA KO approach would be the preferable method for functional and specific miRNA analysis in *Xenopus* NC development.

Analysis of Pax3 expression following miRNA KO showed contrasting phenotypes between miR-196a KO and miR-219 KO (Fig. 5.27 A, B & D). MiR-196a KO led to a loss of *Pax3* expression, and miR-219 KO led to an expansion of Pax3. The region which Pax3 is expanded in miR-219 KO appears superficial looking at the whole-mount image. MO KD of miR-219 and sectioning showed this expansion of NC was in the superficial ectoderm. This may explain why in the q-RT-PCR of whole embryos, there wasn't a significant increase of Pax3 expression. The contrasting Pax3 phenotypes observed following miR-196a KO (loss) and miR-219 KO (gain), are further evidence

that these miRNAs are acting differently and may have different roles in the development of *Xenopus* NC. Other model systems show Pax3 is regulated by miRNAs in embryonic development; for instance, in the context of myogenesis in the chick model system (Goljanek-Whysall et al., 2011; Viaut et al., 2021). Therefore, it is possible miRNAs could be regulating Pax3 in different ways, either directly or indirectly in the context of NC development. Looking at the Pax3 3' UTR, it was found that this does not contain a binding site for either miR-196a or miR-219, therefore it is more likely that our miRNAs are indirectly regulating the expression of *Pax3*. More work could be done to look at direct targets of miRNAs through use of luciferase assays (Viaut et al., 2021).

Pax3 is implicated in the development of melanophores (Milet et al., 2013). The loss of *Pax3* expression following miR-196a KO (Fig. 5.27) may account for the pigment phenotypes observed. The gain of Pax3 following miR-219 KO may show that miR-219 is involved in neural induction and proliferation with expansion of Pax3 seen in superficial ectoderm. This is because work has been carried out to show that primary neurons differentiate in underlying neuroectoderm and proliferate in the superficial ectoderm (Chalmers et al., 2002). *Xenopus* NPB gives rise to placodal ectodermal tissue, NC and HG. A key marker of HG is Xhe2. *Xhe2* expression has been shown to be affected by the level of Pax3 being expressed (Hong and Saint-Jeannet, 2007; Hong and Saint-Jeannet, 2014). As with Pax3, miR-196a and miR-219 KO show contrasting phenotypes in Xhe2 expression, further validating this result (Fig. 5.27); miR-196a KO shows subtle expansion of Xhe2 and miR-219 KO shows loss of Xhe2. This contrasts with the work of Hong and colleagues, where they see an expansion of Xhe2 following expansion of Pax3 (Hong and Saint-Jeannet, 2007). This may be because expansion of Pax3 in our embryos is limited to the superficial ectoderm, whereas Hong's work delivers Pax3 overexpression throughout one side of the embryo by injecting Pax3 mRNA at the 2-cell stage of development into 1-blastomere of the embryo (Hong and Saint-Jeannet, 2014). This suggests Pax3 levels are significant in the proper development of HG, and that our miRNAs may be affecting this network

upstream of Pax3, to affect the levels of Pax3 and in turn perturb the expression of *Xhe2*.

Due to time pressures from the COVID pandemic, there wasn't enough time to learn and utilize TUNEL assays for my experiments. I wanted to know if miRNA KO led to an increase in NC cell death, and if that was possibly causing our craniofacial phenotypes. Instead, I performed a whole-mount *in situ* hybridisation experiments to visualise the spatial expression of c-myc and Snail2 following miRNA KO (Fig. 5.28-29). C-myc is important in maintaining a pool of self-renewing NC cells, and loss of C-myc leads to increased cell death and lack of NC migration (Kerosuo and Bronner, 2016). MO KD of c-myc in Xenopus embryos leads to loss of NC precursors and derivatives (Bellmeyer et al., 2003). C-myc expression following miR-196a and miR-219 KO show a perturbed expression profile, with a weak and laterally shifted phenotype (Fig. 5. 28). This could be indicative of changes in c-myc expression, which in turn is leading to NC cell death or lack of NC migration and differentiation (Bellmeyer et al., 2003; Kerosuo and Bronner, 2016). To know if cell death is truly responsible for the craniofacial and loss of NC expression phenotypes observed following miRNA KO, it would be advantageous in future to do a validatory TUNEL assay, or Caspase-3 assay to evaluate apoptosis of NC cells (Tseng et al., 2007).

To investigate if the loss of NC markers was transient and limited to early neurula development, the expression of Snail2 was examined at late neurula stages, St. 17 (Fig. 5.29). In early neurula development, miR-196a and miR-219 KO leads to a loss of Snail2 expression. Later in development the expression is not recovered shows loss and disorganisation. This may indicate that the migration of Snail2 NC is not progressing normally. This is because Snail2 is involved in the induction of EMT processes involved in NC migration (Li et al., 2019). The reduced profile of Snail2 may also indicate that there is a smaller pool of migratory NC, this could be due to cell death or lack of differentiation of NC. It would be useful in future to look later in embryo development from tailbud to tadpole stages to track the cranial NC migration

following miRNA-196a and miR-219 KD, by using a Snail2 GFP transgenic (Li et al., 2019).

The NC can be used as a model to study cancer development due to the fact they undergo EMT and their migratory nature (Mayor and Theveneau, 2013; Wislet et al., 2018). MiR-196a and miR-219 are both implicated in many aggressive and metastatic cancer populations (Jiang et al., 2018; Schimanski et al., 2009; Wang et al., 2017; Zhuang et al., 2017). Due to this, it could be speculated that miR-196a and miR-219 are potentially implicated in the migration and EMT of NC and may have direct targets implicated in these processes.

5.10.0 Conclusions, ongoing and future work

MiR-196a and miR-219-KO embryos and tadpoles exhibit strong phenotypes. The miR-219 KO leads to craniofacial phenotypes that would be embryonic lethal; this would cause problems for generating lines of miR-KO X. *tropicalis*. To overcome this embryonic lethality, dose-response experiments to reduce the concentrations of sgRNA were performed (Fig. 5.30). It was conducted with the expectation that reduced concentration of sgRNA would still be potent enough to KO miRNA, but with less penetrant, heterozygous, phenotypes to generate viable embryos that would survive into adulthood. Ongoing and future work involves the generation of viable miRNA KO X. *tropicalis* lines.

At the time of submission of this thesis, the approach taken to generate miRNA KO lines of *X. tropicalis* had not yet been validated due to delays caused by the COVID-19 pandemic. We believe that targeting the germ cells of the developing embryo, to generate mosaic heterozygous F0 founders, that are then crossed to produce F1 heterozygotes, which are then further crossed to produce F2 miRNA KO embryos for analysis will be successful at some point.

CHAPTER VI

DISCUSSION, CONCLUSIONS & FUTURE WORK

6.0.0 Discussion

6.1.0 Aims and hypotheses

This chapter will discuss individual key findings from each results chapter and the chapters combined. It will then pose conclusions and areas for future work. It was hypothesised that miR-196a and miR-219 are important in the initial cell fate choices setting up induction and specification of NC. It was also expected that these miRNAs would target directly, or indirectly, genes and gene expression involved in NC, NPB and placodal specification.

In the first chapter of this thesis the key aims, and questions of this thesis were posed. To summarise these were:

- To analyse the spatial and temporal expression of miR-196a and miR-219
- To assay expression of key NC markers and upstream markers that may be targeted by miR-196a and miR-219
- To functionally characterise morpholino knockdown of miR-196a and miR-219
- To develop CRISPR-Cas9 methodology to knockout miR-196a and miR-219 with the view to generate miR-KO lines of *X. tropicalis*.

This work has discovered novel research and key data that will drive this project forward and poses areas for further investigation in the future. I will now summarise these key findings in relation to my research questions, hypotheses, and related published literature with any limitations.

6.2.0 Key findings

6.2.1 Spatial and temporal expression of miRNAs

In the first results chapter the spatial and temporal expression of miRNAs thought to be expressed in NC was examined. MiRNAs have been shown to be expressed in embryonic development previously by members of the lab (Ahmed et al., 2015). Little work has been done to characterise miRNAs in NC development outside of our lab, and many unknowns and gaps in knowledge

remained. One key unknown for this project was to reveal if miRNAs were expressed in the NC in the developing *Xenopus* embryos. Based on small RNA-sequencing and q-RT-PCR data provided by previous work in the lab it was expected that miR-219 would be uniquely expressed in NC, and miR-196a in NC and neural tissue (Ward et al., 2018).

LNA whole mount *in situ* hybridisation in the lab previously did not find an expression profile for mature miR-196a and miR-219 (Ahmed et al., 2015). Therefore, for this project it was important to confirm when and where these miRNAs are expressed as this would give insight into the role of these miRNAs. As optimization of hybridisation was conducted to see if this would improve these results. Where the lab previously used 42^{o}C for hybridisation temperatures, I used 54^{o}C to reduce background and non-specific probe binding signals (Ahmed et al., 2015; Sweetman et al., 2006). After this fine-tuning some expression profiles were generated and showed potential neural and NC expression (Fig. 3.10). Experiments were also performed with LNA probes to assay for species conservation of miRNA expression. The chick embryos showed that miR-196a and miR-219 were expressed in NC and neural tissue (Fig. 3.11), supporting the *Xenopus* miRNA expression profiles. This was to be expected as mature miR-196a and miR-219 are conserved between chick and *Xenopus* (Fig. 3.1), and the LNA probes would be complementary to mature miRNAs miR-196a and miR-219 in both chick and *Xenopus* embryos.

To determine if the miRNA expression profiles overlapped with NC, a double *in situ* hybridisation experiment was used. As the expression profiles generated by LNA probes were less clear, due to the transient nature of mature miRNA expression, I decided to generate standard *in situ* probes based on the pri-miRNA to generate a longer target, as mature miRNAs are far too short to generate a traditional *in situ* hybridisation probe against (Ahmed et al., 2015; Darnell and Antin, 2014; Darnell et al., 2010; Zhou et al., 2018).

Previous work done by the Harland lab adopted a similar approach and designed primers to generate a 1 kb pri-miRNA (Walker and Harland, 2008). The miR-219 expression profile generated by Walker and Harland, showed at the late neurula stage a neural expression profile, and the tadpole stages had a lot of background signalling, but appears craniofacial (Walker and Harland, 2008). Overall, the pri-miRNA probes were giving clearer *in situ* expression profiles with bolder expression, potentially due to the higher hybridisation temperatures of a standard in situ experiment and because of the increased target length of the pri-miRNA which may help with specific binding and reduce non-specific background signalling. The resolution of craniofacial features was rectified by looking at younger tadpoles than Harland and colleagues (Walker and Harland, 2008). The sections of the embryos show some expression of miR-196a and miR-219 in the NC, but also in neural tissue. Reasons for this are currently unclear. This could be due to biogenesis and turnover of miRNA in the developing embryo. To get a clearer view of whether miRNA expression overlaps with NC and NPB, perhaps Sox10:GFP or Pax3:GFP transgenic embryos could be processed by *in situ* and immunohistochemistry to recapture the NC expression (Alkobtawi et al., 2018). This is because the spatial and temporal expression must be understood to give a hint to its functional role. Previous work in the lab has found miRNAs to be co-expressed in neural tissue, and this was thought to be due the widespread expression of the genome in development of the brain and nervous system (Ahmed et al., 2015).

With respect to double *in situ* hybridisation to visualise miRNA and Sox10 NC expression there were technical challenges. It was challenging to develop an expression profile for the miRNAs, and then to develop the second colour profile of Sox10, the Sox10 profile was much weaker than it should appear. The Sox10 was developed with fast red, as the probe was FITC labelled to generate distinguishable colour difference for clear overlap, with fluorescence for detection where there was overlapping. However, this expression was found to be washed out or too weak to determine. Other colours were trialled, but these were too similar to the purple generated by the NBT/BCIP colour reactions developing DIG-labelled probes. Overall, the long-time taken to develop the expression of miRNA with DIG-labelled probe was likely to be

leading to degradation of the anti-FITC secondary antibody bound to the Sox10 FITC probe.

Overall, miRNAs showed NC and neural expression in Chick, *X. laevis* and *X. tropicalis*. This was to be expected for miR-196a which was previously found to be enriched in the NC and neural tissue in animal cap explants, but from the animal cap data, miR-219 was expected to have a cleaner NC profile. This could be due to the transient turnover and biogenesis of miRNAs and warrants further investigation. This could also be due to the artificial nature of animal cap experiments. The tissue is a semi-synthetic tissue generated by overexpression of mRNAs to drive differentiation of the tissue towards a chosen fate. Linker and colleagues have previously discussed how Xenopus animal cap assays are unsuitable for the study of signals and factors implicated in neural induction (Linker et al., 2009). This may have prevented our miRNAs from being enriched in neural tissue animal caps.

Since carrying out this project, newer techniques such as hybridisation chain reaction have been further developed (Choi et al., 2018). After consultation with the manufacturer, it is thought that this technology would amplify a miRNA expression profile, making it clearer and bolder. This is because probes would initially bind to the target miRNA, and then the initial probe would be amplified by a chain reaction with labelled molecules to vastly amplify the original signal cleanly (Choi et al., 2018). Other technologies that could be adapted would be to use RNAscope. This technology works through use of proprietary amplification technology using probes. This is thought to be able to detect miRNAs but may require optimization for use in whole *Xenopus* embryos (Yin, 2018).

6.2.2 Development of a CRISPR-Cas9 method to knockout miRNAs

Initially, sgRNAs were developed to be used singly to individually KO a specific miRNA by targeting the miRNA at the mature miRNA region, or the seed region by inducing small INDEL mutations. Due to relatively small target regions this was limited because as the number PAM sites was restricted, the number of the candidate sgRNA designs was also limited. In addition, the

sgRNAs designed and used individually, could have generated novel mutant miRNAs (Bhattacharya and Cui, 2017). Despite new work outlining which portions of pri-miRNA are significant for Drosha and Dicer processing (Rice et al., 2020), it is unclear if we have significantly reduced expression of our miRNAs or simply created undesirable novel effects such as generation of novel miRNAs (Bhattacharya and Cui, 2017). Therefore, it was important to develop another approach to generate a complete and specific miRNA deletion. We therefore have developed a novel “drop-out” mechanisms. This involved design and use of two sgRNAs simultaneously. During this project another group published some work that knocked out miR-451 in Zebrafish using a similar technique to that developed in this work. Their work also used two sgRNAs to KO miRNAs neighbouring each other (Kretov et al., 2020). This supports the use of our approach and makes us more confident for the ongoing work to generate lines of miRNA KO *X*. *tropicalis*.

To generate lines of miRNA KO frogs, *X. tropicalis* embryos were targeted at the 32-cell stage into 4 of the most vegetal cells to target the germ cells of the developing embryo. This was piloted with sgRNAs for miR-219 KO. These embryos were grown up from Jan’ 2020 and in April 2021 the adults (F0s) were outcrossed with WTs to generate F1 embryos. These were then tested from each of our 5 founder frogs. 40 individual embryos were genotyped, and none showed a heterozygous miR-219 KO. Therefore, it is unclear if the CRISPR on the original embryo injection worked. It would have been better to co-inject these initial embryos with a tracer to know if the embryos were successfully targeted at 32-cell stage. Of 26 embryos, 5 made it to adult frogs (F0), according the EXRC at the metamorphosis stage of development is where many were lost. It could be that the embryos may not be viable, and perhaps in the future if after optimisation this still doesn’t work a conditional knockout for miRNAs may need to be considered. Despite these concerns, validation, and development of the generation of lines of miRNA KO *X*. *tropicalis* are being carried out as this work was not finished during the timeframe of this PhD due to COVID-19 shutdown delays at UEA and at our collaborator the European Xenopus resource centre (EXRC).

6.2.3 Functional characterisation of miRNAs following morpholino knockdown and CRISPR knockout of miRNAs

After KD and KO of miRNAs with MOs and CRISPR-Cas9 respectively, phenotypes observed by whole mount *in situ* hybridisation of NC markers were generally in agreement. Some small disparities though could be seen. For instance, when Snail2 expression was analysed after miRNA-KD and miRNA-KO they showed a similar type of phenotype following miR-196a loss, but slightly different following miR-219 loss (Fig. 4.9 KD, Fig. 5.26 KO). MiRNA-KD showed a stronger KD of Snail2 expression, whereas miRNA-KO showed a weaker, perturbed phenotype. To an extent these differences could be accounted for by the difference in miRNA KD and miRNA KO. With MOs only generating a KD and CRISPR generating a KO, with the caveat that the crispants are likely to be mosaic (Mehravar et al., 2019). It may also be due to CRISPR being a more specific technique, with the CRISPR designed to target specific isoforms of our miRNA. For example, the miR-196a morpholino can target and KD expression of miR-196a and miR-196b. Although being encoded on different chromosomes, as these miRNAs are part of the same family, that they may be co-expressed in the same or similar regions in the developing embryo.

This may account for some of these differences in phenotypes observed between morpholino and CRISPR work and is not uncommon. Previous work in Zebrafish has shown differences in phenotypes observed by morpholino and mutant embryos (Kok et al., 2015). The overall verdict from their work was that it was preferable to put in the labour and time to generate mutants with technologies like CRISPR, as a genetic approach to determine gene function through generation of stable and specific mutants. In addition, they advocated for MO phenotypes to be validated with mutants, such as those generated by CRISPR (Kok et al., 2015). The experiments in this thesis were carried out with careful controls for both MO and CRISPR functional characterisation of miRNA KD and KO including rescue experiments for the morpholino experiments. It would also be beneficial to completely rule-out off-target effect of CRISPR if the miRNA KO embryos NC phenotypes were rescued with the same use of miRNA mimics. Perhaps our initial F0 embryos need to be crossed to overturn any mosaicism in our analysis of F0 crispants

to fully appreciate, and reveal the true extent of the NC, NPB, neural and placodal phenotypes. It would be expected that the phenotypes would largely agree with the work already conducted with the MO work and CRISPR F0s.

6.2.4 Hypothetical model of miRNA effect on neural crest development

One initial aim of this project was to identify direct targets of our miRNAs. This project has failed to address this due to time constraints. The hope was to generate a miRNA KO line of *Xenopus* and perform RNA-sequencing on the embryos to see global enriched and depletion of gene expression following miRNA KO. The genes that are enriched would be strong candidates for further analysis as direct targets of the miRNA. This project shows that following miRNA KD and KO NC gene expression is lost or reduced. It can be inferred from this, those miRNAs are indirectly affecting development of NC, but it is unclear if miRNAs have NC gene targets. However, *in silico* analysis indicates miR-196a and miR-219 have predicted target genes such as *Hox* genes for miR-196a and *Pou* genes for miR-219 (Table 6.1 and Table 6.2), full lists of predicted targets are in Appendix 3 and 4 for miR-196a and miR-219 respectively. Outlined below I provide two working hypothetical models for miR-196a and miR-219 role in the development of neural crest. This will provide a base for further action and validation of miRNA-mRNA targeting in the development of neural crest in *Xenopus*.

Targetscan was used to computationally predict targets of miR-196a in *Xenopus,* key and interesting genes are listed in Table 6.1. MiR-196a is located within a *HoxC* cluster in the genome (Fig.3.1). Hox expression is implicated in anterior-posterior axial patterning (Durston, 2019). The *HoxC* cluster where miR-196a is in the genome contains: *HoxC8-HoxC11* and a target of miR-196a is *HoxC8*. These *HoxC* genes are expressed posteriorly in the developing Xenopus embryo (Plouhinec et al., 2017). Therefore, it may be possible that miRNA may not always be expressed in the same region of the embryos as their mRNA targets, as miR-196a is expressed in neural and NC tissue (Fig. 3.5).

MiR-196a was found to target genes implicated in NC development including: *Sema3a* and *LRIG*. Sema3a is implicated in NC migration, with mouse *Sema3a* mutants showing abnormal NC migration (Koestner et al., 2008). CHARGE syndrome is a neurocristopathy with multiple NC cell abnormalities (Pilon, 2016; Sato et al., 2019). Interestingly, CHARGE syndrome patients have malformation of craniofacial tissues including their ears due to improper ear morphogenesis (Usman and Sur, 2021). LRIG proteins have been found to be implicated in inner ear morphogenesis, and LRIG2 is a predicted target of miR-196a (Table 6.1), (Abraira et al., 2010). We have shown that miR-196a is expressed in the otic vesicle (Fig. 3.5), and that the otic vesicle is a branchial NC derivative (Sadaghiani and Thiebaud, 1987). With miR-196a expressed in otic vesicle; it would be interesting to analyse the role of miR-196a in ear development further with expression analysis of otic vesicle markers like *Agr2* by *in situ* hybridisation in the first instance (Shih et al., 2007).

Table 6.1 - Key predicted targets of miR-196a in Xenopus, as predicted by TargetScan.

Ortholog of target gene	Representative transcript	Gene name
HOXC8	ENST00000040584.4	homeobox C8
HOXA9	ENST00000396345.1	homeobox A9
HOXA5	ENST00000222726.3	homeobox A5
LRIG2	ENST00000361127.5	leucine-rich repeats and immunoglobulin-like domains 2
SEMA3A	ENST00000265362.4	sema domain, immunoglobulin domain (Ig), short basic domain, secreted, (semaphorin) 3A

Targetscan was also used to computationally predict the mRNA targets of miR-219 in *Xenopus*. Some of the key genes targeted are listed in Table 6.2. Eya1 was one of the top hits on this database. Eya1 is expressed in placodal development (Hong and Saint-Jeannet, 2007; Plouhinec et al., 2017; Schlosser and Ahrens, 2004). Within the lab, Eya1 has been validated as a direct of miR-219 by use of luciferase assays (Ward, 2017). Therefore, we can be reasonably sure that the computational prediction tools may be accurate in predicting miRNA targets but will benefit from *in vivo* validation.

One of miR-219's predicted targets is Nol4, a nucleolar protein. Other Nol genes, including Nol11, are implicated in the development of *Xenopus* cranial NC and are thought to be implicated in ribosome biogenesis and ribosomopathies (Griffin et al., 2015). In Fig. 5.23 and Fig. 5.24, miR-219 KO leads to gross craniofacial phenotypes. KD of *Nol11* in *Xenopus* embryos leads to craniofacial phenotypes and highlights how miR-219 could be implicated in neurocristopathies by *Nol* genes (Griffin et al., 2015). Another predicted target of miR-219 is CHD7. This is significant as this gene is implicated in CHARGE syndrome, a neurocristopathy which also has craniofacial phenotypes in patients (Schulz et al., 2014). Interesting, as miR-219 is also expressed in craniofacial tissues (Fig. 3.5), and implicated is potentially implicated craniofacial development Fig. 5.23.

Pou genes were found to be significantly enriched following miR-219 KD in NC tissue (Fig. 4.8). *Pou* genes are pluripotency mediators and are implicated in NC differentiation (Tien et al., 2021). *Pou* genes were also found to be predicted targets of miR-219 (Table 6.2). It could therefore be possible that miR-219 is implicated in the stemness and induction of NC by directly targeting Pou genes. Experiments to show spatial expression of Pou60 were not completed in the time frame of this PhD, but in future could be completed and complemented with luciferase assays to see if *Pou* genes are a direct target of miR-219 in Xenopus NC tissue.

Table 6.2 - Key predicted targets of miR-219 in Xenopus, as predicted by TargetScan.

Ortholog of target gene	Representative transcript	Gene name
EYA1	ENST00000388742.4	eyes absent homolog 1 (Drosophila)
NOL4	ENST00000261592.5	nucleolar protein 4
POU2F1	ENST00000367866.2	POU class 2 homeobox 1
POU6F2	ENST00000518318.2	POU class 6 homeobox 2
CHD7	ENST00000423902.2	chromodomain helicase DNA binding protein 7

Following miR-196a KD, an expanded Zic1 phenotype was observed (Fig. 4.15), this is a neural plate and neural marker. MiR-196a could be acting

upstream of Zic1 or could be targeting other neural plate border markers to then affect the downstream network. There was also loss of En2 following miR-196a KD, this is intriguing and could support the role of miR-196a on anterior-posterior patterning akin to Hox gene expression disruption. I also hypothesise that Wnt signalling could be a potential pathway that is impacted following miR-196a and miR-219 loss as this could explain loss of NC induction (Borday et al., 2018; Honore et al., 2003; Koenig et al., 2010; Lou et al., 2006; McGrew et al., 1999; Merzdorf and Sive, 2006).

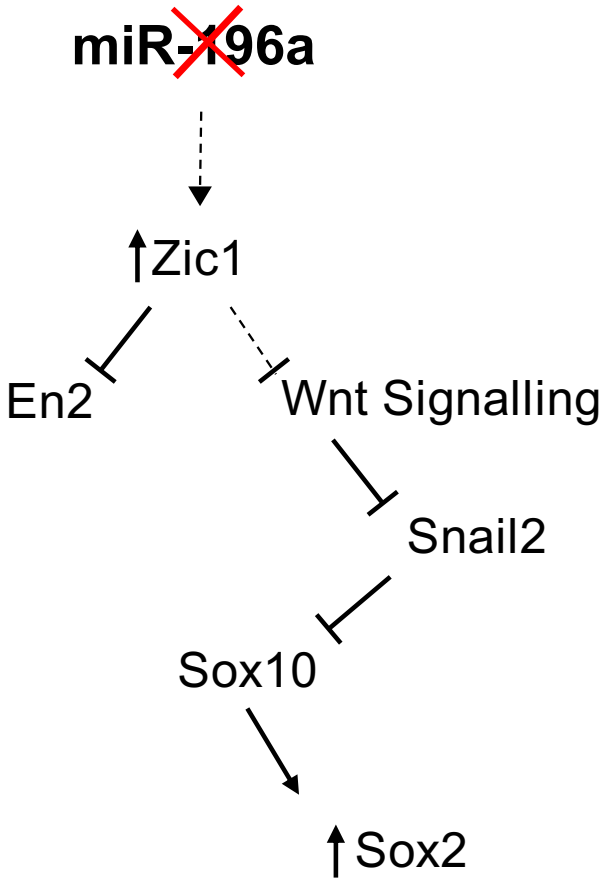

Figure 6.1- Working hypothetical model of miR-196a impact on the development of *Xenopus* neural crest. This figure is based on research from this project and on a literature search (Borday et al., 2018; Honore et al., 2003; Koenig et al., 2010; Lou et al., 2006; McGrew et al., 1999; Merzdorf and Sive, 2006). Dotted lines indicate hypothetical/theory. Solid lines indicate known results from this thesis.

Following loss of miR-219 upregulation of Eya1 is observed. Eya1 is a validated target of miR-219 in the lab and can be seen in Dr. Ward's thesis (Ward, 2017). Therefore, this was used as a starting point for the model.

Following loss of miR-219, Pax3 was significantly enriched in the superficial ectoderm. TargetScan suggests Pax3 is not a direct target of miR-219. It is possible changes in Eya1 could affect the expression of Pax3, as Pax3 and Zic1 are both potential inhibitors and activators of Eya1 respectively, so potentially a feedback loop is being affected by loss of miR-219 (Hong and Saint-Jeannet, 2007).

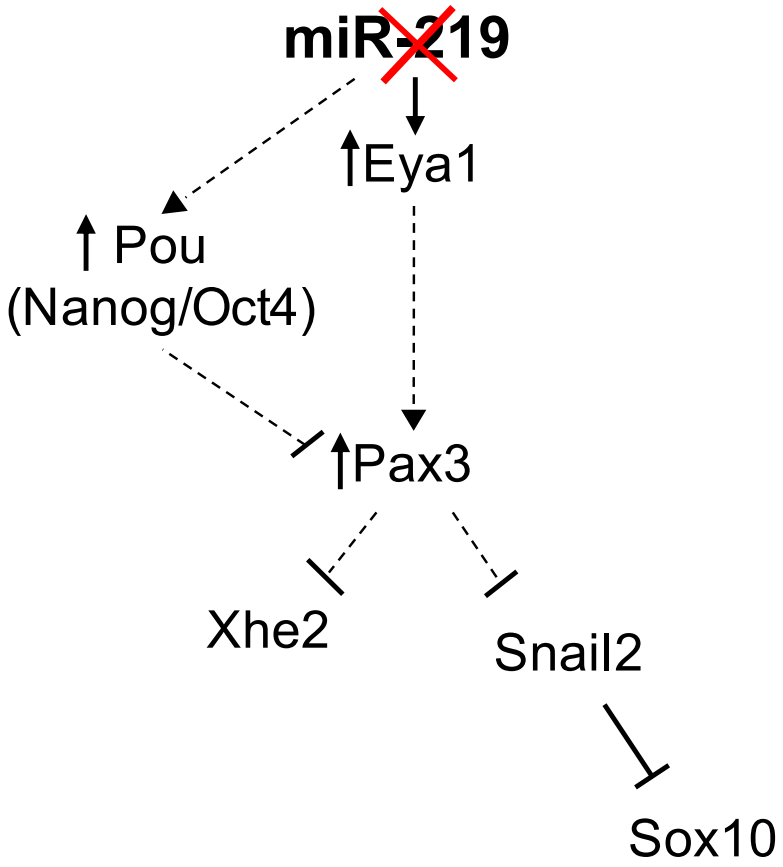

Figure 6.2 - Working hypothetical model of miR-219 impact on the development of *Xenopus* neural crest. This figure is based on research from this project and on a literature search (Borday et al., 2018; Hong and Saint-Jeannet, 2007; Honore et al., 2003; McGrew et al., 1999; Schlosser and Ahrens, 2004; Seal and Monsoro-Burq, 2020; Ward, 2017). Dotted lines indicate hypothetical/theory. Solid lines indicate known results from this thesis.

6.3.0 Overall conclusions and future work

I conclude that miR-196a and miR-219 have different roles in the development of *Xenopus* NC. I hypothesise that these miRNAs may be affecting the development of NC at an upstream level prior to the development and induction of NC. The number of markers for embryo development assay needs

to be expanded to further explore and validate the roles of our miRNAs in NC development. It is vital to further explore the loss of pigment and craniofacial phenotypes generated by miRNA KO further as these may have applications for melanoma and neurocristopathy research. Therefore, I propose to look at pigment and craniofacial development markers, such as *Mitf* and *TCOF1* (Kantaputra et al., 2020; Petratou et al., 2021; Tachibana, 2000). I also believe looking at NC migration, pluripotency and survival will help further reveal the roles of miR-196a and miR-219. This could be conducted through use of crestopheres to analyse NC pluripotency in a NC self-renewing organoid (Kerosuo et al., 2015), NC transgenics with tracking and time-lapse imaging for migration experiments (Alkobtawi et al., 2018; Li et al., 2019) and TUNEL assays for analysing NC cell survival (Tseng et al., 2007).

Work to examine the spatial and temporal expression profile of miRNAs was generated and showed miR-196a and miR-219 expression is not exclusively expressed in NC. Further work could be carried out to get more specific spatial profiles with hybridisation chain reaction (Choi et al., 2018).

Functional characterisation of miRNAs through KD and KO experiments show interesting phenotypes. MiR-196a and miR-219 loss leads to loss of neural crest expression, and disrupted neural, neural plate and placodal gene expression. It would be interesting to investigate the neural phenotypes such as En2 following miR-196a loss and look at other anterior-posterior markers such as Krox20 to unveil potential novel roles of miR-196a in neural patterning.

In silico prediction tools such as Ectomap https://monsoro-lab-ectomap.shinyapps.io/EctoMAP/ and neural crest gene regulatory network online databases such as https://livedataoxford.shinyapps.io/Chick_NC_GRN-TSS-Lab/ could be used in combination with String https://string-db.org/ and Genemania https://genemania.org/ to put together miRNA-NC gene-regulatory networks. Also, miRNA target prediction algorithms could be used; to help shortlist mRNA targets found in future RNA-seq experiments.

Finally, this project showed that it is possible to KO miRNAs with CRISPR and provides a novel and validated protocol for future researchers to fast-track miRNA research in *Xenopus* species. The phenotypes generated by CRISPR suggest roles for miR-196a and miR-219 in developmental diseases such as neurocristopathies. The miR-196a pigment loss phenotype and the miR-219 craniofacial phenotypes warrant further investigation. This, in combination with the development of a validated gene regulatory network of these miRNAs in the development of NC will provide foundations for clinical applications of this work.

7.0.0 References

Abraira, V. E., Satoh, T., Fekete, D. M. and Goodrich, L. V. (2010). Vertebrate Lrig3-ErbB interactions occur in vitro but are unlikely to play a role in Lrig3-dependent inner ear morphogenesis. *PLoS One* **5**, e8981.

Affaticati, P., Le Mevel, S., Jenett, A., Riviere, L., Machado, E., Mughal, B. B. and Fini, J. B. (2018). X-FaCT: Xenopus-Fast Clearing Technique. *Methods Mol Biol* **1865**, 233-241.

Agarwal, V., Bell, G. W., Nam, J. W. and Bartel, D. P. (2015). Predicting effective microRNA target sites in mammalian mRNAs. *Elife* **4**.

Ahmed, A., Ward, N. J., Moxon, S., Lopez-Gomollon, S., Viaut, C., Tomlinson, M. L., Patrushev, I., Gilchrist, M. J., Dalmay, T., Dotlic, D., et al. (2015). A Database of microRNA Expression Patterns in Xenopus laevis. *PLoS One* **10**, e0138313.

Ahmed, M., Xu, J. and Xu, P. X. (2012). EYA1 and SIX1 drive the neuronal developmental program in cooperation with the SWI/SNF chromatin-remodeling complex and SOX2 in the mammalian inner ear. *Development* **139**, 1965-1977.

Akula, M., Park, J. W. and West-Mays, J. A. (2019). Relationship between neural crest cell specification and rare ocular diseases. *J Neurosci Res* **97**, 7-15.

Alberti, C. and Cochella, L. (2017). A framework for understanding the roles of miRNAs in animal development. *Development* **144**, 2548-2559.

Alfandari, D., Cousin, H. and Marsden, M. (2010). Mechanism of Xenopus cranial neural crest cell migration. *Cell Adh Migr* **4**, 553-560.

Alkobtawi, M., Ray, H., Barriga, E. H., Moreno, M., Kerney, R., Monsoro-Burq, A. H., Saint-Jeannet, J. P. and Mayor, R. (2018). Characterization of Pax3 and Sox10 transgenic Xenopus laevis embryos as tools to study neural crest development. *Dev Biol* **444 Suppl 1**, S202-S208.

Alles, J., Fehlmann, T., Fischer, U., Backes, C., Galata, V., Minet, M., Hart, M., Abu-Halima, M., Grasser, F. A., Lenhof, H. P., et al. (2019). An estimate of the total number of true human miRNAs. *Nucleic Acids Res* **47**, 3353-3364.

Ambros, V. (2011). MicroRNAs and developmental timing. *Curr Opin Genet Dev* **21**, 511-517.

Anderson, R. M., Stottmann, R. W., Choi, M. and Klingensmith, J. (2006). Endogenous bone morphogenetic protein antagonists regulate mammalian neural crest generation and survival. *Dev Dyn* **235**, 2507-2520.

Aoki, Y., Saint-Germain, N., Gyda, M., Magner-Fink, E., Lee, Y. H., Credidio, C. and Saint-Jeannet, J. P. (2003). Sox10 regulates the development of neural crest-derived melanocytes in Xenopus. *Dev Biol* **259**, 19-33.

Aoto, K., Sandell, L. L., Butler Tjaden, N. E., Yuen, K. C., Watt, K. E., Black, B. L., Durnin, M. and Trainor, P. A. (2015). Mef2c-F10N enhancer driven beta-galactosidase (LacZ) and Cre recombinase mice facilitate analyses of gene function and lineage fate in neural crest cells. *Dev Biol* **402**, 3-16.

Ashery-Padan, R., Marquardt, T., Zhou, X. and Gruss, P. (2000). Pax6 activity in the lens primordium is required for lens formation and for correct placement of a single retina in the eye. *Genes Dev* **14**, 2701-2711.

Avery, J. and Dalton, S. (2016). Methods for Derivation of Multipotent Neural Crest Cells Derived from Human Pluripotent Stem Cells. *Methods Mol Biol* **1341**, 197-208.

Aybar, M. J., Nieto, M. A. and Mayor, R. (2003). Snail precedes slug in the genetic cascade required for the specification and migration of the Xenopus neural crest. *Development* **130**, 483-494.

Baker, C. V. and Bronner-Fraser, M. (2001). Vertebrate cranial placodes I. Embryonic induction. *Dev Biol* **232**, 1-61.

Baltzinger, M., Ori, M., Pasqualetti, M., Nardi, I. and Rijli, F. M. (2005). Hoxa2 knockdown in Xenopus results in hyoid to mandibular homeosis. *Dev Dyn* **234**, 858-867.

Bang, A. G., Papalopulu, N., Goulding, M. D. and Kintner, C. (1999). Expression of Pax-3 in the lateral neural plate is dependent on a Wnt-mediated signal from posterior nonaxial mesoderm. *Dev Biol* **212**, 366-380.

Barriga, E. H., Franze, K., Charras, G. and Mayor, R. (2018). Tissue stiffening coordinates morphogenesis by triggering collective cell migration in vivo. *Nature*.

Bartel, D. P. (2004). MicroRNAs: genomics, biogenesis, mechanism, and function. *Cell* **116**, 281-297.

Bassett, A. R. and Liu, J. L. (2014). CRISPR/Cas9 and genome editing in Drosophila. *J Genet Genomics* **41**, 7-19.

Bedell, V. M., Westcot, S. E. and Ekker, S. C. (2011). Lessons from morpholino-based screening in zebrafish. *Brief Funct Genomics* **10**, 181-188.

Bellmeyer, A., Krase, J., Lindgren, J. and LaBonne, C. (2003). The protooncogene c-myc is an essential regulator of neural crest formation in xenopus. *Dev Cell* **4**, 827-839.

Berube-Simard, F. A. and Pilon, N. (2019). Molecular dissection of CHARGE syndrome highlights the vulnerability of neural crest cells to problems with alternative splicing and other transcription-related processes. *Transcription* **10**, 21-28.

Betancur, P., Bronner-Fraser, M. and Sauka-Spengler, T. (2010). Assembling neural crest regulatory circuits into a gene regulatory network. *Annu Rev Cell Dev Biol* **26**, 581-603.

Bharti, K., Miller, S. S. and Arnheiter, H. (2011). The new paradigm: retinal pigment epithelium cells generated from embryonic or induced pluripotent stem cells. *Pigment Cell Melanoma Res* **24**, 21-34.

Bhattacharya, A. and Cui, Y. (2017). Systematic Prediction of the Impacts of Mutations in MicroRNA Seed Sequences. *J Integr Bioinform* **14**.

Blum, M., De Robertis, E. M., Wallingford, J. B. and Niehrs, C. (2015). Morpholinos: Antisense and Sensibility. *Dev Cell* **35**, 145-149.

Bondurand, N., Pingault, V., Goerich, D. E., Lemort, N., Sock, E., Le Caignec, C., Wegner, M. and Goossens, M. (2000). Interaction among SOX10, PAX3 and MITF, three genes altered in Waardenburg syndrome. *Hum Mol Genet* **9**, 1907-1917.

Borday, C., Parain, K., Thi Tran, H., Vleminckx, K., Perron, M. and Monsoro-Burq, A. H. (2018). An atlas of Wnt activity during embryogenesis in Xenopus tropicalis. *PLoS One* **13**, e0193606.

Bradnock, T. J., Knight, M., Kenny, S., Nair, M., Walker, G. M. and British Association of Paediatric Surgeons Congenital Anomalies Surveillance, S. (2017). Hirschsprung's disease in the UK and Ireland: incidence and anomalies. *Arch Dis Child* **102**, 722-727.

Brugmann, S. A., Pandur, P. D., Kenyon, K. L., Pignoni, F. and Moody, S. A. (2004). Six1 promotes a placodal fate within the lateral neurogenic ectoderm by functioning as both a transcriptional activator and repressor. *Development* **131**, 5871-5881.

Burke, J. M., Kelenis, D. P., Kincaid, R. P. and Sullivan, C. S. (2014). A central role for the primary microRNA stem in guiding the position and efficiency of Drosha processing of a viral pri-miRNA. *RNA* **20**, 1068-1077.

Burns, A. J. and Douarin, N. M. (1998). The sacral neural crest contributes neurons and glia to the post-umbilical gut: spatiotemporal analysis of the development of the enteric nervous system. *Development* **125**, 4335-4347.

Chalmers, A. D., Welchman, D. and Papalopulu, N. (2002). Intrinsic differences between the superficial and deep layers of the Xenopus ectoderm control primary neuronal differentiation. *Dev Cell* **2**, 171-182.

Chandra, S., Vimal, D., Sharma, D., Rai, V., Gupta, S. C. and Chowdhuri, D. K. (2017). Role of miRNAs in development and disease: Lessons learnt from small organisms. *Life Sci* **185**, 8-14.

Chang, H., Yi, B., Ma, R., Zhang, X., Zhao, H. and Xi, Y. (2016). CRISPR/cas9, a novel genomic tool to knock down microRNA in vitro and in vivo. *Sci Rep* **6**, 22312.

Charpentier, E. and Doudna, J. A. (2013). Biotechnology: Rewriting a genome. *Nature* **495**, 50-51.

Chen, J. F., Mandel, E. M., Thomson, J. M., Wu, Q., Callis, T. E., Hammond, S. M., Conlon, F. L. and Wang, D. Z. (2006). The role of microRNA-1 and microRNA-133 in skeletal muscle proliferation and differentiation. *Nat Genet* **38**, 228-233.

Chen, Y., Pollet, N., Niehrs, C. and Pieler, T. (2001). Increased XRALDH2 activity has a posteriorizing effect on the central nervous system of Xenopus embryos. *Mech Dev* **101**, 91-103.

Cheng, C. and Li, L. M. (2008). Inferring microRNA activities by combining gene expression with microRNA target prediction. *PLoS One* **3**, e1989.

Cheung, M. and Briscoe, J. (2003). Neural crest development is regulated by the transcription factor Sox9. *Development* **130**, 5681-5693.

Cheung, M., Chaboissier, M. C., Mynett, A., Hirst, E., Schedl, A. and Briscoe, J. (2005). The transcriptional control of trunk neural crest induction, survival, and delamination. *Dev Cell* **8**, 179-192.

Cho, S. W., Kim, S., Kim, J. M. and Kim, J. S. (2013). Targeted genome engineering in human cells with the Cas9 RNA-guided endonuclease. *Nat Biotechnol* **31**, 230-232.

Choi, H. M. T., Schwarzkopf, M., Fornace, M. E., Acharya, A., Artavanis, G., Stegmaier, J., Cunha, A. and Pierce, N. A. (2018). Third-generation in situ hybridization chain reaction: multiplexed, quantitative, sensitive, versatile, robust. *Development* **145**.

Clement, K., Hsu, J. Y., Canver, M. C., Joung, J. K. and Pinello, L. (2020). Technologies and Computational Analysis Strategies for CRISPR Applications. *Mol Cell* **79**, 11-29.

Collazo, A., Bronner-Fraser, M. and Fraser, S. E. (1993). Vital dye labelling of Xenopus laevis trunk neural crest reveals multipotency and novel pathways of migration. *Development* **118**, 363-376.

Cong, L., Ran, F. A., Cox, D., Lin, S., Barretto, R., Habib, N., Hsu, P. D., Wu, X., Jiang, W., Marraffini, L. A., et al. (2013). Multiplex genome engineering using CRISPR/Cas systems. *Science* **339**, 819-823.

Cordero, D. R., Brugmann, S., Chu, Y., Bajpai, R., Jame, M. and Helms, J. A. (2011). Cranial neural crest cells on the move: their roles in craniofacial development. *Am J Med Genet A* **155A**, 270-279.

Darnell, D. K. and Antin, P. B. (2014). LNA-based in situ hybridization detection of mRNAs in embryos. *Methods Mol Biol* **1211**, 69-76.

Darnell, D. K., Stanislaw, S., Kaur, S. and Antin, P. B. (2010). Whole mount in situ hybridization detection of mRNAs using short LNA containing DNA oligonucleotide probes. *RNA* **16**, 632-637.

Devotta, A., Juraver-Geslin, H., Gonzalez, J. A., Hong, C. S. and Saint-Jeannet, J. P. (2016). Sf3b4-depleted Xenopus embryos: A model to study the pathogenesis of craniofacial defects in Nager syndrome. *Dev Biol* **415**, 371-382.

Ding, Y., Ploper, D., Sosa, E. A., Colozza, G., Moriyama, Y., Benitez, M. D., Zhang, K., Merkurjev, D. and De Robertis, E. M. (2017). Spemann organizer transcriptome induction by early beta-catenin, Wnt, Nodal, and Siamois signals in Xenopus laevis. *Proc Natl Acad Sci U S A* **114**, E3081-E3090.

Dressler, G. R. and Gruss, P. (1989). Anterior boundaries of Hox gene expression in mesoderm-derived structures correlate with the linear gene order along the chromosome. *Differentiation* **41**, 193-201.

Dubey, A. and Saint-Jeannet, J. P. (2017). Modeling human craniofacial disorders in Xenopus. *Curr Pathobiol Rep* **5**, 79-92.

Dur, A. H., Tang, T., Viviano, S., Sekuri, A., Willsey, H. R., Tagare, H. D., Kahle, K. T. and Deniz, E. (2020). In Xenopus ependymal cilia drive embryonic CSF circulation and brain development independently of cardiac pulsatile forces. *Fluids Barriers CNS* **17**, 72.

Durston, A. J. (2019). What are the roles of retinoids, other morphogens, and Hox genes in setting up the vertebrate body axis? *Genesis* **57**, e23296.

Eisen, J. S. and Smith, J. C. (2008). Controlling morpholino experiments: don't stop making antisense. *Development* **135**, 1735-1743.

Etchevers, H. C., Amiel, J. and Lyonnet, S. (2006). Molecular bases of human neurocristopathies. *Adv Exp Med Biol* **589**, 213-234.

Falabella, M., Sun, L., Barr, J., Pena, A. Z., Kershaw, E. E., Gingras, S., Goncharova, E. A. and Kaufman, B. A. (2017). Single-Step qPCR and dPCR Detection of Diverse CRISPR-Cas9 Gene Editing Events In Vivo. *G3 (Bethesda)* **7**, 3533-3542.

Fan, J., Feng, Y., Zhang, R., Zhang, W., Shu, Y., Zeng, Z., Huang, S., Zhang, L., Huang, B., Wu, D., et al. (2020). A simplified system for the effective expression and delivery of functional mature microRNAs in mammalian cells. *Cancer Gene Ther* **27**, 424-437.

Flynt, A. S., Rao, M. and Patton, J. G. (2017). Blocking Zebrafish MicroRNAs with Morpholinos. *Methods Mol Biol* **1565**, 59-78.

Gao, Z., Kim, G. H., Mackinnon, A. C., Flagg, A. E., Bassett, B., Earley, J. U. and Svensson, E. C. (2010). Ets1 is required for proper migration and differentiation of the cardiac neural crest. *Development* **137**, 1543-1551.

Gessert, S., Bugner, V., Tecza, A., Pinker, M. and Kuhl, M. (2010). FMR1/FXR1 and the miRNA pathway are required for eye and neural crest development. *Dev Biol* **341**, 222-235.

Gilmour, D. T., Maischein, H. M. and Nusslein-Volhard, C. (2002). Migration and function of a glial subtype in the vertebrate peripheral nervous system. *Neuron* **34**, 577-588.

Glinka, A., Wu, W., Delius, H., Monaghan, A. P., Blumenstock, C. and Niehrs, C. (1998). Dickkopf-1 is a member of a new family of secreted proteins and functions in head induction. *Nature* **391**, 357-362.

Glinka, A., Wu, W., Onichtchouk, D., Blumenstock, C. and Niehrs, C. (1997). Head induction by simultaneous repression of Bmp and Wnt signalling in Xenopus. *Nature* **389**, 517-519.

Goljanek-Whysall, K., Mok, G. F., Fahad Alrefaei, A., Kennerley, N., Wheeler, G. N. and Munsterberg, A. (2014). myomiR-dependent switching of BAF60 variant incorporation into Brg1 chromatin remodeling complexes during embryo myogenesis. *Development* **141**, 3378-3387.

Goljanek-Whysall, K., Sweetman, D., Abu-Elmagd, M., Chapnik, E., Dalmay, T., Hornstein, E. and Munsterberg, A. (2011). MicroRNA regulation of the paired-box transcription factor Pax3 confers robustness to developmental timing of myogenesis. *Proc Natl Acad Sci U S A* **108**, 11936-11941.

Gonzalez Malagon, S. G., Lopez Munoz, A. M., Doro, D., Bolger, T. G., Poon, E., Tucker, E. R., Adel Al-Lami, H., Krause, M., Phiel, C. J., Chesler, L., et al. (2018). Glycogen synthase kinase 3 controls migration of the neural crest lineage in mouse and Xenopus. *Nat Commun* **9**, 1126.

Gouignard, N., Maccarana, M., Strate, I., von Stedingk, K., Malmstrom, A. and Pera, E. M. (2016). Musculocontractural Ehlers-Danlos syndrome and neurocristopathies: dermatan sulfate is required for Xenopus neural crest cells to migrate and adhere to fibronectin. *Dis Model Mech* **9**, 607-620.

Grainger, R. M. (2012). Xenopus tropicalis as a model organism for genetics and genomics: past, present, and future. *Methods Mol Biol* **917**, 3-15.

Griffin, J. N., Sondalle, S. B., Del Viso, F., Baserga, S. J. and Khokha, M. K. (2015). The ribosome biogenesis factor Nol11 is required for optimal rDNA transcription and craniofacial development in Xenopus. *PLoS Genet* **11**, e1005018.

Grocott, T., Johnson, S., Bailey, A. P. and Streit, A. (2011). Neural crest cells organize the eye via TGF-beta and canonical Wnt signalling. *Nat Commun* **2**, 265.

Grocott, T., Lozano-Velasco, E., Mok, G. F. and Munsterberg, A. E. (2020). The Pax6 master control gene initiates spontaneous retinal development via a self-organising Turing network. *Development* **147**.

Grunweller, A. and Hartmann, R. K. (2007). Locked nucleic acid oligonucleotides: the next generation of antisense agents? *BioDrugs* **21**, 235-243.

Hamburger, V. and Hamilton, H. L. (1992). A series of normal stages in the development of the chick embryo. 1951. *Dev Dyn* **195**, 231-272.

Harris, M. L., Baxter, L. L., Loftus, S. K. and Pavan, W. J. (2010). Sox proteins in melanocyte development and melanoma. *Pigment Cell Melanoma Res* **23**, 496-513.

Hatch, V. L., Marin-Barba, M., Moxon, S., Ford, C. T., Ward, N. J., Tomlinson, M. L., Desanlis, I., Hendry, A. E., Hontelez, S., van Kruijsbergen, I., et al. (2016). The positive transcriptional elongation factor (P-TEFb) is required for neural crest specification. *Dev Biol* **416**, 361-372.

Heanue, T. A. and Pachnis, V. (2007). Enteric nervous system development and Hirschsprung's disease: advances in genetic and stem cell studies. *Nat Rev Neurosci* **8**, 466-479.

Heasman, J. (2002). Morpholino oligos: making sense of antisense? *Dev Biol* **243**, 209-214.

---- (2006). Patterning the early Xenopus embryo. *Development* **133**, 1205-1217.

Heasman, J., Kofron, M. and Wylie, C. (2000). Beta-catenin signaling activity dissected in the early Xenopus embryo: a novel antisense approach. *Dev Biol* **222**, 124-134.

Helwak, A., Kudla, G., Dudnakova, T. and Tollervey, D. (2013). Mapping the human miRNA interactome by CLASH reveals frequent noncanonical binding. *Cell* **153**, 654-665.

Hemmati-Brivanlou, A., de la Torre, J. R., Holt, C. and Harland, R. M. (1991). Cephalic expression and molecular characterization of Xenopus En-2. *Development* **111**, 715-724.

Hong, C. S., Park, B. Y. and Saint-Jeannet, J. P. (2008). Fgf8a induces neural crest indirectly through the activation of Wnt8 in the paraxial mesoderm. *Development* **135**, 3903-3910.

Hong, C. S. and Saint-Jeannet, J. P. (2007). The activity of Pax3 and Zic1 regulates three distinct cell fates at the neural plate border. *Mol Biol Cell* **18**, 2192-2202.

---- (2014). Xhe2 is a member of the astacin family of metalloproteases that promotes Xenopus hatching. *Genesis* **52**, 946-951.

---- (2017a). Znf703, a novel target of Pax3 and Zic1, regulates hindbrain and neural crest development in Xenopus. *Genesis*.

---- (2017b). Znf703, a novel target of Pax3 and Zic1, regulates hindbrain and neural crest development in Xenopus. *Genesis* **55**.

Honore, S. M., Aybar, M. J. and Mayor, R. (2003). Sox10 is required for the early development of the prospective neural crest in Xenopus embryos. *Dev Biol* **260**, 79-96.

Hsu, J. Y., Grunewald, J., Szalay, R., Shih, J., Anzalone, A. V., Lam, K. C., Shen, M. W., Petri, K., Liu, D. R., Keith Joung, J., et al. (2021). PrimeDesign software for rapid and simplified design of prime editing guide RNAs. *Nat Commun* **12**, 1034.

Hwang, W. Y., Fu, Y., Reyon, D., Maeder, M. L., Tsai, S. Q., Sander, J. D., Peterson, R. T., Yeh, J. R. and Joung, J. K. (2013). Efficient genome editing in zebrafish using a CRISPR-Cas system. *Nat Biotechnol* **31**, 227-229.

Hwang, Y. S., Luo, T., Xu, Y. and Sargent, T. D. (2009). Myosin-X is required for cranial neural crest cell migration in Xenopus laevis. *Dev Dyn* **238**, 2522-2529.

Inui, M., Martello, G. and Piccolo, S. (2010). MicroRNA control of signal transduction. *Nat Rev Mol Cell Biol* **11**, 252-263.

Ishino, Y., Shinagawa, H., Makino, K., Amemura, M. and Nakata, A. (1987). Nucleotide sequence of the iap gene, responsible for alkaline phosphatase isozyme conversion in Escherichia coli, and identification of the gene product. *J Bacteriol* **169**, 5429-5433.

Jang, H. K., Song, B., Hwang, G. H. and Bae, S. (2020). Current trends in gene recovery mediated by the CRISPR-Cas system. *Exp Mol Med* **52**, 1016-1027.

Jiang, C. F., Shi, Z. M., Li, D. M., Qian, Y. C., Ren, Y., Bai, X. M., Xie, Y. X., Wang, L., Ge, X., Liu, W. T., et al. (2018). Estrogen-induced miR-196a elevation promotes tumor growth and metastasis via targeting SPRED1 in breast cancer. *Mol Cancer* **17**, 83.

Jiang, W., Bikard, D., Cox, D., Zhang, F. and Marraffini, L. A. (2013). RNA-guided editing of bacterial genomes using CRISPR-Cas systems. *Nat Biotechnol* **31**, 233-239.

Jin, H. Y., Gonzalez-Martin, A., Miletic, A. V., Lai, M., Knight, S., Sabouri-Ghomi, M., Head, S. R., Macauley, M. S., Rickert, R. C. and Xiao, C. (2015). Transfection of microRNA Mimics Should Be Used with Caution. *Front Genet* **6**, 340.

Jinek, M., Chylinski, K., Fonfara, I., Hauer, M., Doudna, J. A. and Charpentier, E. (2012). A programmable dual-RNA-guided DNA endonuclease in adaptive bacterial immunity. *Science* **337**, 816-821.

Jones, N. C., Lynn, M. L., Gaudenz, K., Sakai, D., Aoto, K., Rey, J. P., Glynn, E. F., Ellington, L., Du, C., Dixon, J., et al. (2008). Prevention of the neurocristopathy Treacher Collins syndrome through inhibition of p53 function. *Nat Med* **14**, 125-133.

Kantaputra, P. N., Tripuwabhrut, K., Intachai, W., Carlson, B. M., Quarto, N., Ngamphiw, C., Tongsima, S. and Sonsuwan, N. (2020). Treacher Collins syndrome: A novel TCOF1 mutation and monopodial stapes. *Clin Otolaryngol* **45**, 695-702.

Karpinka, J. B., Fortriede, J. D., Burns, K. A., James-Zorn, C., Ponferrada, V. G., Lee, J., Karimi, K., Zorn, A. M. and Vize, P. D. (2015). Xenbase, the Xenopus model organism database; new virtualized system, data types and genomes. *Nucleic Acids Res* **43**, D756-763.

Katagiri, C., Maeda, R., Yamashika, C., Mita, K., Sargent, T. D. and Yasumasu, S. (1997). Molecular cloning of Xenopus hatching enzyme and its specific expression in hatching gland cells. *Int J Dev Biol* **41**, 19-25.

Kenyon, J. D., Sergeeva, O., Somoza, R. A., Li, M., Caplan, A. I., Khalil, A. M. and Lee, Z. (2019). Analysis of -5p and -3p Strands of miR-145 and miR-140 During Mesenchymal Stem Cell Chondrogenic Differentiation. *Tissue Eng Part A* **25**, 80-90.

Kerosuo, L. and Bronner, M. E. (2016). cMyc Regulates the Size of the Premigratory Neural Crest Stem Cell Pool. *Cell Rep* **17**, 2648-2659.

Kerosuo, L., Nie, S., Bajpai, R. and Bronner, M. E. (2015). Crestospheres: Long-Term Maintenance of Multipotent, Premigratory Neural Crest Stem Cells. *Stem Cell Reports* **5**, 499-507.

Kim, H. K., Lee, S., Kim, Y., Park, J., Min, S., Choi, J. W., Huang, T. P., Yoon, S., Liu, D. R. and Kim, H. H. (2020). High-throughput analysis of the activities of xCas9, SpCas9-NG and SpCas9 at matched and mismatched target sequences in human cells. *Nat Biomed Eng* **4**, 111-124.

Klymkowsky, M. W., Rossi, C. C. and Artinger, K. B. (2010). Mechanisms driving neural crest induction and migration in the zebrafish and Xenopus laevis. *Cell Adh Migr* **4**, 595-608.

Koenig, S. F., Brentle, S., Hamdi, K., Fichtner, D., Wedlich, D. and Gradl, D. (2010). En2, Pax2/5 and Tcf-4 transcription factors cooperate in patterning the Xenopus brain. *Dev Biol* **340**, 318-328.

Koestner, U., Shnitsar, I., Linnemannstons, K., Hufton, A. L. and Borchers, A. (2008). Semaphorin and neuropilin expression during early morphogenesis of Xenopus laevis. *Dev Dyn* **237**, 3853-3863.

Kok, F. O., Shin, M., Ni, C. W., Gupta, A., Grosse, A. S., van Impel, A., Kirchmaier, B. C., Peterson-Maduro, J., Kourkoulis, G., Male, I., et al. (2015). Reverse genetic screening reveals poor correlation between morpholino-induced and mutant phenotypes in zebrafish. *Dev Cell* **32**, 97-108.

Kretov, D. A., Walawalkar, I. A., Mora-Martin, A., Shafik, A. M., Moxon, S. and Cifuentes, D. (2020). Ago2-Dependent Processing Allows miR-451 to Evade the Global MicroRNA Turnover Elicited during Erythropoiesis. *Mol Cell* **78**, 317-328 e316.

Krichevsky, A. M., King, K. S., Donahue, C. P., Khrapko, K. and Kosik, K. S. (2003). A microRNA array reveals extensive regulation of microRNAs during brain development. *RNA* **9**, 1274-1281.

Kruger, J. and Rehmsmeier, M. (2006). RNAhybrid: microRNA target prediction easy, fast and flexible. *Nucleic Acids Res* **34**, W451-454.

Krutzfeldt, J., Rajewsky, N., Braich, R., Rajeev, K. G., Tuschl, T., Manoharan, M. and Stoffel, M. (2005). Silencing of microRNAs in vivo with 'antagomirs'. *Nature* **438**, 685-689.

Kumasaka, M., Sato, S., Yajima, I., Goding, C. R. and Yamamoto, H. (2005). Regulation of melanoblast and retinal pigment epithelium development by Xenopus laevis Mitf. *Dev Dyn* **234**, 523-534.

Kumasaka, M., Sato, S., Yajima, I. and Yamamoto, H. (2003). Isolation and developmental expression of tyrosinase family genes in Xenopus laevis. *Pigment Cell Res* **16**, 455-462.

Kurauchi, T., Izutsu, Y. and Maeno, M. (2010). Involvement of Neptune in induction of the hatching gland and neural crest in the Xenopus embryo. *Differentiation* **79**, 251-259.

Lee, R. C., Feinbaum, R. L. and Ambros, V. (1993). The C. elegans heterochronic gene lin-4 encodes small RNAs with antisense complementarity to lin-14. *Cell* **75**, 843-854.

Li, J., Perfetto, M., Materna, C., Li, R., Thi Tran, H., Vleminckx, K., Duncan, M. K. and Wei, S. (2019). A new transgenic reporter line reveals Wnt-dependent Snai2 re-expression and cranial neural crest differentiation in Xenopus. *Sci Rep* **9**, 11191.

Li, Z., Xu, R. and Li, N. (2018). MicroRNAs from plants to animals, do they define a new messenger for communication? *Nutr Metab (Lond)* **15**, 68.

Light, W., Vernon, A. E., Lasorella, A., Iavarone, A. and LaBonne, C. (2005). Xenopus Id3 is required downstream of Myc for the formation of multipotent neural crest progenitor cells. *Development* **132**, 1831-1841.

Linker, C., De Almeida, I., Papanayotou, C., Stower, M., Sabado, V., Ghorani, E., Streit, A., Mayor, R. and Stern, C. D. (2009). Cell communication with the neural plate is required for induction of neural markers by BMP inhibition: evidence for homeogenetic induction and implications for Xenopus animal cap and chick explant assays. *Dev Biol* **327**, 478-486.

Litsiou, A., Hanson, S. and Streit, A. (2005). A balance of FGF, BMP and WNT signalling positions the future placode territory in the head. *Development* **132**, 4051-4062.

Liu, K. J. (2016). Animal models of craniofacial anomalies. *Dev Biol* **415**, 169-170.

Lopez-Sanchez, C., Franco, D., Bonet, F., Garcia-Lopez, V., Aranega, A. and Garcia-Martinez, V. (2015). Negative Fgf8-Bmp2 feed-back is regulated by miR-130 during early cardiac specification. *Dev Biol* **406**, 63-73.

Lou, X., Fang, P., Li, S., Hu, R. Y., Kuerner, K. M., Steinbeisser, H. and Ding, X. (2006). Xenopus Tbx6 mediates posterior patterning via activation of Wnt and FGF signalling. *Cell Res* **16**, 771-779.

Lukoseviciute, M., Gavriouchkina, D., Williams, R. M., Hochgreb-Hagele, T., Senanayake, U., Chong-Morrison, V., Thongjuea, S., Repapi, E., Mead, A. and Sauka-Spengler, T. (2018). From Pioneer to Repressor: Bimodal foxd3 Activity Dynamically Remodels Neural Crest Regulatory Landscape In Vivo. *Dev Cell* **47**, 608-628 e606.

Madelaine, R., Sloan, S. A., Huber, N., Notwell, J. H., Leung, L. C., Skariah, G., Halluin, C., Pasca, S. P., Bejerano, G., Krasnow, M. A., et al. (2017). MicroRNA-9 Couples Brain Neurogenesis and Angiogenesis. *Cell Rep* **20**, 1533-1542.

Mali, P., Yang, L., Esvelt, K. M., Aach, J., Guell, M., DiCarlo, J. E., Norville, J. E. and Church, G. M. (2013). RNA-guided human genome engineering via Cas9. *Science* **339**, 823-826.

Mandalos, N., Rhinn, M., Granchi, Z., Karampelas, I., Mitsiadis, T., Economides, A. N., Dolle, P. and Remboutsika, E. (2014). Sox2 acts as a rheostat of epithelial to mesenchymal transition during neural crest development. *Front Physiol* **5**, 345.

Manuel, M. N., Mi, D., Mason, J. O. and Price, D. J. (2015). Regulation of cerebral cortical neurogenesis by the Pax6 transcription factor. *Front Cell Neurosci* **9**, 70.

Marchant, L., Linker, C., Ruiz, P., Guerrero, N. and Mayor, R. (1998). The inductive properties of mesoderm suggest that the neural crest cells are specified by a BMP gradient. *Dev Biol* **198**, 319-329.

Marco, A. (2014). Sex-biased expression of microRNAs in Drosophila melanogaster. *Open Biol* **4**, 140024.

Marco, A., Hooks, K. and Griffiths-Jones, S. (2012). Evolution and function of the extended miR-2 microRNA family. *RNA Biol* **9**, 242-248.

Mayor, R., Morgan, R. and Sargent, M. G. (1995). Induction of the prospective neural crest of Xenopus. *Development* **121**, 767-777.

Mayor, R. and Theveneau, E. (2013). The neural crest. *Development* **140**, 2247-2251.

McGrew, L. L., Takemaru, K., Bates, R. and Moon, R. T. (1999). Direct regulation of the Xenopus engrailed-2 promoter by the Wnt signaling pathway, and a molecular screen for Wnt-responsive genes, confirm a role for Wnt signaling during neural patterning in Xenopus. *Mech Dev* **87**, 21-32.

McNulty, C. L., Peres, J. N., Bardine, N., van den Akker, W. M. and Durston, A. J. (2005). Knockdown of the complete Hox paralogous group 1 leads to dramatic hindbrain and neural crest defects. *Development* **132**, 2861-2871.

Mehravar, M., Shirazi, A., Nazari, M. and Banan, M. (2019). Mosaicism in CRISPR/Cas9-mediated genome editing. *Dev Biol* **445**, 156-162.

Merzdorf, C. S. and Sive, H. L. (2006). The zic1 gene is an activator of Wnt signaling. *Int J Dev Biol* **50**, 611-617.

Milet, C., Maczkowiak, F., Roche, D. D. and Monsoro-Burq, A. H. (2013). Pax3 and Zic1 drive induction and differentiation of multipotent, migratory, and functional neural crest in Xenopus embryos. *Proc Natl Acad Sci U S A* **110**, 5528-5533.

Milet, C. and Monsoro-Burq, A. H. (2012). Neural crest induction at the neural plate border in vertebrates. *Dev Biol* **366**, 22-33.

---- (2014). Dissection of Xenopus laevis neural crest for in vitro explant culture or in vivo transplantation. *J Vis Exp*.

Millar, A. A. and Waterhouse, P. M. (2005). Plant and animal microRNAs: similarities and differences. *Funct Integr Genomics* **5**, 129-135.

Minoux, M. and Rijli, F. M. (2010). Molecular mechanisms of cranial neural crest cell migration and patterning in craniofacial development. *Development* **137**, 2605-2621.

Miska, E. A. (2005). How microRNAs control cell division, differentiation and death. *Curr Opin Genet Dev* **15**, 563-568.

Mohr, S. E., Hu, Y., Ewen-Campen, B., Housden, B. E., Viswanatha, R. and Perrimon, N. (2016). CRISPR guide RNA design for research applications. *FEBS J* **283**, 3232-3238.

Mok, G. F., Lozano-Velasco, E. and Munsterberg, A. (2017). microRNAs in skeletal muscle development. *Semin Cell Dev Biol* **72**, 67-76.

Monsoro-Burq, A. H. (2007). A rapid protocol for whole-mount in situ hybridization on Xenopus embryos. *CSH Protoc* **2007**, pdb prot4809.

Monsoro-Burq, A. H., Wang, E. and Harland, R. (2005). Msx1 and Pax3 cooperate to mediate FGF8 and WNT signals during Xenopus neural crest induction. *Dev Cell* **8**, 167-178.

Moreno-Mateos, M. A., Vejnar, C. E., Beaudoin, J. D., Fernandez, J. P., Mis, E. K., Khokha, M. K. and Giraldez, A. J. (2015). CRISPRscan: designing highly efficient sgRNAs for CRISPR-Cas9 targeting in vivo. *Nat Methods* **12**, 982-988.

Moriyama, Y. and De Robertis, E. M. (2018). Embryonic regeneration by relocalization of the Spemann organizer during twinning in Xenopus. *Proc Natl Acad Sci U S A* **115**, E4815-E4822.

Munoz, R., Edwards-Faret, G., Moreno, M., Zuniga, N., Cline, H. and Larrain, J. (2015). Regeneration of Xenopus laevis spinal cord requires Sox2/3 expressing cells. *Dev Biol* **408**, 229-243.

Naert, T. and Vleminckx, K. (2018). Methods for CRISPR/Cas9 Xenopus tropicalis Tissue-Specific Multiplex Genome Engineering. *Methods Mol Biol* **1865**, 33-54.

Najah, S., Saulnier, C., Pernodet, J. L. and Bury-Mone, S. (2019). Design of a generic CRISPR-Cas9 approach using the same sgRNA to perform gene editing at distinct loci. *BMC Biotechnol* **19**, 18.

Nakayama, T., Fish, M. B., Fisher, M., Oomen-Hajagos, J., Thomsen, G. H. and Grainger, R. M. (2013). Simple and efficient CRISPR/Cas9-mediated targeted mutagenesis in Xenopus tropicalis. *Genesis* **51**, 835-843.

Nieuwkoop, P., Faber, J., (1967). *Normal Table of Xenopus Laevis (Daudin): A Systematical and Chronological Survey of the Development from the Fertilized Egg Till the End of Metamorphosis*. New York: Garland Publishing.

Nieuwkoop, P. D. (1969). The Formation of the Mesoderm in Urodelean Amphibians : II. The origin of the dorso-ventral polarity of the mesoderm. *Wilhelm Roux Arch Entwickl Mech Org* **163**, 298-315.

Ohsugi, K. and Ide, H. (1983). Melanophore differentiation in Xenopus laevis, with special reference to dorsoventral pigment pattern formation. *J Embryol Exp Morphol* **75**, 141-150.

Olena, A. F. and Patton, J. G. (2010). Genomic organization of microRNAs. *J Cell Physiol* **222**, 540-545.

Park, B. Y., Hong, C. S., Sohail, F. A. and Saint-Jeannet, J. P. (2009). Developmental expression and regulation of the chemokine CXCL14 in Xenopus. *Int J Dev Biol* **53**, 535-540.

Parker, H. J., Pushel, I. and Krumlauf, R. (2018). Coupling the roles of Hox genes to regulatory networks patterning cranial neural crest. *Dev Biol* **444 Suppl 1**, S67-S78.

Petratou, K., Spencer, S. A., Kelsh, R. N. and Lister, J. A. (2021). The MITF paralog tfec is required in neural crest development for fate specification of the iridophore lineage from a multipotent pigment cell progenitor. *PLoS One* **16**, e0244794.

Petri, R., Malmevik, J., Fasching, L., Akerblom, M. and Jakobsson, J. (2014). miRNAs in brain development. *Exp Cell Res* **321**, 84-89.

Pilon, N. (2016). Pigmentation-based insertional mutagenesis is a simple and potent screening approach for identifying neurocristopathy-associated genes in mice. *Rare Dis* **4**, e1156287.

Pla, P. and Monsoro-Burq, A. H. (2018). The neural border: Induction, specification and maturation of the territory that generates neural crest cells. *Dev Biol* **444 Suppl 1**, S36-S46.

Plouhinec, J. L., Medina-Ruiz, S., Borday, C., Bernard, E., Vert, J. P., Eisen, M. B., Harland, R. M. and Monsoro-Burq, A. H. (2017). A molecular atlas of the developing ectoderm defines neural, neural crest, placode, and nonneural progenitor identity in vertebrates. *PLoS Biol* **15**, e2004045.

Prykhozhij, S. V., Steele, S. L., Razaghi, B. and Berman, J. N. (2017). A rapid and effective method for screening, sequencing and reporter verification of engineered frameshift mutations in zebrafish. *Dis Model Mech* **10**, 811-822.

Qiu, R., Liu, Y., Wu, J. Y., Liu, K., Mo, W. and He, R. (2009). Misexpression of miR-196a induces eye anomaly in Xenopus laevis. *Brain Res Bull* **79**, 26-31.

Ran, F. A., Hsu, P. D., Wright, J., Agarwala, V., Scott, D. A. and Zhang, F. (2013). Genome engineering using the CRISPR-Cas9 system. *Nat Protoc* **8**, 2281-2308.

Ren, C., Liu, X., Zhang, Z., Wang, Y., Duan, W., Li, S. and Liang, Z. (2016). CRISPR/Cas9-mediated efficient targeted mutagenesis in Chardonnay (Vitis vinifera L.). *Sci Rep* **6**, 32289.

Rice, G. M., Shivashankar, V., Ma, E. J., Baryza, J. L. and Nutiu, R. (2020). Functional Atlas of Primary miRNA Maturation by the Microprocessor. *Mol Cell* **80**, 892-902 e894.

Richbourg, H. A., Hu, D. P., Xu, Y., Barczak, A. J. and Marcucio, R. S. (2020). miR-199 Family Contributes to Regulation of Sonic Hedgehog Expression During Craniofacial Development. *Dev Dyn*.

Riddiford, N. and Schlosser, G. (2017). Six1 and Eya1 both promote and arrest neuronal differentiation by activating multiple Notch pathway genes. *Dev Biol* **431**, 152-167.

Ritter, R. A., Ulrich, C. H., Brzezinska, B. N., Shah, V. V., Zamora, M. J., Kelly, L. E., El-Hodiri, H. M. and Sater, A. K. (2020). miR-199 plays both positive and negative regulatory roles in Xenopus eye development. *Genesis* **58**, e23354.

Rolo, A., Skoglund, P. and Keller, R. (2009). Morphogenetic movements driving neural tube closure in Xenopus require myosin IIB. *Dev Biol* **327**, 327-338.

Ruegger, S. and Grosshans, H. (2012). MicroRNA turnover: when, how, and why. *Trends Biochem Sci* **37**, 436-446.

Ruvkun, G., Wightman, B. and Ha, I. (2004). The 20 years it took to recognize the importance of tiny RNAs. *Cell* **116**, S93-96, 92 p following S96.

Sadaghiani, B. and Thiebaud, C. H. (1987). Neural crest development in the Xenopus laevis embryo, studied by interspecific transplantation and scanning electron microscopy. *Dev Biol* **124**, 91-110.

Sakai, D., Suzuki, T., Osumi, N. and Wakamatsu, Y. (2006). Cooperative action of Sox9, Snail2 and PKA signaling in early neural crest development. *Development* **133**, 1323-1333.

Sakai, D. and Trainor, P. A. (2009). Treacher Collins syndrome: unmasking the role of Tcof1/treacle. *Int J Biochem Cell Biol* **41**, 1229-1232.

Santa-Maria, I., Alaniz, M. E., Renwick, N., Cela, C., Fulga, T. A., Van Vactor, D., Tuschl, T., Clark, L. N., Shelanski, M. L., McCabe, B. D., et al. (2015). Dysregulation of microRNA-219 promotes neurodegeneration through post-transcriptional regulation of tau. *J Clin Invest* **125**, 681-686.

Sater, A. K. and Moody, S. A. (2017). Using Xenopus to understand human disease and developmental disorders. *Genesis* **55**.

Sato, T. S., Handa, A., Priya, S., Watal, P., Becker, R. M. and Sato, Y. (2019). Neurocristopathies: Enigmatic Appearances of Neural Crest Cell-derived Abnormalities. *Radiographics* **39**, 2085-2102.

Sauka-Spengler, T. and Bronner-Fraser, M. (2008). A gene regulatory network orchestrates neural crest formation. *Nat Rev Mol Cell Biol* **9**, 557-568.

Sauka-Spengler, T., Meulemans, D., Jones, M. and Bronner-Fraser, M. (2007). Ancient evolutionary origin of the neural crest gene regulatory network. *Dev Cell* **13**, 405-420.

Scerbo, P. and Monsoro-Burq, A. H. (2020). The vertebrate-specific VENTX/NANOG gene empowers neural crest with ectomesenchyme potential. *Science Advances* **6**, In Press.

Schambony, A., Hefele, J. A., Gentzel, M., Wilm, M. and Wedlich, D. (2003). A homologue of cysteine-rich secretory proteins induces premature degradation of vitelline envelopes and hatching of Xenopus laevis embryos. *Mech Dev* **120**, 937-948.

Schimanski, C. C., Frerichs, K., Rahman, F., Berger, M., Lang, H., Galle, P. R., Moehler, M. and Gockel, I. (2009). High miR-196a levels promote the oncogenic phenotype of colorectal cancer cells. *World J Gastroenterol* **15**, 2089-2096.

Schlosser, G. (2014a). Development and evolution of vertebrate cranial placodes. *Dev Biol* **389**, 1.

---- (2014b). Early embryonic specification of vertebrate cranial placodes. *Wiley Interdiscip Rev Dev Biol* **3**, 349-363.

Schlosser, G. and Ahrens, K. (2004). Molecular anatomy of placode development in Xenopus laevis. *Dev Biol* **271**, 439-466.

Schratt, G. M., Tuebing, F., Nigh, E. A., Kane, C. G., Sabatini, M. E., Kiebler, M. and Greenberg, M. E. (2006). A brain-specific microRNA regulates dendritic spine development. *Nature* **439**, 283-289.

Schulz, Y., Wehner, P., Opitz, L., Salinas-Riester, G., Bongers, E. M., van Ravenswaaij-Arts, C. M., Wincent, J., Schoumans, J., Kohlhase, J., Borchers, A., et al. (2014). CHD7, the gene mutated in CHARGE syndrome, regulates genes involved in neural crest cell guidance. *Hum Genet* **133**, 997-1009.

Seal, S. and Monsoro-Burq, A. H. (2020). Insights Into the Early Gene Regulatory Network Controlling Neural Crest and Placode Fate Choices at the Neural Border. *Front Physiol* **11**, 608812.

Sentmanat, M. F., Peters, S. T., Florian, C. P., Connelly, J. P. and Pruett-Miller, S. M. (2018). A Survey of Validation Strategies for CRISPR-Cas9 Editing. *Sci Rep* **8**, 888.

Shah, V. V., Soibam, B., Ritter, R. A., Benham, A., Oomen, J. and Sater, A. K. (2016). Data on microRNAs and microRNA-targeted mRNAs in Xenopus ectoderm. *Data Brief* **9**, 699-703.

---- (2017). MicroRNAs and ectodermal specification I. Identification of miRs and miR-targeted mRNAs in early anterior neural and epidermal ectoderm. *Dev Biol* **426**, 200-210.

Shi, J., Severson, C., Yang, J., Wedlich, D. and Klymkowsky, M. W. (2011). Snail2 controls mesodermal BMP/Wnt induction of neural crest. *Development* **138**, 3135-3145.

Shih, L. J., Lu, Y. F., Chen, Y. H., Lin, C. C., Chen, J. A. and Hwang, S. P. (2007). Characterization of the agr2 gene, a homologue of X. laevis anterior gradient 2, from the zebrafish, Danio rerio. *Gene Expr Patterns* **7**, 452-460.

Showell, C. and Conlon, F. L. (2009). Natural mating and tadpole husbandry in the western clawed frog Xenopus tropicalis. *Cold Spring Harb Protoc* **2009**, pdb prot5292.

Simoes-Costa, M. and Bronner, M. E. (2015). Establishing neural crest identity: a gene regulatory recipe. *Development* **142**, 242-257.

Sivak, J. M., West-Mays, J. A., Yee, A., Williams, T. and Fini, M. E. (2004). Transcription Factors Pax6 and AP-2alpha Interact To Coordinate Corneal Epithelial Repair by Controlling Expression of Matrix Metalloproteinase Gelatinase B. *Mol Cell Biol* **24**, 245-257.

Sive, H. L., Grainger, R. M. and Harland, R. M. (2007). Synthesis and purification of digoxigenin-labeled RNA probes for in situ hybridization. *CSH Protoc* **2007**, pdb prot4778.

Southard-Smith, E. M., Kos, L. and Pavan, W. J. (1998). Sox10 mutation disrupts neural crest development in Dom Hirschsprung mouse model. *Nat Genet* **18**, 60-64.

Spokony, R. F., Aoki, Y., Saint-Germain, N., Magner-Fink, E. and Saint-Jeannet, J. P. (2002). The transcription factor Sox9 is required for cranial neural crest development in Xenopus. *Development* **129**, 421-432.

Stainier, D. Y., Kontarakis, Z. and Rossi, A. (2015). Making sense of anti-sense data. *Dev Cell* **32**, 7-8.

Stanchina, L., Baral, V., Robert, F., Pingault, V., Lemort, N., Pachnis, V., Goossens, M. and Bondurand, N. (2006). Interactions between Sox10, Edn3 and Ednrb during enteric nervous system and melanocyte development. *Dev Biol* **295**, 232-249.

Steventon, B., Araya, C., Linker, C., Kuriyama, S. and Mayor, R. (2009). Differential requirements of BMP and Wnt signalling during gastrulation and neurulation define two steps in neural crest induction. *Development* **136**, 771-779.

Steventon, B., Carmona-Fontaine, C. and Mayor, R. (2005). Genetic network during neural crest induction: from cell specification to cell survival. *Semin Cell Dev Biol* **16**, 647-654.

Steventon, B. and Mayor, R. (2012). Early neural crest induction requires an initial inhibition of Wnt signals. *Dev Biol* **365**, 196-207.

Sullivan, C. H., Majumdar, H. D., Neilson, K. M. and Moody, S. A. (2019). Six1 and Irx1 have reciprocal interactions during cranial placode and otic vesicle formation. *Dev Biol* **446**, 68-79.

Suzuki, M., Hara, Y., Takagi, C., Yamamoto, T. S. and Ueno, N. (2010). MID1 and MID2 are required for Xenopus neural tube closure through the regulation of microtubule organization. *Development* **137**, 2329-2339.

Sweetman, D. (2011). In situ detection of microRNAs in animals. *Methods Mol Biol* **732**, 1-8.

Sweetman, D., Rathjen, T., Jefferson, M., Wheeler, G., Smith, T. G., Wheeler, G. N., Munsterberg, A. and Dalmay, T. (2006). FGF-4 signaling is involved in mir-206 expression in developing somites of chicken embryos. *Dev Dyn* **235**, 2185-2191.

Tachibana, M. (2000). MITF: a stream flowing for pigment cells. *Pigment Cell Res* **13**, 230-240.

Teng, L., Mundell, N. A., Frist, A. Y., Wang, Q. and Labosky, P. A. (2008). Requirement for Foxd3 in the maintenance of neural crest progenitors. *Development* **135**, 1615-1624.

Theveneau, E. and Mayor, R. (2012). Neural crest delamination and migration: from epithelium-to-mesenchyme transition to collective cell migration. *Dev Biol* **366**, 34-54.

Thompson, R. C., Deo, M. and Turner, D. L. (2007). Analysis of microRNA expression by in situ hybridization with RNA oligonucleotide probes. *Methods* **43**, 153-161.

Tien, C. L., Mohammadparast, S. and Chang, C. (2021). Heterochromatin protein 1 beta regulates neural and neural crest development by repressing pluripotency-associated gene pou5f3.2/oct25 in Xenopus. *Dev Dyn*.

Tomlinson, M. L., Rejzek, M., Fidock, M., Field, R. A. and Wheeler, G. N. (2009). Chemical genomics identifies compounds affecting Xenopus laevis pigment cell development. *Mol Biosyst* **5**, 376-384.

Trainor, P. A. and Krumlauf, R. (2000). Patterning the cranial neural crest: hindbrain segmentation and Hox gene plasticity. *Nat Rev Neurosci* **1**, 116-124.

Tribulo, C., Aybar, M. J., Nguyen, V. H., Mullins, M. C. and Mayor, R. (2003). Regulation of Msx genes by a Bmp gradient is essential for neural crest specification. *Development* **130**, 6441-6452.

Tribulo, C., Aybar, M. J., Sanchez, S. S. and Mayor, R. (2004). A balance between the anti-apoptotic activity of Slug and the apoptotic activity of msx1 is required for the proper development of the neural crest. *Dev Biol* **275**, 325-342.

Tseng, A. S., Adams, D. S., Qiu, D., Koustubhan, P. and Levin, M. (2007). Apoptosis is required during early stages of tail regeneration in Xenopus laevis. *Dev Biol* **301**, 62-69.

Tsubooka, N., Ichisaka, T., Okita, K., Takahashi, K., Nakagawa, M. and Yamanaka, S. (2009). Roles of Sall4 in the generation of pluripotent stem cells from blastocysts and fibroblasts. *Genes Cells* **14**, 683-694.

Usami, M., Mitsunaga, K., Irie, T., Miyajima, A. and Doi, O. (2014). Simple in vitro migration assay for neural crest cells and the opposite effects of all-trans-retinoic acid on cephalic- and trunk-derived cells. *Congenit Anom (Kyoto)* **54**, 184-188.

Usman, N. and Sur, M. (2021). CHARGE Syndrome. In *StatPearls*. Treasure Island (FL).

Vega-Lopez, G. A., Bonano, M., Tribulo, C., Fernandez, J. P., Aguero, T. H. and Aybar, M. J. (2015). Functional analysis of Hairy genes in Xenopus neural crest initial specification and cell migration. *Dev Dyn* **244**, 988-1013.

Vergara, H. M., Ramirez, J., Rosing, T., Nave, C., Blandino, R., Saw, D., Saraf, P., Piexoto, G., Coombes, C., Adams, M., et al. (2018). miR-206 is required for changes in cell adhesion that drive muscle cell morphogenesis in Xenopus laevis. *Dev Biol*.

Viaut, C., Weldon, S. and Munsterberg, A. (2021). Fine-tuning of the PAX-SIX-EYA-DACH network by multiple microRNAs controls embryo myogenesis. *Dev Biol* **469**, 68-79.

Vonica, A. and Gumbiner, B. M. (2007). The Xenopus Nieuwkoop center and Spemann-Mangold organizer share molecular components and a requirement for maternal Wnt activity. *Dev Biol* **312**, 90-102.

Vuorela, P., Ala-Mello, S., Saloranta, C., Penttinen, M., Poyhonen, M., Huoponen, K., Borozdin, W., Bausch, B., Botzenhart, E. M., Wilhelm, C., et al. (2007). Molecular analysis of the CHD7 gene in CHARGE syndrome: identification of 22 novel mutations and evidence for a low contribution of large CHD7 deletions. *Genet Med* **9**, 690-694.

Wakamatsu, Y., Endo, Y., Osumi, N. and Weston, J. A. (2004). Multiple roles of Sox2, an HMG-box transcription factor in avian neural crest development. *Dev Dyn* **229**, 74-86.

Walker, J. C. and Harland, R. M. (2008). Expression of microRNAs during embryonic development of Xenopus tropicalis. *Gene Expr Patterns* **8**, 452-456.

Wang, M., Qin, L. and Tang, B. (2019). MicroRNAs in Alzheimer's Disease. *Front Genet* **10**, 153.

Wang, Q., Zhu, L., Jiang, Y., Xu, J., Wang, F. and He, Z. (2017). miR-219-5p suppresses the proliferation and invasion of colorectal cancer cells by targeting calcyphosin. *Oncol Lett* **13**, 1319-1324.

Wang, Z. (2011). The guideline of the design and validation of MiRNA mimics. *Methods Mol Biol* **676**, 211-223.

Ward, N. J. (2017). miRNAs and their role in neural crest development. In *School of Biological Sciences*: Universtiy of East Anglia.

Ward, N. J., Green, D., Higgins, J., Dalmay, T., Munsterberg, A., Moxon, S. and Wheeler, G. N. (2018). microRNAs associated with early neural crest development in Xenopus laevis. *BMC Genomics* **19**, 59.

Watanabe, T., Yamamoto, T., Tsukano, K., Hirano, S., Horikawa, A. and Michiue, T. (2018). Fam46a regulates BMP-dependent pre-placodal ectoderm differentiation in Xenopus. *Development* **145**.

White, J. A. and Heasman, J. (2008). Maternal control of pattern formation in Xenopus laevis. *J Exp Zool B Mol Dev Evol* **310**, 73-84.

Wilson, L. O. W., O'Brien, A. R. and Bauer, D. C. (2018). The Current State and Future of CRISPR-Cas9 gRNA Design Tools. *Front Pharmacol* **9**, 749.

Wislet, S., Vandervelden, G. and Rogister, B. (2018). From Neural Crest Development to Cancer and Vice Versa: How p75(NTR) and (Pro)neurotrophins Could Act on Cell Migration and Invasion? *Front Mol Neurosci* **11**, 244.

Witkos, T. M., Koscianska, E. and Krzyzosiak, W. J. (2011). Practical Aspects of microRNA Target Prediction. *Curr Mol Med* **11**, 93-109.

Wittig, J. G. and Munsterberg, A. (2016). The Early Stages of Heart Development: Insights from Chicken Embryos. *J Cardiovasc Dev Dis* **3**.

Wlizla, M., McNamara, S. and Horb, M. E. (2018). Generation and Care of Xenopus laevis and Xenopus tropicalis Embryos. *Methods Mol Biol* **1865**, 19-32.

Wolpert, L. and Tickle, C. (2011). *Principles of Development*. Oxford: Oxford University Press.

Wong, N. and Wang, X. (2015). miRDB: an online resource for microRNA target prediction and functional annotations. *Nucleic Acids Res* **43**, D146-152.

Xin, H., Wang, C. and Liu, Z. (2019). miR-196a-5p promotes metastasis of colorectal cancer via targeting IkappaBalpha. *BMC Cancer* **19**, 30.

Xing, F., Song, Z. and He, Y. (2018). MiR-219-5p inhibits growth and metastasis of ovarian cancer cells by targeting HMGA2. *Biol Res* **51**, 50.

Yang, H., Wu, J. J., Tang, T., Liu, K. D. and Dai, C. (2017). CRISPR/Cas9-mediated genome editing efficiently creates specific mutations at multiple loci using one sgRNA in Brassica napus. *Sci Rep* **7**, 7489.

Yaoita, Y. (2019). Tail Resorption During Metamorphosis in Xenopus Tadpoles. *Front Endocrinol (Lausanne)* **10**, 143.

Ye, J., Coulouris, G., Zaretskaya, I., Cutcutache, I., Rozen, S. and Madden, T. L. (2012). Primer-BLAST: a tool to design target-specific primers for polymerase chain reaction. *BMC Bioinformatics* **13**, 134.

Yin, V. P. (2018). In Situ Detection of MicroRNA Expression with RNAscope Probes. *Methods Mol Biol* **1649**, 197-208.

Young, J. J., Kjolby, R. A., Kong, N. R., Monica, S. D. and Harland, R. M. (2014). Spalt-like 4 promotes posterior neural fates via repression of pou5f3 family members in Xenopus. *Development* **141**, 1683-1693.

Zhang, C., Liang, S., Cheng, S., Li, W., Wang, X., Zheng, C., Zeng, C., Shi, S., Xie, L., Zen, K., et al. (2018). Urinary miR-196a predicts disease progression in patients with chronic kidney disease. *J Transl Med* **16**, 91.

Zhang, X., Shen, B. and Cui, Y. (2019). Ago HITS-CLIP expands microRNA-mRNA interactions in nucleus and cytoplasm of gastric cancer cells. *BMC Cancer* **19**, 29.

Zhou, L., Lim, M. Y. T., Kaur, P., Saj, A., Bortolamiol-Becet, D., Gopal, V., Tolwinski, N., Tucker-Kellogg, G. and Okamura, K. (2018). Importance of miRNA stability and alternative primary miRNA isoforms in gene regulation during Drosophila development. *Elife* **7**.

Zhuang, C., Yuan, Y., Song, T., Wang, H., Huang, L., Luo, X., He, H., Huo, L., Zhou, H., Wang, N., et al. (2017). miR-219a-5p inhibits breast cancer cell migration and

epithelial-mesenchymal transition by targeting myocardin-related transcription factor A. *Acta Biochim Biophys Sin (Shanghai)* **49**, 1112-1121.

Zuasti, A., Jimenez-Cervantes, C., Garcia-Borron, J. C. and Ferrer, C. (1998). The melanogenic system of Xenopus laevis. *Arch Histol Cytol* **61**, 305-316.

8.0.0 Appendices

Appendix 1- Plasmid vector for pDR274 Tyrosinase sgRNA generation and Snapgene sequence file of sgRNA sequence for the sgRNA

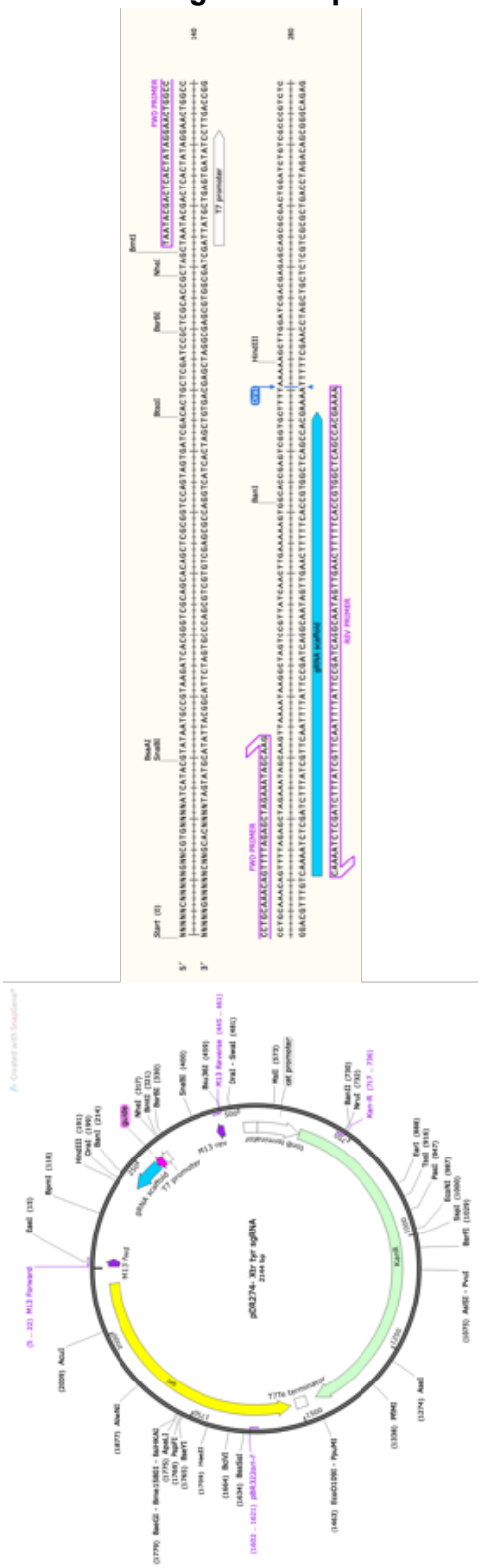

Appendix 2- List of Top 50 differentially expressed genes following miRNA KD with morpholino on NC dissected tissue. Depleted genes in blue, enriched genes in yellow bars.

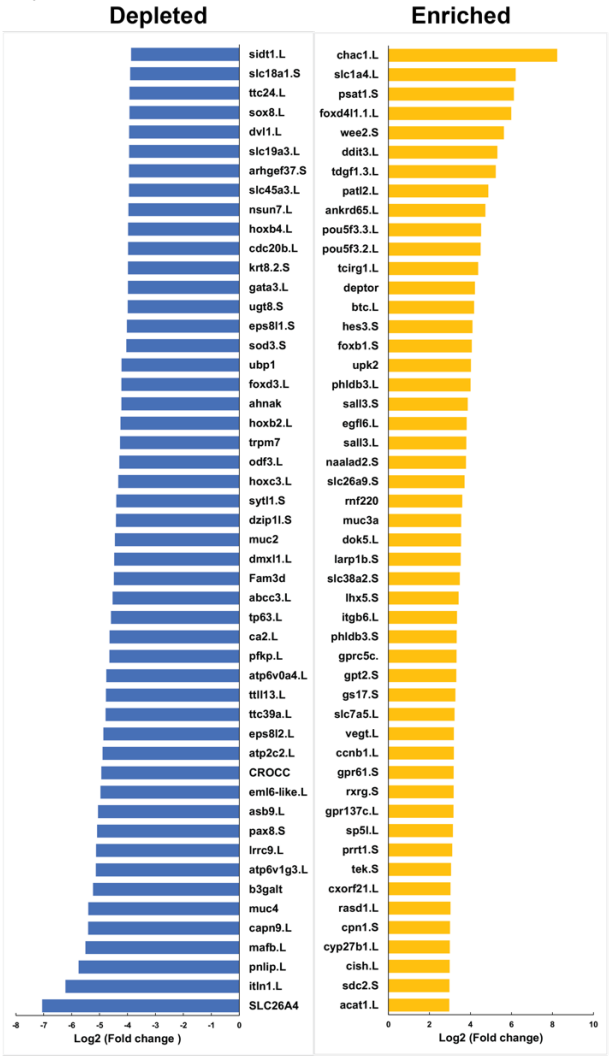

miR-196a

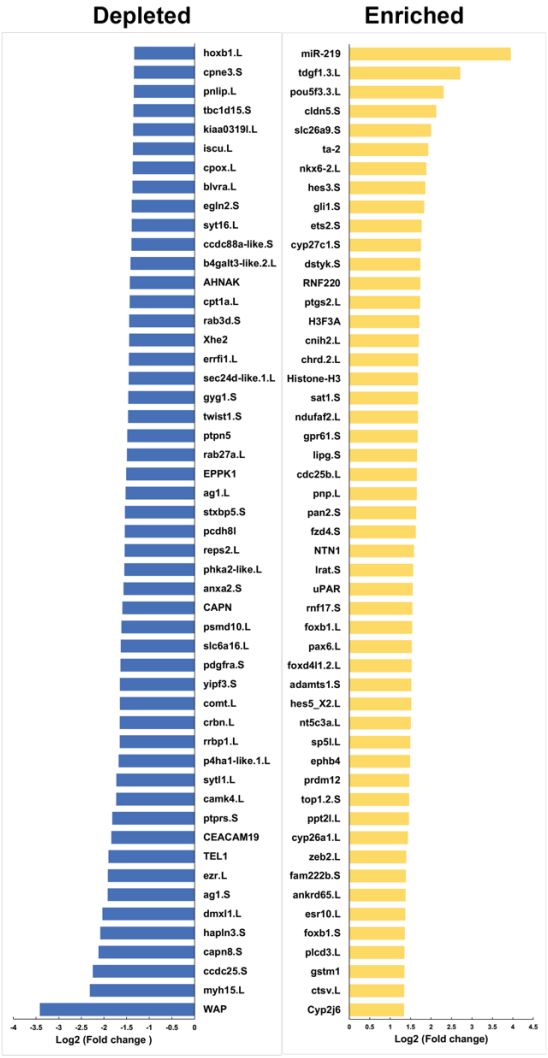

miR-219

Appendix 3-TargetScan, miR-196a Xenopus predicted mRNA targets accessed 22/06/21:

http://www.targetscan.org/cgi-bin/targetscan/vert_72/targetscan.cgi?species=Frog&gid=&mir_sc=&mir_c=&mir_nc=&mir_vnc=&mirg=miR-196a

Ortholog of target gene	Representative transcript	Gene name
HOXC8	ENST00000040584.4	homeobox C8
RP1-170O19.20	ENST00000470747.4	Uncharacterized protein
HOXA9	ENST00000396345.1	homeobox A9
LIN28B	ENST00000345080.4	lin-28 homolog B (C. elegans)
IGF2BP3	ENST00000258729.3	insulin-like growth factor 2 mRNA binding protein 3
VSNL1	ENST00000406397.1	visinin-like 1
ESR1	ENST00000440973.1	estrogen receptor 1
HOXA5	ENST00000222726.3	homeobox A5
SLC9A6	ENST00000370698.3	solute carrier family 9, subfamily A (NHE6, cation proton antiporter 6), member 6
HMGA2	ENST00000403681.2	high mobility group AT-hook 2
CASK	ENST00000421587.2	calcium/calmodulin-dependent serine protein kinase (MAGUK family)
CALM1	ENST00000356978.4	calmodulin 1 (phosphorylase kinase, delta)
POTEE	ENST00000358087.5	POTE ankyrin domain family, member E
EPC2	ENST00000258484.6	enhancer of polycomb homolog 2 (Drosophila)
IGF2BP1	ENST00000290341.3	insulin-like growth factor 2 mRNA binding protein 1
TOX3	ENST00000407228.3	TOX high mobility group box family member 3
BNC2	ENST00000380672.4	basonuclin 2
NR6A1	ENST00000487099.2	nuclear receptor subfamily 6, group A, member 1
EPHA7	ENST00000369303.4	EPH receptor A7
POTEM	ENST00000551509.1	POTE ankyrin domain family, member M
MMS19	ENST00000327277.7	MMS19 nucleotide excision repair homolog (S. cerevisiae)
POTEG	ENST00000409832.3	POTE ankyrin domain family, member G
FOXP2	ENST00000408937.3	forkhead box P2
PPAP2B	ENST00000371250.3	phosphatidic acid phosphatase type 2B
PBX3	ENST00000342287.5	pre-B-cell leukemia homeobox 3
PSENEN	ENST00000591949.1	presenilin enhancer gamma secretase subunit
MBNL2	ENST00000345429.6	muscleblind-like splicing regulator 2
MAP4K3	ENST00000263881.3	mitogen-activated protein kinase kinase kinase kinase 3
LRIG2	ENST00000361127.5	leucine-rich repeats and immunoglobulin-like domains 2
LRP1B	ENST00000389484.3	low density lipoprotein receptor-related protein 1B
SNAP91	ENST00000521485.1	synaptosomal-associated protein, 91kDa

CDV3	ENST00000420115.2	CDV3 homolog (mouse)
NR2C2	ENST00000425241.1	nuclear receptor subfamily 2, group C, member 2
COL1A2	ENST00000297268.6	collagen, type I, alpha 2
AZI2	ENST00000479665.1	5-azacytidine induced 2
CDYL	ENST00000343762.5	chromodomain protein, Y-like
YOD1	ENST00000315927.4	YOD1 deubiquitinase
EYA4	ENST00000367895.5	eyes absent homolog 4 (Drosophila)
FGF14	ENST00000376131.4	fibroblast growth factor 14
NRXN1	ENST00000342183.5	neurexin 1
CDK8	ENST00000536792.1	cyclin-dependent kinase 8
SYNCRIP	ENST00000355238.6	synaptotagmin binding, cytoplasmic RNA interacting protein
ANKRD49	ENST00000544253.1	ankyrin repeat domain 49
COL3A1	ENST00000304636.3	collagen, type III, alpha 1
CELF2	ENST00000379261.4	CUGBP, Elav-like family member 2
MSI2	ENST00000284073.2	musashi RNA-binding protein 2
ZNF507	ENST00000311921.4	zinc finger protein 507
SEMA3A	ENST00000265362.4	sema domain, immunoglobulin domain (Ig), short basic domain, secreted, (semaphorin) 3A
GPC4	ENST00000370828.3	glypican 4
ZNF516	ENST00000443185.2	zinc finger protein 516
GTDC1	ENST00000392869.2	glycosyltransferase-like domain containing 1
USP15	ENST00000353364.3	ubiquitin specific peptidase 15
LETMD1	ENST00000380123.2	LETM1 domain containing 1
PBX1	ENST00000367897.1	pre-B-cell leukemia homeobox 1
PRDM5	ENST00000515109.1	PR domain containing 5
ERI2	ENST00000569729.1	ERI1 exoribonuclease family member 2

Appendix 4- TargetScan, miR-219 Xenopus predicted mRNA targets accessed 22/06/21:

http://www.targetscan.org/cgi-bin/targetscan/vert_72/targetscan.cgi?species=Frog&gid=&mir_sc=&mir_c=&mir_nc=&mir_vnc=&mirg=mir-219

Ortholog of target gene	Representative transcript	Gene name
RORB	ENST00000376896.3	RAR-related orphan receptor B
ZBTB18	ENST00000358704.4	zinc finger and BTB domain containing 18
GNAS	ENST00000371075.3	GNAS complex locus
SIX3	ENST00000260653.3	SIX homeobox 3
FOXJ3	ENST00000372571.1	forkhead box J3
TSC22D2	ENST00000361875.3	TSC22 domain family, member 2
EYA1	ENST00000388742.4	eyes absent homolog 1 (Drosophila)
LEF1	ENST00000265165.1	lymphoid enhancer-binding factor 1
OTX2	ENST00000339475.5	orthodenticle homeobox 2
TENM2	ENST00000519204.1	teneurin transmembrane protein 2
KCNA4	ENST00000328224.6	potassium voltage-gated channel, shaker-related subfamily, member 4
RBM24	ENST00000379052.5	RNA binding motif protein 24
DAZAP1	ENST00000336761.6	DAZ associated protein 1
ROR1	ENST00000371079.1	receptor tyrosine kinase-like orphan receptor 1
ISL1	ENST00000230658.7	ISL LIM homeobox 1
PITPNM2	ENST00000280562.5	phosphatidylinositol transfer protein, membrane-associated 2
RIMS1	ENST00000348717.5	regulating synaptic membrane exocytosis 1
MECOM	ENST00000460814.1	MDS1 and EVI1 complex locus
KCNH8	ENST00000328405.2	potassium voltage-gated channel, subfamily H (eag-related), member 8
NTNG1	ENST00000370067.1	netrin G1
CXXC4	ENST00000394767.2	CXXC finger protein 4
NOL4	ENST00000261592.5	nucleolar protein 4
KCNJ2	ENST00000243457.3	potassium inwardly-rectifying channel, subfamily J, member 2
PCDH17	ENST00000377918.3	protocadherin 17
KLF7	ENST00000423015.1	Kruppel-like factor 7 (ubiquitous)
PDE4D	ENST00000340635.6	phosphodiesterase 4D, cAMP-specific
EFNB2	ENST00000245323.4	ephrin-B2
PCDH19	ENST00000420881.2	protocadherin 19
EYA2	ENST00000327619.5	eyes absent homolog 2 (Drosophila)
SKIDA1	ENST00000449193.2	SKI/DACH domain containing 1
POU2F1	ENST00000367866.2	POU class 2 homeobox 1

POU6F2	ENST00000518318.2	POU class 6 homeobox 2
UBE2V1	ENST00000371657.5	ubiquitin-conjugating enzyme E2 variant 1
CELF2	ENST00000379261.4	CUGBP, Elav-like family member 2
NFIB	ENST00000397575.3	nuclear factor I/B
ZNF827	ENST00000379448.4	zinc finger protein 827
ADCYAP1	ENST00000579794.1	adenylate cyclase activating polypeptide 1 (pituitary)
TMEM189-UBE2V1	ENST00000341698.2	TMEM189-UBE2V1 readthrough
TMEM189	ENST00000557021.1	transmembrane protein 189
SOX5	ENST00000546136.1	SRY (sex determining region Y)-box 5
CD2AP	ENST00000359314.5	CD2-associated protein
STARD4	ENST00000512160.1	StAR-related lipid transfer (START) domain containing 4
CPEB2	ENST00000538197.1	cytoplasmic polyadenylation element binding protein 2
NUMB	ENST00000554546.1	numb homolog (Drosophila)
PPP2R5C	ENST00000422945.2	protein phosphatase 2, regulatory subunit B', gamma
RYBP	ENST00000477973.2	RING1 and YY1 binding protein
HMGA2	ENST00000403681.2	high mobility group AT-hook 2
FGF9	ENST00000382353.5	fibroblast growth factor 9
FBXW7	ENST00000281708.4	F-box and WD repeat domain containing 7, E3 ubiquitin protein ligase
TET2	ENST00000545826.1	tet methylcytosine dioxygenase 2
ELMOD2	ENST00000323570.3	ELMO/CED-12 domain containing 2
TCF12	ENST00000267811.5	transcription factor 12
RBMS1	ENST00000348849.3	RNA binding motif, single stranded interacting protein 1
NCOA2	ENST00000452400.2	nuclear receptor coactivator 2
FLRT3	ENST00000378053.3	fibronectin leucine rich transmembrane protein 3
UBE3A	ENST00000232165.3	ubiquitin protein ligase E3A
SOBP	ENST00000317357.5	sine oculis binding protein homolog (Drosophila)
NFIA	ENST00000403491.3	nuclear factor I/A
RNF165	ENST00000269439.7	ring finger protein 165
CADM2	ENST00000383699.3	cell adhesion molecule 2
SYNCRIP	ENST00000355238.6	synaptotagmin binding, cytoplasmic RNA interacting protein
DDAH1	ENST00000535924.2	dimethylarginine dimethylaminohydrolase 1
TLK1	ENST00000431350.2	tousled-like kinase 1
PHYHIPL	ENST00000373880.4	phytanoyl-CoA 2-hydroxylase interacting protein-like
SOX6	ENST00000316399.6	SRY (sex determining region Y)-box 6
ORC4	ENST00000392857.5	origin recognition complex, subunit 4
DCLRE1C	ENST00000378289.4	DNA cross-link repair 1C
SATB1	ENST00000338745.6	SATB homeobox 1
PTPRM	ENST00000332175.8	protein tyrosine phosphatase, receptor type, M
CLYBL	ENST00000376355.3	citrate lyase beta like

CHD7	ENST00000423902.2	chromodomain helicase DNA binding protein 7
VLDLR	ENST00000382100.3	very low density lipoprotein receptor
ROBO1	ENST00000436010.2	roundabout, axon guidance receptor, homolog 1 (Drosophila)
TRHDE	ENST00000261180.4	thyrotropin-releasing hormone degrading enzyme
ELOVL7	ENST00000508821.1	ELOVL fatty acid elongase 7
MMS19	ENST00000327277.7	MMS19 nucleotide excision repair homolog (S. cerevisiae)
SPTBN1	ENST00000356805.4	spectrin, beta, non-erythrocytic 1

9.0.0 Publications

Mok, G. F., Folkes, L., Weldon, S. A., Maniou, E., Martinez-Heredia, V., Godden, A. M., Williams, R. M., Sauka-Spengler, T., Wheeler, G. N., Moxon, S., et al. (2021). Characterising open chromatin in chick embryos identifies cis-regulatory elements important for paraxial mesoderm formation and axis extension. Nat Commun 12, 1157.

In preparation at time of thesis submission:

Godden et al., (In preparation to submit to Developmental Biology, 2021) An efficient miRNA knockout approach using CRISPR-Cas9 in *Xenopus*

Preprint accessible here: https://www.biorxiv.org/content/10.1101/2021.08.05.454468v1

Godden et al., (In preparation to submit to Developmental Biology, 2021) Investigating the roles of microRNA-196a and microRNA-219 in *Xenopus* neural crest development